Study on Dimensional Measurements Based on Rotating Wire Probe and Acoustic Emission Touch Sensing

by

Salah Elfurjani
B.A.Sc., University of Tripoli, 1991
M.Sc., University of Manchester, 2005

A Dissertation Submitted in Partial Fulfillment of the
Requirements for the Degree of

DOCTOR OF PHILOSOPHY

in the Department of Mechanical Engineering

Supervisory Committee

Study on Dimensional Measurements Based on Rotating Wire Probe and Acoustic Emission Touch Sensing

by

Salah Elfurjani
B.A.Sc., University of Tripoli, 1991
M.Sc., University of Manchester, 2005

Supervisory Committee

Dr. Martin Byung-Guk Jun, **Supervisor**
Department of Mechanical Engineering, University of Victoria, BC, Canada

Prof. Zuomin Dong, **Department Member**
(Department of Mechanical Engineering, University of Victoria, BC, Canada)

Dr. Chris Papadopoulos, **Outside Member**
(Electrical and Computer Engineering, University of Victoria, BC, Canada)

Abstract

Supervisory Committee

Dr. Martin Byung-Guk Jun, **Supervisor**
Department of Mechanical Engineering, University of Victoria, BC, Canada

Prof. Zuomin Dong, **Department Member**
(Department of Mechanical Engineering, University of Victoria, BC, Canada)

Dr. Chris Papadopoulos, **Outside Member**
(Electrical and Computer Engineering, University of Victoria, BC, Canada)

There is an increasing trend towards miniaturization of micro features as well as micro parts. In order to accurately produce these components and the miniaturized features on them, accurate measurement of the component dimensions is required. However, there are limitations in the dimensional measurement of miniature components: micro-probes and Micro coordinate machines (micro-CMMs) suitable for micro-feature measurement are expensive and fragile so it can be difficult to justify the cost for dimensional verification of batch-produced parts (in many cases miniature components are batch-produced). Therefore, a new cost-effective way for dimensional measurement of miniature components is needed. With this in mind, this thesis describes the development of a novel, three-dimensional measurement system using a rotating wire as a probe and acoustic emissions for contact sensing.

This study presents a novel concept of three-dimensional measurements using a rotating wire as a probe and acoustic emission for contact sensing. Experimental results show that the probing system can measure a part with high repeatability. A controller algorithm has been developed for automated scanning within a machine tool. The performance is verified against calibration artifacts. The main contributions of this thesis are as follows: firstly, the traditional contact and non-contact micro coordinate measuring machines including sensing techniques and acoustic emission sensing are reviewed, and a

clear set of knowledge gaps are identified in these fields. Secondly, a novel concept of three-dimensional measurements using a rotating wire as a probe tip and acoustic emission for contact sensing is introduced. The operation and measurements of the rotating micro probing based on acoustic emission (AE) sensing are validated experimentally. Initially, the ability of the rotating microprobe tip based on AE sensing to counteract the measured surfaces interaction rubbing is investigated. Other areas of validation are in the determination of the probing point repeatability, the straightness, and probe tip calibration. Thirdly, the acoustic emission signal and its characterizations of the probe tip touches are studied. The behavior of the rotating probe tip focusses on the threshold, touching time and as well as measured materials type that has an effect on probing accuracy.

Finally, the estimated effective diameter and approximation threshold are modeled. This work is directly aimed at ensuring that the developed rotating probe tip based on AE sensing is capable of operating in an industrial metrology environment.

It is concluded that the developed rotating probe tip based on AE sensing will be able to address the current needs of the micro-CMM community. On the other hand, it is possible that the rotating wire probe tip based on AE sensing can measure micro holes less than the achieved in this work, further increasing its usefulness.

Table of Contents

List of Tables

List of figures

Abbreviations

AET	Acoustic Emission testing
ASTM	American society for testing and materials
ASME	American Society of Mechanical Engineers
AE	Acoustic Emission
A/D	Analog-to-digital
AFM	Atomic force microscopes
CNC	Computer numerical control
CMM	Coordinate measuring machine
dB	Decibel
D_e	Effective wire tip diameter
DAQ	Data acquisition system
DU	Duration
DCC	Direct Computer Control
FFT	Fast Fourier Transform
LLSE	Linear least square estimation
LVDT	Linear variable differential transformer
MNT	Micro/ Nano technology
MEMS	Microelectromechanical system
MARSE	Measured area under the rectified signal envelope
NDT	Non-destructive teste
PSD	Power Spectral Density
PZT	Lead zirconate titanate
PWVM	Probe-Workpiece Voltage Monitoring
RMS	Root mean square
RPM	Revolution per minutes
RT	Rise time
SEM	Scanning electronic microscope
SFM	Scanning force microscopes
SPM	Scanning probe microscopes
SNR	Signal-to-noise ratio

TOA	Time of arrival
UMAP	Ultrasonic Micro and Accurate Probe
WPAES	Wire probing based on AE sensing

Acknowledgments

First and foremost I want to thank my advisor Dr. Martin Jun. It has been an honor to one of his Ph.D. student. I appreciate all his contributions of time, ideas, experience productive and stimulating. The joy and enthusiasm he has for his research was contagious and motivational for me, even during tough times in the Ph.D. pursuit. I would like to extend my best words of thanks to the committee members, Prof. Zuomin Dong, Dr. Chris Papadopoulos.

I would like to acknowledge, Ms. Dorothy Burrows, Ms. Susan Wignall, Barry Kent, Rodney Katz, Minh Ly and Art Makosinski. I would also like to thank Dr. Idress Alokshe, Reza Bayesteh, Geoff B., Max R., Dr. Farid A., Dr. Mohtaram N., Iman, Behzad, Dr. Luo S., Yonghyun, Vahid, Akram, Tim, Dr. Ko J., Ahmad, Mohammad, and Keonhag Lee, We worked together, and I very much appreciated their enthusiasm, intensity, willingness to help me. I gratefully acknowledge the funding sources that made my Ph.D. work possible. I was funded by the Libyan Government.

Lastly, I would like to thank my family for all their love and encouragement. For the presence of my parents here in Victoria for my last semester at UVic. And most of all for my loving, supportive, encouraging friends, whose faithful support during the final stages of this Ph.D. is so appreciated. Thank you.

Lastly, I would like to thank my family for all their love and encouragement. For the presence of my parents here in Victoria for my last semester at UVic. And most of all for my loving, supportive, encouraging friends, whose faithful support during the final stages of this Ph.D. is so appreciated. Thank you.

Salah Said Elfurjani
University of Victoria
July 2016

Dedication

To my wife for her unconditional support, encouragement, for her patience, to my daughters and sons and absolutely everything with love.

To my Parents who worked hard their whole life to enable me my education, brothers and sisters, for their continuous support and encouragement throughout my life, while I have been away from home.

Chapter 1-Introduction

1.1 Motivation and aim

Increasing trends of product miniaturization and needs for 3D complex geometry with relative accuracy of 10^{-3}~10^{-5} demand appropriate quality control of fabricated micro-scale features and components [1]. For dimensional control, most available systems in the manufacturing community are coordinate measuring machines (CMMs) and vision or laser systems. These are confined within the scope of macro-scale. For systems developed to measure meso/micro-scale features and components, it is difficult to justify the high cost and large size of these systems for dimensional verification of the miniature parts with 3D features. Therefore, a new cost-effective way of measuring meso/micro-scale components and features is needed.

Probing technologies using micro-scale probes have been introduced by many researchers and in general they fall mainly into two categories: first method is by touching an object surface with sensing elements such as probe tip and the other is to detect the surface based on non-contact methods using laser or optical sensors [2]. Since devices based non-contact methods tend to be high in cost and their accuracy depends on part surfaces, this thesis focuses on the tactile probing method. Various probing systems with piezoresistance sensors have been developed with cost-effective and robust transducers allowing easy and accurate measurements [3-5]. However, for 3D measurements, three sensors are needed for the probe, which makes the probing units large and complex. Alternative methods have also been adopted for 3D contact micro-probing system such as

micro-probe with optical position detector based on three diode lasers, which limit the probing force less than 1 mN [6-11].

The purpose of this research is to develop a cost effective dimensional measurement system with probing based on an acoustic emission system by utilizing the physical properties and the performance of acoustic emission sensing. This study describe the challenges involved in the sensing mechanism, fabrication of the micro wire probe tip for use as a tactile touch sensor, signal processing, and the solutions to associated difficulties.

Although a numerous literature has been built on the acoustic emission monitoring process in the past few decades, very little consideration has been given to probing application using acoustic emission sensing for dimensional measurement. Physical measurement equipment such as contact probing systems is about more than five decades old and has evolved from a numerical controlled machine tools [2]. Use of non-contact method to overcome the shortage of contact probing system is not very new either. Use of acoustic emission and a rotating probe for touch detection has not been considered for dimensional measurement. Acoustic emission has been used for non-destructive testing (NDT) applications, but utilization of acoustic emission in metrology application has not been observed. This thesis describes the work completed towards the development of rotating micro probe tip based on acoustic sensing system for micro-CMMs.

1.2 Thesis objectives

There are some specific thesis objectives related to this thesis. These objectives will be further adopted in the following chapters, including the definition of few specific research questions.

• Thesis Objective 1 - To design, develop, and validate an acoustic emission based probing system that can measure part dimensions with high measurement accuracy and without surface damage.

• Thesis Objective 2 - To ensure that the developed the acoustic emission probing system can be used in metrology environment and can adhere to existing specification standards.

• Thesis Objective 3 - To understand and analyze acoustic emission signals and the effects of probing process parameters on measurement quality in order to improve the system performance.

• Thesis Objective 4 - To develop and validate probing system's measurement capability by characterizing the geometry of miniature components and features such as pockets and micro-holes.

1.3 Approach and thesis structure

Chapter 1 has described the main motive behind this work, defining Thesis Objectives.

Chapter 2 provides a review of the current state-of-the-art in terms of micro-coordinate measuring machine and micro-probing technology. A wide range of existing technologies on acoustic emission sensing are also discussed, with specific reference to the requirements. Also, this chapter introduces a background information to give framework to this study.

In Chapter 3, the concept and design of the micro probing system based on acoustic emission sensing will be presented. This represents the background knowledge to the thesis, on which the foreground knowledge, developed during this PhD, relies. The research approach that will be used to address the thesis aim is described. This overview

will describe the basic tools that will be used to demonstrate the method of the acoustic emission based probing system.

Chapter 4 provides the experimental measurement work completed towards validating the capability of the rotating probe tip. Development of the rotating micro wire probing system based on acoustic emission sensing is described in detail. The measurement operation of the rotating micro-probe tip will be validated, especially with respect to the surface damage and repeatability measurement. The experimental setup and procedures will be described in detail. A dedicated design of measurements section will clearly define the experiment to be completed, and the results of these measurements will be presented and discussed.

In Chapter 5 introduces a relationship between the frequencies of the generated AE signal, to the different rotational speed, threshold and measured material properties. This chapter also provides evidence that the rotational speed of the probe tip content of the experimental AEs which is proportional to the amount of touches. An estimation model of the threshold is also developed to define an appropriate threshold for measurements.

Presented in Chapter 6 is the fabrication of the rotating straight wire probe, followed by the experimental setup for the measurement of micro-scale holes. Since centrifugal forces result in the probe's wire bending, the effect of spindle speed on the rotating effective diameter (De) of the probe at different overhang lengths is investigated. Three micro-scale holes were fabricated at targeted diameters of 1.0, 0.8, and 0.5 mm, with the femtosecond laser machining setup. Measurement of the micro-scale holes was conducted and the results are as presented, followed by analysis.

The work will be concluded in Chapter 8, which will especially address the successful attainment of the thesis objectives. Finally, future work will be suggested that will help continue development of the micro probing measurements based on acoustic emission sensing towards the requirements of the thesis aim and beyond.

Chapter 2 - Literature review

2.1 Introduction

In this section, the related research for micro measurements and other sensing methods are reviewed. Also, metrological probing systems are studied. The coordinate measuring machines (CMMs) are first presented as basic coordinate measurement understanding. Secondly, tactile probing methods for CMM is introduced and then non-contact probing systems are discussed. Finally, the tool tip and acoustic emission (AE) sensing as another sensing method for positioning, dimensional quality control and monitoring are introduced, and the wire probe sensing based on AE and repeatability as evaluation criteria are studied, respectively.

Modern product technologies, including opto-electronics and microelectromechanical system (MEMS) have seen the development of micro/Nano measurement and associated techniques such as fabrication methods, measurement technologies, and manipulation techniques. Many micro/nanostructure components with tolerance demands such as medical devices, micro motors, fuel injection nozzles with diameters less than 500 μm, components for cameras and computers or hearing devices, and others have recently been assembled, driven by the requirements of micro and nanoscale measurement. In addition, new challenges in metrology are now represented by the increasing miniaturization of products and needs for 3D complex geometry with relative accuracy of 10^{-3}~10^{-5} demand appropriate quality control of fabricated micro-scale features and components [12]. Therefore, sensing measuring systems i.e. contact and non-contact are accelerating the usage of "productive metrology" for 3D measurements instead of conventional contact

systems and the birth of CMM was the key to ensure quality. For dimensional control, most available systems in the market are CMMs, vision or laser systems, scanning force microscopes (SFM), atomic force microscopes (AFM), and scanning probe microscopes (SPM) due to their ability to measure most or all of the individual geometrical features on complex commercial micro products with low uncertainty [13, 14]. The precision / accuracy of CMMs, SFMs and AFMs ranges from a few microns to several hundreds of nanometers, meaning there remain numerous challenges to the measurement precision of the aforementioned probing systems. These challenges, which are significant, arise because the existing surface and coordinate measuring techniques are not suitable for the measurement of microstructures. As main requirements of the system, both a higher accuracy and a smaller probing force are significant; however, both of these attributes are still confronting challenges in 3D metrology. Consequently, many new concepts and designs of micro/Nano probing systems have been proposed. In almost all cases, the probing system is the limiting factor of the machine - either it is not possible to access the feature (main challenge for optical and SPM systems), or the forces associated with tactile CMM-like probes damage the surface or component. Although there is a wide range of probing systems used for Nano-scale metrology tools, usually these are not suitable for measuring three-dimensional (3D) objects. In general, most of the probing systems intended for the measurement of micro-sized components are miniatures of relatively conventional CMM probes or microscopy techniques, which are then enhanced for 3D capability and better repeatability giving the possibility of accurate calibration [4]. Besides, AFMs, SPMs or SEMs may be suitable for surface finish measurement but often lack the capability for three-dimensional measurement at the micro-scale [15]. Obviously,

there is already a large variety of probing systems for Nano-metrology but none of them can fulfil all required tasks satisfactorily. This is due to the differing measuring capabilities of the above probing principles; in micro- and Nano-metrology today, only a sophisticated combination of several probing systems seems to be adequate for quality assurance. The road to multi sensors in Nano-metrology still poses a lot of challenges deriving from two factors: insufficient comparability of the results of different probing systems, and the lack of calibration of the existing and forthcoming probing systems. Positioning and position measuring systems of sufficient range and resolution are available already. During the past decade, researchers successfully introduced two types of technological micro/Nano probing systems. First, there is the touch-trigger probe system, a technique in which the probe tip touches the surface. This is the most commonly used principle for tactile probing, the most well-known example of which is the piezo-resistance sensor with easy, precise and economical measurement, and a robust transducer [3]. The second type of probing system is based on the non-contact method [2], using laser-based optical lenses to measure the surface.

Probing technologies can be classified in two large groups: contact probing systems and non-contact probing systems. Contact probing systems are often called tactile probing systems and since most non-contact probing systems use optical methods for point detection, they are often referred to as optical probing systems [2, 5, 14-16] and in terms of the other method by touching an object surface with sensing elements such as probe tip [3, 6, 11, 17-19]. Furthermore, non-contact probing systems do not have to make (mechanical) contact with the component in order to probe points. Therefore, they measure much faster; additionally, they will not deform a flexible component while probing.

Moreover, the touch-trigger probe system is the tactile probing that is a commonly used method which, have mostly the advantage of being more accurate and reliable. For probing and 3D scanning measurements, at least three sensors need to be joined to the probe, which makes the probing components complicated and large.

Mostly, non-contact systems are typically high in cost and large. Currently, the use of tactile probes on the micro scale is limited by various effects originating from interactions between probe tip and part surface [20]. With the aforementioned various implementations, the majority of the probe system seems to meet the metrological requirements of micro-precision and low probing force. However, as the probe diameter decreased, robust and precise fabrication of the probe becomes difficult, and the sensitivity of the touch sensing systems needs to be significantly improved, resulting in complicated detection devices and algorithms. Consequently, the entire probing system tends to become large in size and ends up being expensive.

Considering cost - and size-efficiency, the tactile probing method was deemed to be more beneficial. In order to measure the scale of any micro part completely, the object in question has to be moved by an ultraprecision 3-axis positioner, as the probe provides information only at the moment of surface-contact with the object [21]. The combination of a contact probe system with a positioning system is generally referred to as the CMM [4], which has been developed since 1950s [13]. Several such μ- and Nano-CMMs which measure meso- to micro scaled parts in nanometer resolution have been developed using one of two types of touch-sensing mechanisms: touch triggered probes, and touch-analog probes. Triggering probes detect the moment of contact and output a signal to lock the current position displayed by the CMM. A typical example based on the above detection

principle and using a vibrating element, whose amplitude is reduced upon surface-contact, can be found in the Mitutoyo Corporation (UMAP 130) [22]. During probing operation the probe approaches the component surface, the probe tip touches the surface and the stylus will deflect. This is detected by the probe sensor which triggers the machine to read out the position of the axes. Many ways have been developed to detect the deflection of the probe [23].

For systems developed to measure meso/micro-scale features and components, it is difficult to justify the high cost and large size of these systems for dimensional verification of the miniature parts with 3D features. Therefore, a new cost-effective way of measuring meso/micro-scale components and features is needed. For measuring such micro-scale parts, traditional CMM's are hindered by the lack of:

- The probing forces in the range of 0.05 N up to 1 N [24]. This probing forces are too high for small probe diameters and damage the workpiece to be checked;
- The limitations probing sphere diameter which is about 1 mm;
- The uncertainty in the range within few μm, which is often upper than the specifications to be measured.

To developed μ-CMM will be based on a commercial CMM whose capabilities have been improved through the use of high-resolution line scales. As in the above mentioned properties of the contacting probes are need to be focusing on them because they can't measure non-rigid components. Therefore, some special CMM's and probing systems for measuring small components have been realized [25]. Furthermore, the accuracy can be improved in two ways. Frist, by software error compensation, and second by developing inherently more accurate machines. Furthermore, the cost of the probe system should be

reasonable compared to the price of a high accuracy CMM. On the other hand, the needs and the demands of measuring cutting tools when it is on the machine before and during the process leads to find other sensing methodology. Therefore, other sensing technique such as tool tip sensing system[26-28], which is has different application such as measuring cutting tool diameters, lengths, positioning the cutting tool tip monitoring and other physical application was developed[29, 30]. For instance, acoustic emission (AE) sensors are used in many fields to monitor and predict the cutting condition i.e. non distractive test, grinding, tool wear, and bearing monitoring etc. [31-36]. This system divided in two groups contact and non-contact sensing, one is tactile sensing device and the other is laser- based optical system. In-process sensors play an important aspect in system at a cost affordable to the industrial application[37]. Finally, each system introduced above is reviewed the basic parameters and methodology in this section:

2.2 Dimensional metrology

Conventionally, dimensional metrology covers measurement of dimensions has been viewed as just another dimensional inspection and in principle also geometries based on distance measurements[38, 39]. Almost, for any machined part there will be an error, which means nominal size will be different form machined component. So to guarantee the product quality this error should be in range of a certain given tolerance limitation. The dimensional metrology equipment consist of On-process Dimensional Measurement (Ultrasonic Methods, Mechanical Methods Optical and Pneumatic Methods) and Post-process Dimensional Measurement (CMM, Micrometer Profile Projector and Block Gauge). However, several definitions can be presented that will be useful in the context of this thesis.

• *Calibration* is process that establishes a relationship between two unknown measurable quantities values and indicates the error of the device and compensates for any lack of trueness by execute a correction.

• *Traceability* the concept of traceability includes a valid calibration and verification (indicates that the measurement error is smaller than a so called maximum permissible error).

• *Precision engineering* is a discipline concerned with the production, manufacture, designing machines, fixtures and assembly of parts with exceptionally low tolerances. The processes tend to be highly accurate, highly repeatable and highly stable over time.

Figure 1 shows a general schematic representation of the dimensional metrology procedure, which described in a simple and accurate concept.

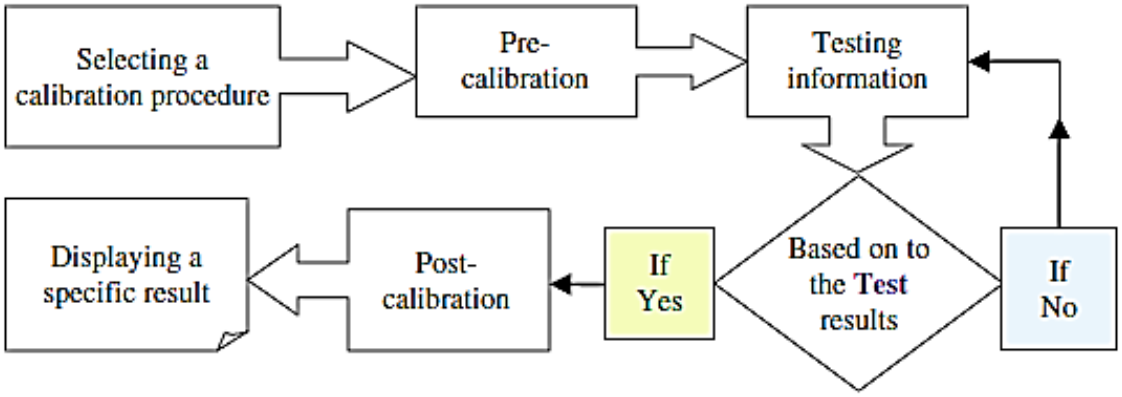

Figure 1 Schematic representation of the procedure in dimensional metrology [40]

2.3 Coordinate metrology on Coordinate measuring machine

The typical 3D "bridge" traditional CMM shown in Figure 2 is used to measure the physical geometrical characteristics of an object in three axes, X, Y and Z, making them very precise Cartesian robots featuring tactile probes, which function as 3-D digitizers with low uncertainty. Usually CMMs are consist of four sections: the probing computer software and on the probing system itself, the machine tool, the operating environment. CMMs might

be controlled by computer or by an operator, the probe system is movable either manually or by servo motors within a certain measuring volume. Also probes may be mechanical, laser, optical, and the recorded points, which collected by suing the probe that positioned manually or automatically via Direct Computer Control (DCC). In addition to being automatized, servo controlled axes bring higher accuracy by way of better reproducing probing. Having revolutionized dimensional metrology, CMMs have been shown to lower inspection costs and increase the productivity of industrial quality systems [13, 14, 25, 41-43].

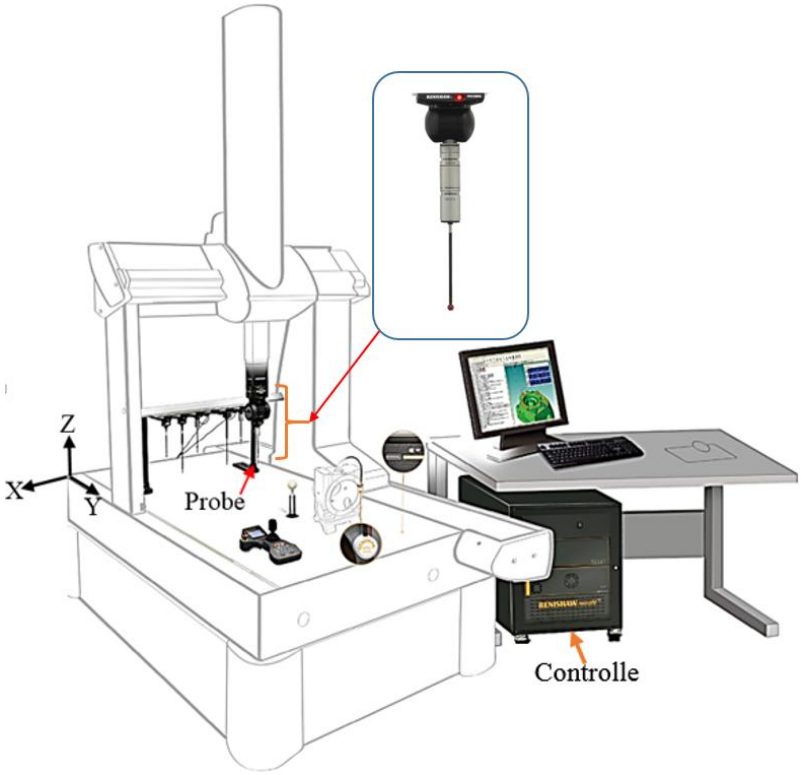

Figure 2 CMM Renishaw's technology[44]

In the CMM measurement process when the probe is traversed along the measured surface and influenced by the probe's contact pressure the probe tip picks up the signals which are either generated by mechanical switching transducers or piezoelectric sensors

and send them to the digital signal processor and counter. Figure 3 shows the schematic diagram of this measurement procedure. Also, the measurement process can be separated into steps*: positioning*, probing, measuring and evaluating. Positioning is the process of moving the part into the measuring workspace of the probing system or vice versa. In traditional CMMs, this is generally done by moving the probing system. Over positioning, it is critical to continuously checking the distance between the measured surface and probing system to avoid collisions [45] and to determine when the maximum safe measuring range is affected. The essential mission of probing process is when the target point is within the probing system is measuring range and a physical joining between the touching element and the surface is verified. Measurement is the comparison of measured dimensions to an accepted standard measurement. Measurement standards for this purpose can be separate integrated into the probing system (e.g. calibrated or calibrated scale).

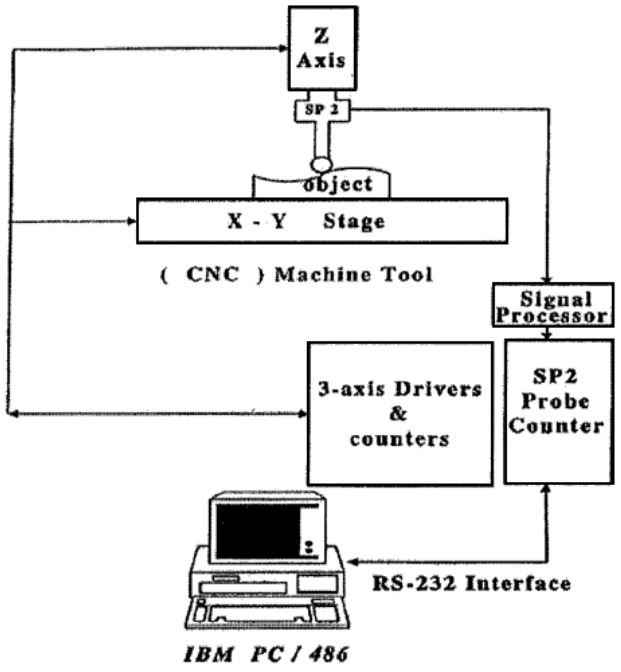

Figure 3 Schematic Diagram measurement procedure for a CMM [46]

2.3.1 Micro CMM's

There are increasing demand for ultra-high accuracy range CMMs due to the increased demand for higher quality control for fine and complex components fabrication by micro system process. However, the need for 3D contact probes is an essential requirement that they should stay at standard for accuracy and reliability of inspection in step with developments in micro-Nano metrology. The progress in miniaturization production now days requires many devices to be used to measure the micro/ Nano technology (MNT) of 3D profile measurement. Material such as polymers need special care with regard to measurement forces for contact probes and this will create a lot more challenging metrology problems beyond the small dimensions and tolerances and complexity [42]. To meet higher quality control in metrological capability regime many µCMM custom was build for micro-scale measurements. Definitely, several laboratories and R&D departments investigate and design their own micro-scale CMMs to addressee the size, quality, and calibration of the probe tip used for inspection. Small-scale CMMs are being recognizable and operational for their possible use in geometric characterization of micro-machined parts was at National Physical Laboratory (NPL) in 1999[47-50] and other research institutions over the following years [2, 25, 51, 52]. The micro-CMMs, also known as miniature CMMs, are shown in Figure 4. The Zeiss F25 µCMM was one of micro-scale metrology CMM developed during the last ten years. The F25 sensing system was developed in direct response to the requirement for quality assurance through the 3D surface topology, form and position of miniaturize components and the resolution on the glass-ceramic line-scales made of Zerodur (Low thermal expansion) on all measurement axes is 7.8nm[53].

Figure 4 Zeiss F25 micro-CMM

2.3.2 The Accuracy and Calibration of CMM's

The measurement operation could not be assisted by putting motor drives on the axes because the probes could not be positioned with great accuracy and the probes were likely to break or the machine itself could become damaged. The development of motorised direct computer controlled machines occurred after the development of a compliant probe. Touch trigger probes work by providing an open switch signal when touched against a component and this signal is used to record the axis position readouts at the instant of touch. The accuracy of a machine, whether software compensated or mechanically corrected, is fundamentally limited by the repeatability of the axes and the stability of the metrology loop. Friction, backlash and changing temperatures are the main sources of nonrepeatability and instability.

As introduced above CMMs are very accurate and suitable for measuring components, but calibration is necessary because it cause deviations of the measured value from the true value. These errors are due to the behavior of a measuring for example, due to the motion of a slider a kinematics error caused due to mechanical incapability in guideways traverse (misalignment is called "pre-travel".), probe tips are not perfectly

spherical, as well as material deposited on ball tip surface (Adhesive wear) as shown in Figure 5 or an abrasive materials (Abrasive wear). So these errors will resulting an offset shifting the probe tip from the given position. Consequently, calibration needed to investigate measuring aspects of machine precision and to know how close the measured value is to the nominal value and to know when we need to replace the probe tip and what is the right probe material should be selected and to compensate the tip radii. In addition, the probe spring force and the high acceleration of probe due to high probe speed approach towards the measured surface, which causes a higher force impact.

The repeatability (precision), resolution and accuracy, are three basic descriptions to remember how well the CMM can position its axes. Resolution is the minimum unit measured by the machine. Accuracy is the highest rotational error between any two points in the machine work volume. Repeatability is the error between a number of successive repeated to move the probe tip to the same spot. Now days, the probe tip calibration well understanding by operators and can be determined automatically in most cases. Laser calibration method is used to achieve higher accuracy measurements and easier set-up than other systems [13, 54-57].

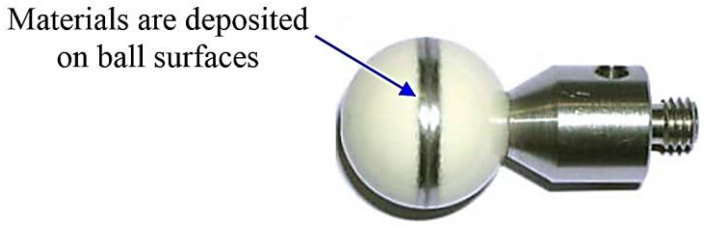

Figure 5 Aluminium material deposited on the surface of the ball [58]

2.3.3 The needs for contact probes

During the last two decades the technology of high 3D geometric measurements of non-contact measurement systems have been developed form meso-to Nano scale. Although of these developments there was a limitation with high aspect ratio micro holes, grooves and the side wall geometry measurement. On the other hand, build and produce a contact probe tip becomes one of the big challenge factors to achieve the desired measurement capability and accuracy. Therefore, conventional CMMs, as dimensional metrology tools, are limited by the size of their probing system to measuring macro- to meso-scaled parts, which has necessitated the design and integration of a contact type micro/Nano-scaled three dimensional coordinate measuring machine. This kind of micro-CMM enables precise measurement accuracy and resolution than conventional macro-scale 3D CMMs. Several such micro- or Nano-CMMs measuring meso- to microscaled components in nanometer resolution, have been improved using one touch triggered probes or touch-analog probes. Triggering probes detect the moment of contact and output a signal to lock the current position displayed by the CMM. A typical example based on the above detection principle and using a vibrating element whose amplitude is reduced upon surface-contact, can be found in the Mitutoyo Corporation[4, 22]. Figure 6 shows the basic tactile probe elements which is the main interaction between the probe tip and measured surface are: the stylus shaft to transfer the contact information and a spring to achieve an isotropic probing force; sensor for evaluating contact information i.e. displacement or force; an interface to the CMM to the control unit for triggering position measurement of the CMM axes[13].

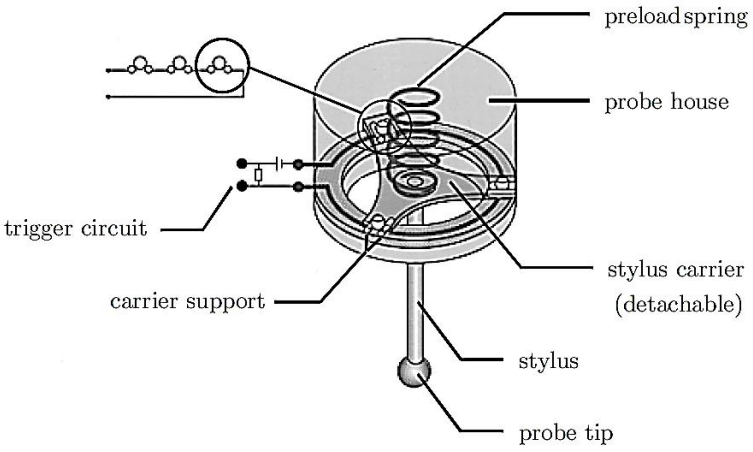

Figure 6 the basic tactile probing design[59]

2.3.4 Probe systems

The probing system is integrated to a CMMs technology and they are three types a scanning probe:

1. An analogue or a scanning probe;

2. A touch trigger probe; and

3. A probe that employs optical technology.

An analogue probe is capable of working either in a mode where it collects points from a number of surface contacts or by scanning the component surface; a touch trigger probe (contact-probe); and a probe that employs optical technology (non-contact) is a sensor, which is intend to get its distance points short after the first touch with sensing parts such as a probe tip[42]. The recognition is performed by physical touching, or by optical methods i.e. charge-coupled device (CCD) cameras and/or laser-based optical sensors, which has a simplified structure. Mechanical probe systems can be categorising into touch trigger systems and measuring probe [60].

Renishaw presented the touch trigger probe with a computer numerical control (CNC) machine in the later century as shown in Figure 7. Once the stylus transferred from its zero point, the resistance of an electrical circuit transformed. At that second the rulers of the CMM are read. Gauging or equivalent probe systems measure the probe tip location continuously. After a surface recognition, the CMM is holding and controlled by signals of the probe system to reach a predetermined probing force. Usually to get the most precise measurement point, the deflection of the probe is added to the position of the CMM axis[19]. Consequently, the probing speed will be lowered to prevent unneeded of high forces at the probing operation. Probing is more time-consuming than in the touch trigger case, because the controlling sequence which take some time[5].

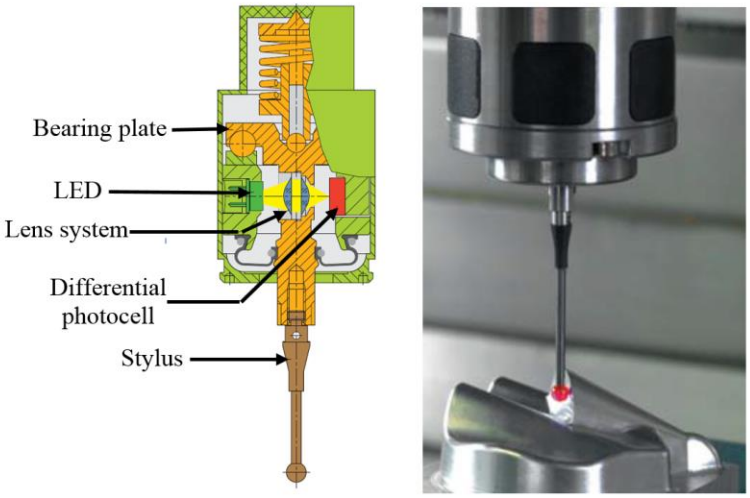

Figure 7 Touch-trigger probe for use in CNC machine [61]

However, the contact method is important but producing a micro scale probes has some difficulties. Although, during scanning the parts the non-contact methods avoids the surface damage but it is a cost due to complexity of the accuracy of the system.

2.3.5 CMM probes

The CMMs probe /sensor has multi functions such as positioning, probing, measuring and evaluating to determine the position of a surface point of a part. The probes of CMMs which “touches” (with one of traditional methods i.e. tactile, or optically, and hybrid sensors) that presented by several researches supposed to have a low probing force not to damage the measured surface for tactile probe and should not suffer from more uncertainty sources than contact probes for noncontact sensors, which its standardization is still inadequate and cannot measure undercuts or holes. The only Hybrid i.e. Zeiss F25 can work independently coupled as a team to compensate the shortage of each other. The accuracy of sensor/probe is strongly influence on the CMMs. Thus, the producers have identify each probe with its specification and advantages. There are some categories of CMMs probe types such as the mechanical probes, optomechanical probes, silicon-based probes and vibrating probes [13, 37, 62].

The following sections will present a different probing systems that are applied to measure micro/Nono parts with small measurement uncertainties and low probing forces.

2.3.5.1 Contact (Tactile) Probing Systems

The main challenges for the contact method between touch-trigger probing elements and the measured surface are the probing force. This type of probing system are using systems similar to linear variable differential transformer (LVDT's) or Piezo resistive or capacitive sensors to locate the detection of the probing element. Micro-/Nano-repeatability is achievable with the determination of the surface detection sensitivity, and the probe design such as a probe tip sphere, and diameter and stylus length. Several researches like Metas probing system shown in Figure 8 which results in probing forces of about 0.5 mN and

has a repeatability in the range of 5 nm [52, 63]; NPL probing system shown in Figure 9 with an isotropic stiffness of 10 N/m and a measurement range of ±20 µm[47]; IBS Triskelion shown in Figure 10 has Probing forces of approximately 0.5 mN. The measurement range is ±10 µm[64]; Xpress Gannen XP shown in Figure 11 with the stiffness at the probe tip about 400 N/m and the measurement range 30 µm[20]; TU Eindhoven or Pril shown in Figure 12 has a measurement uncertainty approximately 1 µm and speeds up to 70 mm/s[59, 60, 65] . These systems have presented low probing force with uncertainties in the range of only 10 nm low enough not to damage both a micro-probe tip and measured surface.

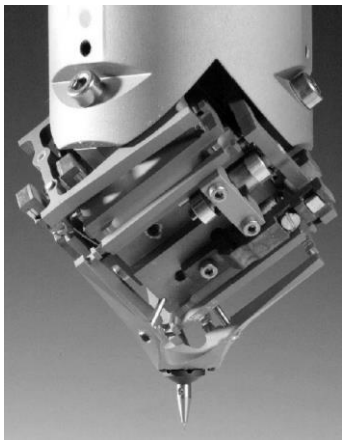

Figure 8 probing system, based on parallel kinematics[52]

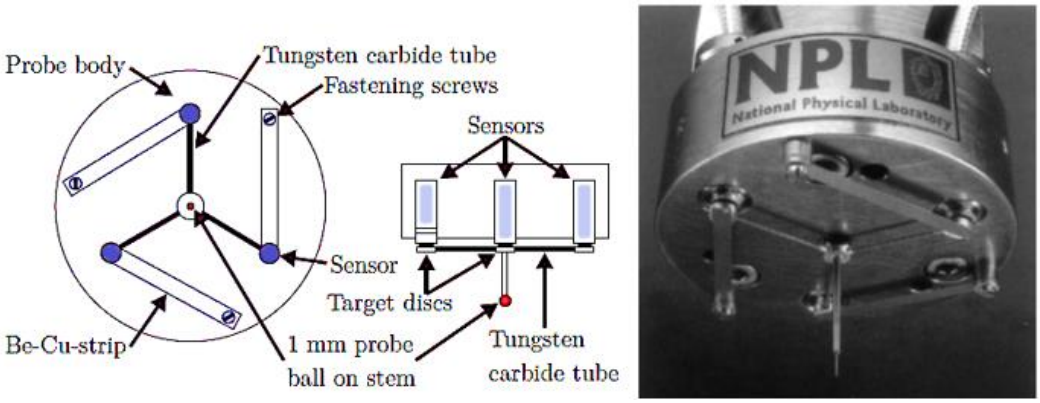

Figure 9 Assembly and picture of NPL of probing design system [23]

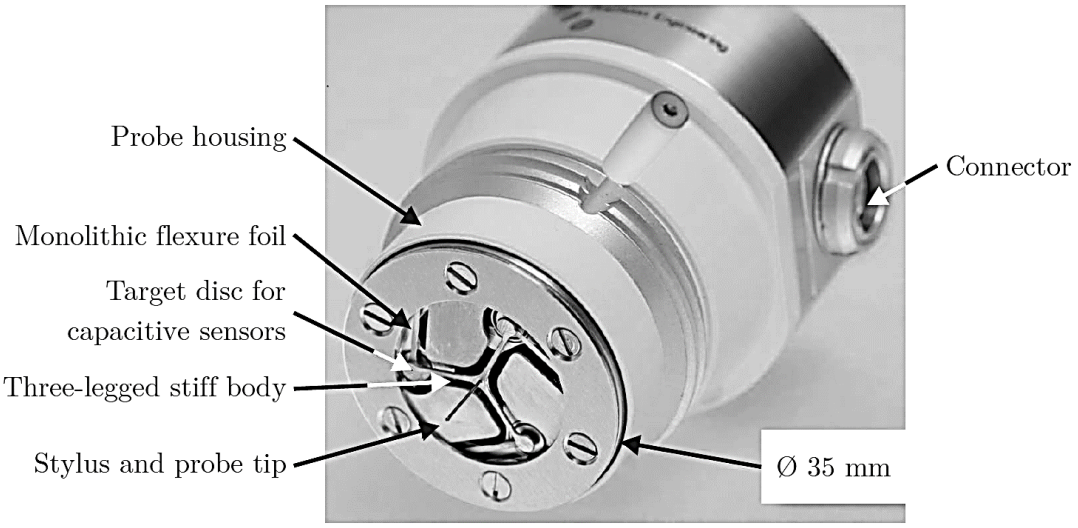

Figure 10 IBS Triskelion probing system[64]

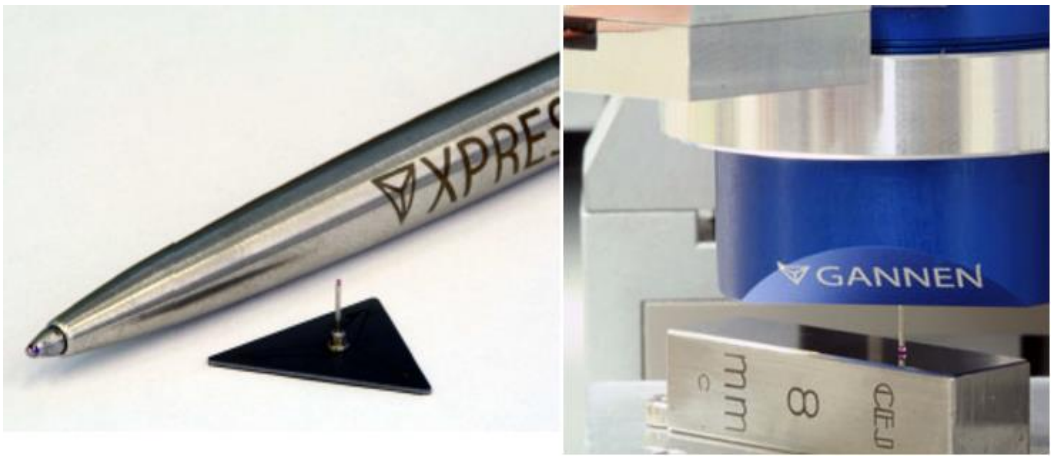

Figure 11 The Gannen XP - High-precision tactile probing system[20].

On the left: The chip of the probing system.

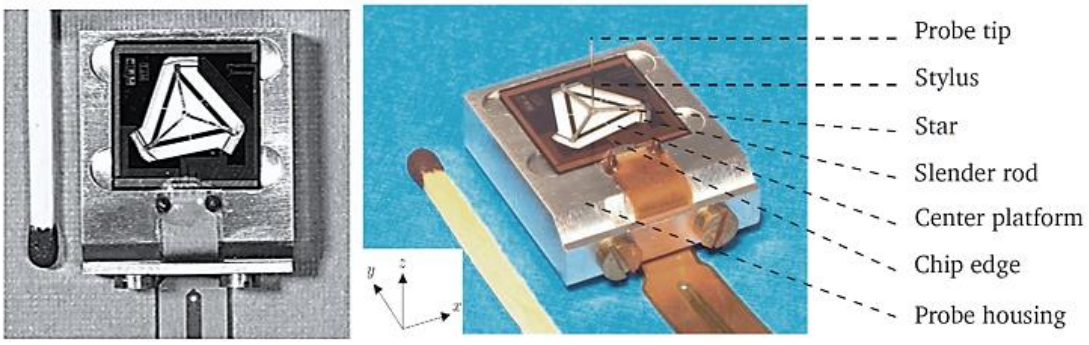

Figure 12 3D-probing system based on three slender rods [59]

2.3.5.2 Opto-mechanical probing systems

The opto-tactile micro probe 2-3D-probing systems have been established, all based on a fibre probe as shown Figure 13, [7, 66-69]. The probing system use a stylus, a glass fiber is used at the end of which, a probing sphere from glass is mounted, which has diameter down to 20-25 µm and microscope with CCD camera to detect the X- and Y-position of the probing sphere. The movement in z-direction is detected with a second CCD camera to determine the deflection of the probing element.

For measuring in small holes and for depths of the probe up to 1 mm, probing uncertainties is between 0.2 – 0.5 µm. The probing forces are in range of some µN, it is very sensitive and without any damaging on the measured surface. These type of sensors was use for characterization of micro-structures was reported from Japan [23, 70].

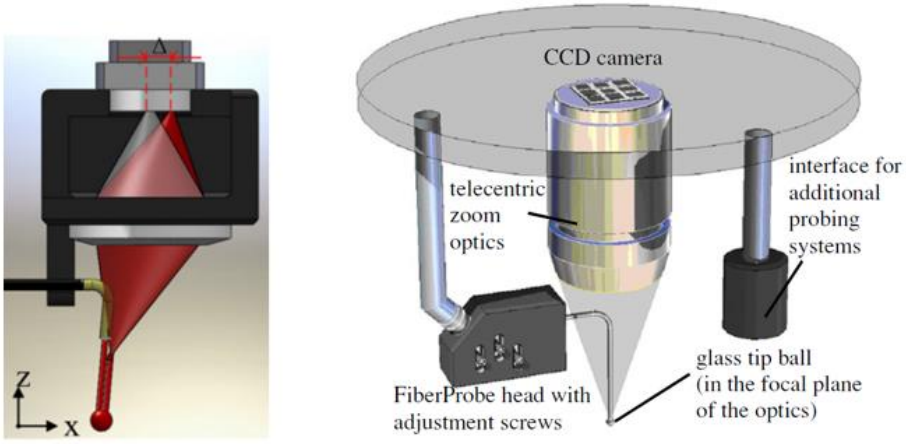

Figure 13 Opto-tactile micro based on a glass fiber, left schematic setup of the 2D-probing system , right realised 3D-probing system[4, 71].

2.3.5.3 Micro-probe based on silicon membrane

Micro-probe by [18, 23] contains of a membrane with integrated piezo-resistive strain gauges, a stylus and ruby ball with a diameter of 0.30 mm, attached to the end of the stylus used approach to attempt to reduce probing forces, as shown in Figure 14. In both cases,

Piezo- resistive strain gauges, a micro-probe tip attached to the center of membrane were etched onto the silicon membrane to detect three-dimensional deformation of the membrane and can thus be used to measure a displacement of the probe tip. The styli are shortened to a length of 5 mm, and fixed to the boss with epoxy resin. Wheatstone-bridges connected to piezo-resistive elements to send signals, so all three directions can be calculated. For membrane length between stylus and edge of 1 mm, a thickness of 30 μm that joined to the stylus of a micro-probe has stiffness is approximately 800 N/m in z-direction and 160 N/m in the xy-plane. The measurement uncertainty of the membrane probe could not be obtained from literature but is estimated to be between 50 - 100 nm.

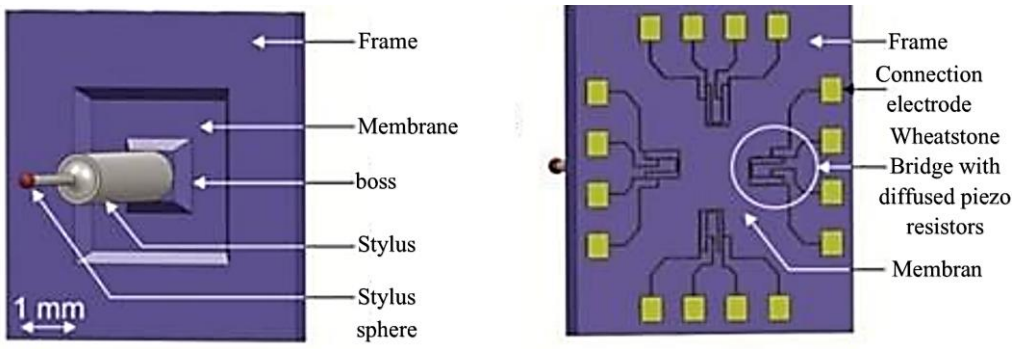

Figure 14 New packaging-concept of the 3d-microprobe [72]

2.3.5.4 Scanning contact probe using floatplane and focus sensor

A 3D mechanical probe design using DVD-Pickup heads as a sensing element has been developed. When the given probe tip is in contact and then deflected by the measured surface, four mirrors mounted onto respective extended arms will amplify the up/down displacement at each mirror position, and plate will be displaced as shown in Figure 15. These displacements can be detected by four corresponding laser focus probes. The dimension of the mechanism can be simulated by finite element method to obtain optimum design, the standard deviation was estimated at 10 nm. Because of the symmetrical

geometry, the force-motion sensitivity should be symmetrical in X-Y plane, where the contact force of about 109 mN [73-76].

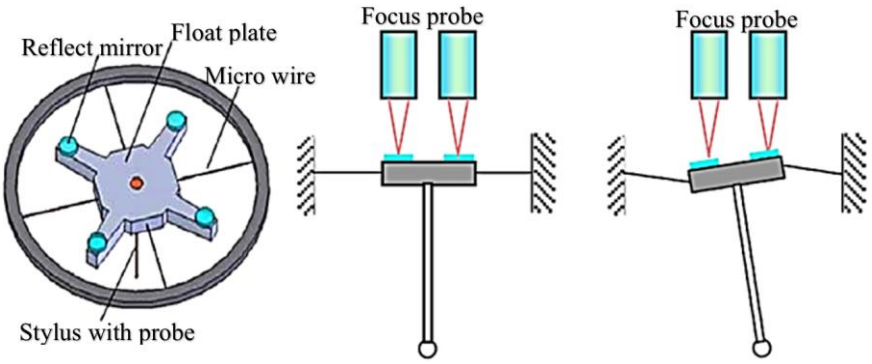

Figure 15 the DVD-Pickup heads Probe floating mechanism [76]

2.3.5.5 Compact 3D optical sensor

The new development analogue contact probe is consist of a rube sphere tip joint to tungsten stylus, an elastic mechanism composing of a plane mirror, a floating plate and four V-shaped leaf springs and a 3D optical sensor. Figure 16 shows the probe mechanism. The large motion in horizontal plane and uniform stiffness will generated by the V-shaped four-leaf spring structure. The 3D optical sensor is detecting the vertical displacement and the dual-axis tilts of the plate with respect to the plan mirror fixed in the center of the floating plate. When the probe tip is in contact force with measured surface the floating plate made the probe a stable rest position. The probe tip movement in 3D is detected by the 3D optical sensor that comprises a miniature polarizing interferometer and a micro autocollimator. Experimental results show that the system can meet the requirements for microstructure measurement where the probe can achieve ± 10 μm × ± 10 μm × 10 μm ($X \times Y \times Z$) measurement range, equal stiffness (within 1 mN μm − 1), and 30 nm measurement standard deviation[77].

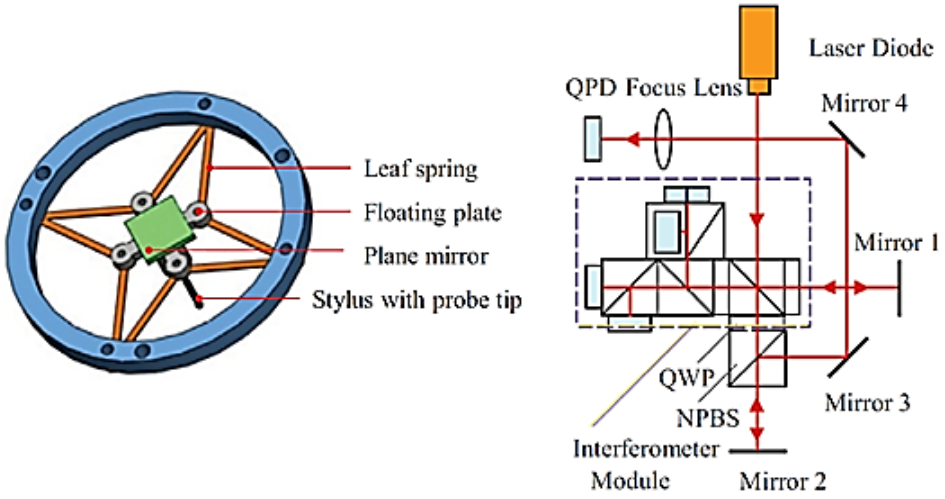

Figure 16 The design of the probe, Left, the probe system, Right, the Sketch of the 3D optical sensor[77].

2.3.5.6 Micro-probe using piezo interferometry

Micro-scale holes are usually measured with SPMs, SEMs, or optical profilometers, which are not used for routine measurements. These devices are generally considered to be 2½ dimensional measurement devices; this is because it is difficult to measure the inside profile using these devices. Thus, internal geometry specifications, such as in-hole roundness, cannot be measured or characterized [78-82]. The use of CMMs with probe tips as small as 300 μm in diameter has been reported. There are, however, limitations as stiffness issues arise with thinner styli, as the contact force deflects the stylus shaft and causes measurement errors [81]. In an effort to solve some of the problems associated with micro-hole measurements, different probing methods and technologies have been suggested, such as vibration-scanning probes, fiber deflection probes, vibrating optical fiber probes, and optical trap probes [83-87]. Although these methods can be used to measure dimensions inside micro-scale holes, they can be costly to develop and maintain.

The presented probing system and its application is based on a Fizeau interferometer, which is normally used in surface testing[88]. The probing system components are adjustment unit, the laser interferometer and the probing head. The micro-probe is coupled to flexure hinges, which support elastically the probe unit, which are manufactured by laser cutting from a thin foil with adequate thickness of 0.06 mm as shown in Figure 17, which keep the probing force low. The probing idea is based on a piezo interferometer to sensing the probe sphere deflection, which is caused a change in the orientation and the distance of the interference fringes. Additionally, an unwanted deformation of the surface under test, caused by too high probing forces, can be detected in the interference pattern over the whole diameter of the laser beam only in its intensity, but not in its shape. This type of probing system has repeatability reached to be 0.19 μm.

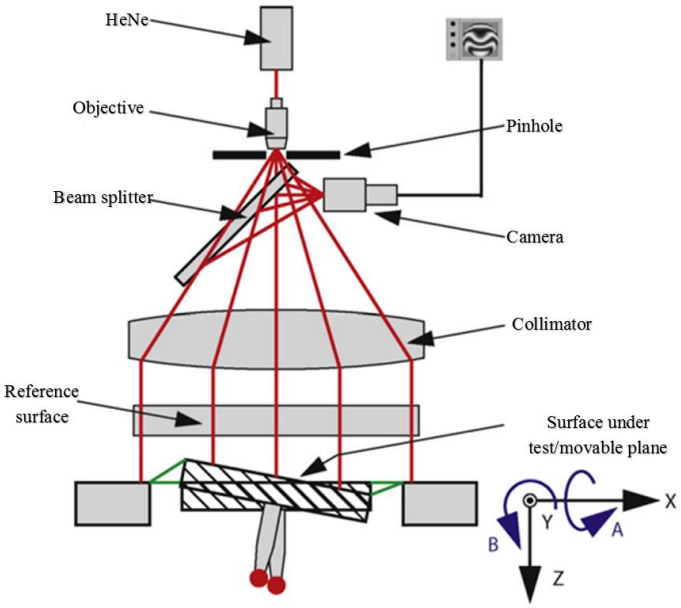

Figure 17 Setup for 3D-probing system using piezo interferometry [88]

2.3.5.7 Slender piezo-resistive cantilever

A new development designed chip holder, which allows simultaneous fixing of the contacting of the piezo-resistive sensor electrodes and the chip. This rigid element can be also tilted to perform 3D investigation, which is inapplicable with traditional scanning force microscopy (SFM). The deflection of the cantilevers (1.5-5 mm in length, 30-200 μm in width and 25-50 μm in height) [89] is transformed into an electric signal proportional to the applied strain either capacitance or directly or indirectly (piezo-electric layer on the cantilever or piezo-resistive layer or elements) following a change in resistance of the sensing network. The Wheatstone bridge located close to the cantilever clamping used to cantilever deflection[90, 91]. A probing tip was generated at the cantilever bottom side and has value of ~ 250 μm for the smallest tips shown in Figure 18. Tiling the sensor head to measure the surface on sidewalls and inclined surfaces. In addition, it is possible to determination of the 3D geometry of micro and Nano parts, when the absolute position and orientation of the sensor is known. At high scanning speeds (> 1 mm/s) and low probing forces (< 100 μN) the sensor has fulfils the requirements of form and roughness measurements with machined surfaces

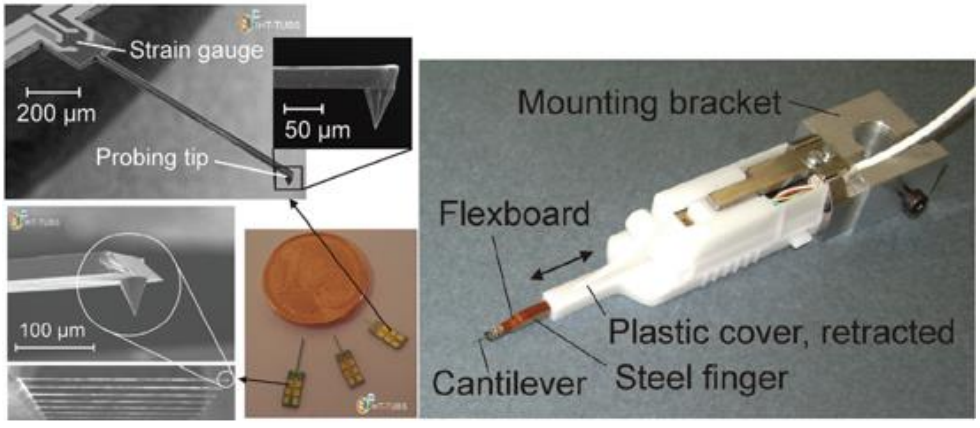

Figure 18 A sample of slender piezoresistive cantaliver sensor with integrated tip[89]

2.3.5.8 Vibrating probing systems

Mitutoyo UMAP (Ultrasonic Micro and Accurate Probe): Mitutoyo Corporation has developed this probing system to measure the profile of ink-jet and fuel injection nozzles as shown in Figure 19. This system uses the change in the vibrational amplitude of the vibrating the glass probe tip. The probe tip is 30 μm in diameter and it will contact measured surface and the friction force will generating voltage signal and resonate frequency which picked up by the sensing electrode. This amplitude is reduced on contact with the measured surface. The repeatability is about 0.1 μm, the contact force about 1 μN [4, 17, 83, 92-94].

2.3.5.9 Standing wave sensor

A high aspect-ratio microscale tactile probe referred to as a standing wave sensor has been developed. The free length probe with 7μm in diameter and 3.5mm in length fixed into a rigid quartz oscillator shank. The free end of the shank generates an amplitude of oscillation greater than the probe shank diameter a diagram of the operating principle of the Virtual probe is shown in Figure 20. The probe can repeatability resolve surface features of 5 nm, the probing force is up to 100 μN. This method has scanning technology ability to access narrow, deep features i.e. measure glass ferrules, fuel injection nozzles [84, 85, 95-98].

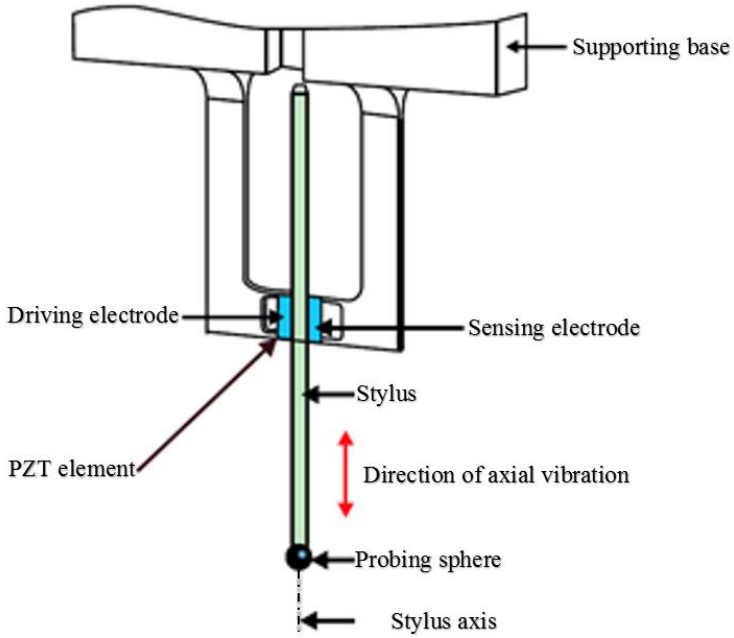

Figure 19 probing system with vibrating probing element [17]

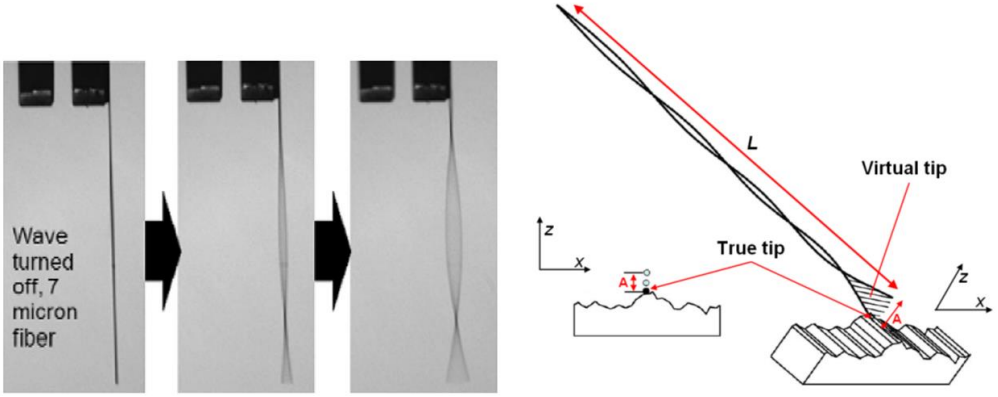

Figure 20 Left a close up view of standing wave fiber operating with a free length; Right schematic of the operating principle [85]

2.3.6 Non-Contact Probing System

Presently, many different types of optical sensors have been used. With non-contact methods based on optical lenses can be measure micro/Nano components by some to the nanometer accuracy, such as, optical focus probe method, SPM (Scanning Probe Microscope) and the hologram diffraction methods. The most optical probing methods have sensitive to the

reflectivity of the measured surface. Also the most recognized of the non-contact technology is the measuring speed compared with the contact methods, whereas most of the optical probing systems have limitation on achieving high aspect ratio, which is confined mainly due to the Rayleigh criterion. Flexible parts can be probed without being deformed and very small structures can be measured which could not be resolved with a conventional tactile probe[99]. In this section, three types of non-contact probes are introduced, which seem to enhance these weak points of the optical micro-probing system. *Nano-CMM with a laser-trapping probe* has the following advantage comparing to the contact systems: High sensitivity; Low measuring force; High sphericity of the probe; dynamically controllable probe characteristics.

So all these benefits will element the surface damage and probe deflection resulted in contact methods. The concept of the system as shown in Figure 21 a glass microsphere that is optically trapped in air by using a single-beam gradient-force optical trap. The probe sphere is sinusoidally vibrated approaches to the measured surface in the orthogonal plane along the optical axis of the trapping laser, following which position sensing is performed by detecting the changes in the vibration signal[100]. Form experimental results, it was found that the laser-trapping system has repeatability of sensing 32 nm. The uncertainty of the Nano- CMM against the flatness and microsphere was estimated to be 335 nm.

Auto focusing micro-probe using DVD pickup: this system using many optical lens, and because DVD player pickup applied as an auto focusing laser probe which reducing the complexity and the cost. In principle as shown in Figure 22, initially, a 650 nm wavelength light source is release by laser diode, and which is polarized by a grating plate. Following, after passing through a beam splitter and a quarter wave plates, by an objective lens, the light beam is accurately focused 2 mm above the measured surface in diameter of 1.0 mm.

The reflected beam is converted to signals to image on a four-quadrant photo detector using the quarter wave plate. The auto-focusing probe is built in the Nano-resolution position stage to form a prototype non-contact micro-CMM [2]. The experimental results confirmed the achieved accuracy is within 30 nm below 30 mm and 0.1 mm for up to 1 mm.

Probing system based on spherical capacitive plate

This 3D probing system technique is based on a spherical capacitive plate for a non-contact probing at nanometer resolution. This method can be used for submicron measurement of small structures with dimension larger than 3 mm and depth down to 100 mm. The spherical capacitive plate shown in Figure 23 is used to convert the micro gap between the plate and the measured surface being measured into a capacitive signal [101]. Experimental results indicate that when the probe tip diameter is 3mm, the measuring system has a resolution 5 nm and nonlinear error is less than 10 nm in the full-range.

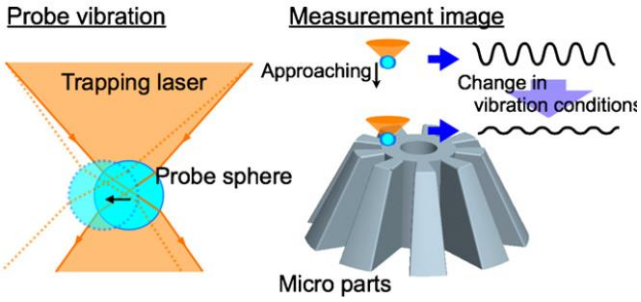

Figure 21 Conceptual sketches of the laser-trapping probe[100].

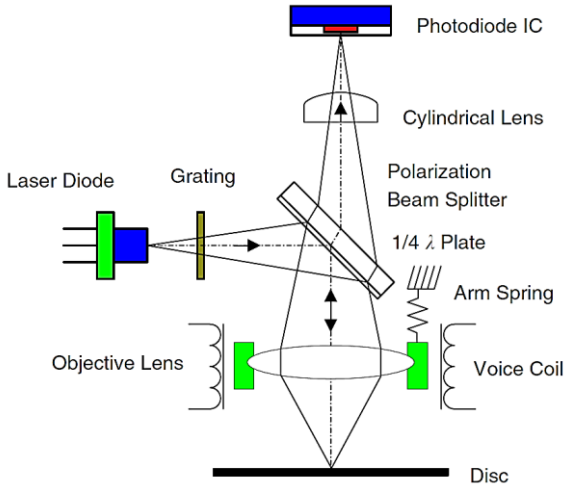

Figure 22 Principle of autofocusing probe [2]

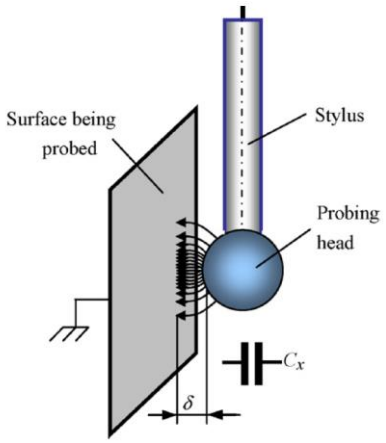

Figure 23 the principle of spherical capacitive plate[101].

2.3.7 Sensing Techniques in Machining Process Monitoring

Traditionally the touch and tactile sensor devices are distinguished in direct and indirect measurements, which measures the parameters of a contact between the sensor and an object. In the consideration of tactile and touch sensing, the following definitions are commonly used:

Touch Sensing: this is the detection and measurement of a contact force at a defined point. A touch sensor can also be restricted to binary information, namely touch, and no touch.

Tactile Sensing: this is the detection and measurement of the spatial distribution of forces perpendicular to a predetermined sensory area, and the subsequent interpretation of the spatial information. A tactile-sensing array can be considered to be a coordinated group of touch sensors.

Slip: this is the measurement and detection of the movement of an object relative to the sensor. This can be achieved either by a specially designed slip sensor or by the interpretation of the data from a touch sensor or a tactile array [102, 103].

With direct methods the desired information is obtained by the actual value of the measured variable. Indirect methods involve the measurement of one or more variables related to the analyzed phenomenon. This interaction obtained is confined to a small defined region. The information of interest is then estimated by means of empirical relations or models. For example the tool wear can be assessed directly by measuring the extension of the corollary with a vision system, or indirectly by using a relationship between spindle power and wear level. Directs methods are generally very accurate but difficult to implement in an existing machine and can also impose some limitations in the machining operation (e. g. cutting without lubricant). This make direct methods more suitable for laboratory applications than for workshop usage.

Indirect methods are less accurate than the direct ones but on the other hand they are easier to implement and then more common in practical applications. Since the work of [27], the most used sensors for monitoring and control applications have been dynamometers, accelerometers, current sensors and AE sensors which monitoring force, power, acoustic emission and vibration. However also different techniques are used including vision systems, temperature sensors, strain gauges and displacement sensors.

Tactile-Sensing Methods

A new technical solution system presents a cost-effective and reliable method for setting up the work coordinate system for ultra-precision miniature machine tool operations. This technique adopts a method for detecting the contact between the cutting tip and the machined surface within Machine tool-Fixture cutting Tool-Workpiece System, which employs an on-machine tool workpiece voltage monitoring system. The concept of the tool tip detection Tool-Workpiece Voltage Monitoring system have been developed for detecting a tool breakage during micro machining operations described in and the same Machine tool Working Coordinate Systems is employed to detect the tool tip. Figure 24 shows the approaches most commonly adopted and depicts the general principles of this system. By creating a close electrical circuit between the spindle and the workpiece, voltage variations generated at contact of the tool tip against a machined surface and can be detected with a specially designed sensor. Then, the conversion of the voltage variation is processed into a digital signal and then sent to the CNC controller. On the other hand, the sensitivity of this methodology is sufficient to detect accurately the contact between the cutting tool tip and the machined surface and can improve the precision and the quality of the machined micro components[28].

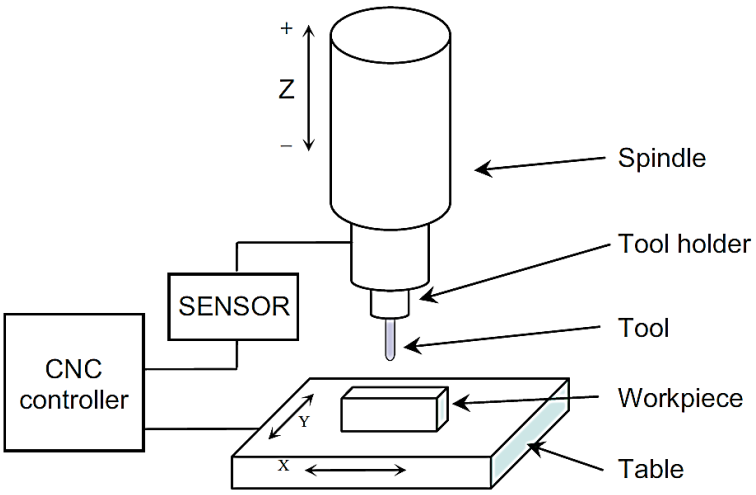

Figure 24 The general principle for detecting the tool-workpiece contact[28].

2.4 Acoustic emission-Sensing Methods and theory

AE is defined as a phenomenon of all engineering materials where elastic stress waves are transmitted into the micro-structural of the material structure rapidly when it subjected to an external stimulus (change in pressure, load, or temperature). Any form of atomic level material dislocations even with 1/1000th of an atomic radius can generate AE [104]. Some of these waves will be reflected, and some will be converted into a surface wave and are released due to the rapid release of stored strain energy emitted as high frequency mechanical vibrations from localized sources within and/or on the surface of a material [105-113]. The frequency range of the waves could cover the inaudible range over the audible range (acoustic or lower than 20 kHz) due to changes in the microstructure of materials . The sonic waves higher than the audible range are defined as ultrasonic waves. Rigorously speaking, AE waves are neither ultrasonic nor acoustic [110].

Acoustic Emission concept

The wear, friction, plastic deformation, micro-fracture, and impacts are usually the sources of acoustic emission. When elastic weaves propagated inside the body and reach the

surface of the material they can be detected by AE sensors. AE can thus provide the early information on defect/deformation in any material or structure. If the atomic bonds break during an integrity test, the energy released propagates through the material according to the laws of acoustics. These waves become strained or compressed under external forces, and spring back when released, which can be detected by piezoelectric transducer placed on the surface to records the waves and the signals. The measurement sequence such as the piezoelectric sensors, data acquisition system and preamplifier is shown in Figure 25.

Depending on the signal-to-noise ratio (S/N ratio) the stored signals can be either low- or high-pass filtered to eliminate the noises. A preamplifier is necessary to minimize the interference and prevent the signal loss, for further processing in the voltage range 0.01mV-100 V and the filter to remove the noise and finally an amplifier. To refine the frequency range and avoid aliasing, they are then amplified and filtered [114]. Then sent to data acquisition system (DAQ) where the analog data and convert it into digital data to extract the information about the nature of the source [104, 107]. The analog-to-digital (A/D) converter converts continuous-time signals into discrete-time signals, which are then stored. These signals converted to dynamic motions as a voltage signals typically range in amplitude from a few microvolts to a couple of millivolts in different frequency ranges usually have a bandwidth of several kHz to a few MHz [107, 115]. This electrical signal may be analyzed in either the time domain or the frequency domain to provide a framework to determine much of the information contained in a signal. In engineering materials, the band width from several kHz to several 100 kHz or 1 MHz is recommended in the measurement. Table 1: Frequency range of different types of AE studies for various media[117]. Table 1: Frequency range of different types of AE studies for various

media[117]. Shows the frequency range of various types of acoustic emission studies for various media.

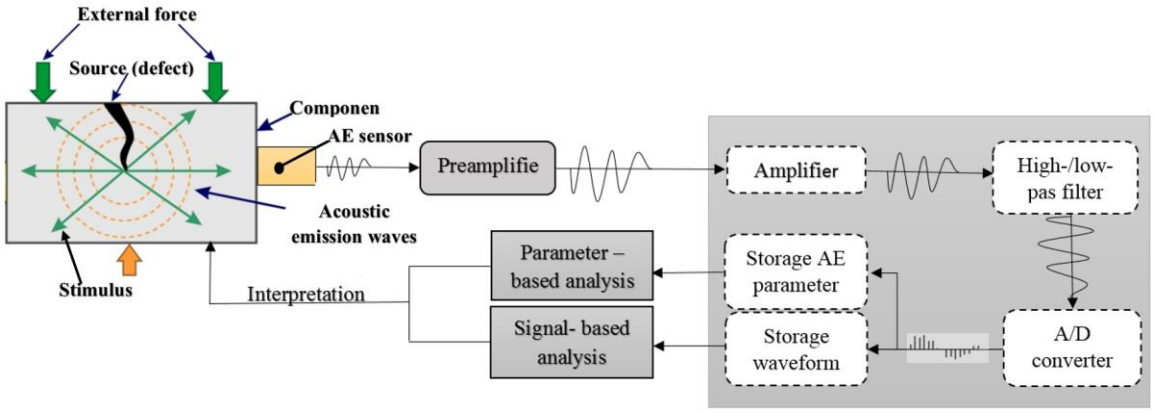

Figure 25 Presents a traditional AE system setup of a propagation crack [116]

Table 1: Frequency range of different types of AE studies for various media[117].

Frequency range	Acoustic emission studies on
10−100 Hz	Micro-earthquakes
200−300 Hz	Small clear specimens, geological material
100 kHz−2 MHz	Solid wood and wood-based composites

2.4.1 Acoustic emission instrumentation

AE system instruments are available in a variety of arrangements ranging from large multi-channel systems to minor and portable equipment. Figure 26 shows a typical acoustic emission system apparatus consists of:

- Sensors used to detect AE events
- Preamplifiers that amplify initial signal. Typical amplification gains are 20-60 dB.
- Cables are typically of coaxial type to transfer signals on distances up to 200-300 m to AE devices.
- Data acquisition device perform filtration, parameters evaluation, data analysis, charting and performs analog-to-digital conversion of signals.

Figure 26 Acoustic Emission sensors and a multichannel data acquisition system.

On other words these systems have common devices, including AE sensors, preamplifiers, filters, and amplifiers for making signal measurable, storage varies widely depending on the demands of the application and then display[111].

Figure 27 shows a block diagram of a generic four-channel acoustic emission system

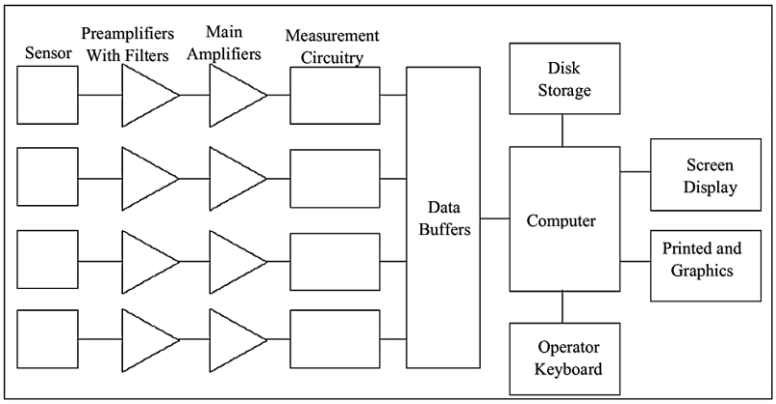

Figure 27 a block diagram of a generic 4 channel AE system [111].

2.4.2 Acoustic emission sensor design

Acoustic emission sensor is a device that transforms a local dynamic material displacement caused by a stress wave to an electrical signal. This is achieved through transducers which convert dynamic motions at the surface into an electrical voltage signal

due to the change in stress in the crystal. So the selection of the correct AE sensor very important.

AE sensors are typically piezoelectric sensors typically consists of several elements. The active element is a piezoelectric ceramic with electrodes on each face. This element might be in desk or cylinder shape with few a few mm in height and from 1-5 mm in diameter.

One electrode is connected to electrical ground and the other is connected to a signal lead. Behind the active element is usually a backing material, often made by curing epoxy containing high density tungsten particles. The backing is usually designed so that acoustic waves easily propagate into it with little reflection back to the active element. In the backing, much of the wave's energy is attenuated by scattering and absorption. A ware plate protects the active element. A thin layer of a couplant or an adhesive bond is used between the contact surfaces of the sensor and the tested object [118]. The transducer is housed in a suitable enclosure with a wear plate and connector as illustrated in Figure 28.

The sensor is excited by the stress waves hitting its face, and it transmits an electrical signal to a nearby preamplifier and then onto the main signal processing equipment. In piezoelectric sensors, commonly named piezoelectric effect, a communication between the mechanical and the electrical state of (Lead zirconate titanate) PZT materials, is applied. Contraction of the PZT material due to an applied pressure yields a proportional voltage increment. The piezoelectric effect is reversible [119, 120]. The key element in an AE sensor is a piezoelectric transducer. When a mechanical strain is applied in a piezoelectric material, a measurable potential difference is produced across the transducer. This phenomenon is reversible, i.e., by application of a potential difference across the

transducer; a mechanical vibration can be induced in the piezoelectric crystal. For linear piezoelectricity, there is a linear relation between mechanical vibration and potential difference allowing direct measurement of distortion from the output voltage.

AE sensors are produced in a way that the resonance is damped out. This way, all the frequencies of the wave is recorded at the same sensitivity as shown in Figure 28. Recorded by sensors are directly attached to the surface of the tested material. It must be considered that they are normally operated at resonance and therefore do not allow broadband detection of AE signals. Resonant sensors are responsive to movement in its typical operating frequency range of 30 kHz to 1 MHz. However, the frequency ranges of the expected signals are often fairly well known, making it possible to choose the right sensor before the experiment [110]. Whereas, a stress wave consists of many frequency components. The higher frequency components will attenuate more quickly as the wave travels and can only be detected close to the source. Background noise such as air hose sound and passing trucks, will be lower frequency. Therefore, the resonant frequency of the sensor is chosen to give maximum sensitivity without background noise. Ideally, the AE signal that reaches the mainframe will be free of background noise and electromagnetic interference. Before, converting the electrical signal at the output of a piezoelectric sensor normally needs to be filtered and amplified. This process is also known as "signal conditioning". The conditioned signal is then sampled and all further processing is then performed digitally. The AE sensor is the very most important device in the AE system. However, there is undefined problems to be solved such as: effect of mounting condition on sensitivity, sensor sensitivity and degradation of the sensitivity and its method evaluation. These elements will affect the peak voltage, change duration time, detected AE

signals, and so on. The main consideration in transducer selection are operating frequency, sensitivity and environmental and physical characteristics. Thus it is quite important to put these factors in the account during using AE equipment [121].

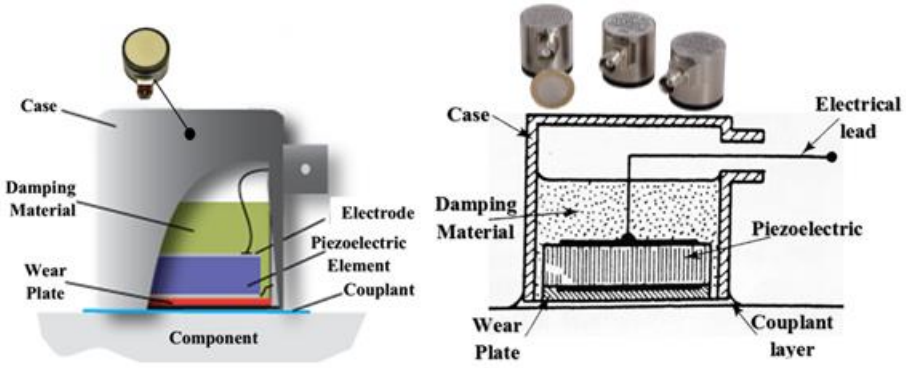

Figure 28 Schematic diagram of a mounted typical AE sensor design [111, 122, 123].

2.4.3 Preamplifier

The preamplifier often located closer to the piezoelectric crystal, which generate usable electric current in the AE sensor and transforms the signal to a voltage as shown in Figure 29. The function of preamplifiers is to increase the strength of the input signal to a more suitable range. Because the magnitude of the voltage is very small. Usually, the preamplifier is mounted integral in the sensor and a very few commercially available that incorporate the amplifier with the sensor.

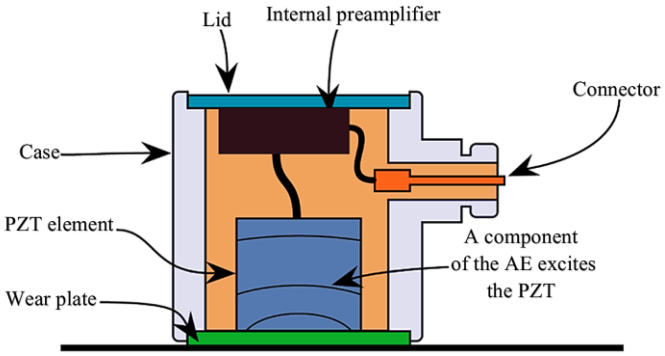

Figure 29 A schematic view of a piezoelectric transducer integrated with preamplifier

Amplifying and frequency filtering are the two components of signal conditioning. Preamplifiers were designed to be used with all available AE systems that have their power supplied via the output signal. The signal is usually amplified by 20 dB to 60 dB (most commonly 40 dB), which is between 10 and 1000 times the input signal. Some preamplifiers are also fitted with analogue filters to eliminate low frequency noise the equipment presented in Figure 30. The 2/4/6 preamplifier is designed to be used with all AE systems. These filters are supplied in the Lows Pass (LP), High Pass (HP), and Band Pass (BP) configurations.

Filtering in the preamplifier (together with transducer selection) is the primary means of defining the monitoring frequency for the acoustic emission operation. This may be improved by additional filtering at the computer[111].

Figure 30 Preamplifier 60, 40, and 20 dB [124]

The main use of preamplifiers is to bring the voltage/signal to a higher level for measurement, and be able to amplify a very small signal, in the order of some microvolts without any interference; so that any electromagnetic noise picked up on the long cable will have relatively less effect. Also to provide circuitry that can deliver the signal down long lengths of cable with Minimum loss. The acoustic emission is shock wave inside a stressed material, where a displacement (unit of distance) ripples through the material and moves its surface. A transducer on that surface undergoes this displacement as a pressure.

The pressure is measured as force per unit area in Pascal (Pa), equivalent to Newton per square meter ($N.m^{-2}$).

The signal from the transducer is sometimes related to velocity ($m.s^{-1}$), displacement (m) or acceleration ($m.s^{2}$). Properties of piezoelectric transducers are related to electric charge: a pressure on the element creates a charge (measured in Coulomb) on the electrodes. A rapidly charge fast enough to allow the use of either voltage or charge amplifiers. After this, signal processing may analyze and store data in terms of signal strength in volt Second ($V{\cdot}S$), energy in joule (J), signal in volt (V) or power in watt (W).

Hertz, Bel and Decibel

Frequencies usually correspond to bandwidths for specific applications. Frequency is measured in hertz (HZ), where 1 Hz =1 cycle per second. The term loudness refers to amplitude in audible frequencies. Some acoustic waves are audible; others have frequencies above or below audible frequencies (ultrasonic- Frequencies above 20 hertz or subsonic- Frequencies below 20 hertz, respectively). A Signal at an inaudible frequency has measurable amplitude but it is not called loud or soft [111]. A customary unit for measuring the amplitude of an acoustic signal is the decibel (dB), one tenth of a bel (B) and sometimes written dB (v). The decibel is not a fixed measurement unit but rather expresses a logarithmic ratio between two conditions of the same dimension (such as voltage or energy). In auditory acoustics, an arbitrary sound pressure such as 20 µPa can be used for the reference level of 0 dB. In acoustic emission, the reference level 0 dB_{AE} is defined as a signal of 1 µv at the transducer before any amplification. The fundamental decibel is:

$$N_{dB} = 10\ log_{10}\ \frac{P}{P_o} \qquad (2.1)$$

Where P is the measured power and P_o is the reference power in watts. In sense, the power is a square function of voltage:

$$N_{dB} = 10\ log_{10}\ (\frac{V}{V_o})^2 \quad (2.2)$$

$$= 20\ log_{10}\ (\frac{V}{V_o}) \quad (2.3)$$

Where v is the measured potential and V_0 is the reference potential in volts.

2.4.4 AE data acquisition

Data acquisition is the process of sampling signals that measure real physical phenomenon such as voltage, current, temperature, pressure, or sound and converting the resulting samples into digital numeric values by using a computer with programmable software. Also, it can record and organize the AE data. Data acquisition systems (abbreviated with the acronym DAS or DAQ) typically convert analog waveforms into digital values for processing. The components of data acquisition systems include:

• ***Transducers and sensors*** that convert physical parameters to electrical signals.

• ***Signals***: Physical phenomena can be converted into measurable signals by the appropriate transducers.

• ***Signal conditioning circuitry*** to convert sensor signals into a form that can be converted to digital values.

• ***DAQ hardware***, ***Driver and application software***: Analog-to-digital converters, which convert conditioned sensor signals to digital values. Signals are basically categorized into two groups: Analog signals and Digital signals. Main concern for data acquisition results from the A/D (analog to digital) conversion and the triggering.

After the preamplifier, the AE signal is transmitted to the AE data acquisition system by a cable. Signal data are mostly digitized by employing a personal computer system. A monitoring system can analyze such parameters as count, hit, event, rise time, duration, peak amplitude, energy, RMS (root mean square) voltage, frequency spectrum, and arrival-time difference. Meanwhile, DAQ also quantize time which is parceled into discrete intervals as shown in Figure 31.

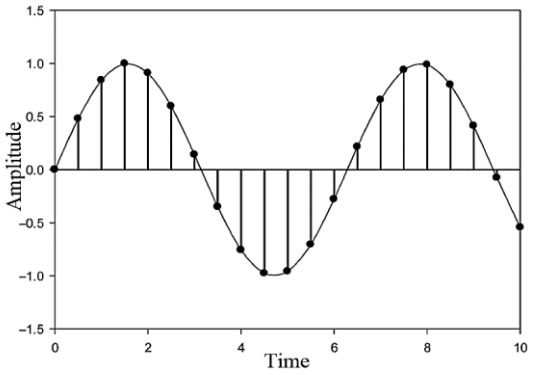

Figure 31 Signal sampling into discrete time intervals

This analog signal, which will be converted is input to the sample and hold, and upon the reception of a pulse from the external sampling control circuit a voltage measurement of the analog input signal is made and converted into a flow of digital values, for example a continuous time and continuous-amplitude analog signal is converted to a discrete-time and discrete-amplitude digital signal. Hence, the rate needs to be defined at which new digital values are sampled from the analog signal. The rate of new value called sample frequency or sample rate which is sample per unit of time (Sec.) taken from continues signal. To enable a perfect signal reconstruction after sampling, the sampling frequency should be high enough. The Nyquist sampling theorem is a fundamental theory that defines the necessary relationship between the highest frequency contained in a signal and the minimum required sampling rate. It stated that the sampling frequency should be at least

twice the highest frequency contained in the signal being sampled. If a function x (t) contains no frequencies higher than fc Hz (the highest frequency contained in the signal) and fs is the sampling frequency, then it is required that fs ≥ 2fc [125, 126]. DAQ can eliminate unwanted signals or frequencies (filter), or amplify the signals that generated by the sensor must be clean and band limited. Anti-aliasing filters are required so that the signals can be properly transformed to the frequency domain. Fast A/D units have to be used to ensure that a large number of events are recorded [15]. Usually, the A/D converter is equipped for each channel of the recording unit. Most of the time data acquisition software can instantly plot graphs and analyze the data, which is helpful for inspectors to understand what is happening during the test. A sketch of AE instrument is shown in Figure 32.

Figure 32 AE Data Acquisitions system

2.4.5 System computer

The First elements in the computer are the main amplifiers and thresholds, which are adjusted to determine the test sensitivity. Main amplifier gain in the range of 20-60 dB are most commonly used. Thereafter, the available processing depending on the size of the system. Similarly, the signal data being gathered to be displayed and stored and sometimes

computer can be houses the threshold settings and main amplifiers, which can be adjusted to control the sensitivity of the experiment. All these data will passed through the computer to a disk file of signal descriptions[111].

2.4.6 Acoustic emission wave analysis

Waveforms of the AE signals feature shown in below is illustrates some common terms associated with AE signals. They are created by joining various single points named samples. Understanding an AE Signals needs the knowledge of some basic terminology which is essential to analyze and interpret these signals. For this, modern AE systems use detection thresholds. The voltage threshold may be adjustable, fixed or floating and depends on the signal-to-noise ratio, size of the structure and test set-up as shown in Figure 33. The time of the first threshold crossing is called "arrival time of the burst" and is needed for location calculation. If the AE signal exceeds the threshold in either positive or negative direction, this means the start of a hit (a hit is a detected burst). The amplitude of the signal refers to the peak voltage of the response and is expressed on a relative decibel scale. Rise time is defined as the time between the first AE hit and the maximum peak amplitude, and the duration of the signal refers to the time interval between the first and last AE threshold crossing. After a certain time, when the AE burst signal died out, the trigger gets activated again. It has to be considered that the same event can trigger multiple channels in a sensor array. Digital systems sample the AE signal e.g. every 100 ns, which means 10 million times a second. The unit of the more than 1000 samples, which shows the huge amount of memory required for a single burst [127, 128].

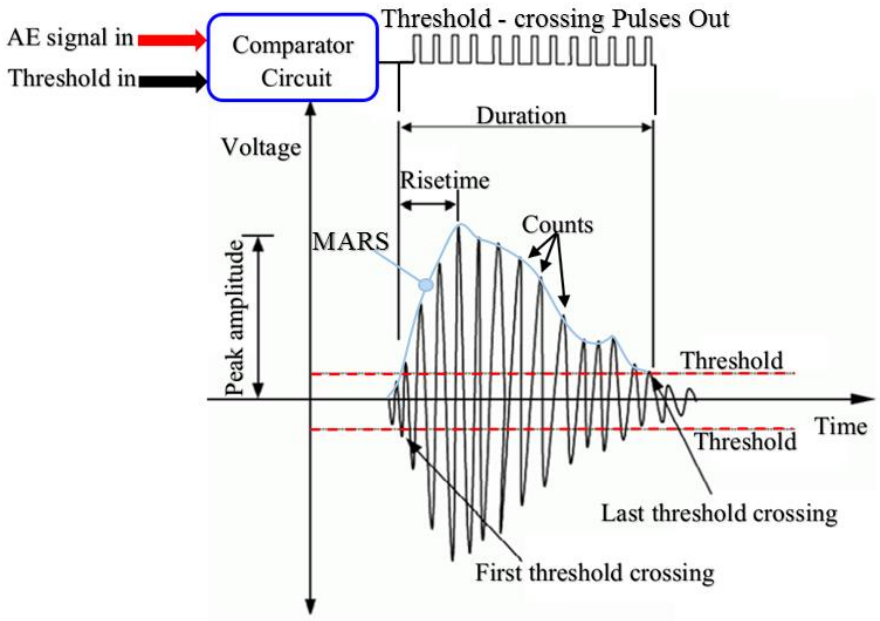

Figure 33 Common AE features from captured signal [129].

A typical AE signal feature shown in the in the above image is adopted and defined below and also called basic AE parameters.

Acoustic emission signal: electrical signal from an acoustic emission sensor produced by the acoustic emission wave.

Threshold: is the voltage level on an electronic comparator such that signals with amplitudes larger than this level will be recognized.

MARSE: (measured area under the rectified signal envelope) the area under the envelope of the rectified voltage signal. Specifically, MARSE is defined as [130]:

$$S_r = \frac{1}{2}\int_{t_1}^{t_2} f_r(t)\,dt \qquad (2.4)$$

Where:

f_r = rectified signal envelop.

t_1 = time at first threshold crossing.

t_2 = time at last threshold crossing.

Peak amplitude is the greatest measured voltage in a waveform and is measured in decibels (dB). The peak amplitude is usually reported in decibels (dB) due to the wide range of typical values in voltage unit. Voltage is converted to decibels using the following equation:

$$A = 20 \log \left(\frac{V}{V_{ref}}\right) \quad (2.5)$$

Where:

A = Amplitude.

V = Voltage of peak excusion (peak (signal).

V_{ref} = Reference voltage(electronic noise), typically 1μV (Voltage generated by 1 mbar pressure of the face of sensor).

The electronic peak noise is the maximum voltage within a defined time period without acoustic emission.

Counts it refers to the number of pulses emitted by the measurement circuitry if the signal amplitude is greater than the threshold.

$$\text{Number of counts } N = \frac{\omega}{2\pi\beta}\ ln\ \frac{V_o}{V_t} \quad (2.6)$$

Where: V_t is threshold voltage, β is duration time, ω is angular frequency and V_o is initial signal amplitude.

Hit (Sensor Hit): "The detection and measurement of an AE signal on a channel" (ASTM E 1316).

Frequency: the frequency is the number of cycles per second of the pressure variation in a wave, measured in hertz. An acoustic emission waveform usually consists of several frequency components.

Event (AE Event): “A local material change giving rise to acoustic emission” (ASTM E 1316).

Source (AE Source): “The position of one or more AE events” (CARP, 1999)

Signal strength is mathematically defined as the integral of rectified voltage signal over the duration of the AE waveform packet.

Energy: generally defined as a measured area under the rectified signal envelope [131, 132].

Background noise: acoustic emission noise which can be rejected by raising the detection threshold or frequency filtering.

Burst signal duration: time difference between the first and the last crossing of the detection threshold by a burst signal.

Burst signal parameters: specific characteristics describing a burst (e.g. peak amplitude, duration, rise-time, energy).

Burst signal rise-time: time difference between the first threshold crossing and the peak amplitude of the burst signal.

This is shows that the raw signal data during AE sensing has an important volume of information and it is very sensitive related to micro scale level.

Generally, there are two kinds of AE signals which can be divided into successive type signal and sporadic type signal; the first is the continuous emission, which can arise from background noise, corrosion, and leakage in i.e. pipes or friction. It has varying amplitudes and frequencies but signal never end, these signals are general associated with plastic deformation in ductile materials. The other type is burst emission also called transient signals with high amplitude, the origin of which can be cracks or other flaws and

occurs only when the flaw is propagating, here the begin and end of the signal deviate clearly from the background noise as shown in Figure 34. Therefore the structure needs to be under load during the inspection, and usually, continuous signal are generally unwanted (noise) signals [104]. All of these detected AE events are added to give what is termed the raw AE signal.

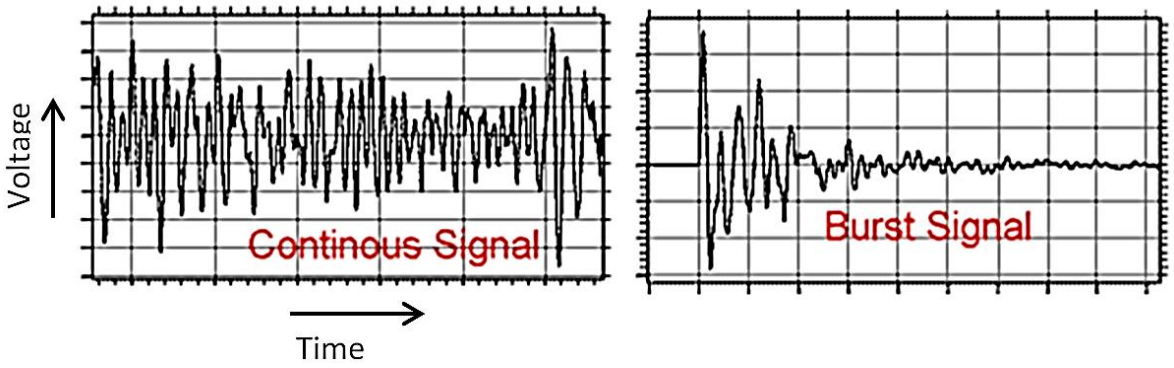

Figure 34 Continuous and burst AE signals[114].

Signals produced by causes other than acoustic emission and are not relevant to the purpose of the test, some types of noise are:

Switching regulators noise: noise of switching power supplies and Electro-magnetic noise.

Hydraulic noise: turbulent flows, boiling of fluids and leaks.

Mechanical noise: Movement of mechanical parts in contact with the structure e.g. fretting of pressure vessels against their supports caused by elastic expansion under pressure.

Floating threshold: Used to distinguish between the background noise and acoustic emission events under conditions of high, varying background noise.

Cyclic noise: Repetitive noise such as that from reciprocating or rotating machinery.

The purpose of the floating threshold shown in Figure 35 is to automate the process of setting the threshold on each channel. This will keep it acceptably above noise background variation, while still remaining as sensitive as possible to avoid emission

activity. The floating threshold shown in figure 35 makes online monitoring a practical reality, but its use should be restricted by the proper selection of sensors and electronic band passing. The floating threshold response to a high-energy transient signal should be slow so as not to affect signal feature measurements.

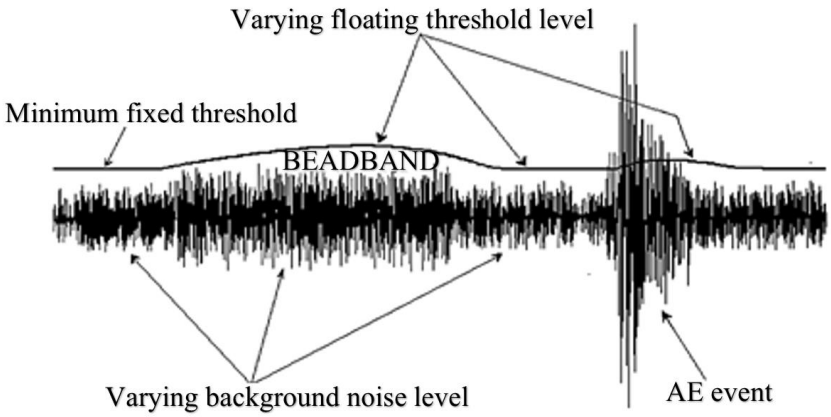

Figure 35 AE signal with flow noise in burst type signal [133]

2.4.7 Time Domain analysis

Analyzing the measured signals in the time domain is to evaluating the similarities in digital signals between two signals. In order to extract information useful for condition monitoring such as wave shapes and amplitudes for a group of signals are compared. For several signals, this is the most logical and intuitive way to view them. It can show the arrival time of the signal; an increase or decrease in the amplitude at a given position in the signal; or the pattern of waveform and any changes of waveform parameters over time through as simple as a visual checking. Figure 36 shows the time domain waveforms gives out an example to demonstrate the denoising effect of a rubbing AE signal.

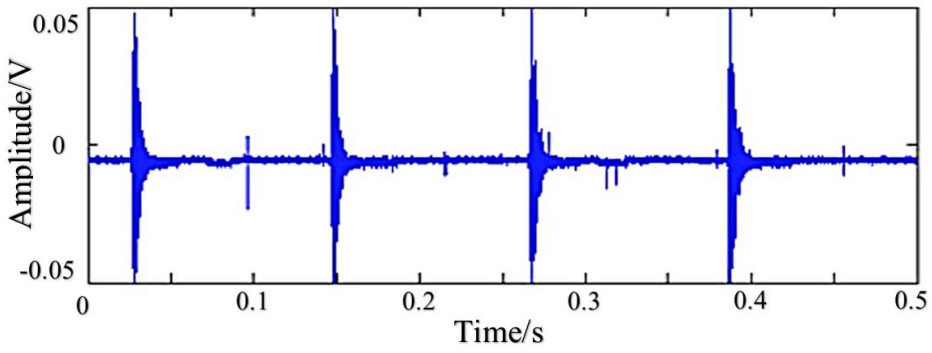

Figure 36 AE of rotor-bearing system analysis results of rubbing AE [134]

2.4.8 Frequency Parameters and Frequency Domain Analysis

Presently such frequency-domain features as shown in Figure 37 play an important role in AE data interpretation. The resolution of frequency parameters is depending on the sampling rate and the waveform length employed[110].

1. Frequency centroid: a calculated frequency feature reported in kilohertz, which results from a sum of magnitude time's frequency divided by a sum of magnitude, as equivalent to the first moment of inertia.

2. Peak frequency: a frequency feature reported in kilohertz, which is defined as the point in the power spectrum at which the peak magnitude is observed.

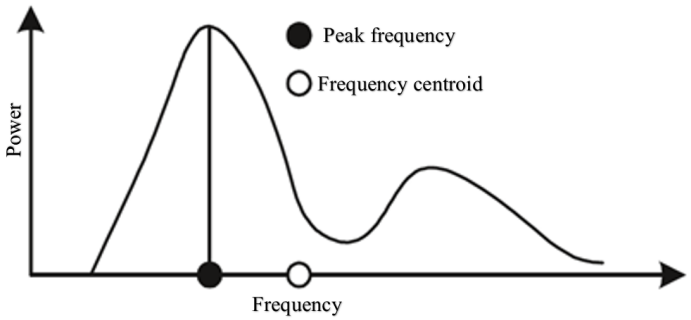

Figure 37 Configuration of peak frequency and frequency centroid

Frequency domain analysis offers further options for analysis of AE discrete signals, this analysis can provide information with regard to discrete signal components in certain frequency range. In general, frequency analysis involves the decomposition of time-series data into the frequency, and is regarded as the most useful method for signal processing. The frequency domain involves transforming the time domain signal to the frequency domain using a Fourier transformation (FFT). FFT is based on the principle that a general periodic function can be expressed as the superposition of a series of sine and cosine terms.

A continuous signal may be reconstructed without information loss if the sampling frequency is greater than twice the highest frequency component in the signal (Nyquist frequencyf_{max} ($the\ maximum\ resolvable\ frequency$) =

$f_{Nyquist}$ ($the\ Nyquist\ frequency$) = $\frac{f_s\ (the\ sampling\ frequency)}{N\ (the\ number\ of\ samples\ acquired)}$).

According to the Shannon Sampling Theorem, the maximum resolvable frequency must be half the sampling frequency (f_{max} =$f_{Nyquist}$ = $\frac{f_s}{2}$). A further approach commonly used is to filter the signal to separate it into its constituent parts. If the filter is carefully constructed then this can then allow increased focus on specific events through enhanced signal to noise ratios (SNR). A low/high or band-pass filter is usually applied to avoid aliasing. Spectra are averaged in order to reduce the variance of spectral estimates. For an N-point measured signal series $X(n)$ in the time domain, with a sampling period of T, the discrete Fourier transform is given as:

$$X(k) = \sum_{n=1}^{N} x(n) e^{-j2\pi(k-1)\frac{(n-1)}{N}} \qquad k = 1,2,\dots,N \tag{2.7}$$

$$X(n) = \frac{1}{N}\sum_{k=1}^{N} X(k) e^{-j2\pi(k-1)\frac{(n-1)}{N}} \qquad n = 1,2,\dots,N \tag{2.8}$$

To plot the frequency spectrum, the scale of the frequency axis should be determined based on the sampling rate $f_s = \frac{1}{T}$ and the total number of sampled data points N. The frequency resolution after FFT is $f_s = \frac{N}{T}$, where T is the acquisition time, f_s is the sampling frequency and N is the number of samples acquired. However, other algorithms have been developed which implement the FFT in order to estimate the distribution of the signal energy in the frequency domain, the principal methods for this are known as the Power Spectral Density (PSD) and Welch's PSD estimate[135]. Furthermore, time- frequency domain analysis is an attractive approach which analyses AE signals in the time frequency domain as shown in Figure 38. This is useful because many acoustic emissions are transient signals whereas stationary characteristics are assumed by the classical Fourier approach.

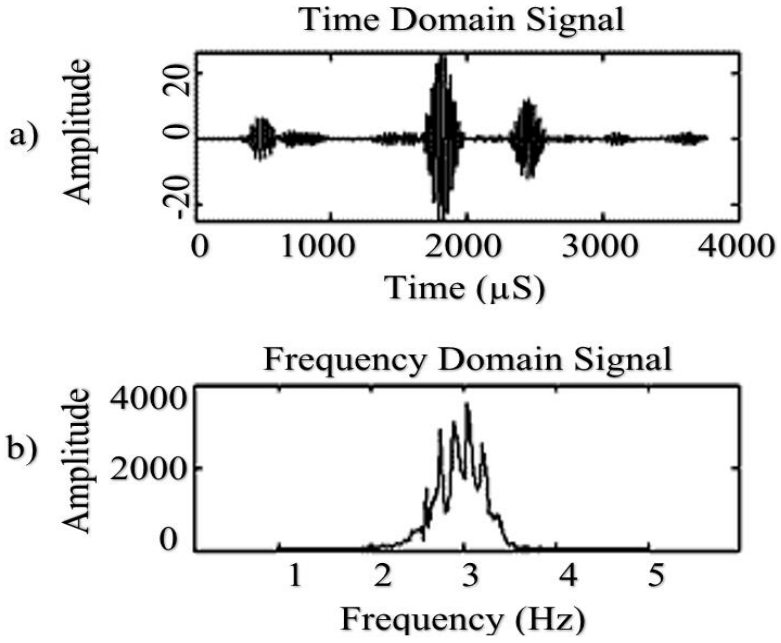

Figure 38 typical received: a) time domain b) frequency domain

2.4.9 Acoustic emission root mean square (RMS)

Root mean square (RMS) is a powerful tool to estimate the average power of a discrete AE signal data and is proportional to the area under the envelope waveform of a discrete signal. Refer to the AE RMS application regular time constant is between 10^{-4} and 0.1 seconds [136]. AE RMS is a suitable parameter to evaluate the failure and damage extent of the material and is an important parameter to be used in non-destructive tests by acoustic emission technique. Once an AE hit is generated, all of the data (AE_{raw}) that create the signal are 'averaged' over a predefined segment that is directly dependent on a chosen RMS time-constant. It can be also defined as a rectified time-averaged value, calculated over a discrete interval, and is reported as a voltage in terms of AE sensor response and can be written as:

$$Rout\ Mean\ Squar\ (r.m.s)AE = \sqrt{\frac{1}{\Delta T}\int_0^{\Delta T} AE^2\ (t)dt} = \sqrt{\frac{1}{N}\sum_{i=1}^{N} AE^2(i)} \qquad (2.9)$$

Where ΔT is the integration time constant and N is the number of discrete AE data within ΔT and represents the signal from each sampled point. AE_{RMS} can be obtained by using an analog RMS filter or digitally by calculating with a chosen ΔT according to the right part of the equation. There is no general rule in selecting suitable ΔT to obtain AE_{RMS}, however ΔT=1 ms provides a good resolution for grinding process, and have been used for many researchers. It should be noted that, since arithmetic mean of all measured AE signals are forced to be zero, standard deviation and RMS can be regarded as one formula given in equation[136, 137].

2.4.10 Acoustic sensing challenges and obstacles

The challenges of using AE techniques were found in many research papers, while some issues are described by others in published literature. Challenges and obstacles associated with various machinery applications of AE, in the context of commonly stated benefits. There are many challenges can be identified in successful application of AE monitoring technique: sensor calibration, noise which may produce acoustic signals similar to the genuine AE signals, hardware, and software, non-stationary signals, variability in operating conditions, signal differentiation. High level of continuous noise such as fluid flow may obscure some weak AE signals[114], accurate source localization[138], damage quantification[139], noise removal and source differentiation[140]. Also the background, service environments are generally very noisy, both continuous and impulsive, makes AE signals less accurate[141]. Challenges still exist in using AE technique for monitoring applications, especially in the area of analysis of recorded AE data, as large volumes of data are usually generated during monitoring. Thus, signal discrimination and noise reduction are very difficult, yet extremely important for successful AE applications[142]. Moreover, evaluation criteria does not exist in form of commonly accessible data, for example, the threshold of AE is set firmly to the knowledge and experience of the service provider.

2.5 Conclusion:

In this chapter a broad range of probing systems is introduced, which are developed in a recent decade for micro-Nano-components. Current work on the probing system by many researcher have a lot improved the feasibility for the Nano metrology. However, none of them seem to meet all the requirements such as probing force, accuracy, and simplicity in

structure for the micro-Nano-metrology. Thus, each system utilized the appropriate combination of the a few sensing methods to minimize the limitations of the one sensing system. Nonetheless, the presented probing systems still confronted still many challenges. The recent experimental results shows the measurement uncertainty of the membrane probe is as lower than 100 nm and the probing force is achieved to less than 1 mN. In non-contact method (laser- trapping system), the repeatability is verified to 32 nm. In general, majority of the reviewed micro-CMM probes have attempted to address one or more of the obstacles faced when completing measurements at the micro-scale such as stylus dimension, probing error, force effect on measured surfaces. These challenges will directly impact on the ability of the research results to address one of the Thesis Aims: "to develop and operate a contact rotating probe tip based on AE sensing that it enables existing micro CMMs to reliably measure few 100s μm features in 2-3D to a high accuracy.

The background knowledge of the concept of the rotating probe tip based on AE sensing will be presented in Chapter 3, and a research approach will be developed.

Chapter 3-Development of Rotating Wire Probe and Acoustic Emission Touch Sensing

This chapter provides development and fabrication of rotating wire as a probe and acoustic emission contact sensing to be effective in dimensional metrology. This chapter presents three probes to be used on high accurate micro CNC machine.

3.1 Data acquisition system and storage

The data acquisition system used at the UVic (University of Victoria) Facility is described in the following sections. It is composed of hardware from National Instruments and software developed using C# to collect and analyze the data. Specifications of sensors and high speed cameras used for data collection were also provided.

3.1.1 Data acquisition device

The raw signal from the preamplifier and the processed output from the integrator were monitored, and a National Instruments PXI-6133 acquisition card is used for data acquisition. These cards have 8 analog input channels which feature 14 bit sampling at 2.5 MHz. Sampling rate was set to 1 MHz for all experimentation. NI BNC-2110 panel was connected to the PXI cards allowing for input signals to be easily connected to the DAQ. Communication between the DAQ and computer system in the control room is done by a SH68-68-EP Shielded Cable (National Instruments).

3.1.2 AE sensors

The main concerns behind sensor selection are operating frequency, bandwidth, and sensitivity. A transducer is a device that produces a measureable voltage signal proportional to the amount of released energy. When stressed physical waves arrive to the

part surface, small displacements will occur. AE sensors are used to detect this mechanical movement and convert it into an electrical signal. Typically, AE sensors are categorized into two kinds; resonant and wideband. Resonant sensors are more sensitive to AE sources at particular frequencies, where the piezoelectric materials of these sensors oscillate at greater amplitude than the other frequency. By matching resonant transducer with the expected frequency of AE events, a greater contrast between the noise and the real AE signal can be achieved that can improve the signal-to-noise ratio significantly. On the other hand, wideband sensors are much better for larger frequency range rather than resonant sensor. Generally, wideband sensors have a relatively flat frequency response across their working range. The transducer is housed in a suitable enclosure with a fixture plate. The sensor is excited by the stress waves hitting the measured surface mounted on the fixture, and it transmits an electrical signal to a nearby preamplifier and then onto the main signal processing equipment. However, all data used for wavelet transform analysis in this study was obtained from WD Broadband sensors an AE sensor calibration.

3.1.3 AE preamplifier

The preamplifier has a wide dynamic range and can drive the signal along a length of cable. The preamplifier typically provides a gain of 40 dB and includes a high-pass or band-pass filter to eliminate the mechanical and background noise. To gain and excellent cable drive capability the preamplifier is usually placed close to the sensor. PAC 2/4/6 preamplifiers were used throughout this study shown in figure 30.

3.1.4 Couplant and cable

When a sensor is simply placed in the fixture object, only a very weak signal is passed through the sensor. However, if a small thin layer of couplant is placed between object and

sensor face, a much larger signal is obtained so couplant is crucial to the accuracy of the measurement procedure and has a high fidelity when signals transmit. A couplant is a material which assistances the transmission of an acoustic wave between the measured surface and sensor. Material such as grease based couplant have much higher viscosity than liquid or gels. Therefore the couplant layer is necessary to get rid of bubbles and make couplant layer as thin as possible to guarantee good acoustic transmission and more suitable for rougher surface application. A couplant material is primarily used to remove any air film at the interface of sensor and surface part due to the microstructure of two contacting surfaces. Air gap at this interface will cause loss of energy transmission because the acoustic impedance of air is much lower than that of measured surface and sensor surface. Consequently, placement of a thin layer of couplant material with higher acoustic impedance will replace the air between two surfaces and increase the transmission of energy and can provide an excellent sound transmission which is comparable with greased based couplant but with a relatively strong bond [143]. The connecting cables should be chosen to eliminate electro-magnetic noises interference.

3.1.5 Sensor holding fixture

Mounting the Sensor is necessary to hold the sensor in a fixed position. Typically, when the sensor is coupled to the measured surface, it is secured with tape hold-down. Mounting fixtures also provide constant pressure for optimizing the transmission of energy from the measured part to the sensor when high viscosity couplant is used. However, precautionary measures should be taken so that no electrical contact between the sensor case and specimens occurs in the presence of these mechanical mounting fixtures. In this research, ultrasonic couplant has been used to couple the contact surface of sensors to the fixture

surfaces. It is strongly recommend to read acoustic emission codes and standards i.e. American society for testing and materials (ASTM) [144] these standards helps a lot to avoid mastics during experimental work.

3.1.6 Background Noise

Background noise is unwanted signals picked-up from sources that are not relevant to the source being monitored and can have electrical and/or mechanical origins. Precautions against such interfering noise should always be taken, even though enormous progress has been made since the early use of AE technology. In rotating wire probe tip based on AE sensing events will almost certainly be generated from more than just the source of interest and will be a complex combination of tip rubbing, spindle sound and flow generated AE. These AE signals must be identified or eliminated in order to discriminate them from the signals of interest generated by the engine.

A basic starting point for eliminating these unwanted signals is the selection of an appropriate frequency range for the measurement process. Background noise coming from longer distances usually consists only of frequency components below 20 kHz, and so has only a small influence on the measurements higher than 20 kHz. It has been found that 100 Hz to 50 kHz is a suitable range for the study. Electrical noise problems can be eliminated by using differential sensors or sensors with built-in preamplifiers and selecting correct thresholds. Further studies are needed to narrow the range and improve the accuracy of AE sensing.

3.1.7 Data analysis

Recorded text data files are saved and to accomplish this task a MATLAB code was created to import these files and create three dimensional plots and to find empirical data such as the peak and rise time. It is also used to create plot images.

3.1.8 Micro machine's stage calibration

The main requirements for machine calibration are accuracy, identity, completeness, error evaluation, and simplicity. The micro machine manufacturer (ALIO) has data for all calibration requirements done by Renishaw calibration interferometer system and the correction tables were stored in the machine controller.

3.1.9 Experimental techniques

The right mounting of sensor to the fixture plate is one of the most important parts of AE sensing system. An essential requirement for sensor mounting is a sufficient acoustic coupling between the sensor face and the placing surface inside the fixture plate. The sensor and housing surface in the mounting fixture must be clean and clear and smooth for maximum couplant adhesion. Only a thin layer of appropriate couplant should be applied so it can fill gaps caused by surface roughness and eliminates air gaps to ensure good acoustic transmission.

The following describes the methods used to mount sensor and measured part during all AE sensing operation.

1) The top of fixture plate is cleaned to remove all irregularities to ensure maximum area contact between measured surface and the top of fixture plate;

2) Melt a sufficient layer from thermal glue (65 C˚) on the top of fixture plate, and mount the measured part on it. Once the temperature has dropped after mounting the part;
3) The sensor mounting location is cleaned to remove all irregularities to ensure maximum area contact between sensor face and fixture bottom surface. This is for optimizing the AE transfer coupling;
4) A couplant is applied between sensor contact face and the contact spot on the bottom of the fixture plate to ensure the optimum transmission of AE signal. Ultrasonic couplant is predominantly used in this measurement methodology;
5) The sensor is placed on it is place and pushed slightly to ensure an adequate layer of couplant covers the surface of the sensor. The sensor is secured by piece of rubber and tape for the whole measurement duration, which ensures that a constant pressure is applied between the sensor and the contact location;
6) Both fixture plate and AE sensor including the mounted measured part fixed on the machine stage.
7) The sensor cable connected to amplifier and then connecting the amplifier to corresponding channel at the rear of the AE data acquisition system using BCN cable;
8) A well mounted sensor should record a signal with amplitude refer to the AE sensor working frequency;
9) The sensing mechanism will demonstrating in the following section.

3.2 The rotating micro wire probe tip base on AE sensing background knowledge

The AE-based touch-sensing system was first developed and applied in micro-milling operations by Keith et al [145]. Recently, a new probing system that consists of a wire probe and AE sensor for touch detection has been reported [87, 146-150]. It was demonstrated that use of a rotating wire and AE sensor can be quite promising as a cost-effective and accurate probing system [144]. The wire probe is relatively easy to fabricate, and the AE-based detection method is very cost-effective and highly sensitive. Besides, the spinning probe overcomes the "snap-in" and adhesion of the probes to the workpiece surface during the touching operation, which is a major problem for typical micro-scale probes. However, only the feasibility of the new probing system was reported, and in-depth evaluation of the system as well as automated scanning capability has not been demonstrated.

3.2.1 The concept and design of the tilted rotating wire probe tip based on acoustic emission sensing system

A new AE-based probing system with a wire-based probe was developed to address this issue with reduced cost and size, and ease of application. The basic design structure of a wire probe tip stylus of this system and its assembly based on AE sensing is shown in Figure 39. A stainless steel high strength wire is bonded to the end of the stylus. The wire is then bent at an angle, β, 45º such that, as the stylus spins, the rotational diameter of the wire tip becomes the probe effective diameter (D_e). The effective diameter can be written as:

$$D_e = 2\,R_e = 2\,L\,Sin\,\beta \tag{3.1}$$

The effective diameter determines the smallest feature size that can be measured with the probe. As shown in Eq. (3.1) [87, 146-149], the effective diameter depends on the length and angle of the wire. Fabrication of small diameter probe can be achieved simply by attaching a short length wire. As long as the wire extends out farther than the edge of the stylus, the wire probe can be used for contact sensing..

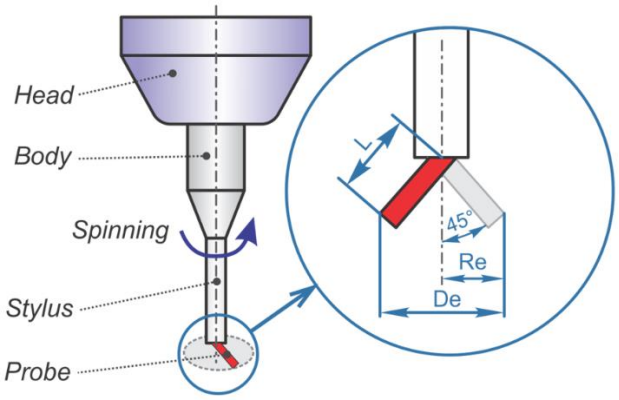

Figure 39 Diagram of the wire probe tip and geometry

For the probe tip structure, simple and low-cost interchangeable probe was fabricated. Thin stainless steel wire with diameter of 177 µm was bonded into a stainless steel tube with the inner diameter of 254 µm. The wire is then bent at the angle of 45°. Figure 40 shows an SEM image of the probe and the wire tip using SEM Hitachi s-4800. An edge can be seen at the end of the wire because the wire is cut using a cutter. Some burrs are also visible on the wire tip caused by wire cutting.

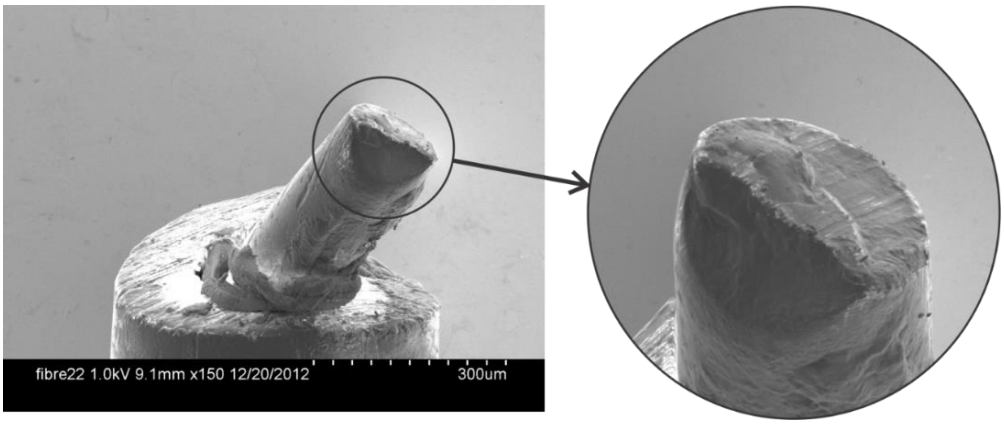

Figure 40 SEM image of a typical probe tip ready for measurements

3.2.2 Probe tip diameter and stylus fabrication

As a probe tip is fixed on the stylus, the part of the stylus needs to have a smaller diameter than the tip itself. This to guarantee that measured surface parallel to the stylus can be measured without the hazard of contact between stylus and wall of the measured component as shown in Figure 41 .

A technique of fabricating probe stylus with the angle probe tip to form a micro probe tip has been developed by the authors, where thermal glue melted up to 85 C^0 and used to mount the tip into the stylus to form a micro-angle, sphere, and straight tip, the tip is glued with a film by deposition process with rotating the tip. Such as the rotating probe tip is able to make use of thinner styli, consequently smaller probe tips can be used. The radius of the measuring part of the stylus determines the smallest probe tip that can be used on a probe. Furthermore, at the present set of circumstances, it is very challenging to produce spheres with very small diameters that are appropriate in shape and roughness to be used as tips.

Three different types of probe were designed and developed for probe system evaluation; they are denoted as: type a, a bent probe with 45 degree angled tip; type b, a ball tip probe; and type c, a straight tip probe. The bent and the straight probes were made

of thin stainless steel wire with diameter of 177 µm, whereas the ball tip probe was made with a stainless steel sphere of diameter 800 µm that exhibited good sphericity. A schematic of the probes are shown in Figure 42.

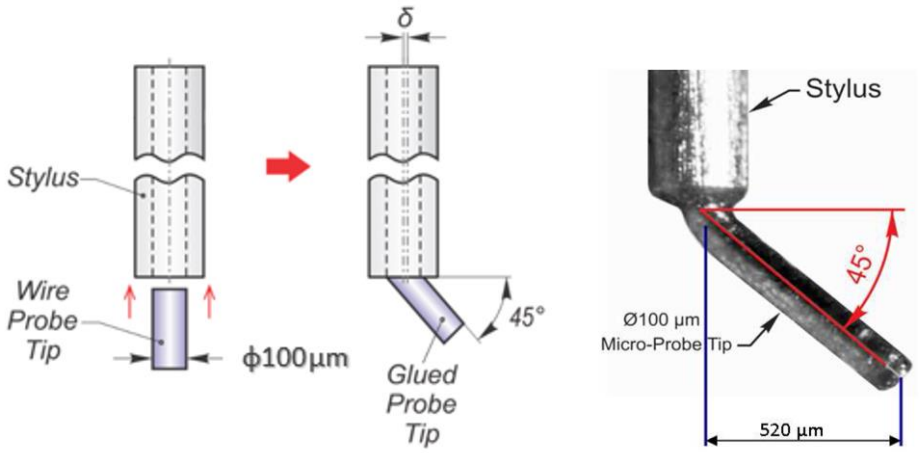

Figure 41 A fabricated 45˚ probe and its geometry

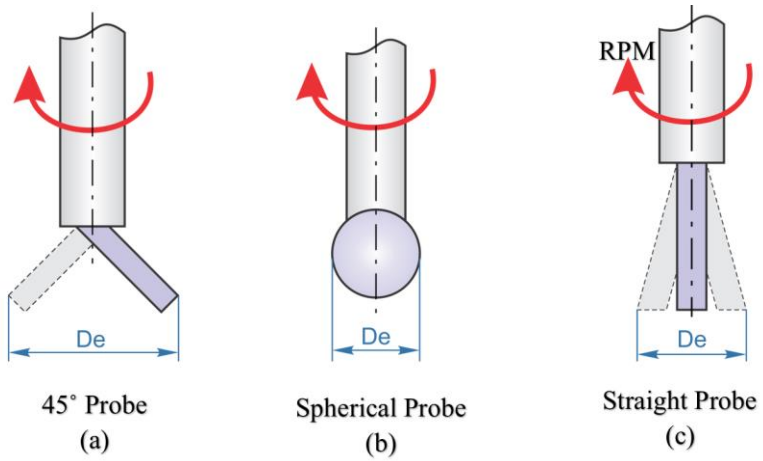

Figure 42 Schematic of three types of probe

3.2.2 The contact mechanism of the tilted rotating wire probe tip based on acoustic emission sensing system

The measurements of the micro-scale dimensions were measured using a precise, of custom-made µCNC machine (ALIO Industries) with three linear stages. Having resolution of the XYZ stages less than 100 Nanometers (table command resolution of 0.1 µm and

maximum spindle speed of 80,000 rpm- NSK E3200 spindle). The probe is rotated using a NSK E800Z spindle with the maximum rotational speed up to 80,000 rpm were used to test the wire-based probing system. A Physical Acoustics Nano 30 acoustic emission (AE) sensor placed beneath the fixture plate that holds the sheet with micro-holes. The AE sensor was used to detect contact when the rotating probe was translated using the linear stage within the measured surface.

The contact sensing method using a wire probe and an AE sensor is illustrated in Figure 43. The probe is rotated and commanded to approach the object at a given approaching feed. As soon as the tip made contact with the part surface, the AE sensor picked up a burst of generated AE signals. The AE signal is generated due to the rubbing or impact between rotating wire probe tip and the part surface. There is a slight dependency of the distance between the contact location and the AE sensor on the generated AE signal magnitude. Thus, care must be taken in setting the threshold value used to detect the contact burst, so that the magnitude of the burst is larger than the AE noise, but small enough for highly sensitive contact detection. For contact sensing, the AE signal was sampled at 100 kHz and sent to the designed control software. The input digital signals from the AE sensor were formed as an array of numbers from the data acquisition driver board. The signal processing module determined the point of contact between the probe and the component. When the magnitude of AE signals crosses the threshold point, contact is detected, and the wire probe is stopped by calling a function in command manager to generate a command for the CNC controller. Pulses generated from subsequent AE generation were neglected. The contact coordinates of the probe were recorded, and the probe immediately went back to the start position [146-149].

The probing system can detect contact regardless of the approaching direction. Thus, one sensor can be used to detect contact in all three orthogonal directions (X, Y, and Z). However, the contact mechanism is slightly different in the Z direction. In the X and Y directions, duration of wire rubbing against the object surface is much shorter than in the Z direction, in which the wire tip is in contact with the surface for the entire revolution. The proposed method of Acoustic emission based touch sensing is presented in Figure 44 will be used.

On other words we can briefly summarize the operation in steps as following:

- A probe tip wire is fixed on a spindle rotates at rounds per second.
- A component fixed on a machine stage. Dimension measurements of its surface points are our goal.
- AE sensor fixed inside, where it listens to contacts between and the probe tip and the component.
- Output of the sensor connected to a preamplifier which used amplified and filtering the signal.
- Output of the amplified signals are connected to data acquisition channel in order to convert conditioned sensor signals to digital values.
- Output of connected to measuring machine to be compared with a threshold, where that threshold is adjusted to be as zero in non-contact situation.

The main advantages and disadvantages of the use of AE in Acoustic emissions phenomena in wire probe tip sensing are:

Advantages:

– AE are non-directional, therefore usually only one sensor suffices,

– AE are very sensitive to micro physical phenomena, thus offering good possibilities for early-stage failure detection,

– The frequency of the AE transient wave is dependent on the measured material characteristics rather than on the rotational speed of the probe tip. Based on this, it has been seen that AE offers good chances for detecting all signals at different spindle speed,

– Mechanical noise has low amplitude in the range of AE, which means the signal has a high signal-to-noise ratio.

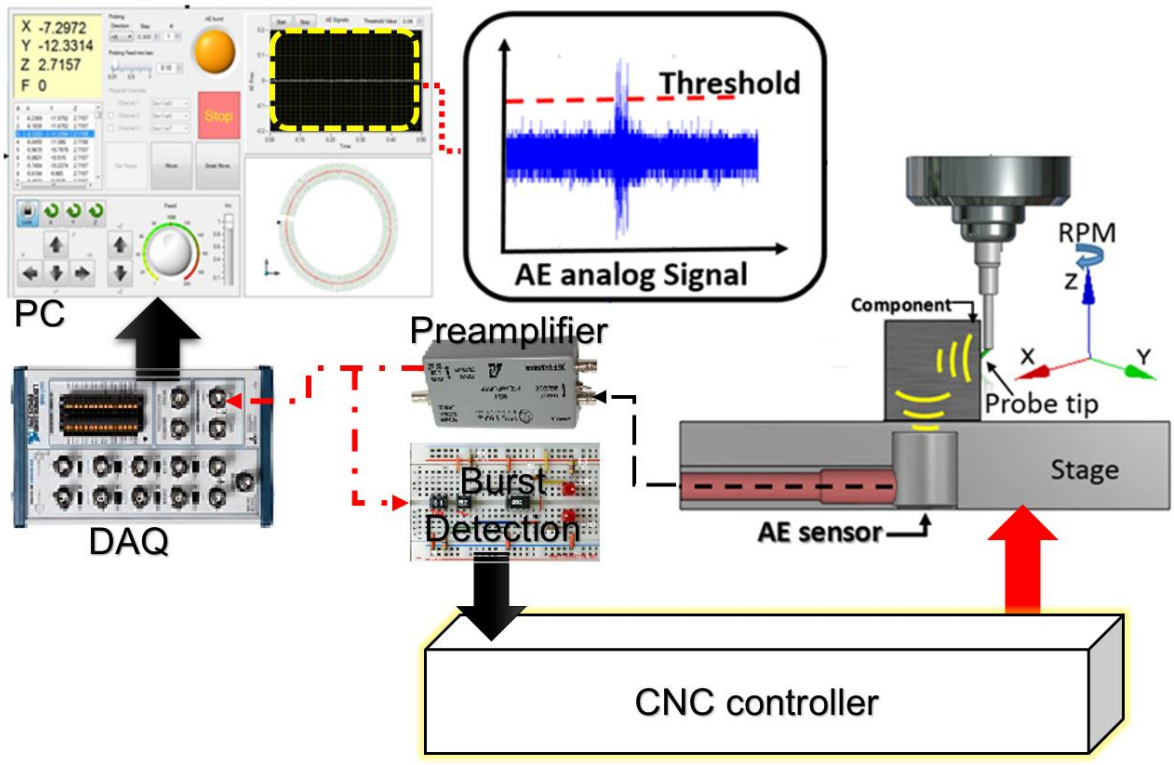

Figure 43 Micro-probe measurement touch sensing system

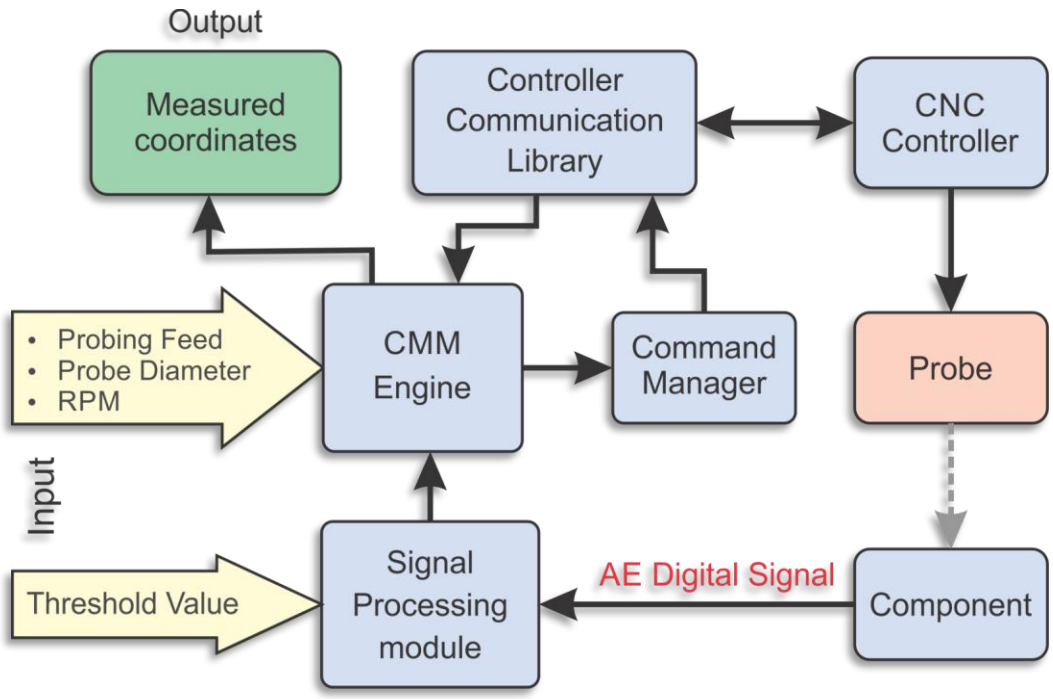

Figure 44 System fram work for AE based touch sensing

Disadvantages:

– The AE waves travel from the rubbed point in all directions reducing its amplitude as the distance from the rubbed point increases, a phenomenon termed attenuation,

– AE are sensitive to interfaces. When the waves meet changes in the propagation medium (e.g. interfaces or changes of material between fixture and measured component), only one part of the AE wave is further transmitted and other part is reflected.

These two disadvantages can in some cases be diminished by placing the sensor closer to the measured part center.

On the other hand, higher roughness of the measured surfaces produces more asperity contact and, therefore, higher levels of AE. In addition, the probe tip speeds has two contrary effects on the AE. First, as the speed increases the number of touches reduced, which results in less asperity contact so eliminate surface damage and probe wear. Second,

the increase in the probe tip rotational speed results increases in higher AE levels. Different results can be found on different surface measurements depending on the probe tip geometry. This well not affect the measurement repeatability. The influence of these parameters on the AE can be considerable and thereby should be taken into account in the analysis of AE signals from measured part.

Other possible sources of AE signals during the measurement process are:

a) Unwanted sound from spindle air pressure,

b) Elastic deformation of probe tip peak, and

c) The machine stages movements.

3.2.3 Automated profile Scanning Algorithm strategy and Control Software

A control software has been developed to control the probing system with an user interface. The interface also allows translation of the axes. For manual contact position measurement, the probe is first brought to a position near the surface of the object and then it is commanded to approach the surface at a given feed rate. Once contact is made, the probe retracts to the orginial position. The interface also displays probe's current position, and the recorded contact positions are graphically displayed on the interface along with the approach direction for the corresponding contact position. The control software allows automated scanning of an object in the X-Y plane regardless of the object's geometry in the plane based on an algorithm developed as shown in Figure 45. Two initial positions (*P0* and *P1*) need to be measured for the automated scanning. The direction of the probe, step-over distance *Rs* and offset distance from the surface *Ro* are set by the user. By connecting P0 and P1, line segment *L1* is generated. Circle *C1* is then created with center

P1 and radius *Rs*. The line segment *L2* is then extended in the direction of *L1* to obtain *P2* as shown in Figure 45. The X and Y coordinates of *P2* (X_{P2} and Y_{P2}) can be found as,

$$X_{P2} = 2X_{P1} + X_{P1}S^2 + \sqrt{-4X_{P1}{}^2S^6 + 4R_s{}^2S^4 + 4X_{P1}{}^2S^2 + 4R_s{}^2} \tag{3.2}$$

$$Y_{P2} = S(X_{P2} - X_{P1}) + Y_{P1} \tag{3.3}$$

where X_{p1} and Y_{p1} are X and Y coordinate of P1, and

$$S = Y_{P1} - Y_{P0} / X_{P1} - X_{P0}\ , \tag{3.4}$$

and similarly, X_{p0} and Y_{p0} are X and Y coordinate of P0.

The approach direction at *P2* is set to be normal to *L2* and denoted as *N2*. The length of the line *N2* is determined by the offset distance *Ro*. The probe then approaches the component surface from *P3*, which is the intersection of *C2* and *N2*. The *X* and *Y* coordinates of *P3* (X_{P3} and Y_{P3}) can be found as,

$$X_{P3} = 2X_{P2} + X_{P2}S'^2 + \sqrt{-4X_{P2}{}^2S'^6 + 4R_o{}^2S'^4 + 4X_{P2}{}^2S'^2 + 4R_o{}^2} \tag{3.5}$$

$$Y_{P3} = S'(X_{P3} - X_{P2}) + Y_{P2} \tag{3.6}$$

where S' is given by

$$S' = -1/(Y_{P1} - Y_{P0} / X_{P1} - X_{P0}) \tag{3.7}$$

Then, the probe path is set in the direction of *P3-P2*, which is approximately normal to the component surface as shown in Figure 45. The subsuequent approach paths (*N3*, *N4*, etc) and start positions (*P5*, *P7*, etc) can be determined in the similar manner.

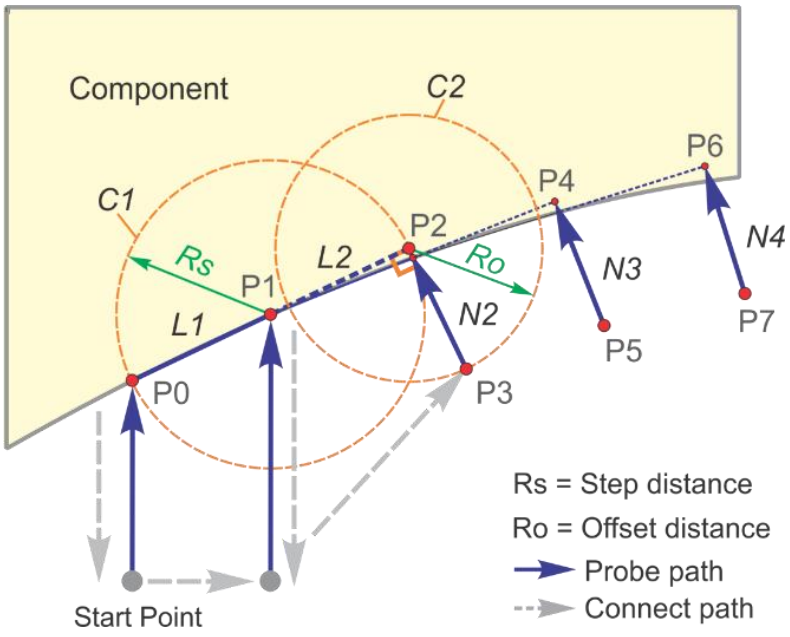

Figure 45 Probe path gereration for automated measurement

The flowchart of the algorithm for automated scanning is shown in Figure 46. In the algorithm, required input parameters include probe effective diameter, spindle speed (RPM), probing feed (f_p), step-over distance (Rs), offset distance (Ro) and initial direction (I_{dir}), which are set by the user.

The algorithm takes two initial measurements in the I_{dir} direction set by the user. In other words, when i (measured point counter) is less than two, probe path is set along idir direction. Probe approaches the surface at the feed rate of f_p until the contact between the probe and the component surface triggers. The first contact position is stored as the first item (i.e., P [0]) in the P list, which is an array of two points. The second contact point is then stored in P[1]. Once two initial points are stored in the P list, new probe path is calculated based on Eqs. 3.2-3.7, and the next contact point is obtained. Then, the P list is updated such that it stores the last two contact points in the list. This procedure continues until the measured points form a closed path. All the contact points of the surface are stored a separate array as measurements.

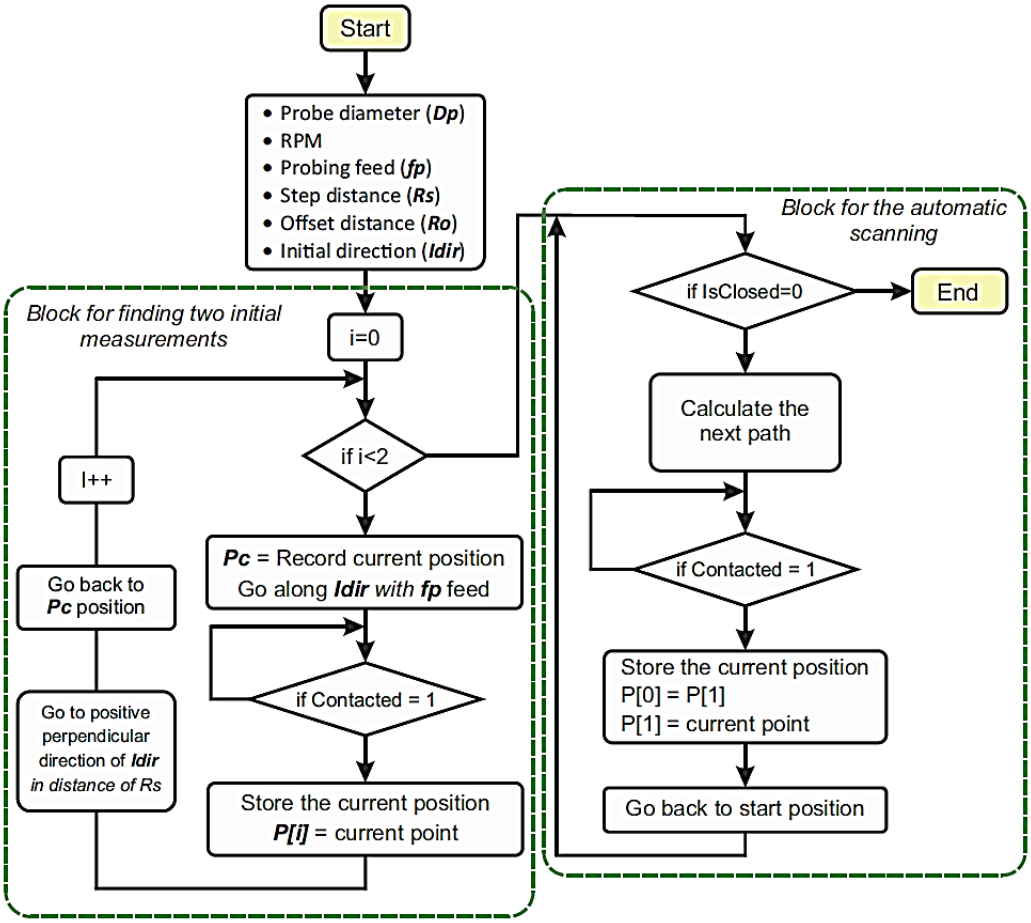

Figure 46 Automated scanning algorithm

3.3 Measuring probe tip path

In position control applications there are many ways to move from one point to another. One of the requirements in rotating wire probe tip measurement procedure is to keep the feed rate at a constant value along the entire probe tip path. To reach the desired feed rate, controllers implement different types of approaching feed profiles (Trapezoidal / S-curve profile). The velocity ramps up linearly to a final velocity F over time T_a. Then the velocity ramps down linearly from F to zero over time T_d. In order to start measurement operation from a certain point with an approaching feed rate of *f*, 3-axis stage should start accelerating from a distance of at least ½ *f* t_a and start decelerating to a distance of at least ½ *f* t_D to stop

at a touched point. This will be a challenge when dealing with start points, touching points, and rapid returning points. In these points feed rate will not be constant. This will casing a delay and increase touching time and thereby number of touches.

3.4 Conclusion:

This chapter has described the theoretical work conducted with regards to the development and evaluation of a new cost-effective probing system using wire-based probe and acoustic emission based touch sensing. A dimensional probing system using a rotating wire and AE sensor for touch detection and an automated scanning algorithm have been developed.

From the previously define micro-CMM probing requirements, and also the thesis objectives – To develop and validate a new micro-CMM that can be applied to AE sensing:

1. The designed stylus has a stylus probe tip effective diameter below than 500 µm, an aspect ratio similar to existing micro manufactured CMM probe tip, and is suitable for use with a rotating wire probe tip based on acoustic emission sensing.
2. The rotating wire probe tip based on acoustic emission sensing can operating with a probe point repeatability less than 1µm and measure micro holes depths as it can be seen in next chapters where they presents the results of the dimensional probing system measurements. These measurements will be described in more depth throughout this research, but mainly in Chapter 4 and 7.
3. Easy to fabricate calibrate rotated wire probe tip.

Following the work contained within these first four chapters, especially chapter 4, and 7, the technical measurement work of this thesis can now be processed.

Chapter 4 - Measurement system performance

4.1 Introduction

In this chapter, we present an experimental measurement assessment of the probe tip effect on a measured surface. A parametric study was conducted to identify the relationship between damage on the surface caused by the measurement tip and key machining and measurement parameters. Better understanding of these parameter will help to avoid surface damage and measurement errors. Three different versions of the wire probe tip were proposed to determine the least surface-damaging design. The probes had identical geometry but were made of different materials—thus each had a unique elastic modulus and hardness. The surface damage that each probe scratched on to the measured surface were determined to be between zero to few hundred of nanometers. Experimental measurements were conducted to evaluate the repeatability of the three probes. Experiments were also conducted to verify the performance of each probe against verified calibration artifacts including several block gauges and a cylindrical plug gauge. Proper selection of a wire probe tip depends on the specific application and is necessary to have the highest measurement precision in each application. Experimental measurements show that using more than one acoustic emission (AE) sensor has good results with micron-level accuracy and thus, may be used to improve the surface integrity.

The organization of the chapter is as follows. The new probe designs are introduced to be used in conjunction with AE sensing. Probes made from different materials have been developed and evaluated. Probe sensitivity and repeatability with respect to AE sensing methods for touch detection have also been examined. The results from each probe

are compared with one another with regards to the surface damage of the tested, measured samples. Experiments are conducted to evaluate the measurement performance of the probes against calibration artifacts. The effects of process conditions such as threshold and effective diameter are also studied and presented, followed by discussions on the results. Finally, the conclusions are presented.

In general, measuring small parts with a contact probe is difficult because the required contact can cause wear of the probe as well damage to the measured surface. To address this challenge, research has been conducted into different physical contact probe tip geometries as well as the number of AE sensors used. Prior research was conducted initially into the angle probe tip design (with only one AE sensor). Work done in this chapter verified and built upon this prior research and also examined straight probe tip and ball probe tip geometries as well as various configurations of AE sensors. A summary of these probe designs is given in Table 2.

It was determined that using multiple AE sensors reduced the number of tip contacts required to make a measurement and thus, greatly reduced the number of scratches on the surface. It was also determined that selecting the appropriate probe tip geometry depends greatly on the measurement material; however, due to the mechanical and physical properties of the measurement method, only sound conductive materials can be measured.

Table 2: Methods for probe tip measurement based AE contact detection

Probe tip shapes geometry			**Multi AE sensor**
Angle probe tip	Straight probe tip	Ball probe tip	1-3 Acoustic emission sensor

In this research, single and multi-acoustic emission sensor arrays were compared to determine the best method for quality of measurements. The challenge of using AE sensors for the probe tip contact detection is to eliminate as much resulting surface damage as possible (and to the required tolerance of surface quality and accuracy) while still generating contact signals distinguishable from background, and environmental noises.

Factors such as measurement requirements, environmental conditions, measuring methodology, measured component geometry, mounting and fixing of the component, measuring device, calibration, measurement software, measurement uncertainty, and operator contribute to the measurement performance. Every measurement process will have some level of uncertainty. No perfect measurement methodology exits. Thus, the measurement result is not complete without the accompaniment of a quantitative statement of its uncertainty. Therefore, both the measurement uncertainty of rotating wire probe tip based on AE sensing system and the experimental work detailing block gauge calibration techniques are introduced in this chapter. The effect of measuring parameters on measurement operation, effects of spindle speed and approaching speed on the effective diameter of the wire-based probe and measurement accuracy are also presented. Also, wear of the wire-based probe and damage on the measured surface are also investigated. This is done by means of standard gauge blocks. A Mitutoyo gauge block set (ASME grade 0) was used as a test piece and the contact between the wire and the gauge surface was measured using one AE sensor (Physical Acoustics Nano 30) so that they will not influence the measurement uncertainty. In addition, the probing system was also used as a metrology tool to measure micro-milled features.

4.2 **Measurement Procedures**

A micro-computer numerical μCNC ALIO machine was used (table command repeatability is less than 50 nanometers table and maximum spindle speed of 81,000 rpm). An advanced technology (AT) compatible computer is interfaced to both CNC and AE system. When the probing tip is measuring, the AT compatible computer based data acquisition system collects the AE signals, and stores it for analysis. Furthermore, a workpiece material, for example, a Mitutoyo block gauge, is directly mounted on the center of a fixture plate along with three AE sensors (NANO30). The AE sensors were installed underneath of the center of this plate and were amplified through a 2/4/6 preamplifier with 40 dB selected gain which transmitted the signals to the receiver. The first step of the experimental setup is to determine and then filter out the environmental noise from the spindle frequency spectrum. The threshold for this noise was set at either 10, 20 or 30mV (with a set approaching speed of 0.05mm/sec), depending on which threshold provided the fewest number of contact events.

The measured parts used in this study are various Mitutoyo block gauges as well as lab-machined parts made from various materials such as brass, aluminum, mild steel, acrylic. These parts were mounted on the stage with 65˚C thermal glue. The probe tip was made from PTFE coated stainless steel wire. The wire diameter was 0.25 mm diameter and the effective diameter (De) of the probe tip was 650 μm. The probe tip was rotated at 1000 - 80,000 RPM depending on the test requirements, and the approaching feed was 0.05 mm/sec.

Since the AE signal has a high frequency (in the kHz range), the raw frequency data was processed by an analog circuit and sampled at fixed control intervals by the data

acquisition system. The sample rate was set at 100K during all data acquisition. The experimental setup for measurements is shown in Figure 47.

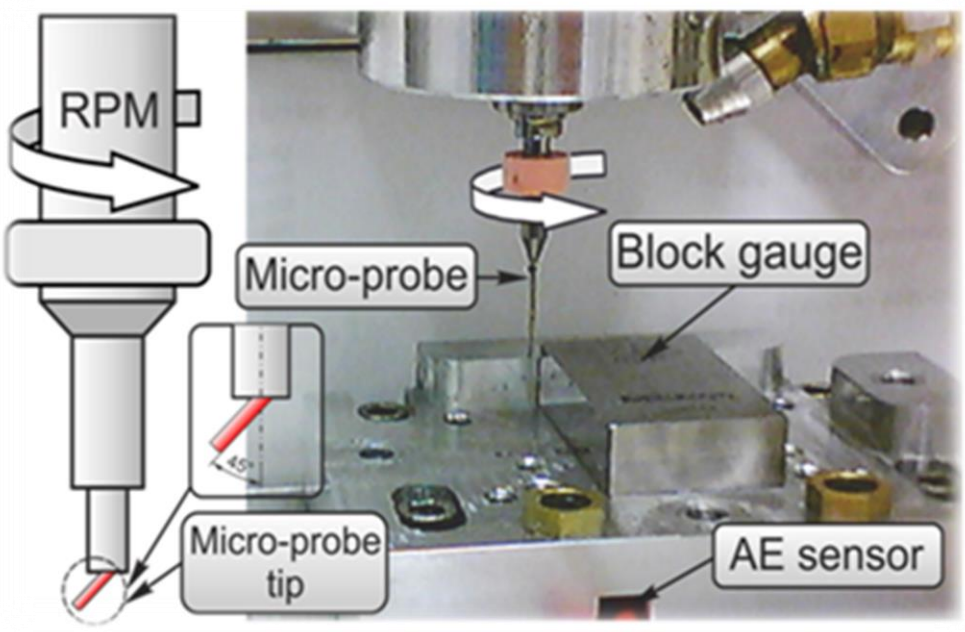

Figure 47 Experimental setup for evaluation of the probes[147]

The repeatability of the AE sensing method for touch detection has been examined. Experiments are conducted to evaluate the measurement performance of the probe artifacts. The effects of process conditions such as threshold and probe tip speed are also studied and presented, followed by discussions on the results.

4.3 Probes wear and surface damage

To examine the wear of the probe wire and the surface damage from the touching operation, each probe was commanded to approach the surface of a gauge block, and as soon as a touch is detected, the probe was moved to the contact position and remained for a period, causing the wire to go through a large number of touches. The probe first went through 10,000 touches at one location, then 20,000 at a different location. The number of touches was increased similarly at ten different locations up to 100,000 touches, resulting

in 550,000 touches in total. For all operations, the feed rate was 0.05 mm/sec and the spindle speed was 60000 RPM. After the touches at each location, the effective diameter was measured again to determine the amount of probe wear. In order to examine the probe wear and surface damage, additional experiments were conducted with a new probe of 105 μm diameter. Also, three new probes were tested for probe wire wear with a new probe of 170 μm diameter.

4.3.1 Probe wear

The effect of the number of touching operations on the probe tip wear for each probe is given in Figure 48, which shows similar wear behavior for all three probes. It can be observed that as the number of touches increase, probe tip wear initially increases rapidly and then stabilizes. After 550,000 touches against a gauge block, total probe wear is around 25 μm. However, for most components, the total number of touches required to measure the dimensions will be much less than 10,000 touches. The average wear after 10,000 touches was only around 2 μm. Thus, dimensional variation due to probe wear during the measurement of a given component's dimension will be less than a couple of microns. Before measuring a new component, the probe needs to be recalibrated against a calibration object.

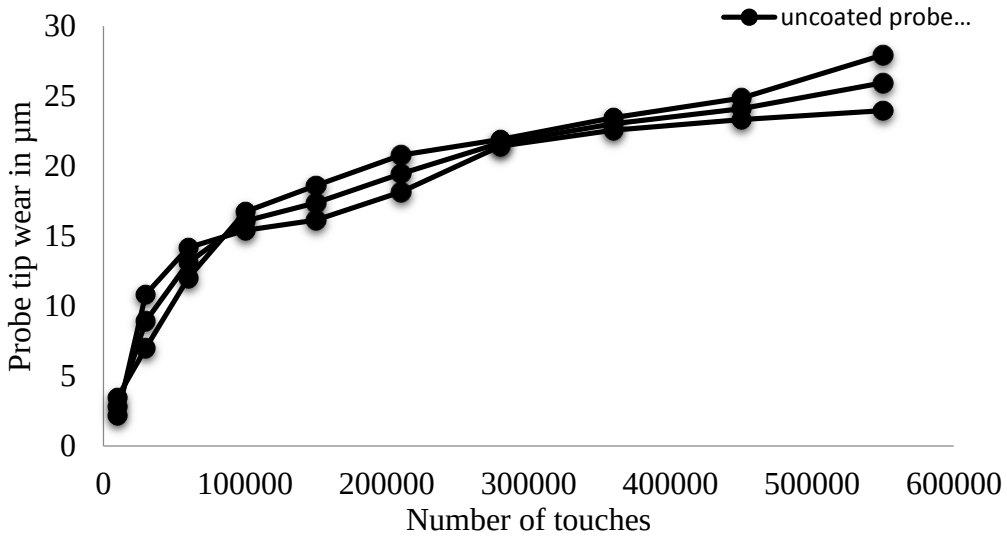

Figure 48 Probe wear represented by decrease in effective diameter

To investigate the possibility of reducing probe wear and surface damage further, probes with stainless steel wire with PTFE coating (McMaster-Carr) were tested. Figure 49 shows the PTFE coated probe wear measurement results. As can be seen, probe wear, even after 550,000 touches, is much less than 10 µm.

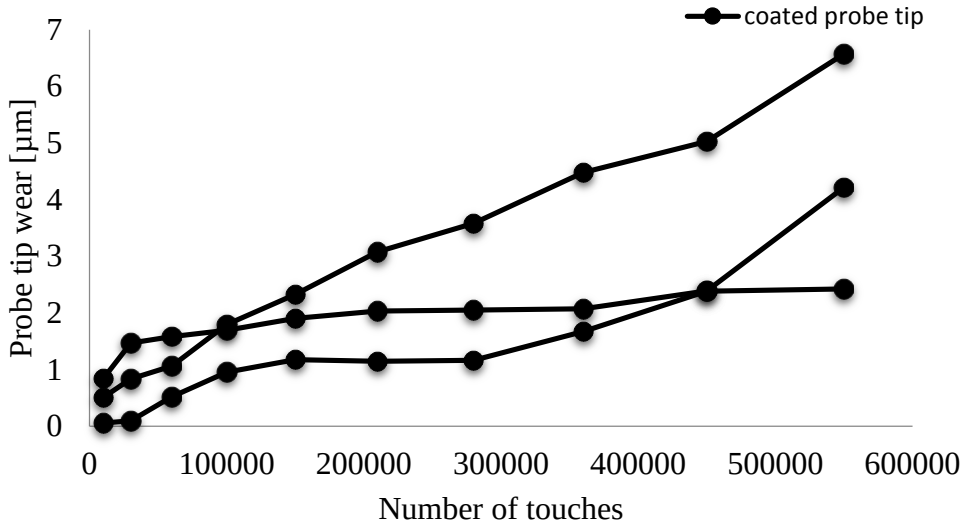

Figure 49 Probe wear with PTFE coated wire

Measurements are conducted to evaluate and compare the probe wear of the three probes (bent, straight and ball probe tip). The effect of the touching operation on component

surface and the probe tip wear was given in Figure 50, which showed that the probe tip wear for all touching operations increased gradually as time progresses. It is observed that probe tip wear increases rapidly as touching time increases, resulting in the total amount of wear of 28, 17, and 30 μm for angle, sphere, and straight probes respectively.

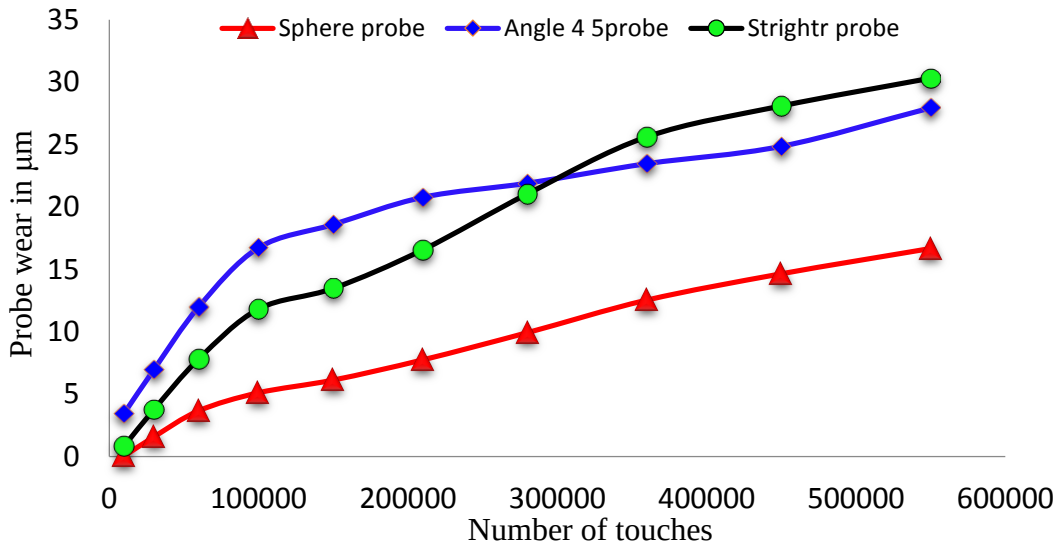

Figure 50 Total probe wear represented by decrease in effective diameter

To examine the wear of the probe wire made of three different materials each probe was commanded to approach the surface of a gauge block as mentioned earlier. For all operations, the feed rate was 0.05 mm/sec and the spindle speed was 60000 RPM. After the touches at each location, the effective diameter was measured again to determine the amount of probe wear. The effect of touching operations on the probe tip wear for each is given in Figure 51, which shows similar wear behavior for all three probes. It is observed that as the number of touches increases, probe tip wear initially increases rapidly and then stabilizes. After 550,000 touches against a gauge block, total probe wear is around 30 μm. However, for most components, a total number of touches required to measure the dimensions will be much less than 10,000 touches. The average wear after 10,000 touches

was only around 1.11 μm. Thus, dimensional variation due to probe wear during the measurement of a given component's dimension will be less than a couple of microns.

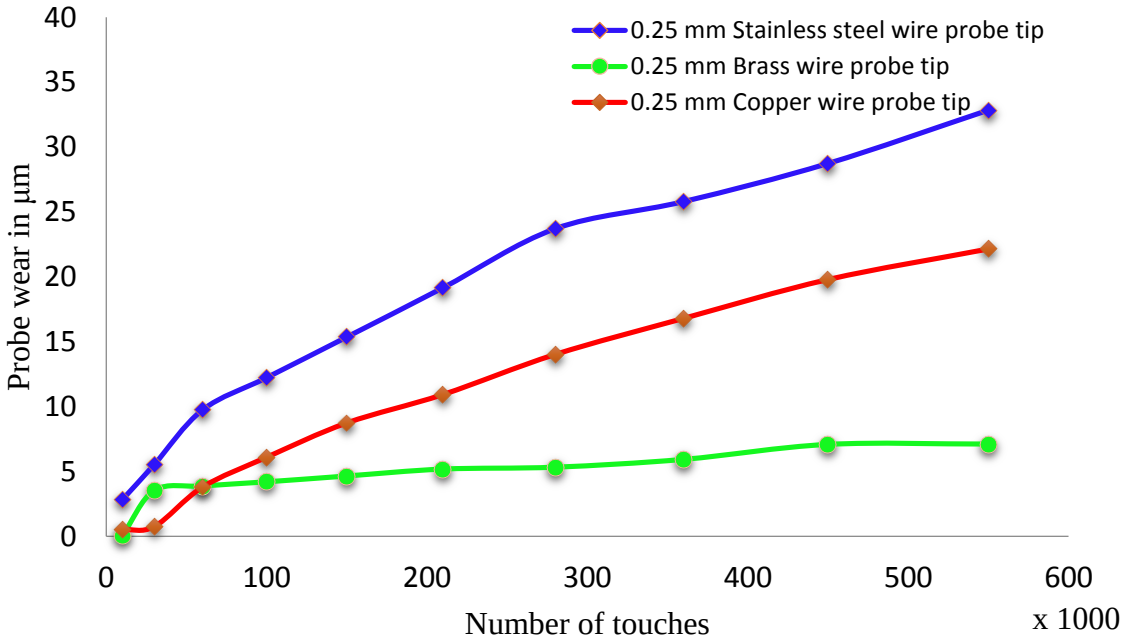

Figure 51 Probe wear represented by decrease in effective diameter

4.3.2 Surface damage for the three wires of material

In order to see the surface damage caused by the touches, the gauge block surface was observed using SEM (Hitachi s-4800) and an optical profiler (Talysurf CCI, Taylor Hobson). Figure 52 shows an SEM image of the surface damages after 550,000 touches. The optical profiler measurement revealed that the surface damage (a scratch) was 400 nm, 1.2 μm, 5.9 μm in depth, width, and length, respectively. The surface damage after 10,000 touches was difficult to be seen from the SEM image, indicating negligible surface damage even on the mirror finish surface of the block gauge. All the touches were conducted at the spindle speed of 60,000 rpm.

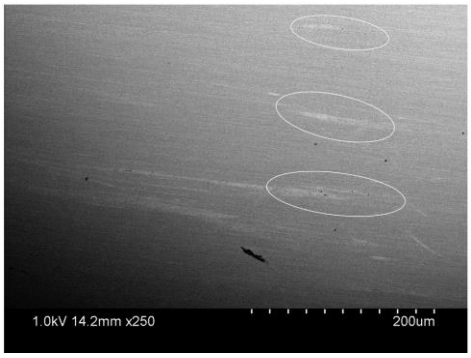

Figure 52 SEM images of surface damages for touch locations on the mirror finish surface of the block gauge

The surface damage on the 10,000 touch location could not be seen by both methods. We were able to locate the surface damage after 550,000 touches as shown in Figure 53, indicating negligible surface damage even after 550,000 touches. The optical profiler measurement revealed that the surface damage was 400 nm, 1.2 μm, 5.9 μm in depth, width, and length, respectively.

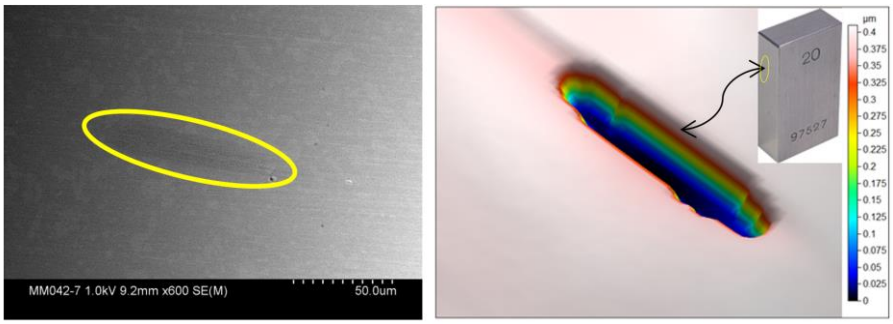

Figure 53 SEM and Talysurf CCI optical profiler images of surface damages for touch locations on the mirror finish surface of the block gauge

To see the surface damage caused by the touches, the gauge block surface was observed using an Optical scanner microscope (Zeiss). The surface damage on the 10,000th touch location could not be seen by both methods. We were able to locate the surface damage after 550,000 touches as shown in Figure 54, indicating negligible surface damage even

after 550,000 touches. The optical profiler measurement revealed that the surface damage is much less than 100 nm, in depth.

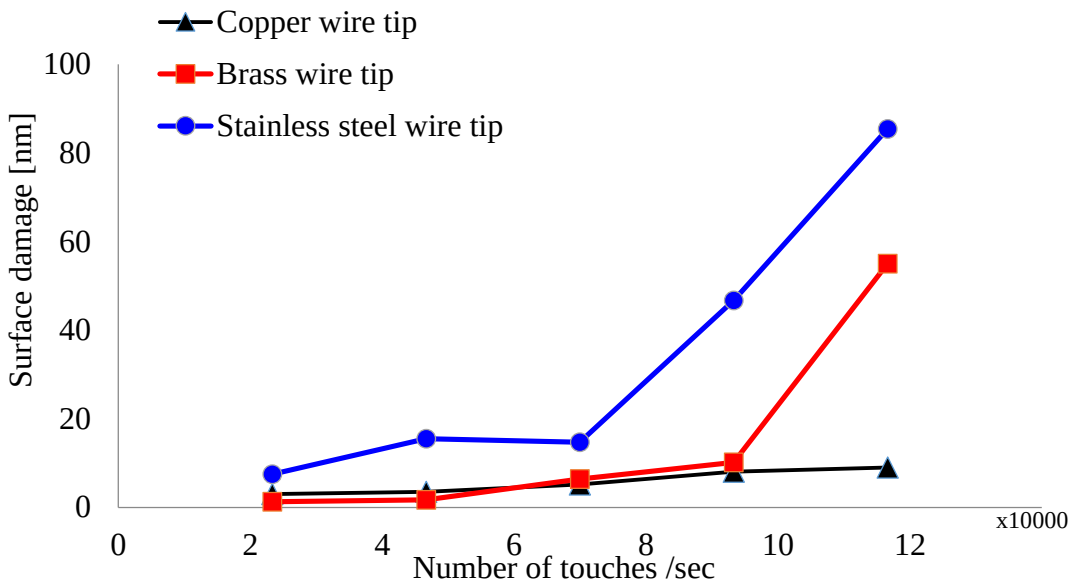

Figure 54 Surface damage Vs number of touches

Generally, during automated touch detection, the surface damage also increases due to the time delay when AE sensor is sending the signal to the controller at touching period. The real contacting time during one touch is on average of $3x10^{-3}$ seconds (at 0.05 mm/sec approaching feed and 70 x 10^3 RPM spindle speed).

In Figure 55 the contacting time was kept for 100 seconds for both AE methods and all probe tip materials. Keeping the point of contact between the probe tip and the measured surface as small as possible is necessary to exceed the AE signal threshold. The surface damage is negligible when the surface is approached from the Z axis with all solid metals (especially with hard metals) because when the probe approaches the surface from the Z axis, the probe undergoes continuous touching of the surface. When the probe approaches from the X or Y axis, the probe undergoes discontinuous touching, thus requiring many more contacting events, ultimately leading to more surface damage.

The reason for keeping the probe tips touching up to 100 seconds is to examine the probe tip life and to find the ideal wire material for multiple applications. This technique works much better with solid metals than with soft materials because of the decreased acoustic conductivity of soft materials. Also, it is evident that a single AE sensor will produce more surface damage when compared against multi AE sensor systems for both materials when using stainless steel and brass probe tips. Due to its hardness, stainless steel and brass probe tips show more damage than copper tips without exhibiting any dependency on the number of AE sensor.

Probe wire tip Dia. 0.25 [µm]	Surface damage [µm] in Z axis			
AE sensors	Single		Multi	
Materials	Steel	Aluminum	Steel	Aluminum
Contacting time in sec.	100			
Stainless steel probe tip				
Brass probe tip	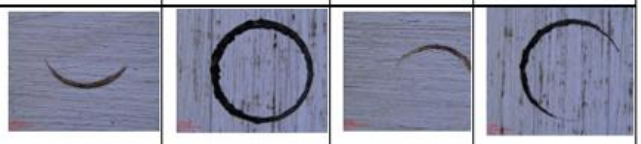			
Copper probe tip	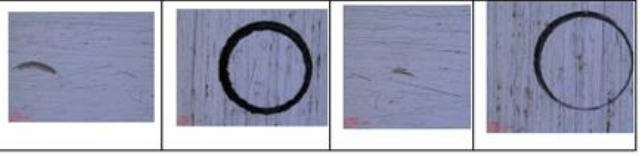			

Figure 55 Zeiss images of the surface damage in Z- axis

Copper probe tips have fewer scratches and the shallowest scratch depth, even after 100 seconds of contact time (as shown in Table 3). Hence, instead of using stainless steel or brass probe wire tip, a copper wire tip can be used for soft and hard materials. Further investigation will be conducted with soft materials and other probe tip designs.

Table 3: The effect of probe tip material on the measured surfaces

Method	Single AE	Multi AE	Single AE	Multi AE
Average depth of scratches	μm			
	Stainless Steel		Aluminum	
Stainless steel probe tip	28.76	26.83	53.74	43.69
Brass probe tip	27.1	14.23	60.5	70.3
Copper probe tip	18.81	14.84	45.39	32.85

The strength of the AE signals depends on the material where elastic energy releases and turns into elastic wave which propagates through and to the component surface. The stainless steel modulus of elasticity is much higher than the aluminum and thus, creates less elastic energy for the same number amount of probe tip impact. Therefore, to detect the contact more precisely in aluminum, instantaneous impact has to be increased while maintaining damages at minimum level by increasing the approaching feed rate.

4.3 Measurement uncertainty

Experiments were conducted to evaluate the sensing capability, repeatability, effective diameter, probe wear, and surface damage. Effective diameter variations and measurement accuracy affected by process conditions are investigated. Finally, probe wear and surface damage are examined.

The three different probes shown in Figure 42 were used to measure widths of different gauge blocks. These measurements were performed using the automated scanning method described in the last chapter. To find the gauge block's width, we have to measure the effective diameter of the probe by using a different gauge block width. Before any measurements, the probe needs to be calibrated against a reference part.

The measurement procedure (as described in Section 4.2) was done to verify the effectiveness of the probing system with respect to the probe approaching feed, probe

straightness, etc. For the AE micro probe tip repeatability tests, a reference standard block gauge was fixed on the surface of the stage as illustrated in Figure 47. The probe tip was run at 60,000 RPM. The standard deviation on the reproducibility of each tip was determined from the data sets gathered in these experiments.

The angle, sphere, and straight probes tip are used to evaluate the probing system using one AE sensor. The experiments were conducted to calculate the variation in effective diameter. The effect of measurement accuracy by process condition, the repeatability of the probing system, probe wear, and surface damage are also investigated. Measurements of calibration artifacts were then performed to verify the accuracy of the probing system.

The probing system was also used as a metrology tool to measure micro-milled features. In order to conduct the experiments effectively and efficiently, the original system has been modified by adding control software to control the probing system with a user interface. The interface also allows for the translation of the axes. The control software allows for automated scanning of the part surface in the X-Y plane, regardless of the component's geometry in the plane.

Calibration was necessary to determine the probe's effective diameter. The effective diameter of the rotating 45˚ probe tip was measured using a 20 mm width (B_w) block gauge (Mitutoyo, Grade 0) for precise measurement. Because the block gauge may not be positioned perfectly perpendicular to the approach direction for contact detection, contact positions at multiple locations on both sides of the block gauge were determined in order to compensate for the tilt angle (θ) between the block gauge width and the approach direction. From the contact positions from both sides, the tilt angle can be calculated, and

the length L can be determined. Then, the effective diameter can be calculated by subtracting the length L from the average length between the contact positions of both sides.

Figure 56 shows how one face of the block was scanned to record 5 points as a straight edge, and a point on the other face was obtained in the middle of the edge. A normal line connecting the line and the point was taken as the summation of the block's width and the effective diameter. .

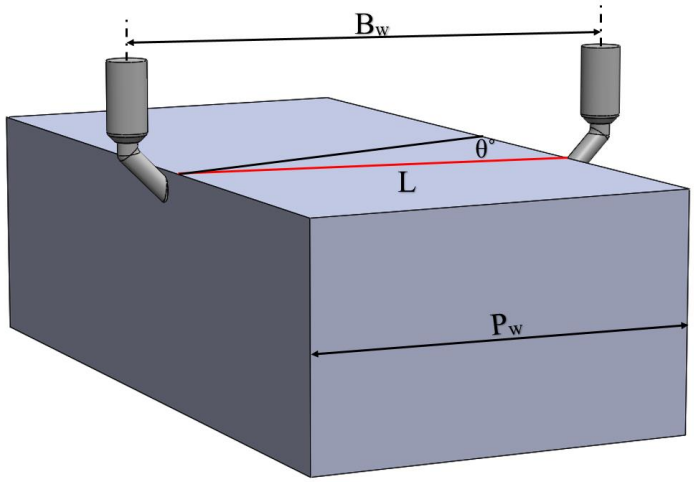

Figure 56 Gauge blocks used to find D_e for each probe

4.3.1 Repeatability measurements

The next test assessed the system performance. The repeatability of this calibration is an important parameter for a dimensional touch probe; the results of the evaluation of repeatability tests in the X and Z directions of the three different probe types are shown in Figure 57 to Figure 59. A Mitutoyo gauge block (ASME grade 0) was used for the experiment.

The probes were commanded to contact the gauge block surface, and the contact position was recorded. This contact detection was repeated 100 times over the same position. The contact position variations in the X and Z axis are shown in Table 4.

Table 4: Repeatability of the 100 recorded measurements at a given location on the gauge block.

Axis	45^0 probe tip	Sphere probe	Straight probe
X (µm)	0.56464	0.84745	2.12638
Z (µm)	0.81942	0.20082	0.69036

For the angle probe, the repeatability in the X-axis is slightly better than that of the Z-axis. This may be due to longer touch times between the probe tip and the surface in the Z direction. On the other hand, with the other two probes, the opposite was observed where the Z-axis touches had better repeatability rather those in the X direction. Further study is required to understand the factors affecting the repeatability and ultimately to reduce the effects of these factors.

.

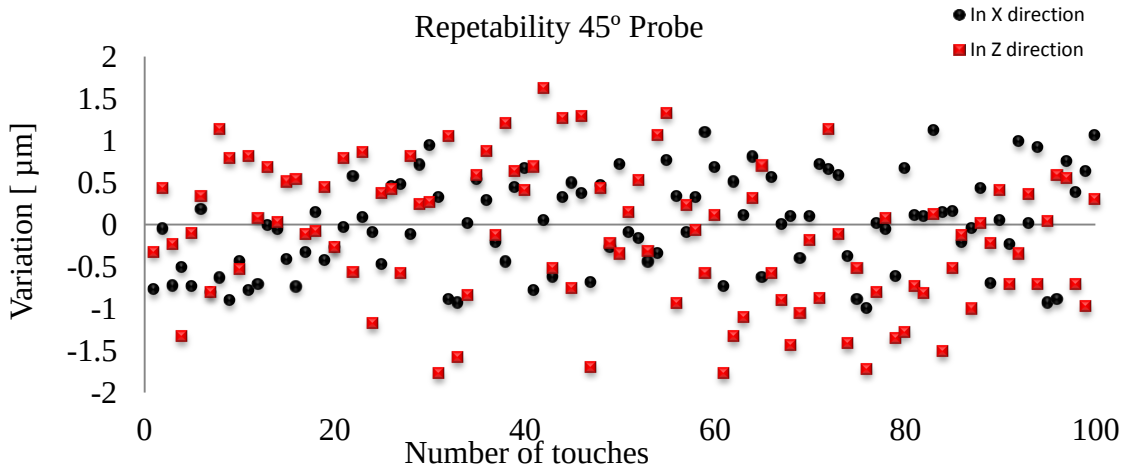

Figure 57 the repeatability results for angled wire probe

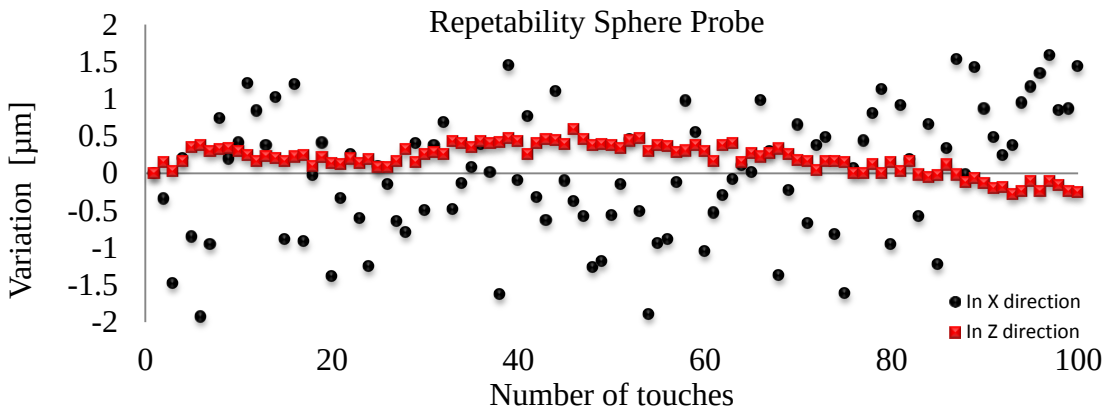

Figure 58 the repeatability results for a gauge block along the X and Z for sphere probe

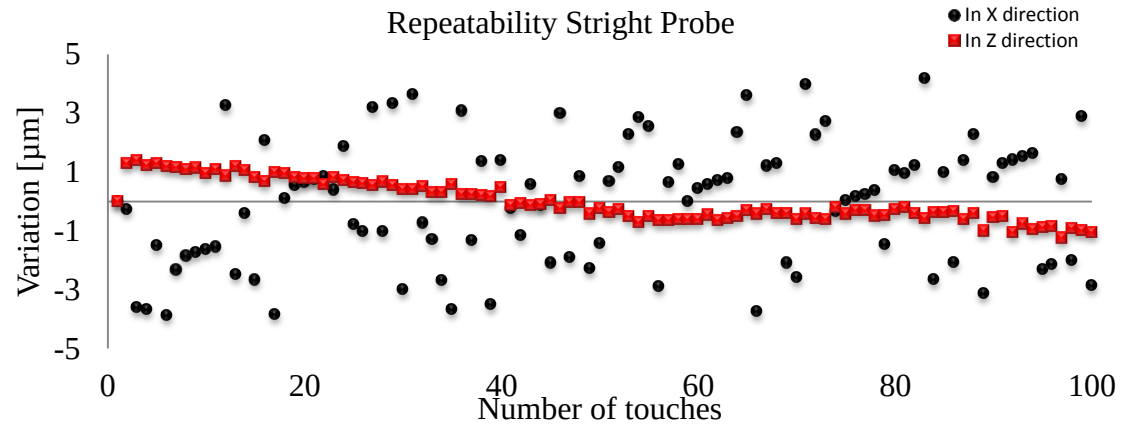

Figure 59 the repeatability results for a gauge block along the X and Z for straight probe

Also, the repeatability of angle probe tip was examined, and the results of the repeatability evaluation experiments in the X and Z directions are shown in Figure 60 and Figure 61 respectively. A Mitutoyo gauge block (ASME grade 0) was used for the experiment. The probe was commanded to contact the gauge block surface, and the contact position was recorded. This contact detection was repeated 90 times over the same position. The contact position variations in the X axis shown in Figure 60 shows that it has a variation of $\sigma = 0.861$ µm. It seems that in the beginning, contact was detected slightly away from the surface. This may be due to a burr on the probe wire caused when it was cut or debris left on the component surface or probe. Figure 61 shows that the repeatability in

the Z axis is σ = 0.593 µm, and it seems to be slightly better than the X axis and this might be due to the wire contact with the surface is longer in the Z axis, which may generate more prominent AE signal, leading to better repeatability.

Similarly, we run the same measurement condition using CMM machine (Mitutoyo 710). Figure 62 shows that it has a variation of σ = 0.536 µm.

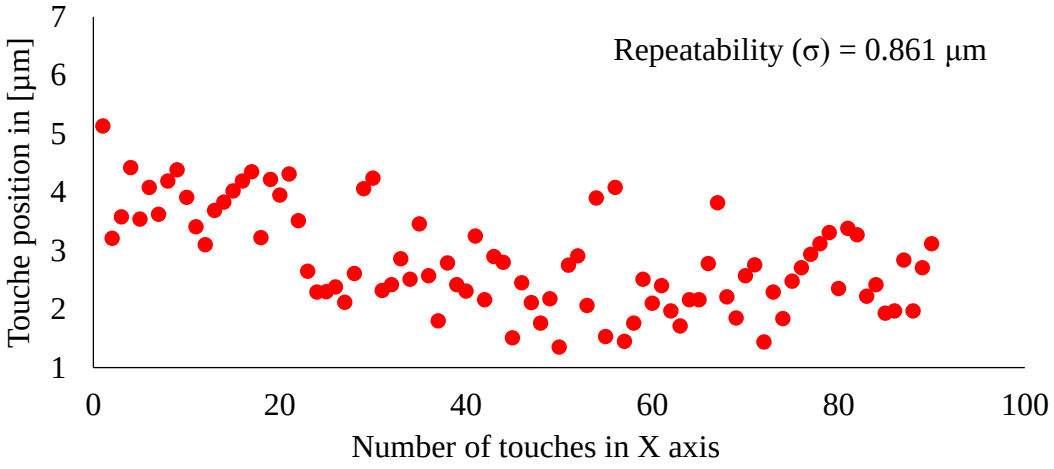

Figure 60 Repeatability results against a gauge block in X-axis

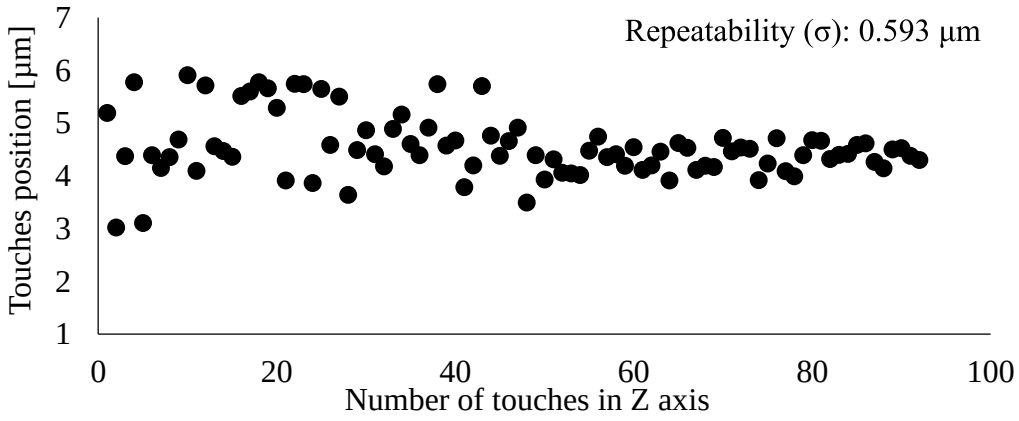

Figure 61 Repeatability results against a gauge block in Z axis

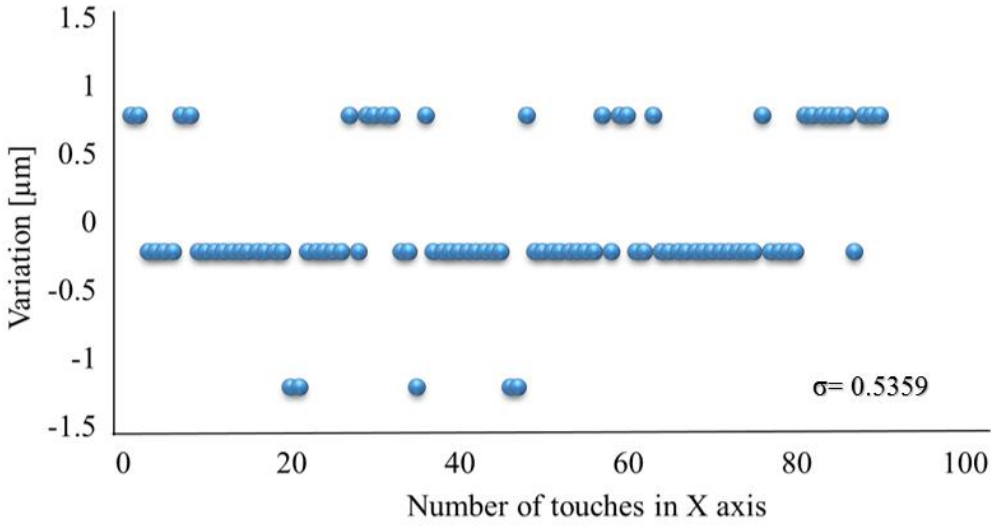

Figure 62 Repeatability results against a gauge block in X-axis using Mitutoyo CMM

Figure 63 through Figure 66 show results of repeated individual measurements for the same position using three different wire probe tip materials (stainless steel, brass, and copper). A Mitutoyo gauge block (ASME grade 0) was used for the experiment and a single AE sensor was installed in the center of the plate for the first part of the experiment. Three AE sensors were installed in the center of the plate in a triangular arrangement for the second part of the experiment. The probe was commanded to contact the gauge block surface at 0.05 mm/sec approaching feed and 70 x 10^3 RPM rotating speed, and the contact position was recorded. In these figures, the repeatability range in the X-axis for the three different probes has a variation of σ as shown in Table 5, as it can be seen from the table that using multi-acoustic emission sensors much better than single AE sensor.

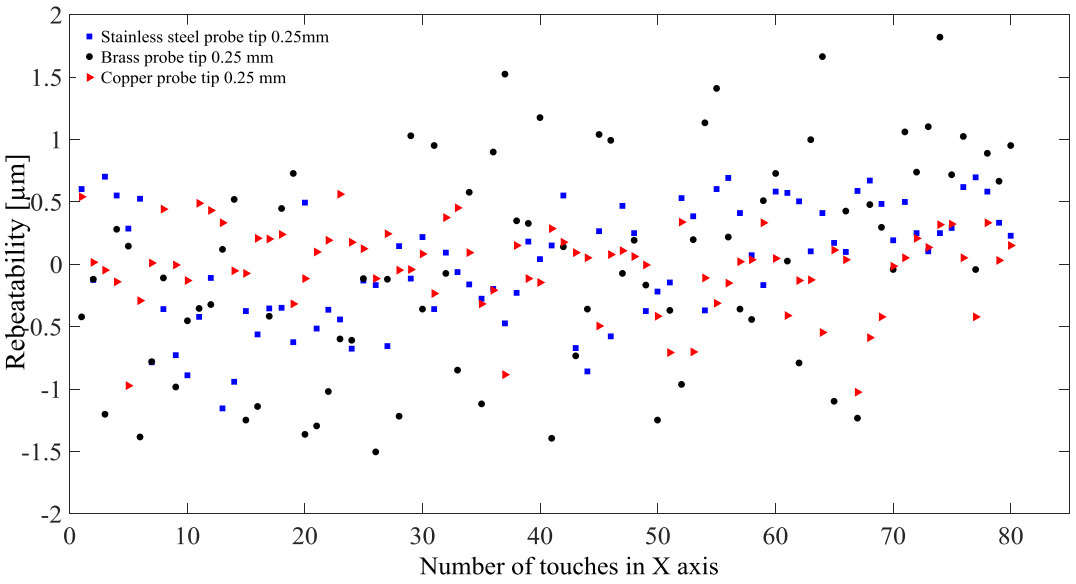

Figure 63 Repeatability results against a gauge block in X-axis – Single AE sensor

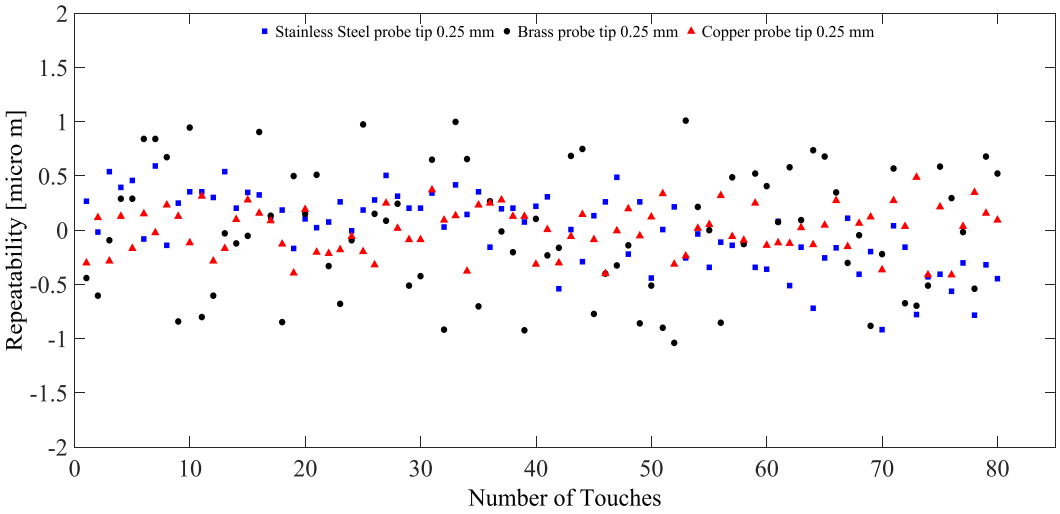

Figure 64 Repeatability results against a gauge block in X-axis – multi AE sensors

The repeatability in the Z axis is shown in Figure 65 and Figure 66 and the variation of σ from these plots is summarized in Table 6. The tests appear to have more repeatability when conducted with multi AE sensors; this may because there is less time delay from the first arrival and first threshold crossing of the AE triggering system. Furthermore, in the Z axis direction, the probe is in continuous contact with the surface when compared with the

X-axis direction. In the X-axis direction, a hitting wave is formed from probe contact, whereas in Z-axis direction, the rotational friction will realize much more energy due to prolonged probe contact. In terms of material effects, the brass and the copper probe wire tips have the almost same performance as the stainless steel probe tip.

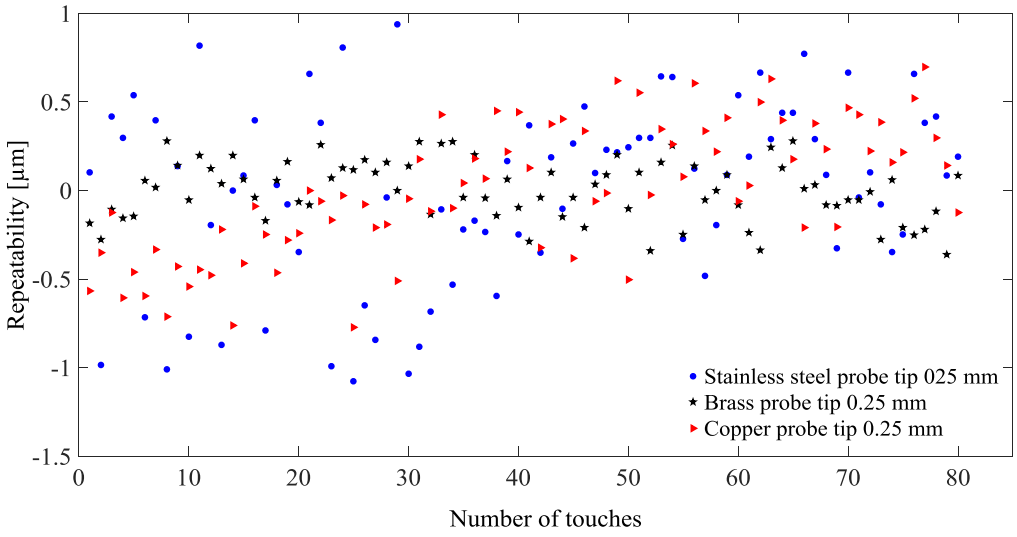

Figure 65 Repeatability results against a gauge block in Z axis- Single AE sensor

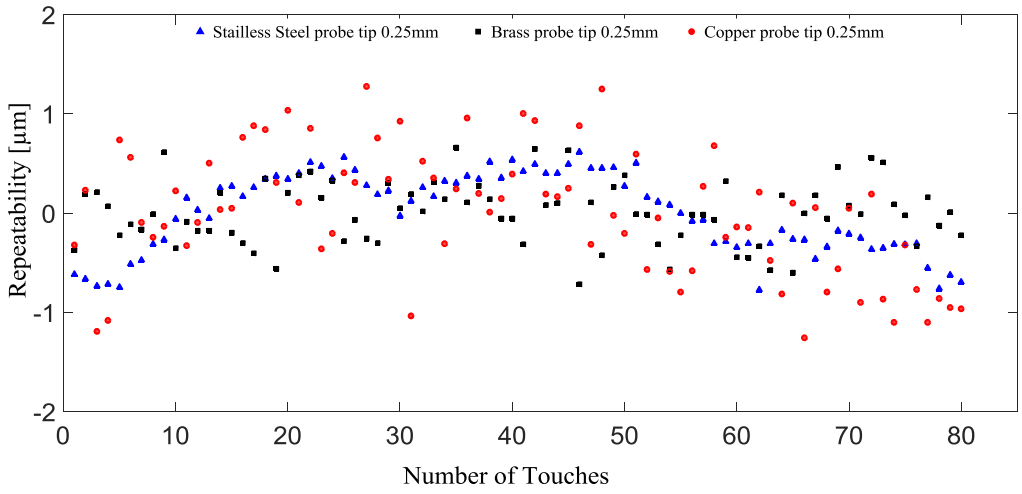

Figure 66 Repeatability results against a gauge block in Z axis – multi AE sensors

Table 5 Repeatability results against a gauge block in X- axis

AE sensors	Repeatability (μm)		
	Stainless steel tip	Brass tip	Copper tip
Single	0.475	0.851	0.335
Three	0.341	0.577	0.220

Table 6: Repeatability results against a gauge block in Z- axis

AE sensors	Repeatability (μm)		
	Stainless steel tip	Brass tip	Copper tip
Single	0.509	0.785	0.8158
Three	0.403	0.316	0.640

Contact position variations in the X axis were recorded for measurements made on two samples, a piece of composite material and a piece of glass. The variations were $\sigma = 0.641$, 0.251 μm, respectively, as shown in Figure 67 and Figure 68.

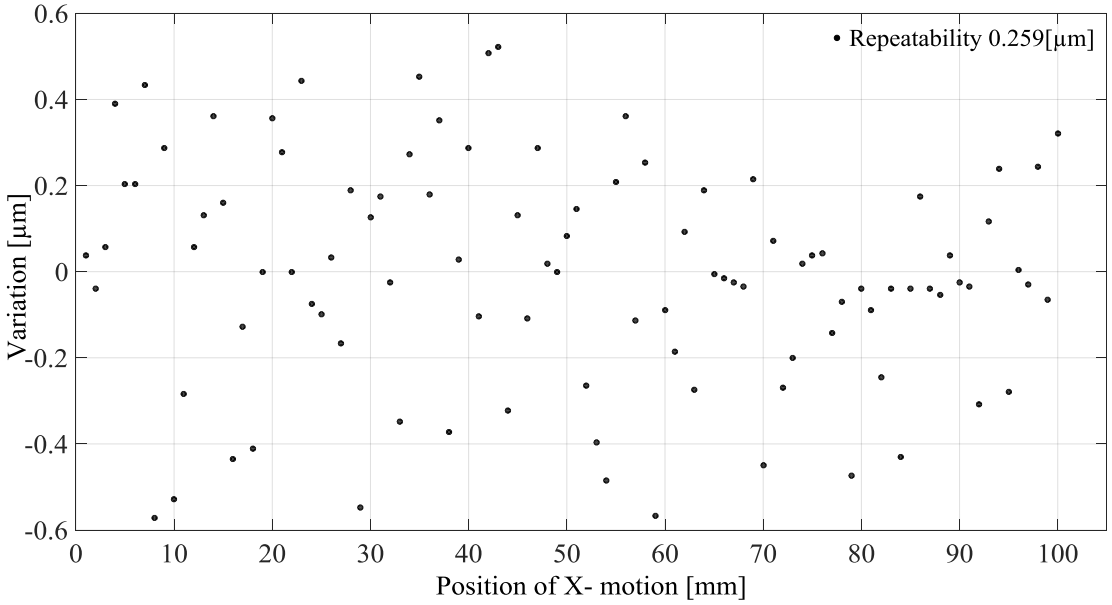

Figure 67 Repeatability results against glass material in X- multi AE sensors

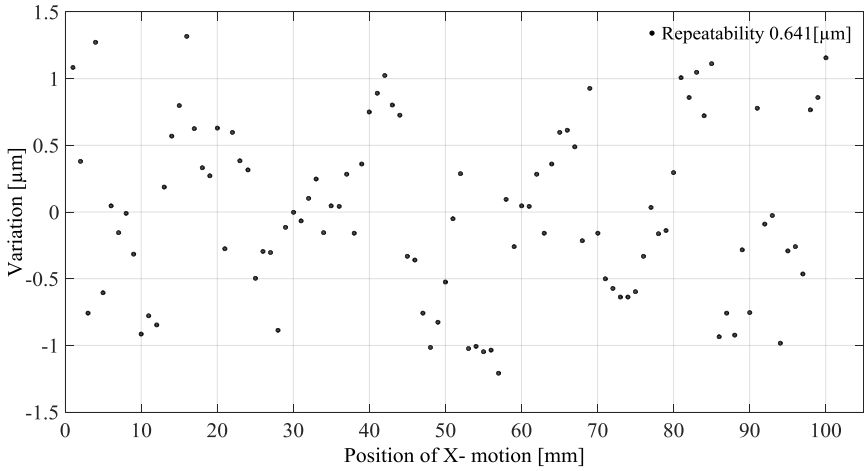

Figure 68 Repeatability results against a composite material in X-multi AE sensors

4.3.2 Effect of threshold on repeatability and effective diameter

The threshold is an important parameter that improves the detection procedure during probing. The process performance of acoustic emission based on rotating touch wire probe system is measured with a repeatability test. A repeatability test is conducted by repeatedly measuring the same measured surface. A Mitutoyo gauge block (ASME grade 0) was used for this test. The probe was commanded to contact the gauge block surface, and the contact position was recorded. This contact detection was repeated one hundred times over the same location for the five different thresholds (10, 15,20,25,30 millivolts). After each measurement cycle, the probe tip returns to its starting position. For each of the measurements, the approach distance and the probe tip speed were kept constant. Table 7 shows the repeatability results of detecting the tool tip using the same method described above.

Table 7 : The threshold effect on measurements repeatability

Threshold Voltage	10	15	20	25	30
Repeatability in µm	0.197	0.178	0.165	0.21	0.256

Experiments were carried out with various thresholds at 40K RPM spindle speed and 0.05 mm/sec approaching feed. It was found that smaller threshold values have better repeatability standard deviations; however, the threshold had to be set above the noise floor. The repeatability tests were conducted with different materials: carbide, mild steel, aluminum, acrylic and brass. It was found that the repeatability results for the mentioned materials were as follows: 0.191, 0.210, 0.274, 0.323, and 0.336 µm, respectively. Figure 69 shows the repeatability at the spindle speed of 60 K RPM and 0.05 mm/sec approaching feed and 10 millivolts. In general, repeatability improves with decreasing the threshold value (up to the noise floor). Figure 70 shows that there is different energy released form the different tested materials, which might explain the repeatability variation between them.

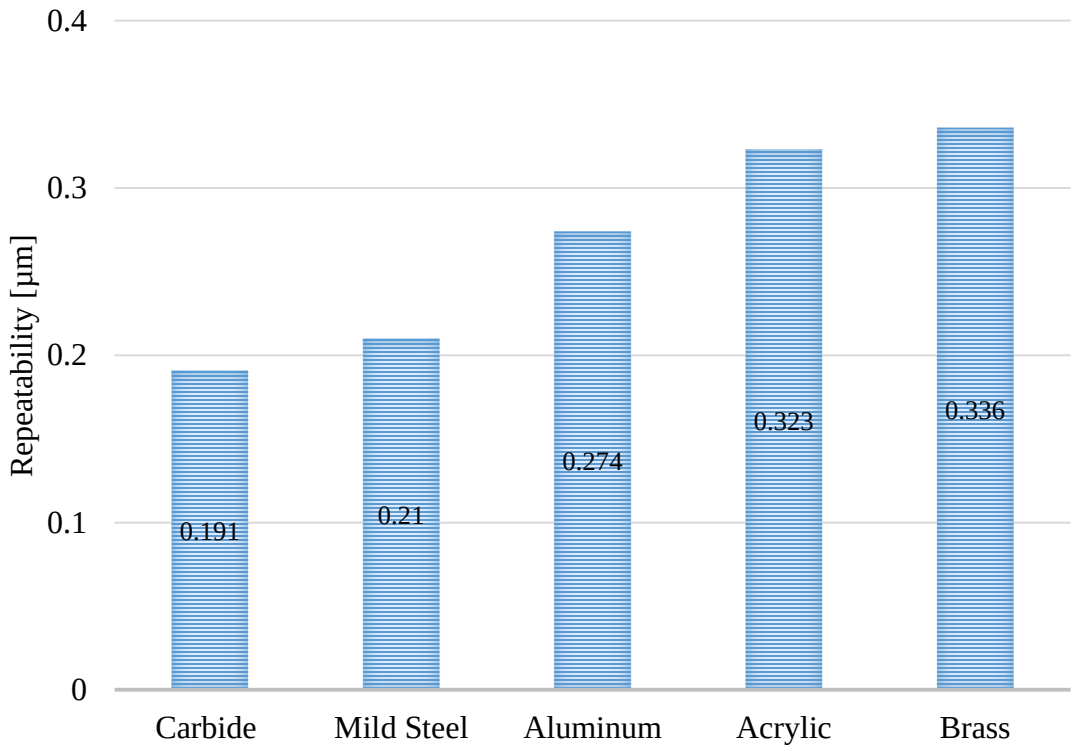

Figure 69 The repeatability of different measured materials

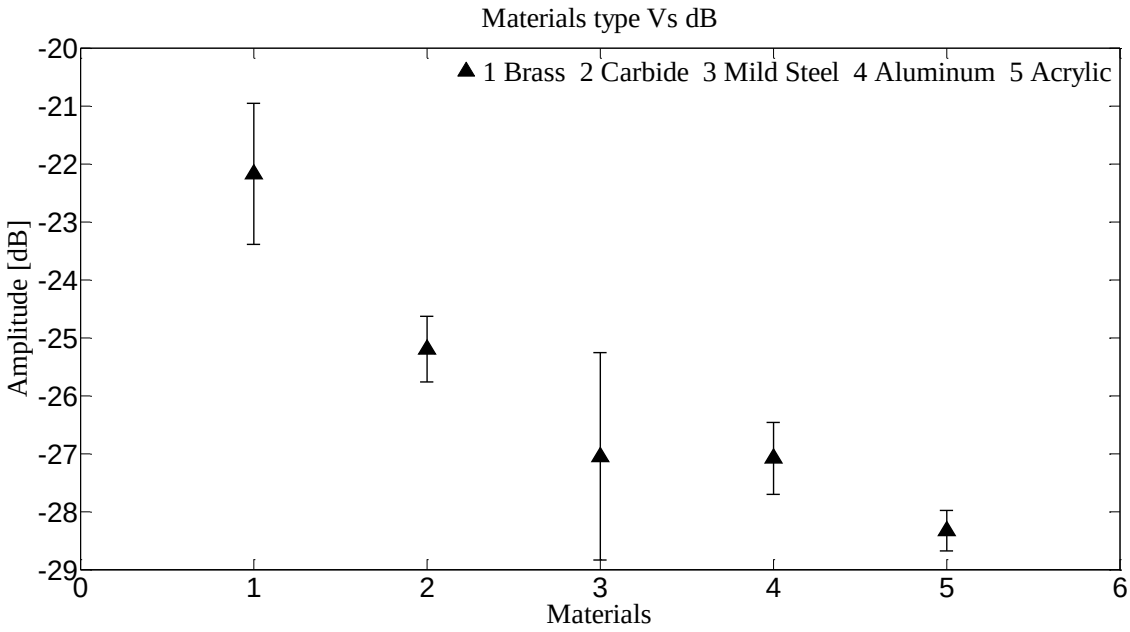

Figure 70 The decibel magnitude of different materials

In addition, Figure 71 and Figure 72 prove how does high threshold effect on the same measured point, this is because the probe tip keep moving forward till the tip releasing energy over this threshold, and this will increase the touching duration time and the overshoot or in other words delaying the touch-off detection, a series of experiments will be conducted in the following sections. On the other hand, the spindle motor has different frequencies so there will be a fluctuated noises during the different rotational speed, which may be caused by the refracted curve at this experimental conditions. Thus, if the spindle wasn't using air pressure, and has silencer which enables the spindle to rotate with stabile noises, it is expected to have better repeatability results.

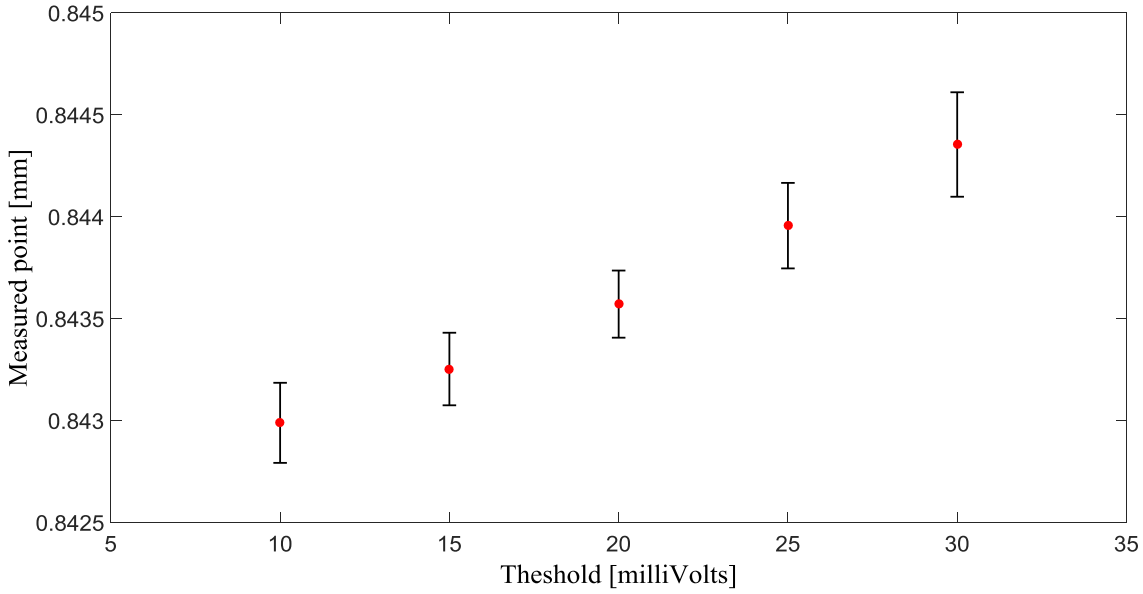

Figure 71 The repeatability of measurement at different threshold

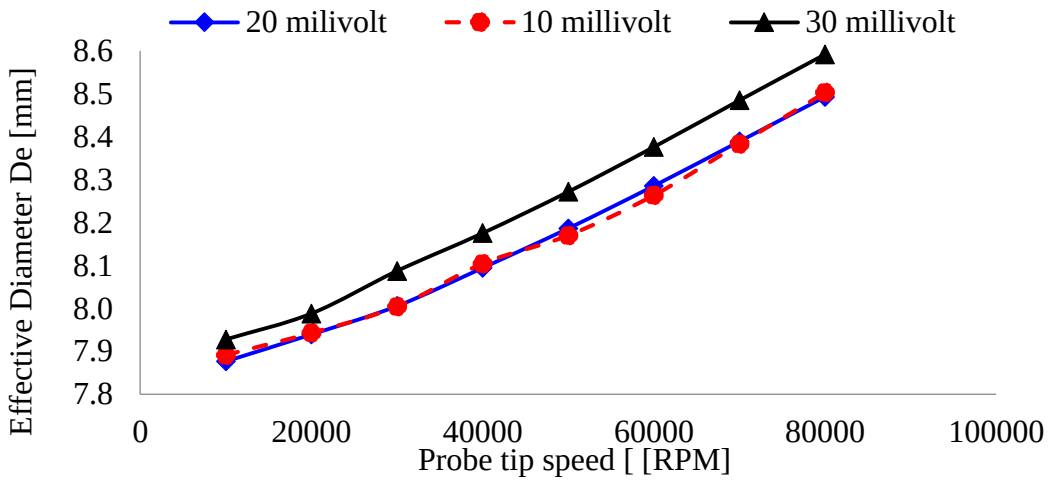

Figure 72 the effect of threshold on the effective diameter

4.3.3 Gauge block width measurements

Experiments were conducted to measure the widths of different gauge blocks. All measurements in this section were performed using the automated scanning method described in the previous section. In order to measure the width differences of the same material gauge block (tungsten carbide, Mitutoyo, ASME grade 0), the effective diameter of the probe (De) was first determined using a 20 mm gauge block. For the probe used in

this experiment, a normal line connecting the line and the point was taken as the summation of the block's width and the effective diameter as it was shown in Figure 56. D_e was measured to be 1.629 μm. Three sets of experiments were conducted. The probe was used to measure the widths of three gauge blocks of different sizes (10, 15, and 20 mm), and each gauge block was measured five times. Figure 73 shows the results of gauge block width measurements. Only the deviations from the corresponding gauge block's width are plotted. The width measurement deviation is on average 0.517 μm. This slightly increased deviation higher than the gauge block's tolerance may be due to the wire tip roughness, and stage accuracy.

Other probe tips are used in this experiments; De was measured to be 1600.3, 890.5 and 679.7 μm for angle, sphere and straight probes respectively. Nine sets of experiments were conducted each probe tip was used to measure the widths of three gauge blocks of different sizes (10, 12.7, and 20 mm), and each gauge block was measured five times. Figure 74 shows the results of the gauge block width measurements. Only the deviations from the corresponding gauge block's width have been plotted. Each touch operation was repeated five times. The repeatability, expressed into (3σ) for angle probe, sphere, and straight probes are 0.786, 1.382 and 1.326 respectively.

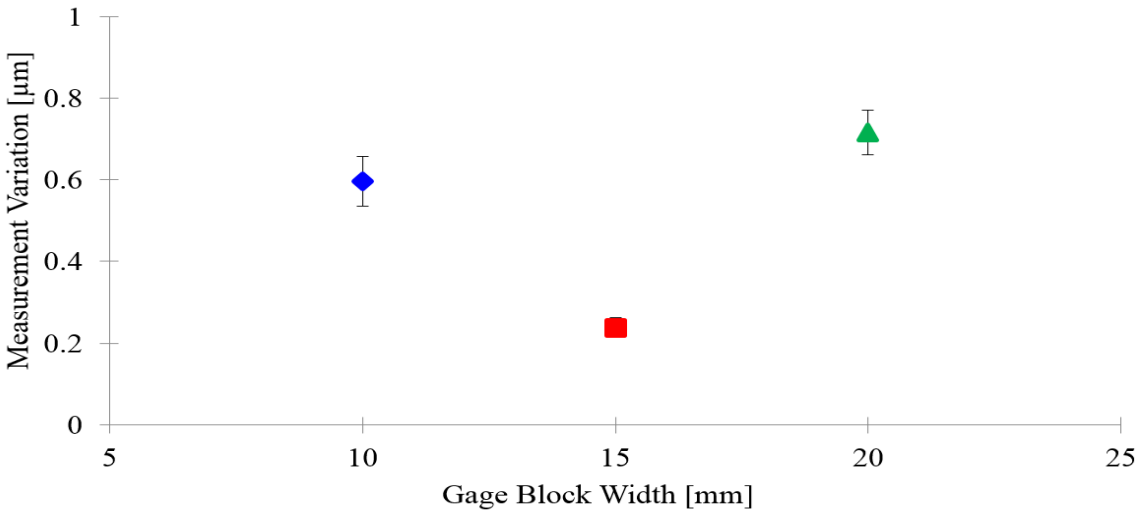

Figure 73 Gauge block width measurements result. Only width deviations are plotted

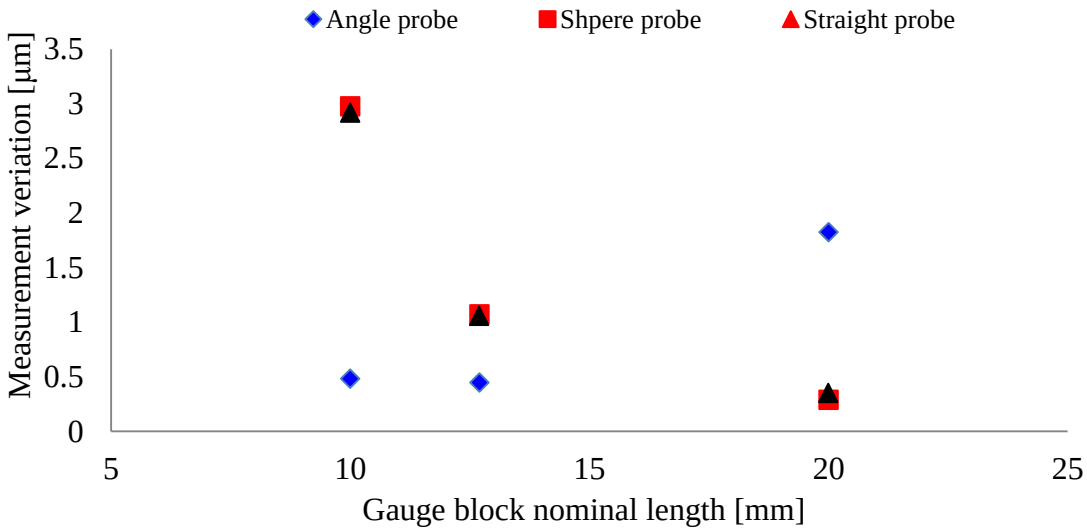

Figure 74 Gauge blocks width measurements result . Only width deviations are plotted.

Three sets of experiments (as shown in Figure 75 to Figure 77) were conducted. The probes were used to measure the widths of four gauge blocks of different sizes (5, 10, 15, and 20 mm), and each measurement result of gauge block width is the average of five measurements. Only the deviations from the corresponding gauge block's width are plotted. The width measurement deviation shows that multi AE sensors have better response compared with one AE sensor.

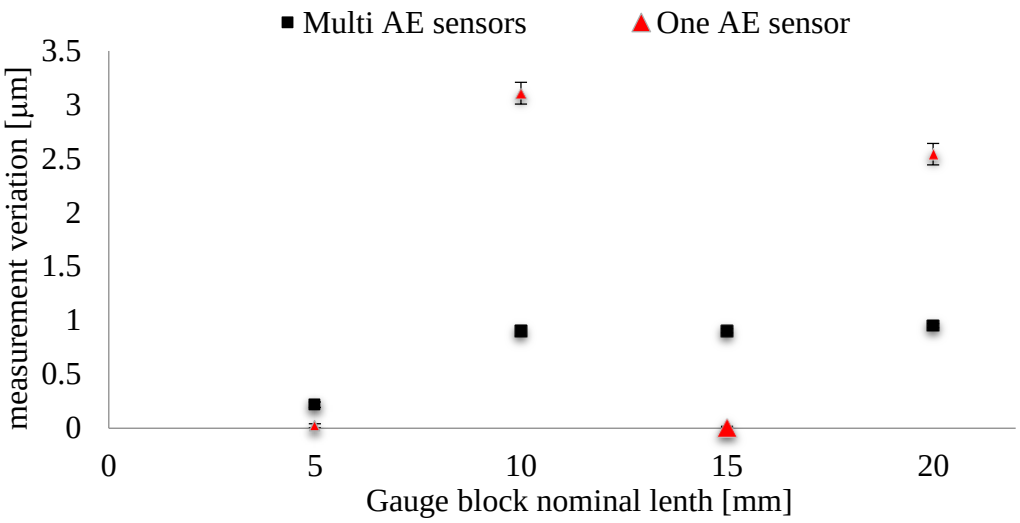

Figure 75 Mitutoyo gauge width measurements with wire Stainless steel probe.

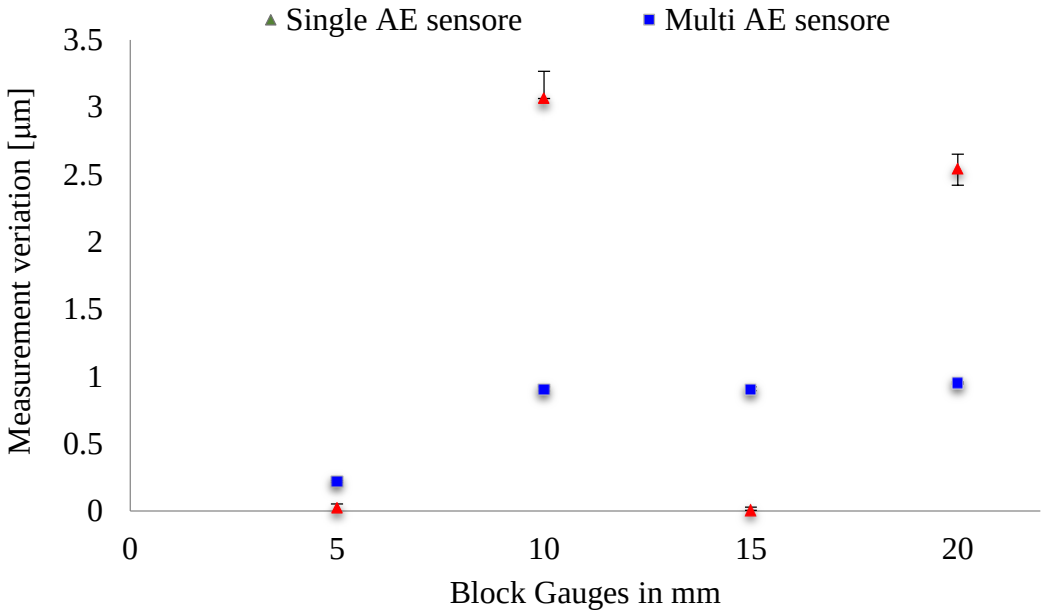

Figure 76 Mitutoyo gauge block width measurements with Brass wire probe tip

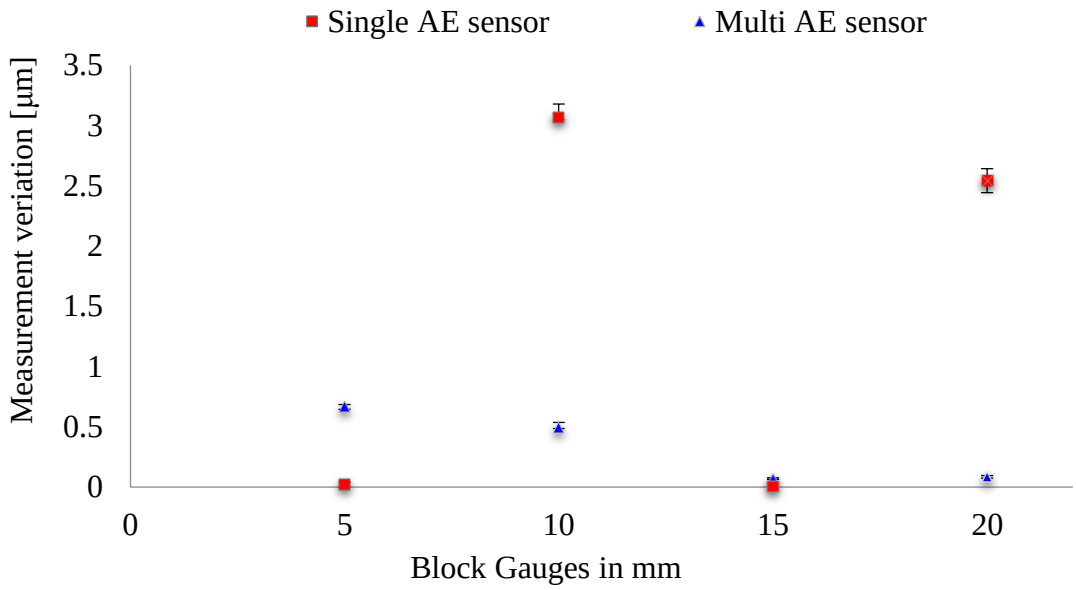

Figure 77 Mitutoyo gauge block width measurements with wire

the copper probe tip

It can be seen that brass and copper wire probe tips have the same performance of stainless steel wire probe tips. Table 8 shows that multi AE sensors have better repeatability than single AE sensor.

Table 8: Repeatability of single and multi AE sensor of effective diameter

Number of AE	Repeatability (µm) of effective diameter measurements		
	Wire probe tip of		
	Stainless Steel	Brass wire	Copper wire
Single AE	0.524	1.625	0.737
Multi AE	0.476	0.7	0.667

4.3.4 Cylindrical block measurements

Automated measurements were also performed on a cylindrical plug gauge. A cylindrical plug gauge of 12.7 mm diameter (McMaster-Carr) was scanned to obtain the block's diameter and the circular form. 90 points around the cylinder were taken to measure the

cylinder form. The plug gauge is 50.8 mm long and has a tolerance of 5 µm. A photo of the cylinder gauge and the measurement results are shown in Figure 78.

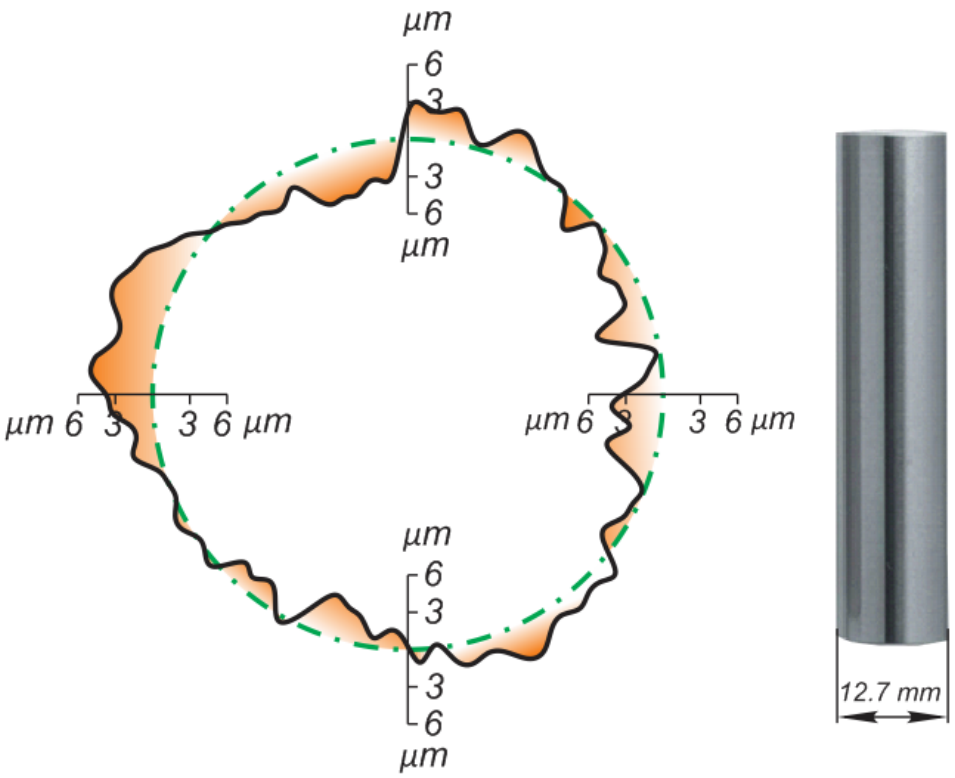

Figure 78 measurements on a 12.7 mm calibration gauge block.

Moreover, the repeatability of the three different probe materials was tested for both AE sensors methods, and the results are shown in Table 9 and Figure 79. The cylinder diameter was measured to be 12.706 mm. The measured diameter and the deviation of the measurement points from the cylinder diameter are close to the tolerance of the cylinder.

Table 9: Repeatability of single and multi AE sensor of cylinder gauge measurements

AE	Repeatability (µm) of cylindrical gauge block measurements		
	Stainless steel tip	Brass tip	Copper tip
Single	2.951	2.45	4.2
Multi	2.109	2.278	3.272

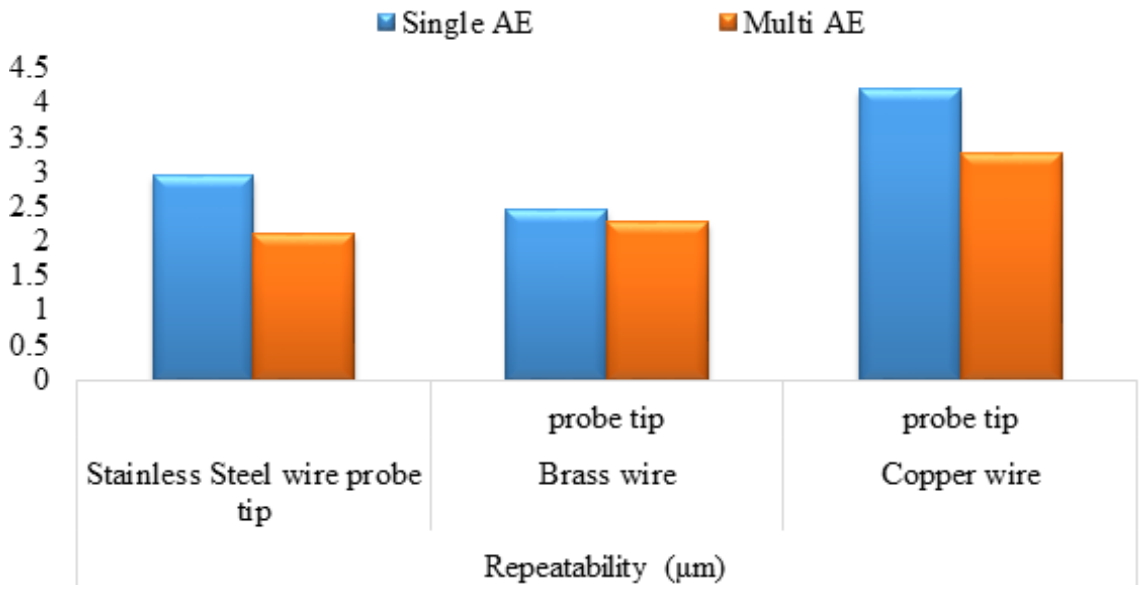

Figure 79 repeatability result of cylindrical gauge block

4.3.3 Evaluation with artifacts

It is worthwhile to note that before straightness experiments, the probe was calibrated to determine the effective rotating diameter of the probe. Automated measurements were also performed on a cylindrical plug gauge. A cylindrical plug gauge of 12.7 mm diameter (McMaster-Carr) was scanned to obtain the block's diameter and the circular form. 100 points around the cylinder were taken to measure the cylinder form. The plug gauge is 50.8 mm long and has a tolerance of 5 µm. A photo of the cylinder gauge and the measurement results are shown in Figure 80.

The cylinder diameter was measured to be 12.706 mm. The measured diameter and the deviation of the measurement points from the cylinder diameter are close to the tolerance of the cylinder. The probing system was used to measure and verify the dimensions of machined features.

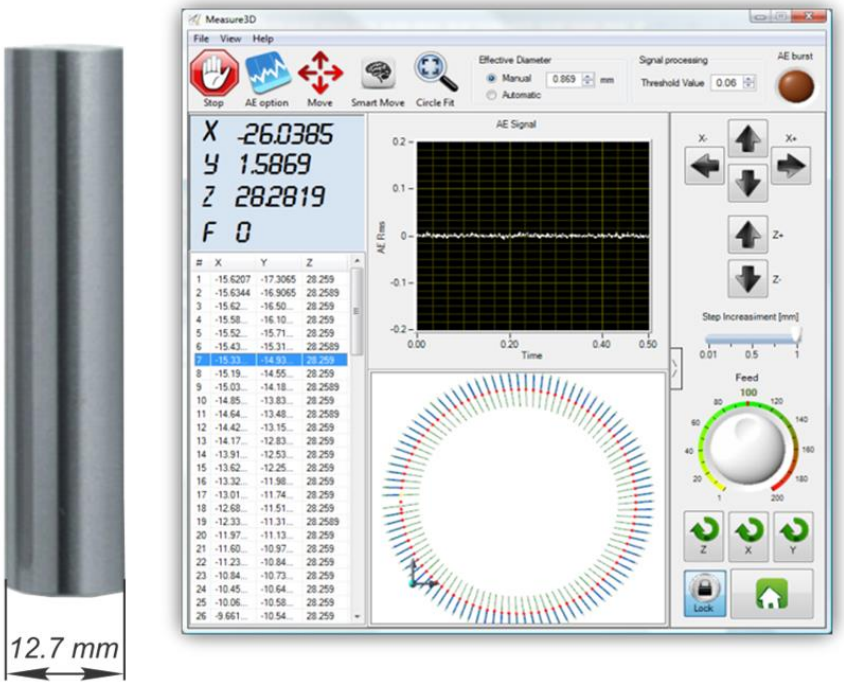

Figure 80 Measurements on a 12.7 mm calibration gauge block.

A cylinder of 12.7 mm diameter was machined as shown in Figure 81 (a) and measured using the automated probing system. The diameter was measured to be 12.695 mm. The form error and deviation from the nominal value are shown in Figure 81 (b), which shows the three-lobe type form error associated with the cylinder. It shows that the automated probing system can accurately measure the cylinder diameter and the form error. Deviations of the positions of the measured points from the pocket design geometry were as high as 12.0 μm because it was a rough milled cylinder.

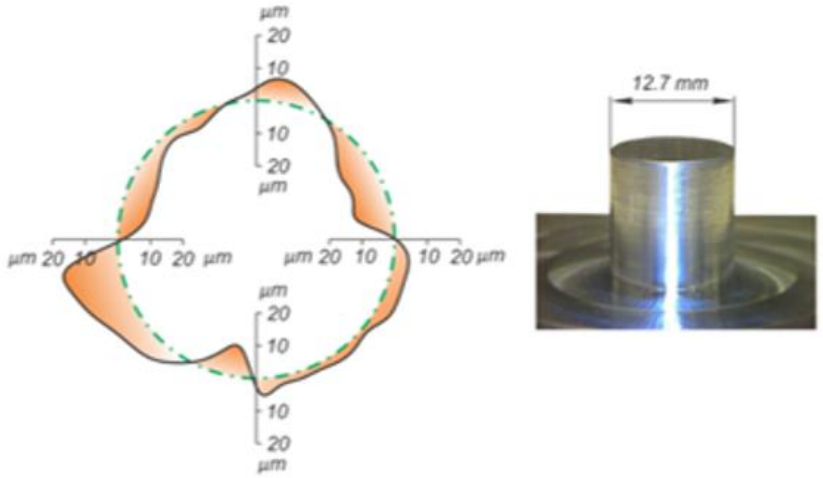

(a)

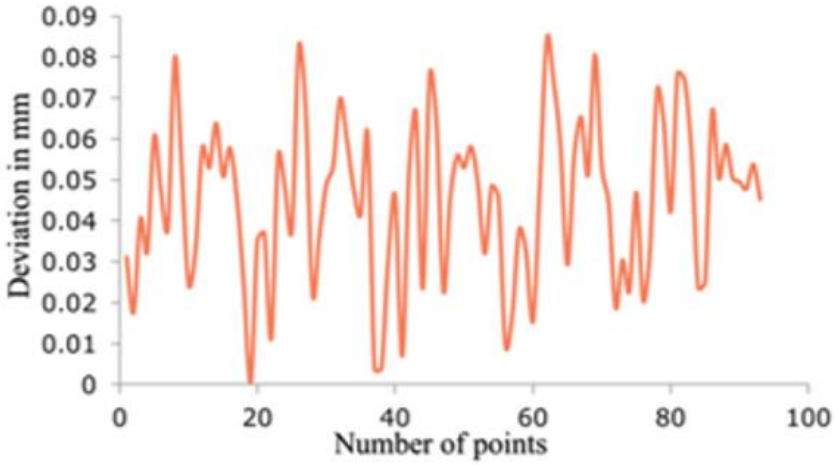

(b)

Figure 81 Automated scan results of a rough machined cylinder

Measurement of a rough milled bore-hole of 5 mm diameter was also conducted, and the measurement Figure 82 results are shown in Figure 82.

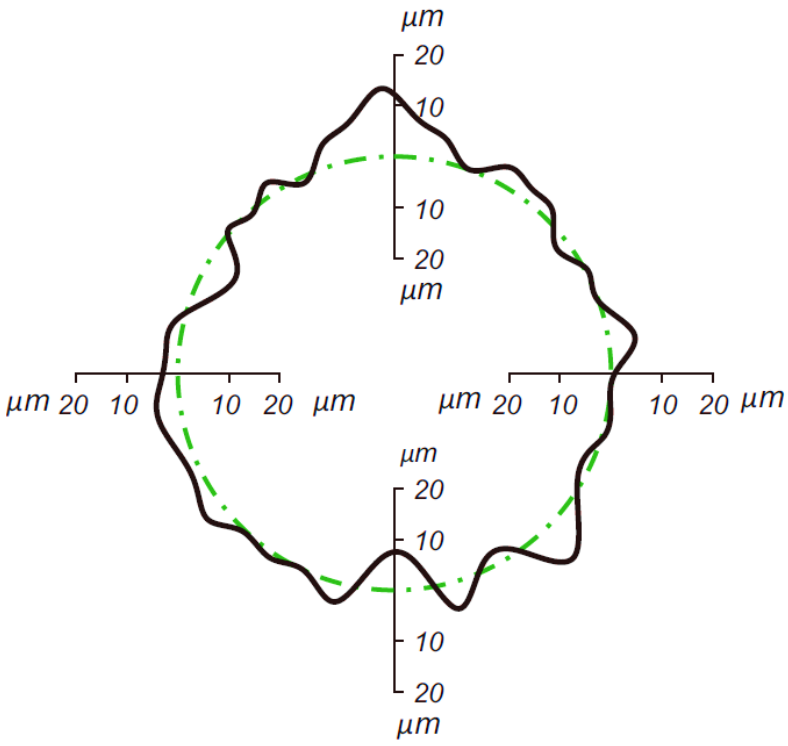

Figure 82 Automated scan results of a rough machined hole of φ 5 mm

The diameter was measured to be 5.0297 mm. The form error of the hole is also accurately captured. A micro end-mill machined pocket shown in Figure 83 (a) was also scanned. The points taken during the automated scanning are shown in Figure 83 (b) with the pocket design geometry shown as a solid line. Deviations of the positions of the measured points from the pocket design geometry were as high as 80.0 µm because it was a rough milled pocket. These results show that the probing system can be effectively used to measure and verify the dimensions of machined features.

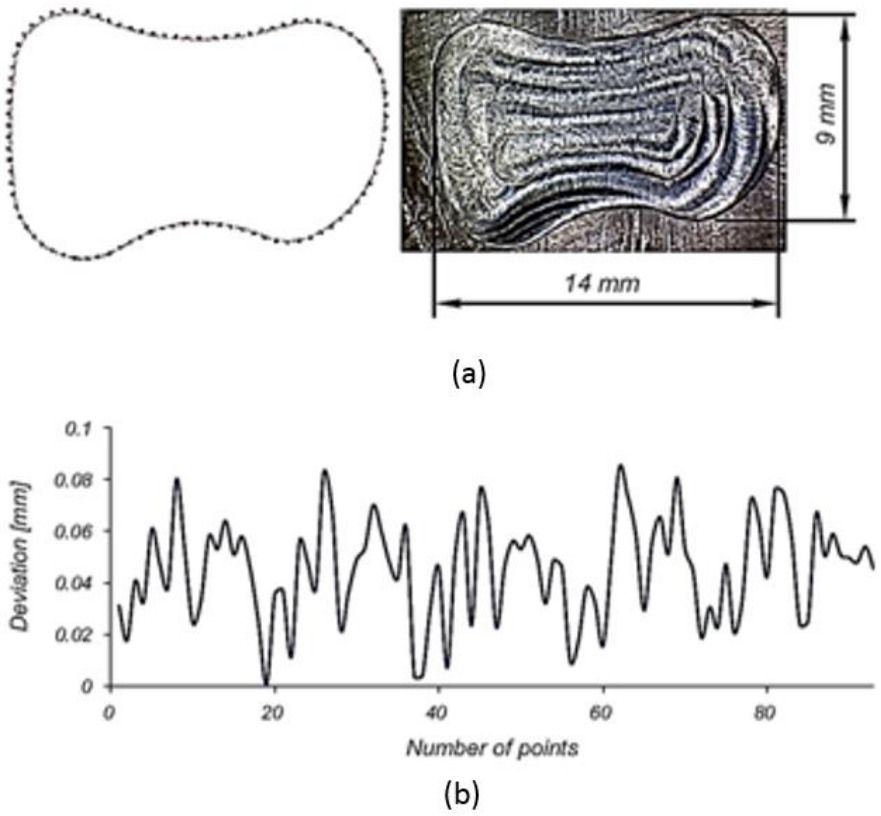

Figure 83 Automated scan results of a micro-milled pocket

Measurements were also performed on a cylindrical plug gauge with a diameter of 12.7 mm (McMaster-Carr), which was scanned to obtain the block's diameter and the cylinder form. Also, the three micro probes tip where tested, measurements were made using 20 points on the circumference, and this number can be considered as an acceptable minimum around the cylinder were taken to measure the cylinder form. The plug gauge was 50.8 mm long and had a tolerance of 5 µm. A cylinder gauge and the measurement results are shown in Figure 84, and Table 10. The measured diameter and the deviation of the measurement points from the cylinder diameter were close to the tolerance of the cylinder. The form error was closer to the form error of the cylindrical plug gauge.

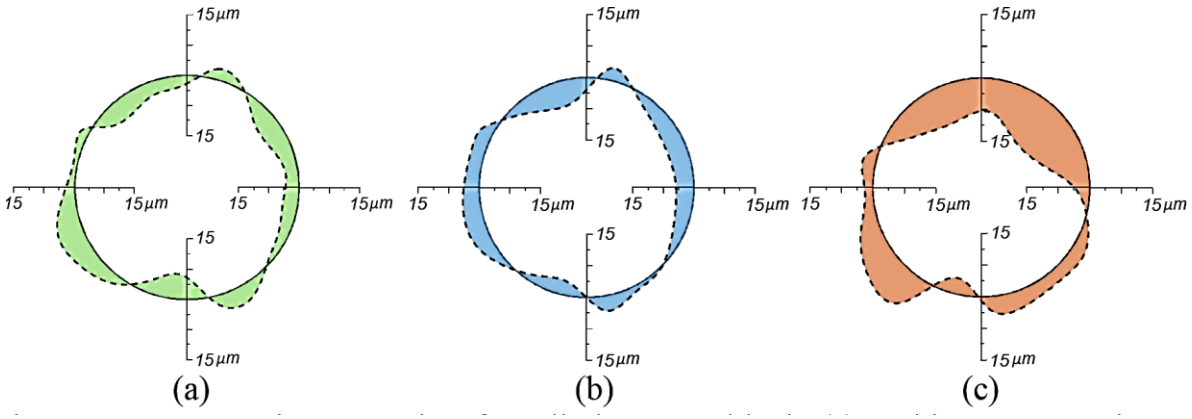

Figure 84 Automated scan results of a cylinder gauge block: (a) Probing system using 45 º probes, (b) Probing system using Sphere probe and (c) Probing system using a straight probe.

The three probe tips were used to measure and verify the dimensions of machined features. Figure 85 and present the measurement results of the cylinder form of a milled cylinder with a diameter of 12.7 mm.

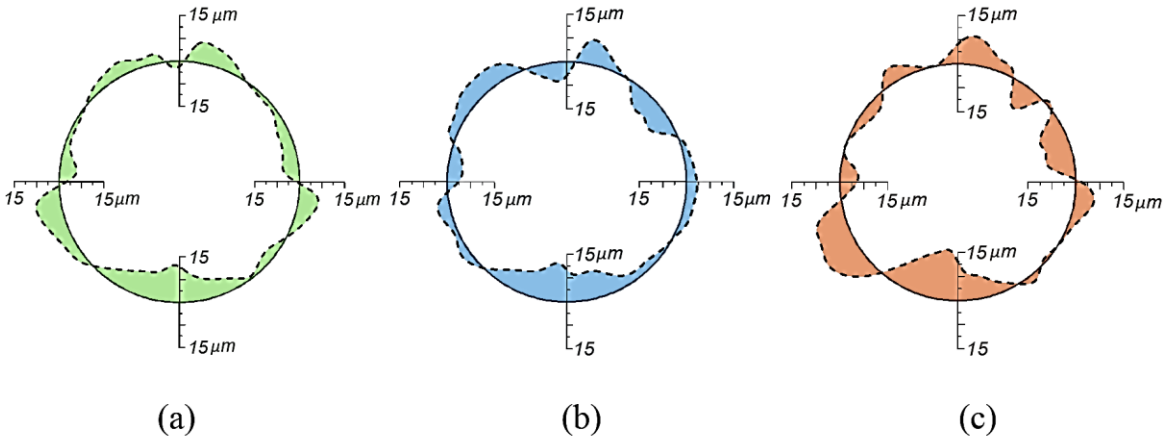

Figure 85 Roundness of the probing system point-by-point measurement in the XY-plane: (a) Probing system using 45 º probes, (b) Probing system using Sphere probe and (c) Probing system using a straight probe.

Table 10 Block gauge and machine cylinder measured result

Measured part		Deviation [μm]		
		Angle wire probe	sphere probe	Straight probe
Cylindrical block gauge	Min.	7	6	12
	Max.	7	5	21
Machined cylinder	Min.	9	8	12
	Max.	12	12	15

4.3.5 Straightness measurements

Measurements were also conducted to evaluate the repeatability of probe measurements by measuring straightness of a 20.0 mm gauge block. The gauge block's straightness was measured by determining positions of one face of a gauge block along the 25.0 mm length of the block using the probe. Because the gauge block is not fixture perfectly normal to the probing axis, any line slope in the measurements was taken out. The variation in the measurements along the straight face of the block is shown in Figure 86. It shows that the block's straightness is within σ = 0.869 μm, which is similar to the variation in the repeatability. Considering the block's width tolerance of 0.15 μm, the measured straightness seems to be slightly larger. This may be because of the wire tip roughness and the locational dependence of the AE sensor, causing variations in the repeatability. This locational dependence can be minimized by using multiple AE sensors at different locations to cover a larger area.

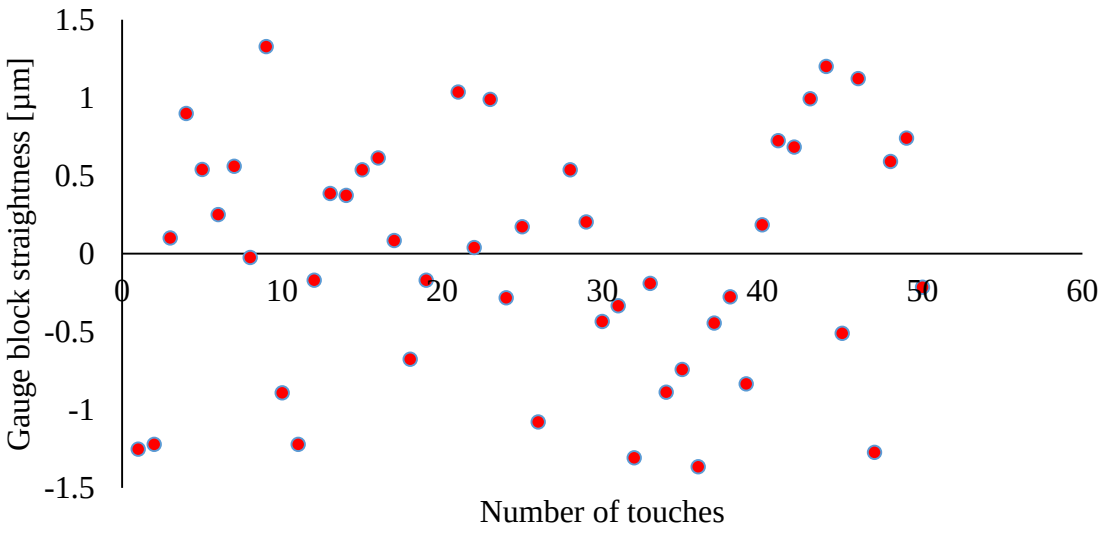

Figure 86 Straightness measurement of a 20 mm gauge block

Measurements were also conducted to evaluate the straightness of the three different probes tip by measuring the straightness of a 20 mm gauge block. The gauge block was not fixed without alignment to the probing axis; therefore, any line slope in the measurements was removed. The probes is commanded to move point-by-point so that the system can detect the out-of-straightness of the motion. Figure 87 is the result of x-direction straightness error it demonstrates good linearity for angle, and sphere probes tip of our system with only 0.55, and 1.4 mm respectively error, and 3.8 mm within the range of 50 mm. Also. Figure 88 and Figure 89 is the result of x-direction straightness error for composite and glass materials, and straightness is within σ = 0.75, 0.341 respectively µm.

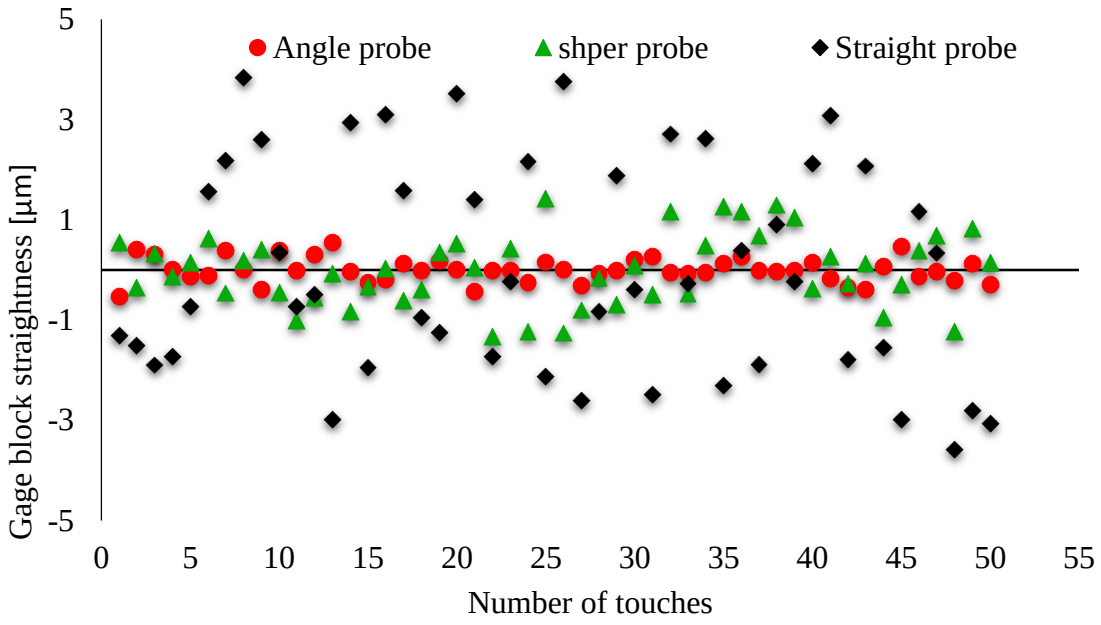

Figure 87 Straightness results for a gauge block along the X for the three different probes using one AE sensor

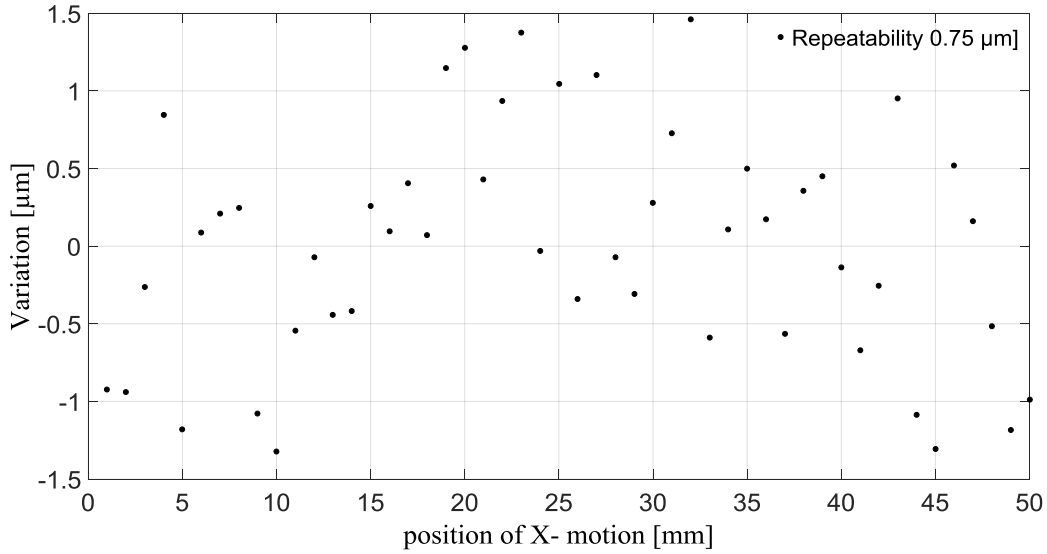

Figure 88 Straightness results for a composite material along the X for the angle probe using multi AE sensors

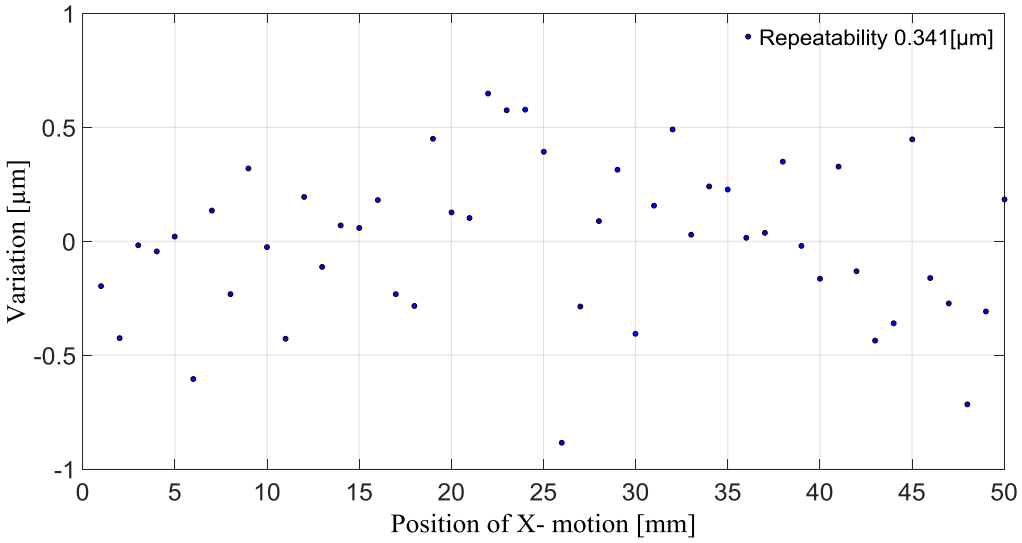

Figure 89 Straightness results for a glass material along the X for the angle probe-multi AE sensors

In our measurement experiments, we also use the multi-probe measurement method to measure the straightness motion error of each linear stage to evaluate the repeatability of the three different probes measurements by measuring straightness of a 20 mm gauge block. In the straightness measurement test, the stage was moved from 0mm to 25 mm along the block surface using the probes. Essentially, the block's straightness was measured. Because the gauge block is not fixtured perfectly normal to the probing axis, any line slope in the measurements was taken out.

The variation in the measurements along the straight face of the block for both methods are shown in Figure 90 and Figure 91 which demonstrates good linearity of our system. By comparing the results of the repeatability for these three probes shown in Table 11, we can conclude that the multi-probe measurement method adequately performs the measurements of the straightness motion errors with small standard deviations. In other words, measuring with these three different probe wire materials are easily influenced by the using multi AE sensors.

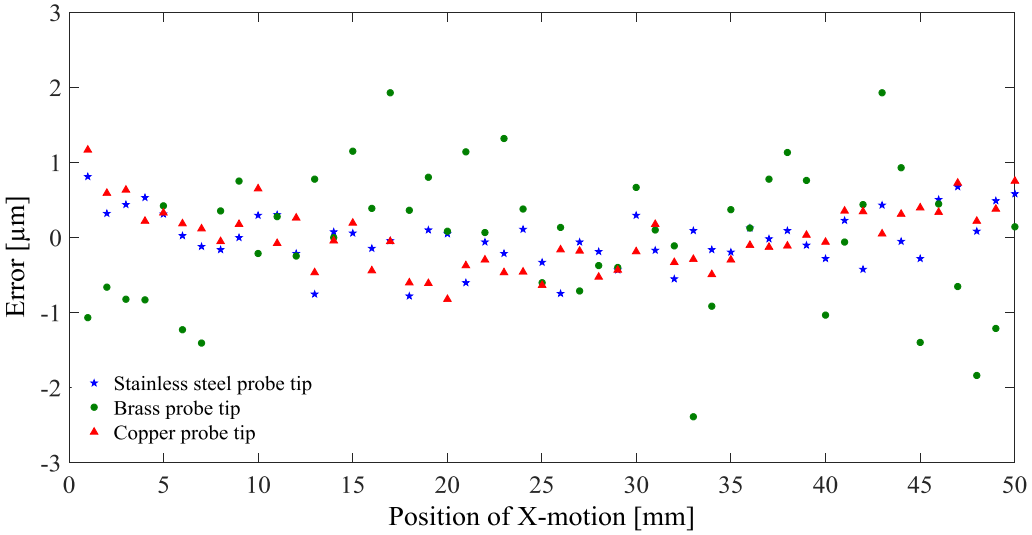

Figure 90 Straightness measurement of a 20 mm gauge block- Single AE sensor

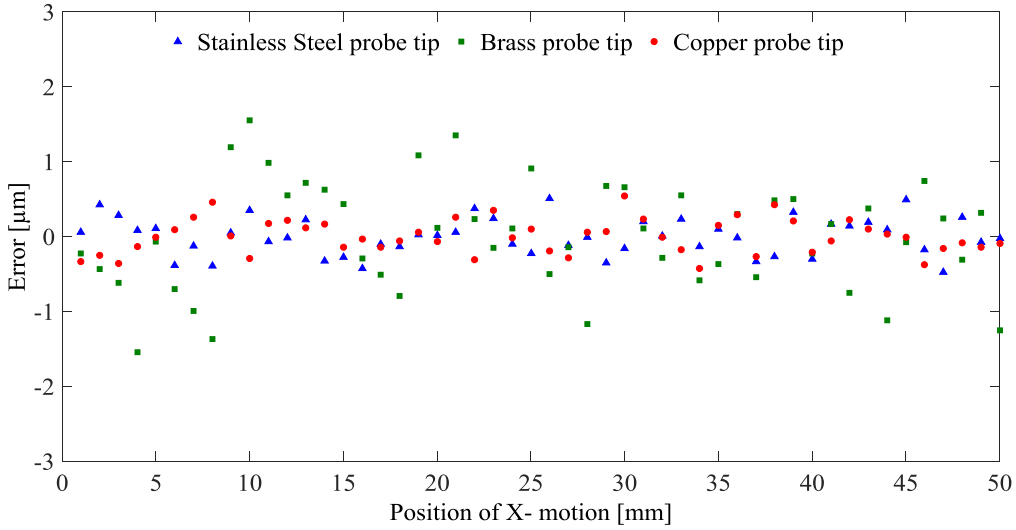

Figure 91 Straightness measurement of a 20 mm gauge block- multi AE sensors

Table 11: Straightness measurement repeatability of three different probes materials

AE	Repeatability (µm)		
	Stainless steel tip	Brass tip	Copper tip
Single	0.365	0.919	0.424
Multi	0.249	0.730	0.229

4.3.6 Measurements of flatness deviations

Requirements of flatness deviation evaluation of technical surfaces are essential to control flat surfaces of parts and in checking the geometric quality of manufacturing process. Also, often to qualify a surface as a primary reference to which the other part features are referred with position tolerances and the specification of fitness. Flatness is a condition of a specified surface having all elements in one plane ANSI [16, 17]. Also, flatness refers to the minimum distance (D) between two parallel planes (or lines) enclosing a set of measurement points taken on the surface that is checked for flatness, as shown in Figure 92. The requirement of fitness is via a tolerance zone defined by two parallel planes within which the surface must lie. Since fitness tolerance has no datum, the parallel planes that form the tolerance zone can be oriented in any direction.

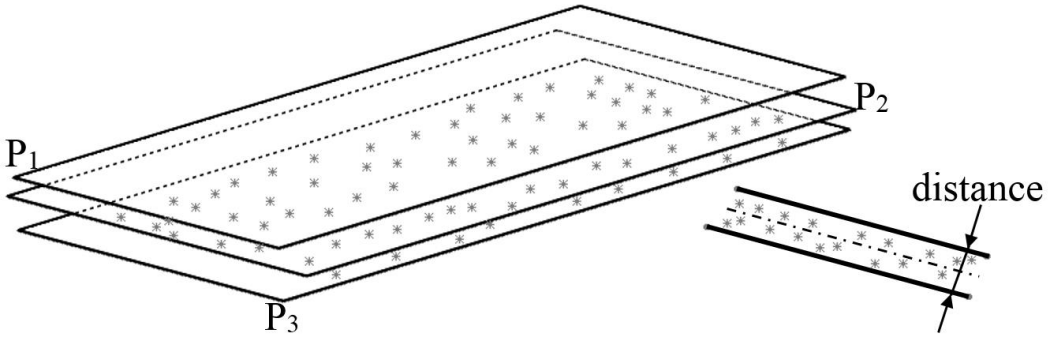

Figure 92 Flatness is the minimum distance between two planes containing measuring points

4.3.6.1 Measurement strategies

The limited sampling methods are employed that give specific rather than general information concerning the assessment of flatness form. These include: grid method, polar grid, specified grid, points method, parallel (uniform sampling strategy). The

following closed mesh point distribution measuring pattern will be proposed to determine the D as defined in Figure 93.

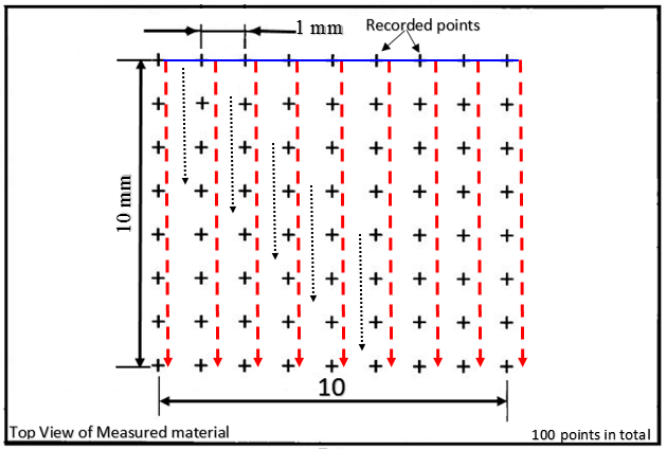

Figure 93 Parallel measuring pattern. The number of lines is case dependent

The principle of parallel extraction method is a higher density of closed mesh points in the direction of the profile about the density of points orthogonal to the profile. Linear least square estimation method (LLSE) is one of the most applied statistical techniques to model data [18] or minimum area method which is used to obtain the flatness in this measurements, as shown in Figure 94.

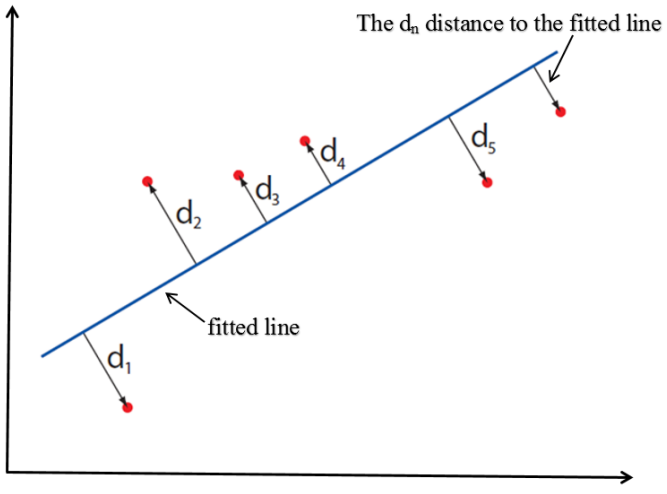

Figure 94 Graphic expression of least square method

4.3.6.2 Finding the Best Fit Plane

In Figure 93 , the plane P_1 is the best-fit plane for the points calculated using the LLSE. The planes P_1 and P_3 are two parallel planes (parallel to the plane P_2) enclosing all the points. According to the definition, the distance between the planes P_1 and P_3 is a minimum. Equivalently, the distance is the sum of the maximum distances between the points on both sides of the fitted plane (plane 1) and the plane itself.

Assuming that a point is represented as (x_i, y_i, z_i) and the plane is represented as ($\widehat{x_0}, \widehat{y_0}, \widehat{z_0}$) and ($\widehat{a}, \widehat{b}, \widehat{c}$,), the deviation from this point to the plane is:

$$\acute{d}_\iota = \hat{a}\,(x_i - \widehat{x_0}) + \hat{b}\,(y_i - \widehat{y_0}) + \hat{z}\,(z_i - \widehat{z_0}) \qquad (4.1)$$

For a set of *n* points, the distance between two parallel planes is:

$$D_{ev} = \max(\acute{d}_\iota) - \min(\acute{d}_\iota) \qquad i = 1{:}\ n \qquad (4.2)$$

The deviation (D_{ev}) has to be smaller than the tolerance specification for the flatness.

4.3.6.3 Measurement procedures

During the experiment, the glass, block gauge and composite material (manufactured by *Carbon-Composite Technology*) were placed on the machine stage, and they were measured point by point to and from in the direction shown in Figure 94. First, the movement was in Y direction, and one movement was 1 mm. There were 10 movements in the total length of 10 mm, and the same movement in the X direction. There were 100 points in total except block gauge there were 90 points due to the width limitation. The highest value, lowest value, and flatness were calculated, and the 3D schematic diagram was displayed in Figure 95 to Figure 97.

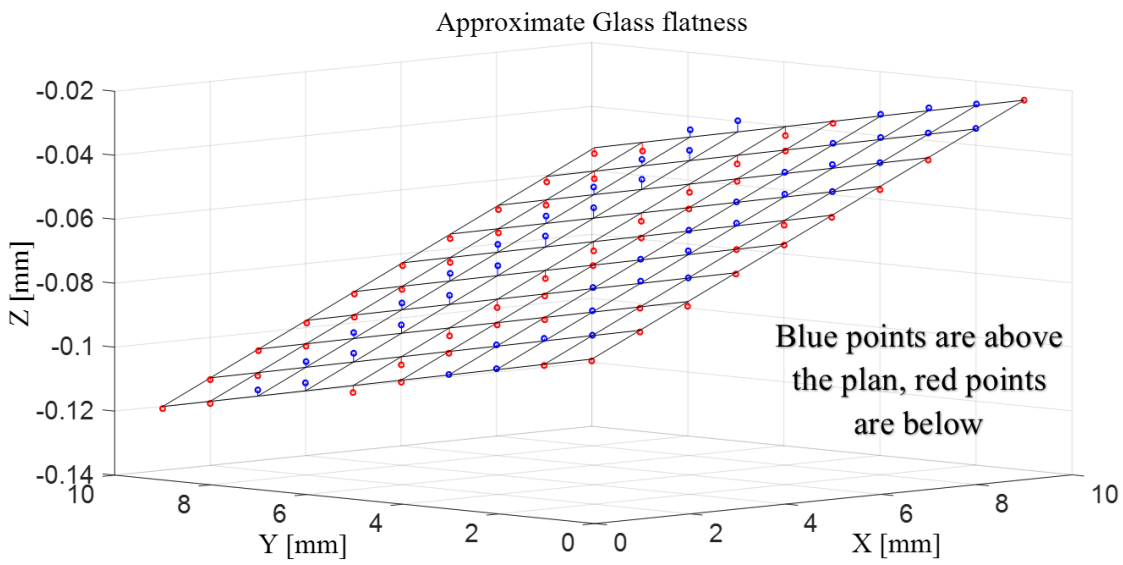

Figure 95 Flatness deviations of the investigated Glass surface plate

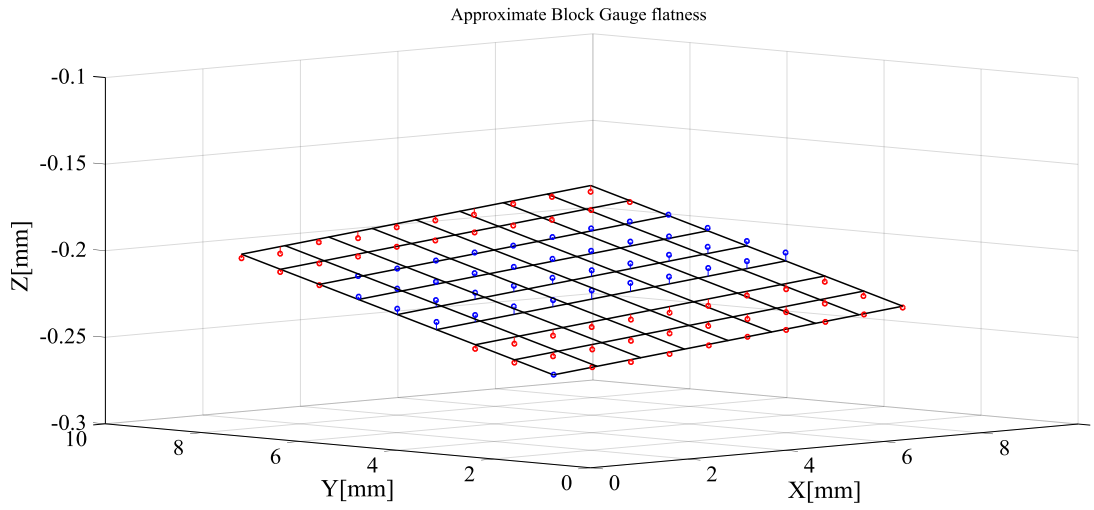

Figure 96 Flatness deviations of the investigated Block gauge surface

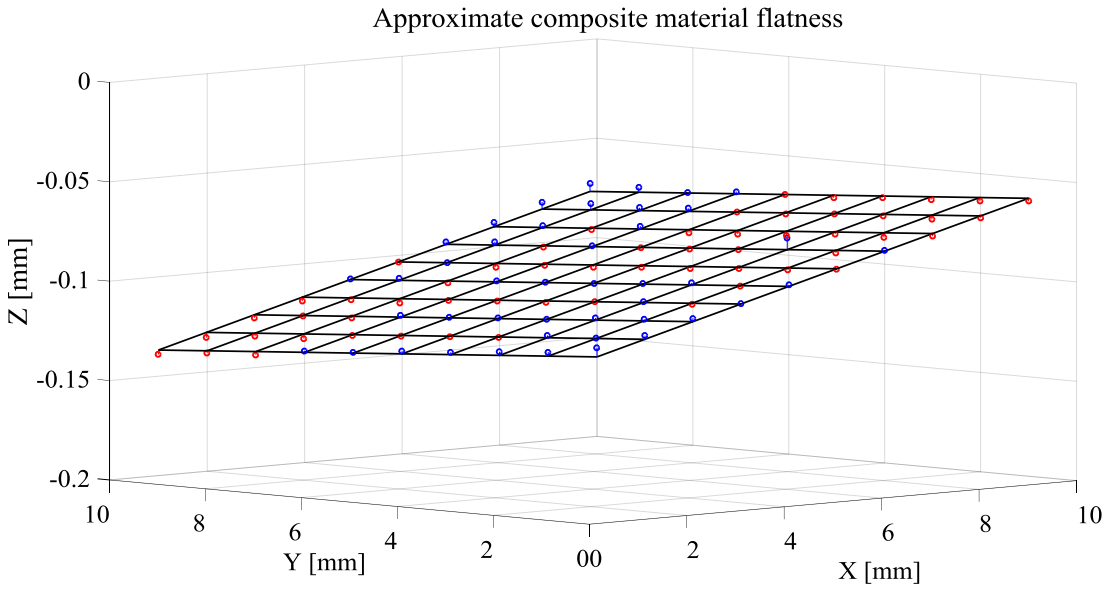

Figure 97 Flatness deviations of the investigated composite material surface

The profile of the surfaces was graphically illustrated in the figures from 96-98. They show that the AE sensing method can measure the out-off flatness. These figures depicted and confirmed the flatness of the measured surfaces of glass, block gauge and composite materials. The surfaces are shown their slops either slightly toward or downward of the reference datum due to the arbitrary selection or "tilting" of the reference plane. But the slopes are uniform and indicating the flatness nature of the three measured surfaces. The use of color to highlight points or area above and below the reference plane is helpful in understanding topography; the plane passes through the point mean, and it is the perpendicular distance to each centered point. The fitted plane minimizes the sum of the squared errors for measured materials surfaces as shown in Table 12.

Table 12 the flatness squared errors of measured materials surfaces

Measured material	Glass	Gauge block	Composite materials
the sum of the squared errors in µm	0.2602	0.6405	0.2287

4.4 Influence of Measurement Parameters

4.4.1 Effect of Spindle Speed

Figure 98 shows the effects of the spindle rotational speed and the approaching speed on the measurement accuracy of the probe. Eight different speeds from 10,000 to 80,000 RPM were selected at the approaching speed of 0.05 mm/sec, a wire diameter of 177 μm, and bend angle of 45 degrees. It shows that the effective diameter increases with increasing spindle speed. The total increase in effective diameter was 9 μm. The effective diameters obtained in Figure 98 was used to measure the length of the gauge block at a given spindle speed. The measured block gauge lengths are accurate with a variation less than 100 μm. Spindle speeds higher than 70,000 RPM are close to the maximum that the spindle can handle and cause a further increase in the effective diameter. This may be due to unwanted dynamics such as eccentricity and centrifugal forces at the high spindle speeds. However, because the effective diameter (D_e) is calibrated before measurement, as long as the process conditions are maintained consistent with a given component, the measurement accuracy is not compromised.

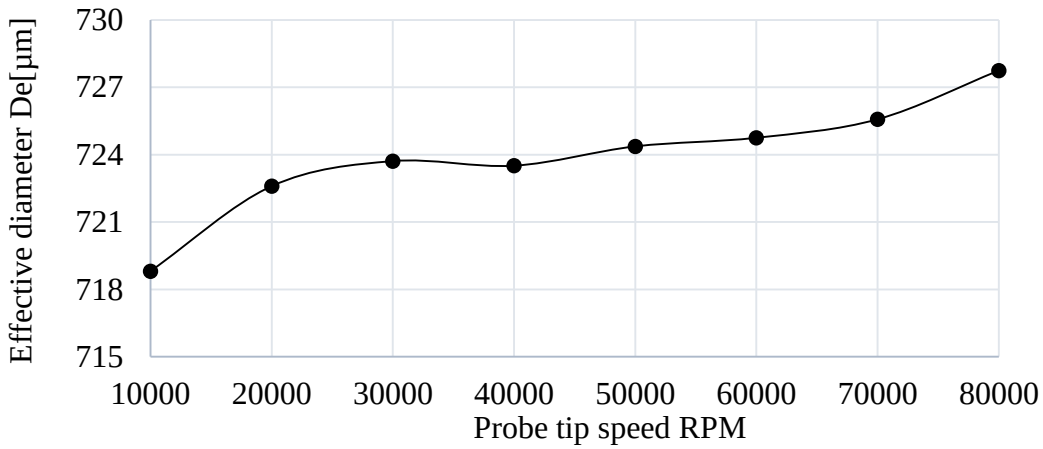

Figure 98 Effect of spindle speed on effective diameter

4.4.2 Effect of Approaching Speed

Figure 99 shows the effects of the approaching feed rate on the measurement accuracy of the probe. The variation in the effective diameter measurement is less than 0.4 µm. It shows that for the feed rate range tested; there is no effect of increasing the approaching feed on the effective diameter. This shows that selection of a feed rate for calibration of the effective probe diameter is quite flexible. However, care must be taken when selecting high feed rates because of high feed rates are not recommended due to probe's positional overshoot once the touch is detected. Higher the feed rate, farther the overshoot will be, resulting in more touches between the rotating wire and the workpiece surface, causing increased probe wear and surface damage. So the approaching feed rate does not seem to have much effect on the probe's effective diameter.

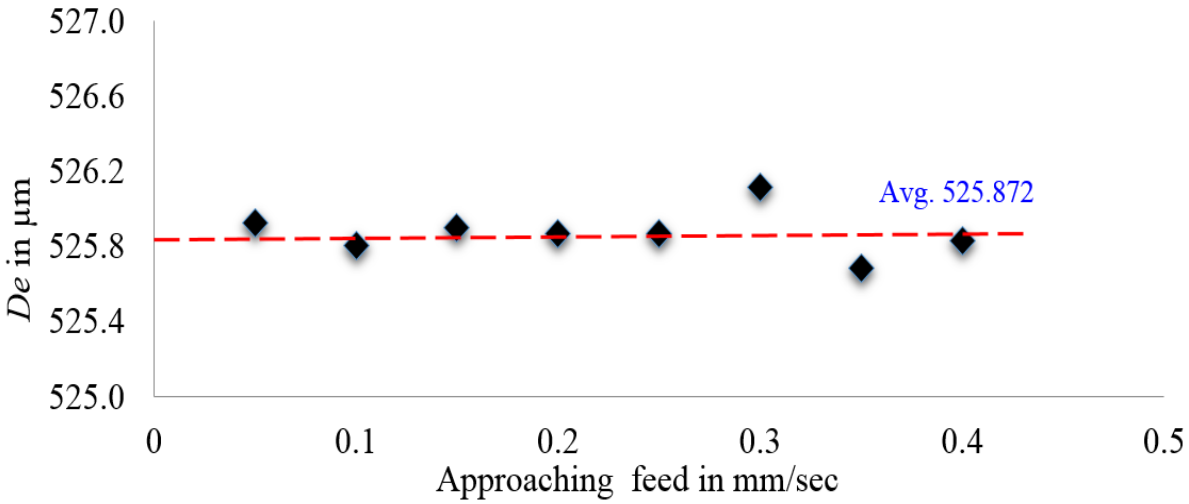

Figure 99 the effect of approaching feed on effective diameter

Furthermore, in Figure 100 shows the effects of the approaching feed rate on the measurement accuracy of the probe. It shows that the measurement accuracy decreases as the feed rate is increased.

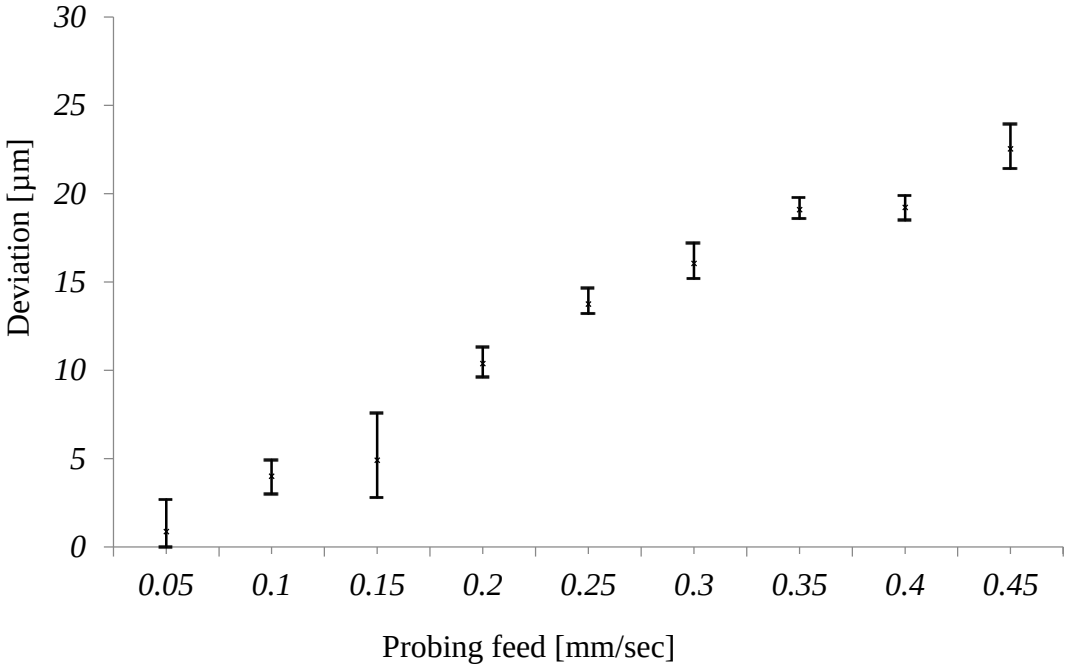

Figure 100 the effects of the approaching feed

4.5 Probe Tip Stability

It is well know that a straight elastic thin elastic stainless steel wire, when rotated from one end about its natural axis, may be lose it is stability. At certain values of RPM two equilibrium configurations will be possible: one in which the rotating probe tip remains straight and one in which it is deflect so its axis bent under the effect of centrifugal forces. The stability of our system is very important, When the straight wire probe tip rotates at high different speeds, the resulting centrifugal force will cause the free end of wire tip to bend out as shown if Figure 101. The inertia force or centrifugal force is proportional to the eccentricity of G [151], which is R_e+ u; Let the deflection of the straight wire probe tip is (Re + u). The distance to the center of gravity is then R_e + u. The probe tip rotates at ω rad/s. The wire stiffness is *k* N/m the deflection force is hence

$$F = k\, R_e \qquad (4.3)$$

The centrifugal force is

$$F_c = M\omega^2 (R_e + u) \tag{4.4}$$

The equation force we have

$$k\, R_e = M\omega^2 (R_e + u) \tag{4.5}$$

$$R_e = \frac{M\omega^2 (R_e+u)}{k} = \frac{M\omega^2 R_e}{k} + \frac{M\omega^2 u}{k} \tag{4.6}$$

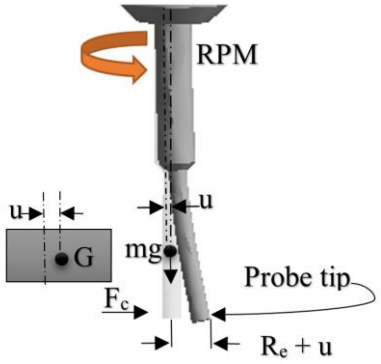

Figure 101 the effect of rotational speed on 2 mm straight probe tip

$$R_e = \frac{M\omega^2 u}{k(1-\frac{M\omega^2}{k})} \tag{4.7}$$

As it known $\omega_n^2 = \frac{k}{M}$ (4.8)

$$R_e = \frac{\omega^2 u}{\omega_n^2 \left(1-\frac{\omega^2}{\omega_n^2}\right)} = \frac{u}{\left(\frac{\omega_n}{\omega}\right)-1} \tag{4.9}$$

From that we can see that when

$\omega_n = \omega$ $R_e = u/0$ which is infinity. This means that no matter how small the imbalance distance u is, the probe tip will rotating at natural frequency.

The frequencies at different speeds can be calculated as following:

$$f_n = \frac{\pi}{2}(n+\frac{1}{2})^2\sqrt{\frac{gEI}{wL^4}} \tag{4.10}$$

Where n=2, 3… the lowest speed almost corresponding to n=1.

In this research, free vibration analysis of the straight probe tip under variations boundary condition is carried out. The natural frequencies of the straight probe tip are analyzed by using finite element method. This uses the Modal solution method. The system using the assumption of Euler-Bernoulli beam theory. The natural frequency calculation for 2 mm probe tip length and 250μm in diameter due to its own weight only and the first five critical frequencies is as following:

Using Euler-Bernoulli Beam theory we found:

$$EI\ \frac{d^4 y}{dx^4} + \ \rho\ A\ \frac{d^2 y}{dt^2} = 0 \tag{4.11}$$

$$Y(x,t) = X(x)T(t) \tag{4.12}$$

This makes equation 6.9:

$$\frac{EI}{\rho\ A}\ \frac{d^4 X}{dx^4} T(t) + \ X(x)\ \frac{d^2 T}{dt^2} = 0 \tag{4.13}$$

Solution for displacement is:

$$X(x) = \ C_1\ Cos(x\lambda) + \ C_2\ Sin(x\lambda) + \ C_3\ Cosh\,(x\lambda) + \ C_4\ Sinh(x\lambda) \tag{4.15}$$

Where:

$$\lambda = (\frac{\rho\ A}{EI}\ \omega^2)^{\frac{1}{4}} \tag{4.16}$$

For the straight probe tip, the displacement and slop are zero at the top of the styles, while the moment and shear are zero at free end. Thus the boundary condition are:

At x = 0 y=0, $\frac{d\ y}{dx} = 0$ and at x= L $\frac{d^2 y}{dx^2} = 0, \frac{d^3 y}{dx^3}$

This proves that:

$C_2\ = \ -C_4$, and $C_1 = \ -C_3$

Solving for $C_1\ and\ C_2$ we found:

$$Cos(\beta L)\ Cosh\,(\beta L) = \ -1 \tag{4.17}$$

The roots of this equation are

$$\beta_n\ L = \frac{(2n-1)\pi}{2} \tag{4.18}$$

The equation for time breaks down into:

$$T(t) = b_1\ Sin\ [(\beta_n{}^2 \sqrt{\frac{EI}{\rho\ A}})\ t] + b_2\ Cos\ [(\beta_n{}^2 \sqrt{\frac{EI}{\rho\ A}})\ t] \tag{4.19}$$

So the frequency in rad/sec is:

$$\omega^2 = \frac{\beta_n{}^2}{L^2} \sqrt{\frac{EI}{\rho\ A}} \tag{4.20}$$

Converting to Hz, we get the natural frequency as shown below:

$$f_n = \frac{\omega_n}{2\pi} = \frac{\beta_n{}^2}{2\pi L^2} \sqrt{\frac{EI}{\rho\ A}} \tag{4.21}$$

Figure 102 shows the natural frequency of 2 mm straight probe tip and its deformation and shows the extracting the first 5 natural frequencies.

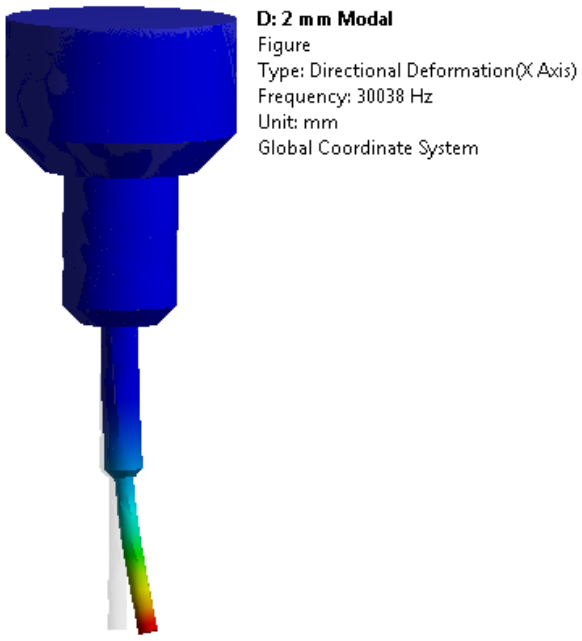

Figure 102 the effect of natural frequency of straight probe deformation

For probe tip lengths more than 2 mm the effective diameter is not useful for measurements because it is bigger than we expected. So it can be seen form the Table 13 that the critical speed that might case vibration to system start at 1802 K RPM and we have 80K RPM in our measurement system, which means there will be no effect of vibration on our measurement accuracy system.

Table 13 extracting the first 5 natural frequencies of straight probe tip

n	Natural Frequency f_n [Hz]	Critical probe tip speed K RPM
1	30038	1802.28
2	30077	1804.62
3	80803	4848.18
4	81044	4862.64
5	147840	8870.4

On the other hand, the friction between the bent rotating tip and measured surface (rubbing surface) are very important feature in micro wire probe tip based on acoustic emission. It needs to be extremely small, but the colliding between the contact face of probe tip and the measured surface become critical due to the stiffness of measured part and more importantly due to soft measured materials. This, so called "tip-part surface rub problem" has a focal point of our investigation since developing this new measurement methodology. Therefore, our motivation is to eliminate the contact friction and reducing number of probe tip touches during measurement process. Typical impingement as in figure 103, when the rotating wire probe tip radially interfere with the measured surface. This radial interference originates tangential, radial as well as axial forcing between the probe tip face and the measured surface which case some respective deformation. The amount of this deformation is certainly important but not as critical from the surface damage concerns.

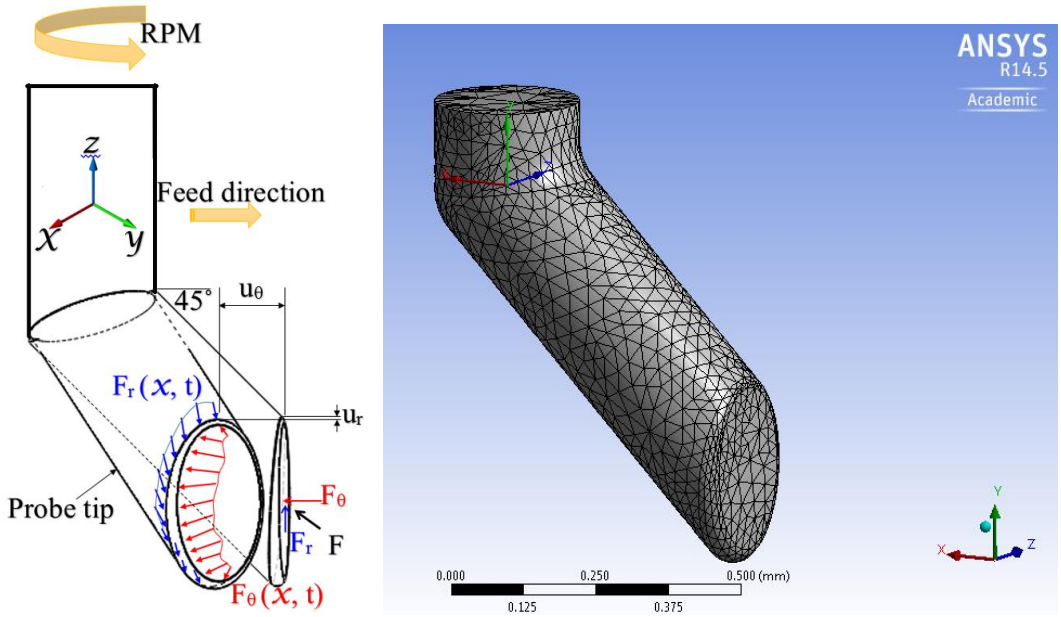

Figure 103 Load on the probe tip

Similarly, the natural frequencies of the bent probe tip (1 mm) are analyzed by using finite element method. The natural frequency for 1 mm probe tip length and 250µm in diameter due to its own weight only and the first five critical frequencies is shown in Table 14

Table 14 extracting the first 5 natural frequencies of bent probe tip.

	Natural Frequency f_n [Hz]	Critical probe tip speed K RPM
1	78399	4703.94
2	80513	4830.78
3	445000	26683.8
4	453000	27166.8
5	541000	32464.8

As it can be seen form the Table 14 that the critical speed that might case vibration to system start at 4703.94 K RPM, which means there will be no effect of vibration on our measurement accuracy system for bent probe tip too.

4.6 Bent Probe Tip Contact Length

The contact length between the probe tip and the measured surface as shown in Figure 104 is a fundamental parameter in rotating WPAES. There is a relationship between the actual size of the contact length, with probe tip diameter, effective diameter and angle of contact based on the variations of the geometrically calculated value. This simplification can cause an unexpected surface damage from reality for both the front of probe tip and measured part, measurement sensitivity as well as result in probe tip wear if it has a small Young's Modulus.

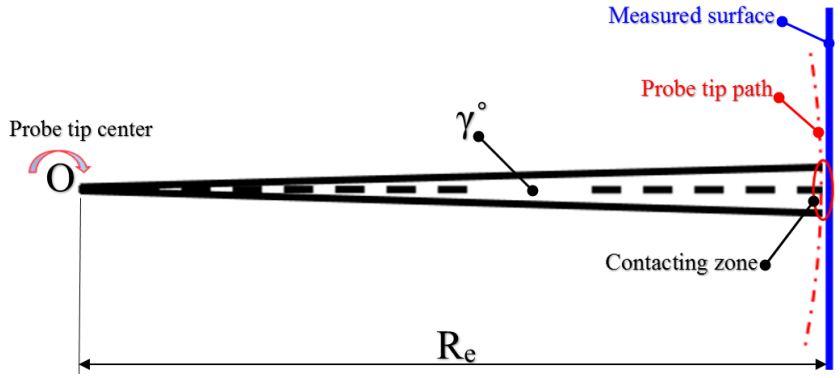

Figure 104 the contact length between the bent probe tip and the measured surface

$$L = \frac{\gamma \, \pi \, R_e}{180} \qquad (4.22)$$

Total contact length is assumed to be the same as the wire diameter, but this value has been seen to reach even higher values depending on measuring conditions. The main reason for this is the elastic deformation within the measuring contact zone due to the applied normal force at the interface. Figure 105 illustrates the contact length model, which is dependent on following individual components: the geometric measured surface contact zone, the elastic deflection between the probe tip and the measured surface and the microscopic contact at the micro level.

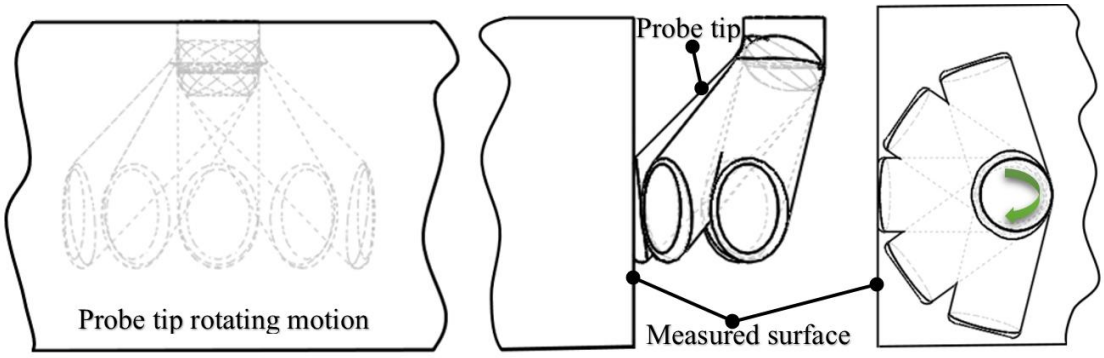

Figure 105 Model of the probe tip and measured surface contact

The radius of the effective diameter and the measured surface contact length each increase as the normal force is exerted during measurement procedure. This elastic deformation results in the actual contact length is negligible with rigid materials. The contact length is not only useful for modeling, but is also essential in understanding damage system dynamics; such as contact stiffness.

4.7 Conclusion

The experiments were conducted to investigate the effect of process parameters, and the results have demonstrated the ability of the probing system to measure a part with micron-level accuracy.

The results of the evaluation indicate that the probing system can be used to measure a micro-scale part within one-micron accuracy with negligible surface damage on the part. Also, the measurement repeatability and accuracy of the used probes are excellent, micro probing based on acoustic emission, for example, is capable of performing measurements with a repeatability and accuracy.

The measurement repeatability and accuracy of the three probes are excellent, micro probing based on acoustic emission, for example, is capable of performing measurements with a repeatability and accuracy. The geometry of the probes and the use of the AE sensor

enable the probing system to be cost-effective and easily scalable for micro-scale components.

For the repeatability evaluation experiments, x and y coordinates are recorded after contacting the gauge block. Each touch operation was repeated 100 times and the repeatability is expressed into sigma (σ) as an evaluation indicator. Moreover, multiple AE sensors and the setting of the appropriate thresholds optimizing the measurement quality.

The automated scanning algorithm behavior works effectively on the 2D plane. Measurement sensitivity and the diameter of the probe tip are limited by the diameter of the stylus on which the probe tip is attached. Despite these specifications, there still are some limitations concerning the performance of these probes on the micro scale. A rotation microprobe will be able to overcome these limitations, thus resulting in a probe that is capable of performing measurements on micro-sized features, such as holes with a diameter below 1 mm, and with micrometer uncertainty and repeatability with negligible surface damage on the part.

On the other hand, the angle wire and sphere tips of the probes need to decrease in size. As a probe tip is assembled on the stylus, the stylus needs to have a smaller diameter than the tip itself. This to ensure that walls parallel to the stylus can be sensing without the risk of contact between stylus and component.

Wire-probe wear and surface damage have been examined it was found less wear probe and surface damage, and this is due to better comparator sensitivity. There is no effect of the approaching feed on the effective diameter. There is an obvious effect of rotating speed on the effective diameter. As it can be seen that the effective diameter is increased once, the rotational speed increased.

In general, a dimensional probing system using a rotating wire probe tip and AE sensor for touch detection and an automated scanning algorithm have been developed. Also, the following conclusions can be drawn from this chapter:

Experimental results of the probe wear and surface damage show that they can be assumed to be negligible for dimensional measurement of most components. Much less than 1.0 μm probe wear was observed even after 10,000 touches against the surface of a block gauge. The surface damage on the block gauge surface was hardly seen after 10,000 touches. Only after 500,000 touches, scratches caused by the wire-based probe were observed on SEM. Measurement results of machined features show that the probing system can be effectively used to measure and verify the dimensions of machined features.

Automated scanning of calibration artifacts and machined features have been achieved. The probing system is capable of less than 1.0 μm repeatability. The results of the evaluation indicate that the probe wear and surface damage show that they can be assumed to be negligible for dimensional measurement of most components. Measurement results of machined features show that the probing system can be effectively used to measure and verify the dimensions of machined features. The flatness measurements using AE sensing method show a satisfactory accuracy for miniature surfaces.

The probe tip will not going to resonant and there will be no potential failure observed in the probe tip. The maximum spindle ration rotation in our system is 80k rpm which means 1333.333 Hz and as we can see the smallest Natural frequency from the calculation is 78.4 kHz. If we use 15 mm probe tip length the probe tip will resonate but the maximum used probe tip length in current system is 1 mm.

Chapter 5- Signal analyzing of probing measurement system based on AE sensing and threshold estimation

5.1 Introduction

During Wire probing based on AE sensing (WPAES) procedure, and while carrying out AE detection, it is often found that the background noise is very high (compared to the AE signal). AE signals include various noises and interferences. Most of the noises have spread frequency spectrum such electromagnetic, cyclic, Hydraulic, and white noise, where they spread over the entire frequency bandwidth. Theory of operation requires spindle rotation. In this method, a high rotational accuracy, high dimensional stability and high stiffness air spindle was used. Physically, spindle air flow produces the amount of noise. The results classified these noises as the mean noise component. There is no probe tip contact without rotation, and no rotation without air flow. Therefore, we need to filter these noise signals to get the original signal picked up by AE sensor where this noises level appears in the DAQ as voltage. Where certain “well chosen” voltage called “threshold voltage” is equivalent to the pure interfere noise level without original signal. So it is necessary to understand the types of noise sources and to ensure the elimination of their influence. Usually, frequency domain and time-space domain methods are used technique for signal processing to filter out the noise content from the original signal, based on noise features. Reducing the number of the probe tip touches during measurement process will reduce the surface damage. So analyzing the AE signal, it is essential to eliminate or reduce the noise.

The aim of this chapter is to eliminate or reducing the number of scratches on the measured metal components surface i.e. steel, aluminum, any other metal alloys which

caused due to probe tip penetration into the measured surface. In order to see the surface damage caused by the touches, the Mitutoyo gauge block was observed using SEM as shown in Figure 53. Even though, the scratches are unseen on hard metals but not with softer, so as much as we reduce the number of probe touches the depth of scratches will be negligible and as a result the probe tip wear will be closer to zero. There is more than one factor which dominates the underlying probing mechanism and minimizing these scratches on the measured surface; it is proposed to predict a proper acquisition threshold of the Acoustic emission (AE) sensor. So that the AE sensor can respond to a less numbers of probe tip touches on the surface and not the week signals are not missed due to a high threshold. Also, workpiece material needs to be considered as a parameter to predict the scratches of measured surfaces. On the other hand, the amplitude of the generated AE signals can be affected the amplitude of the generated AE signals due to the available surrounding noise that may interfere with the acquisition of data.

5.2 Understanding the Acoustic Emission Signal

In our case, the noises are covered by many other noise sources in the system like, environmental and the used equipment. The noises generated from the air supply pressure, machine stages movements, and the surrounding noise. The background noises are usually caused by power supply, preamplifier, and DAQ card, and propagate acoustic signals in a wide range of frequencies. All these noises and others will effect on the selected threshold magnitude therefor identifying these noises are a most serious obstacle in AE measurements, so we have to eliminate them from the frequency spectrum that produced for the probe tip touching. The frequency ranges which carried the maximum amount of energy are very important for the probing detection. These noises can affect the AE

measurement and the amplitude of the generated AE signals. So through real-time programmable filtering technique consists of these frequency ranges were recorded. To do so, a Matlab code is generated to take Fast Fourier Transform (FFT) filtering analyzing the raw signals to show the important frequencies contained in the acquired AE signal. Due to ambiguous functional dependency in the time domain, we carried out an evaluation in the frequency domain, and power spectra density (PSD) of the raw AE signal. From the results it can be observed that the backgrounds noises are all over the bandwidth. Based on the analysis of AE signal sources, AE derived from component probing consists of continuous and transient signals, which have distinctly different characteristics. Continuous signals are associated with the dynamic motion of the machine stages, spindle rotation, and air pressure out let compressed air which is mainly uncontrolled and unwanted noise signals, while burst or transient signals result from either probe tip rubbing or by the machine stage occasional stopping shown in Figure 106.

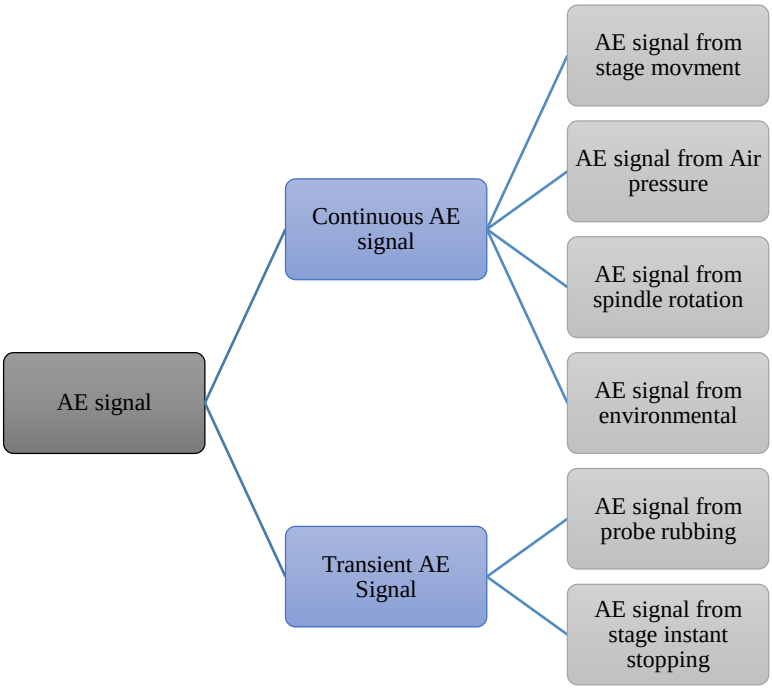

Figure 106 AE signal type in probing process

A plot of an AE signals response is a mix of burst type, and continuous type resulting from contact between the rotating probe wire-tip and measured surface as shown in Figure 107. There is a slight dependency of the distance between the contact location and the AE sensor on the generated AE signal magnitude. Thus, care must be taken in setting the threshold value used to detect the contact burst so that the magnitude of the burst is larger than the AE noise but small enough for highly sensitive contact detection.

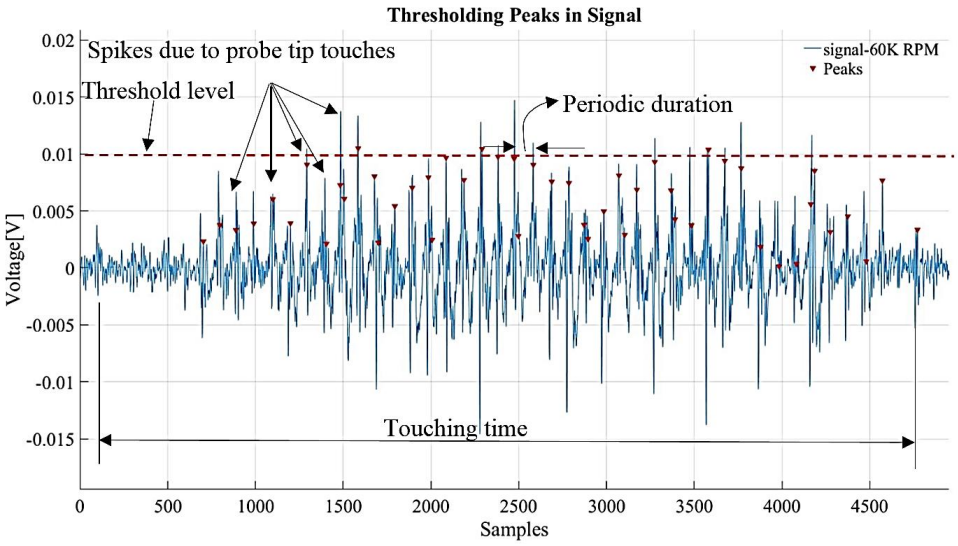

Figure 107 AE Bursts signal from microprobe tip-surface contact (10 millivolt threshold)

The signal feature of the output of the AE sensor mounted into the fixture underneath the measured component (closer to the component surface) when the rotating probe is commanded to approach measured surface at a constant approaching feed is shown in Figure 108. The main features that could be observed form filtered AE waveform are the details of every single probe tip touch i.e. duration, amplitude and to validate the recommended threshold.

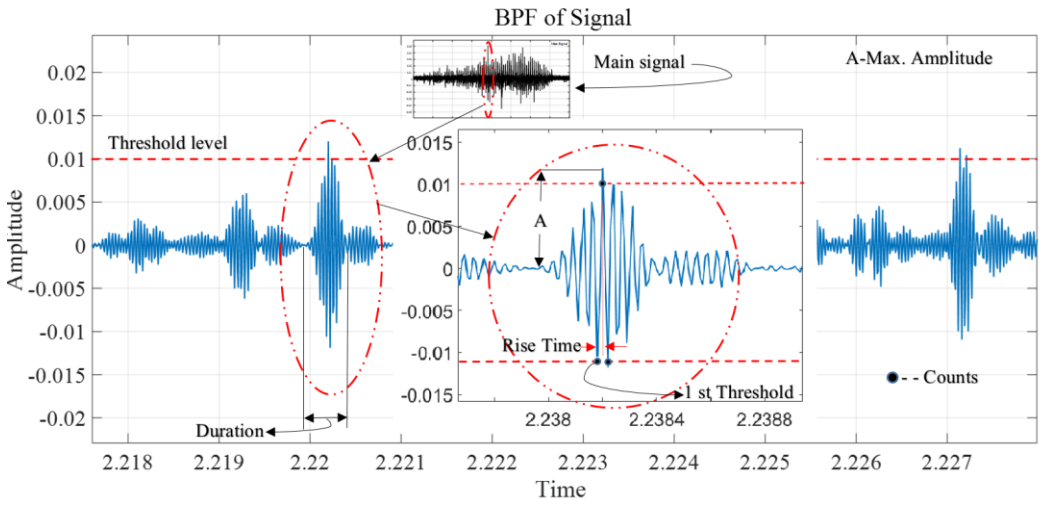

Figure 108 the acoustic emission waveform and burst AE signal features

5.3 Effect of Spindle Speed and threshold

To study the effect of the spindle speed, different speeds from 10,000 to 80,000 rev/min (RPM) were selected at the approaching speed of 0.05 mm/min. Also, Threshold Voltage considered being one of the factors to affect the repeatability on measured surface. The selected threshold was between 10 to 30 millivolts to determine the burst of generated AE signal as a contact from other noises. If the threshold voltage set is below 10 millivolts, the noises don't allow the probe tip to approach the surface due to noises threshold. If the threshold voltage is set higher than 25 millivolts, then the generated amplitude of the produced AE burst signal above the threshold voltage will be much higher than the acceptable threshold to be generated between the probe tip and as measured surface, and might resulting in the deeper surface damage of a softer material part. The effect of spindle speed on duration touches time at different tested thresholds was given in Figure 109, which showed that increasing spindle speed, threshold increased the duration touches time. Similar results for the effect on a number of touches shown in Figure 110. The number of touches in Figure 110 also prove the effect of the threshold voltage, when the 10 millivolts

are selected, the probe tip at 20 and 40 K RPM is less, which is comparable to the other thresholds. However, as the threshold voltage increase, the time duration are reduced, which seems to agree with the overshoot.

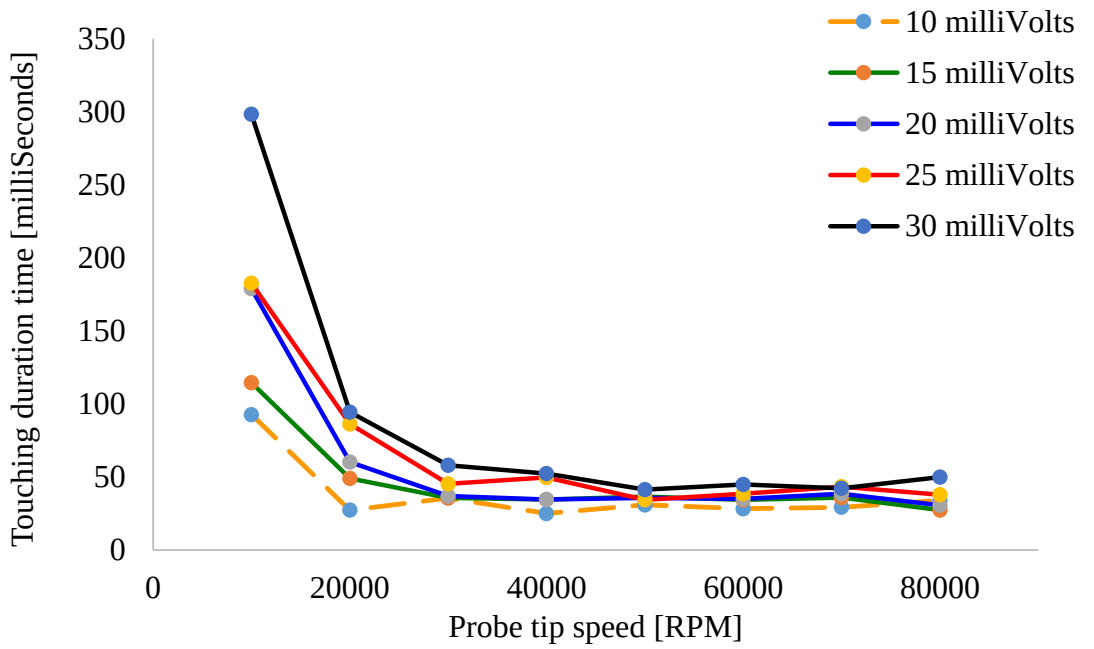

Figure 109 the duration of touching at different RPM

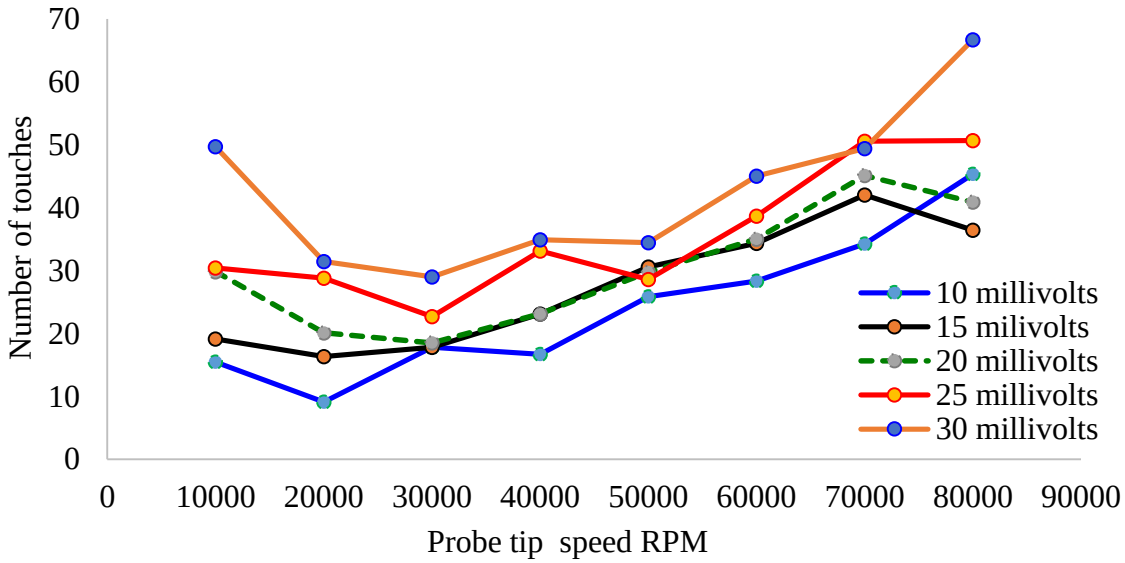

Figure 110 the number of touches at different RPM

5.4 Frequency-Domain Display

AE signals are very important information to analyzing the AE signal features; frequency domain gives spectral information by transforming these signals form time domain to frequency domain. The frequency domain can be achieved by using FFT transform of the time waveform.

Figure 111 shows the FFT spectrum of the air pressure frequency noises were located between 0 to 50 kHz, raw AE data at 60K RPM during sensing and we can see the first peak in the AE spectrum occur at a frequency of 1000 Hz. The main problem was still to distinguish between these sounds from the air flowing through, the stages motion, and the environmental noises. All of these were continuous acoustic emissions which were mixed.

The noises data, the spectrum of noisy data is illustrated in Figure 111. The frequency band from (0-50 KHz) was chosen based on a detailed analysis of the whole frequency spectrum. The next other surrounding noises are the raw signals of the machine stages motion, and air pressure peaks which are generated, frequency broadband noise is produced which, mixed with environment noises. These noises in the probing system can limit the overall system sensitivity and hampers accurate interpretation. This will add complexity requires a full description of both the burst physical characteristics and the background noises by which the AE burst has been generated. It can be seen that the environmental noises are permeated into it. For measuring the dimension Alio micro - system machine needs air pressure to run the spindle and due to the continuous bleeding of the excessive air from the spindle air out let. So the aim of the following air pressure noise analysis was to figure out the frequency of the air pressure which flowed through the spindle at 4 MPa

when the machine is off. The spindle located closer to the measuring component, and the AE sensor was in the center underneath the component when raw data recorded.

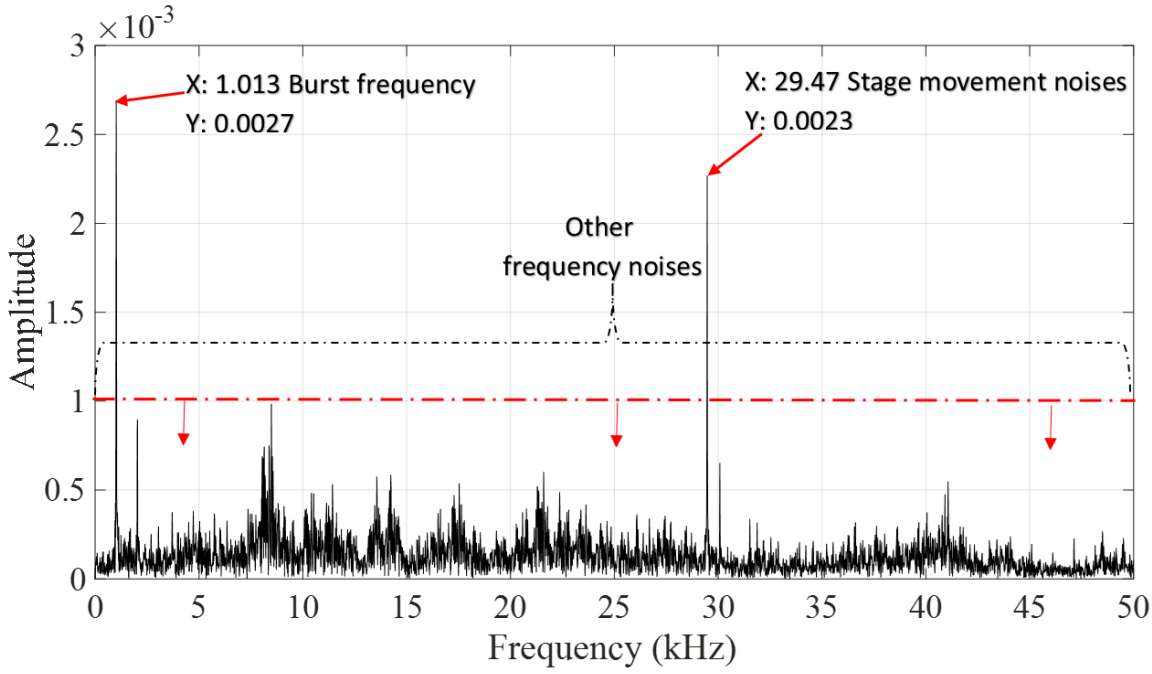

Figure 111 the signals generated during the stage motion (Al-60K RPM)

On the other hand, from the spectral analysis of the signal, three major frequency peaks show the results recorded data of previously mentioned noises, and as it can be seen in Figure 112 there is overlapping between machine noises, air pressure, background noise usually oscillates at low frequencies (0–50 kHz). These three frequency bands were found to be constant signal characteristics of all the noise background with a different number of amplitude. The use of frequencies over too wide a band is susceptible to excessive background noise, limiting sensitivity and resolution of the AE probing technique. Thus, there is no guarantee of a complete filtration of the noise since the measured sound and the noise overlap. The Spindle rotates at very high speeds with media pressure up to 4 MPa so the signal transfer to the amplifier is a problem due to the rotating spindle, which also because a periodically swelling signals making preprocessing necessary.

The spectrogram showed in Figure 107 that the large increase in acoustic emission waves when a probe tip is touching the measured surface. This is reasonable because during hitting the surface large amounts of acoustic emission are generated by several rubbing simultaneously between the tip and the surface. When probe tip did not touch the surface, the spectrogram was similar to those seen when in between, including the sound spectra of noises caused by air pressure, spindle rotation sound and others. In general, we can summarize the spindle speed frequencies are merged with air pressure sound; this means all the spindle speeds have one frequency, and we can use any speed if does not increase the number of scratches.

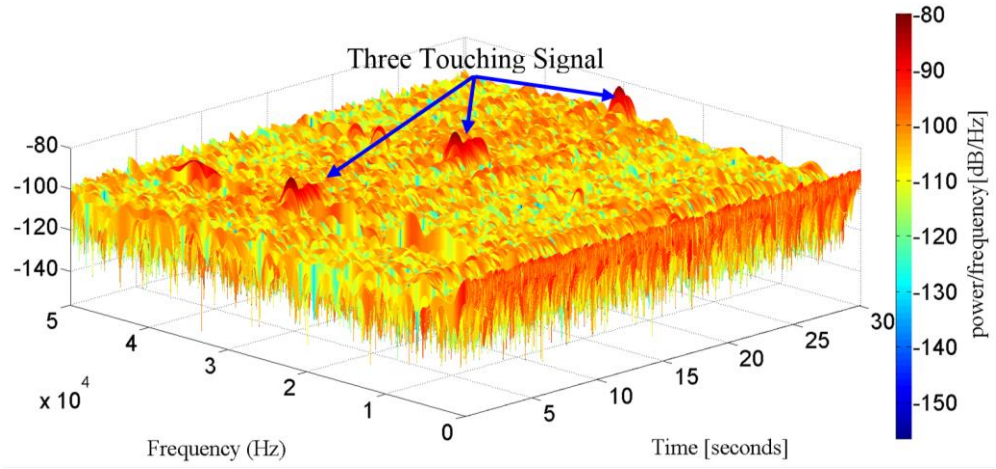

Figure 112 Spectrogram during AE probing

5.5 Signal Filtering

The AE probing measurement system has been challenging tasks in micro probing machine. AE sensor can be used to conduct and to identify the relationship between damage on the measured surface of the component, number of probe tip touches and the threshold level. When the probe tip moves toward at a given approaching feed and speed, and once it touches the measured surface the unfiltered signal exceeds the

threshold, feed motion stops, and it steps back on the same time, AE signals are recorded and identifying the contact point coordinate. So depending on the threshold magnitude selected a larger damage is expected.

To analyze the AE signal, it is essential to eliminate or reduce the noises. The effects of the background noise on the measured AE signal are considerable can be reduced by using the real-time programmable filter which is programmed in MATLAB that is part of the AE measurement system. The noise can also be reduced by decreasing the gain and increasing the threshold. Since the background noises were characteristic frequencies ranges, a bandpass filter is designed with to eliminate the background noise caused by environmental noises, preamplifier, and DAQ card, machine stages and air pressure from burst frequency. The raw signals were amplified and filtered, and its spectrum is illustrated in Figure 113 and Figure 114. Besides, the stages during stopping and returning points generating a signals which collected by the AE sensor and all these signals are unwanted signal or in other words are noises.

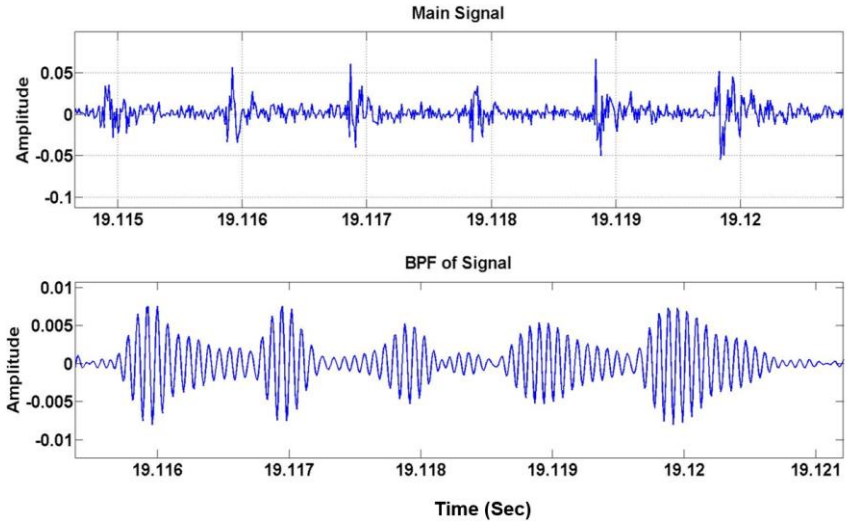

Figure 113 The frequency domain before filtering and the bottom on after filtering

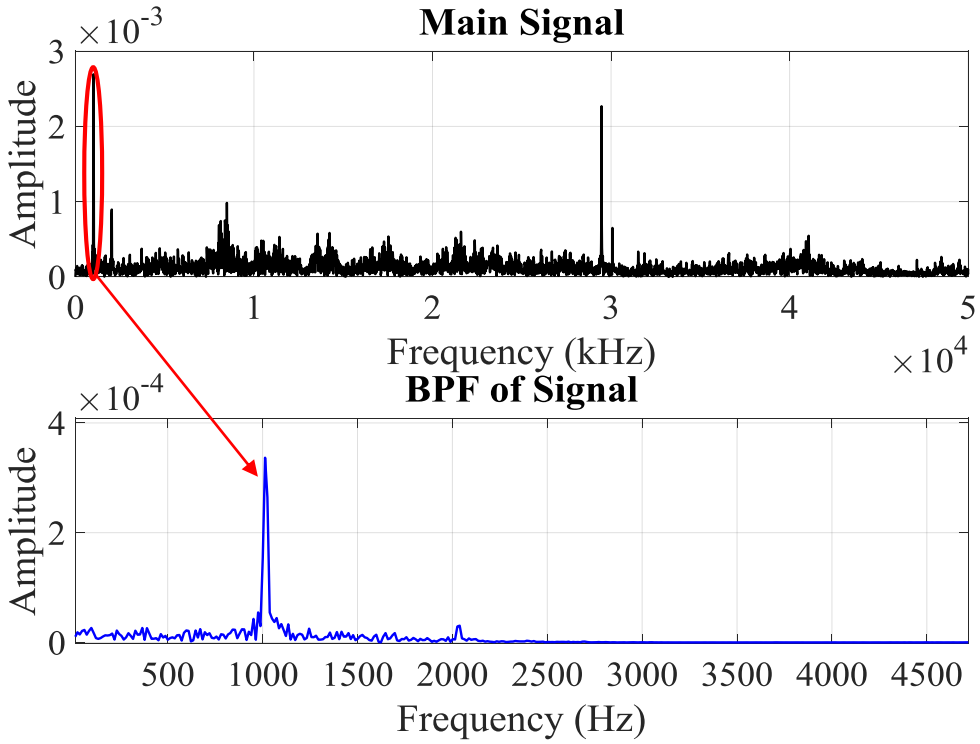

Figure 114 the AE spindle time domain of some spikes before and after filtering

5.6 Burst Detection

The acoustic emission touch-off detection system relied on a high-speed DAQ to capture and process acoustic emission signals via a running program on a PC, and the UMAC controller (PTalkDT ActiveX). A burst of acoustic emission energy was taken to indicate probe tip touch-off. Due to delays inherent in AE signal processing and communication between the micro CNC machine controllers, the effective advance rate of the probe tip was limited to about 50 milliseconds without considering feedback time delay.

The parameters which can be extracted from the probe tip sensing AE signal depend on the type of the signal. For the burst of generated AE signals, the parameters are AE energy, single rise time, AE event, AE counts, AE count rate, and AE peak amplitude as shown in Figure 115. The AE count is the number of times that the probe tip sensing AE

signal crosses the recommended threshold limit. AE count rate is the rate at which probe tip is sensing AE signal counts occur. Energy generated by the probe tip sensing in AE signal corresponds to the energy released by the probe tip. The duration (t_{AE}) is the time between the first and the last crossing of the AE threshold.

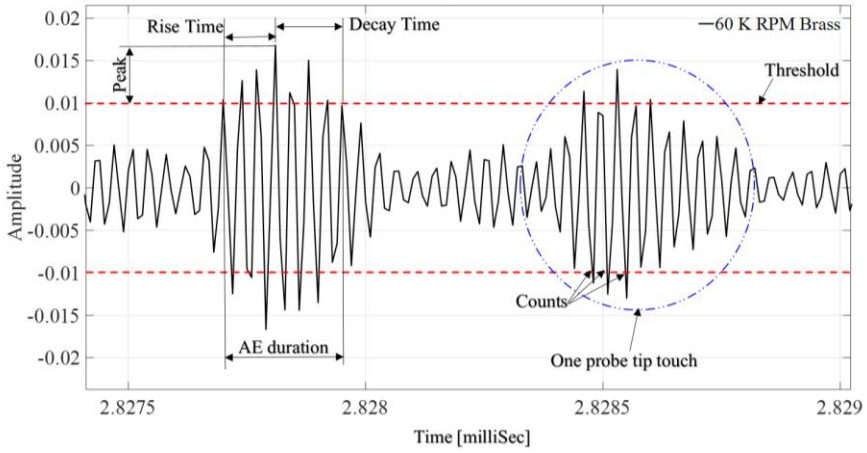

Figure 115 the burst of the probe tip sensing filtered AE signal and its characteristic parameter

Based on Figure 110, the number of AE counts (C_{AE}) is 7, the probe tip sensing AE signal amplitude 16.81 millivolts, AE duration:

(t_{AE}) is ≅ 0.25 milliSec.

AE count rate (Cr_{AE}) can be determined by:

$$Cr_{AE} = \frac{C_{AE}}{t_{AE}} \tag{5.1}$$

$$Cr_{AE} = \frac{7}{0.25 * 10^{-3}}$$

$$Cr_{AE} = 28000/\text{Sec.}$$

5.6 Single Burst Test

As aspect of the acoustic wave that has not been investigated yet is the duration time and the signal amplitude of the acoustic wave. To ensure the AE signal is in fact a burst

signal, AE signals were collected at different probe tip speed. Three different materials were compared, each one having different duration time, and AE signal amplitude. Figure 116 to Figure 118 and Table 15 indicate that the AE signals have different respond at every single rotational probe tip during touches for different materials. It can be seen there is a clear and distinct increase in released energy and touching duration time as the rotational speed increased at constant approaching feed rate. This increase in time at low rational speed i.e. 10K RPM (167 rev/sec) because there is no enough frictional burst to pass the threshold level, so AE released energy is also increased. On the other hand, as it can be seen at high rotation speed the released energy is higher, the touching duration time is less and within the acceleration and deceleration time (default time is 50 mSec.) of the micro Alio machine stage servo motor controller where the Trapezoidal / S-curve profile is considered. The figures also demonstrate that the high volume of a number of touches produces high amplitudes, and this is depending on measured materials type. So we also have to take into consideration the less duration touching time and number of touches as well as the threshold level for each measured materials. Regardless of the different probe tip speed, tested materials, the sparks have a different AE signal amplitude and have a signal duration time between 29 to 45 mSec.

Table 15 the amplitude and total duration time for different tested materials at different probe tip speed.

Materials	Acoustic wave output	Speed		
		10 K RPM	30 K RPM	80 K RPM
Carbide	Amplitude of AE signal	17	29	31
	Duration time – msec.	43	44	31
Brass	Amplitude of AE signal	34	51	115
	Duration time – msec.	36	32	29
Acrylic	Amplitude of AE signal	26	33	52
	Duration time – msec.	42	45	32

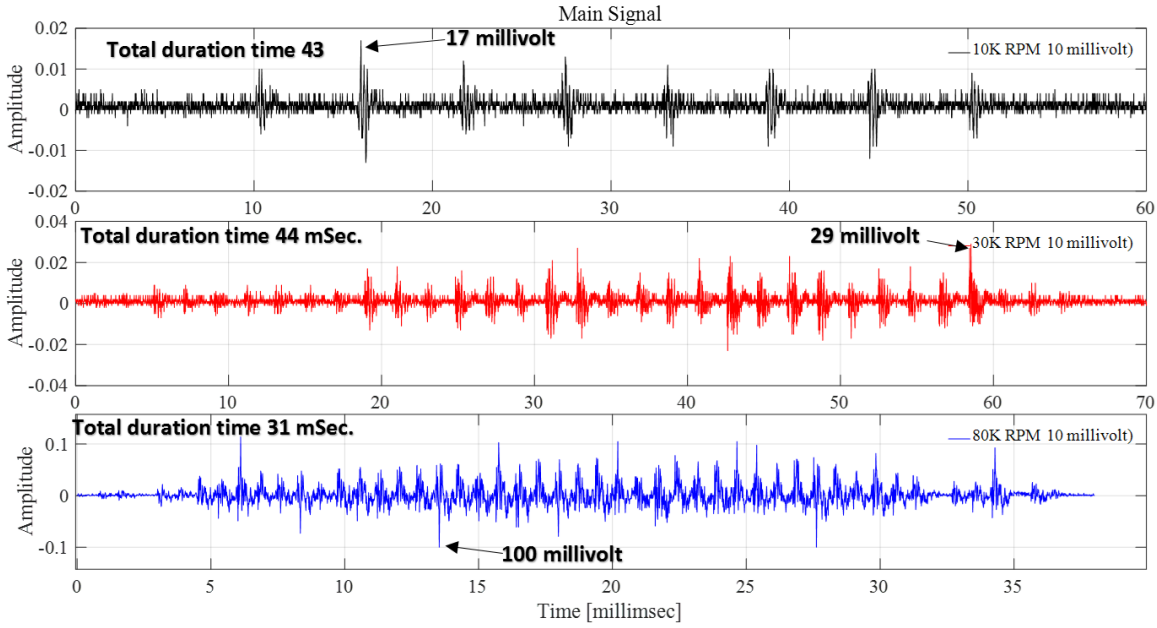

Figure 116 the AE burst signals of three different rotating speed for carbide steel material1 mm probe tip length

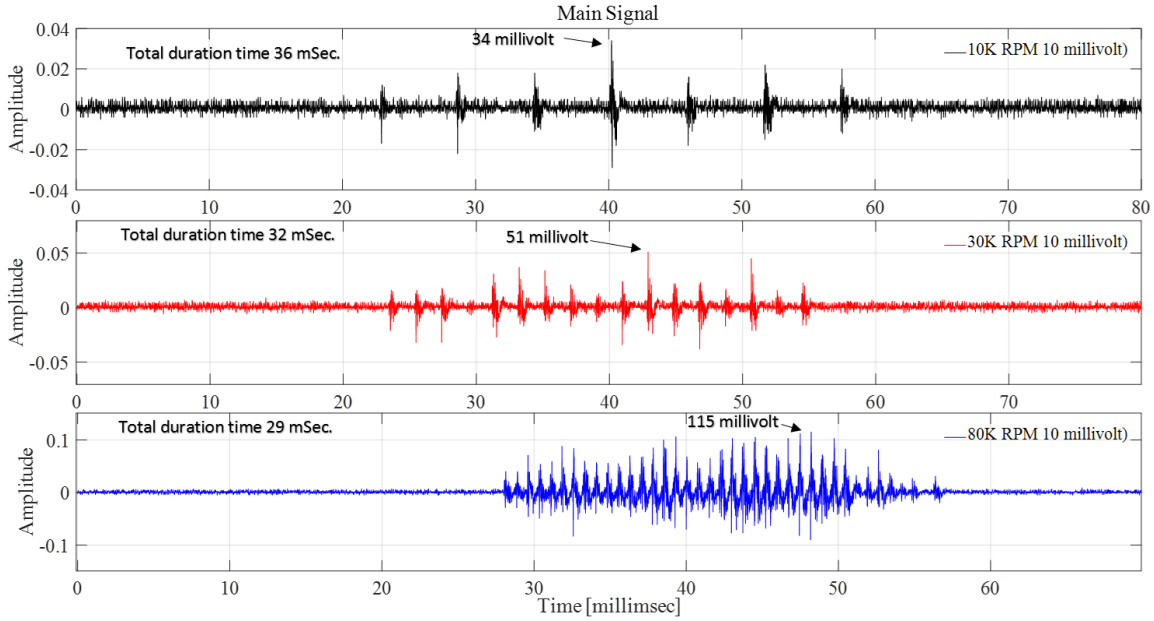

Figure 117 the AE burst signals of three different rotating speed for brass material – 1 mm probe tip length

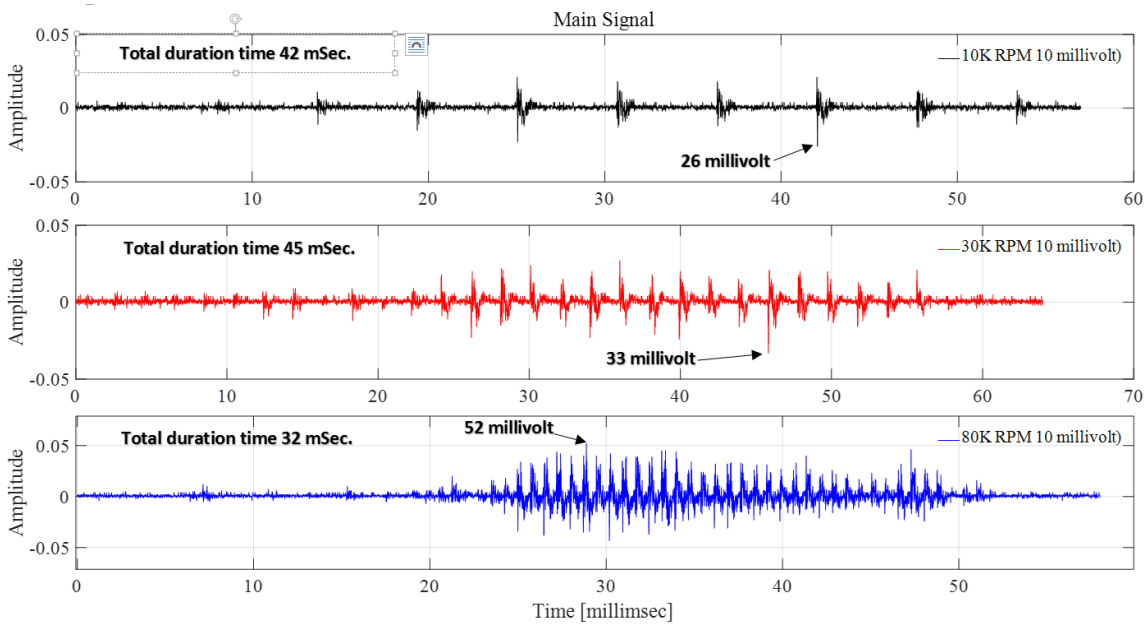

Figure 118 the AE burst signals of three different rotating speed for Acrylic material -1 mm probe tip length

5.7 Power of signal

To understand the behavior of signals we tested the power signal for different materials. The power of a signal is the sum of the absolute squares of its time-domain samples divided by the signal length, or, equivalently, the square of its RMS level.

$$P = \frac{1}{T}\sum_{t=1}^{T} x^2\ (t) \qquad (5.2)$$

Where x (t) describes the signal for time 1 to t.

Figure 119 shows the power for each AE signal for different material at 60 K RPM. The figure shows that the metallic materials have higher power comparing with none-metallic materials. Next section we will examine the power spectral density for each material to figure out the behavior of materials during sensing.

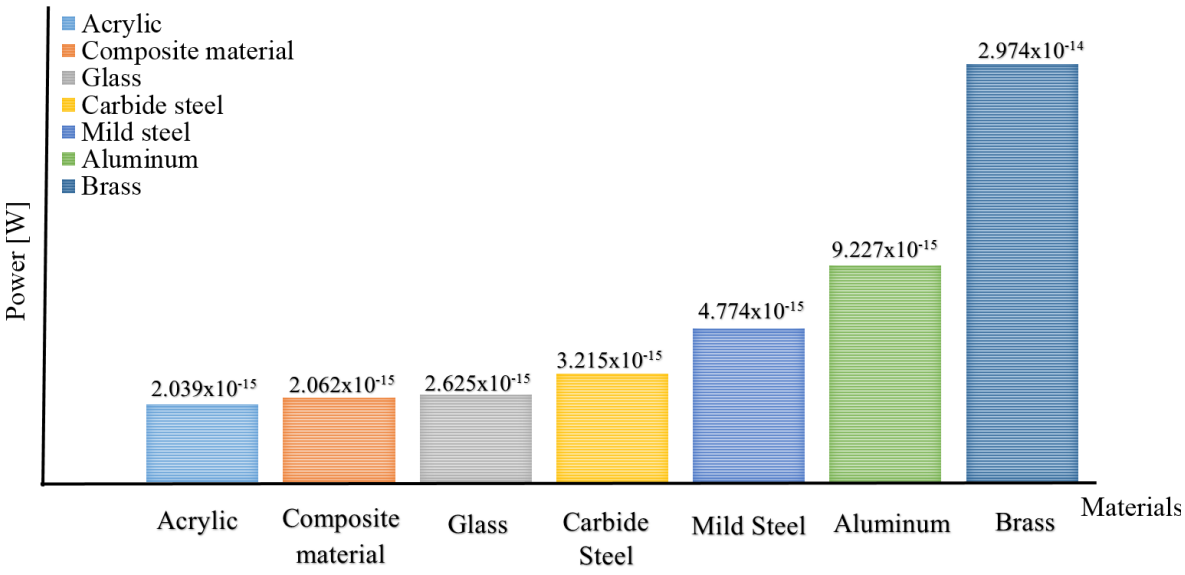

Figure 119 the power signal for each tested materials

5.8 Spectral density analysis

Noise may also be assessed by spectrum analysis. The spectral behavior of acoustic signals for different measured materials is studied during sensing. As seen from Figure 120 and Figure 121 the materials have a different amplitude of energy and as it can be seen it was so low for glass and composite material which means that their frequencies variations are weak. In the opposite, the power spectral density of acoustic emission signals was the strongest for brass followed by aluminum, mild steel, acrylic, carbide composite material and glass. It is also interesting to note that the frequency of AE signal for each material is the same. These results are specific of the WPAES parametars and material properties used for these testes such as the probe tip speed, approching feed, measured material, etc. On the other hand, using the same AE measurement method on a block gauge, teste and compare the effect of three different threshold on power spectral density as shown in Figure 122. We can obtain three very different power spectral density of acoustic emission signals.

It can be seen that the amplitude of the power spectral density of acoustic emission signals increases with increased threshold at the same frequency.

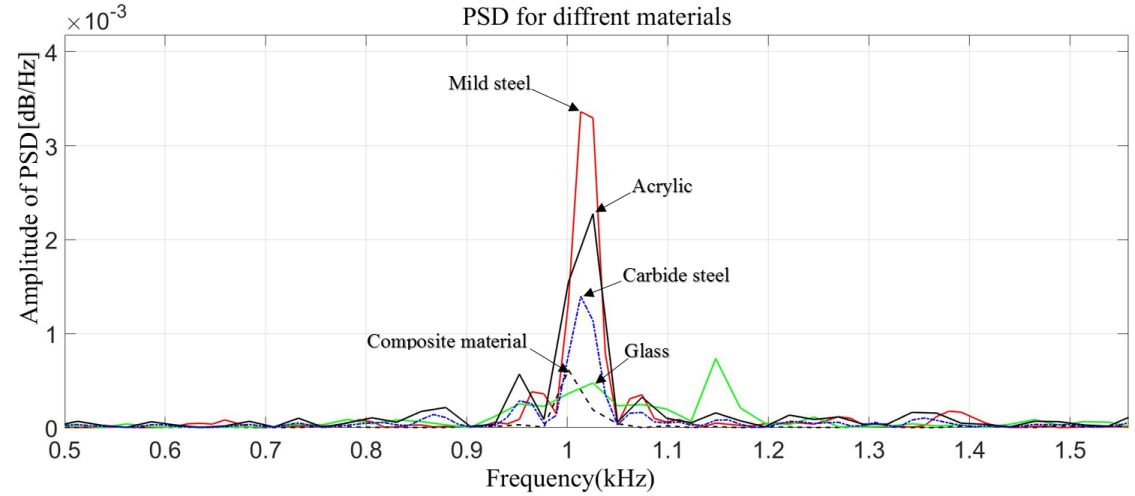

Figure 120 Power spectrum density of five different tested materials

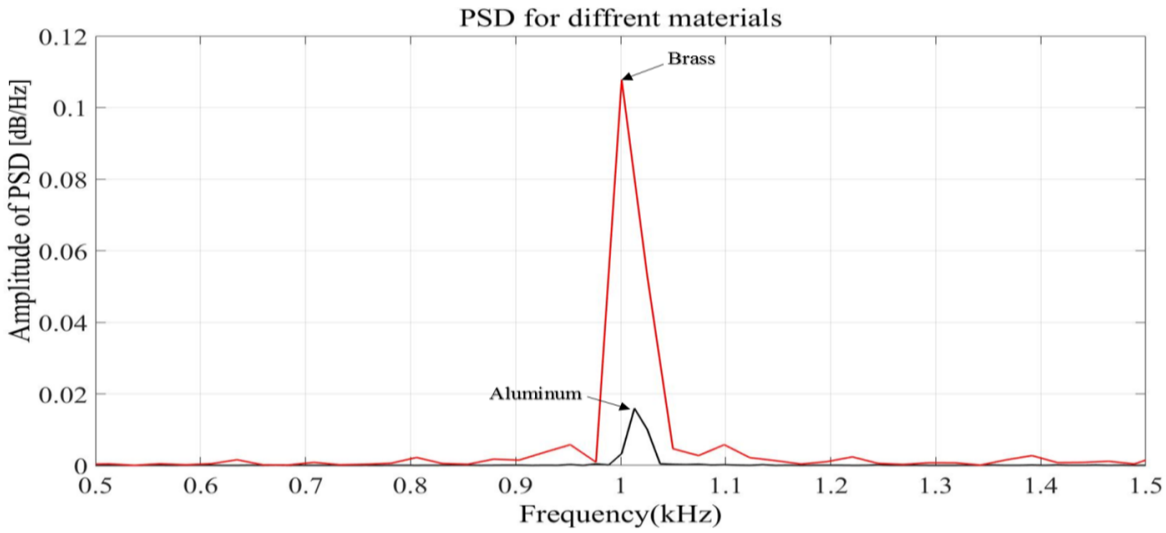

Figure 121 Power spectrum density of Brass and aluminum

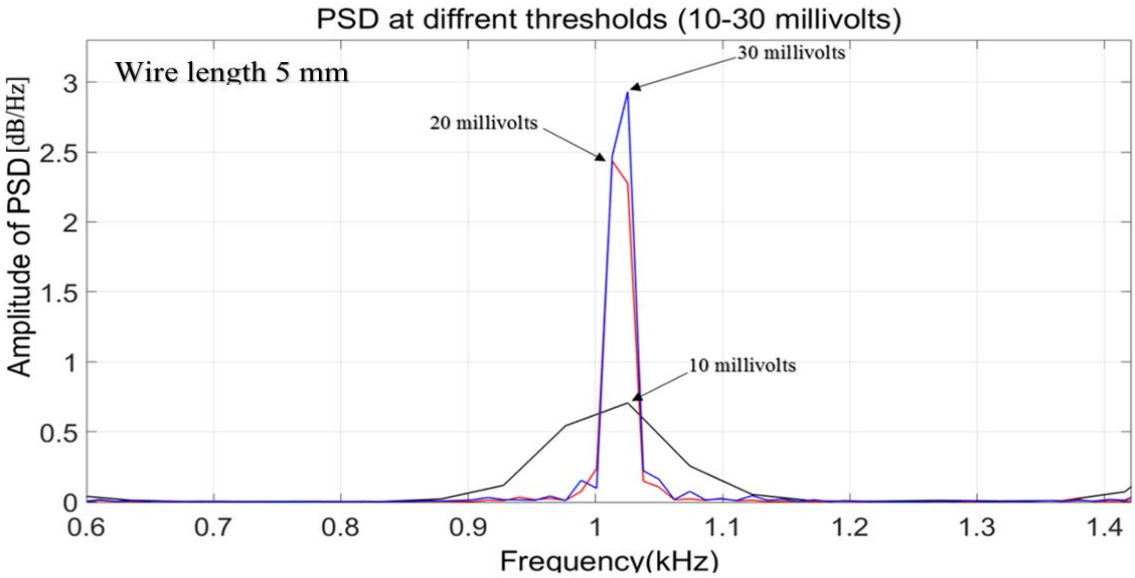

Figure 122 Power spectrum density at different threshold level

Moreover, Figure 123 shows that the sound intensity during rubbing for each selected probe tip speed. As it can be seen from the figure a clear increase in the amplitude of sound intensity as much as the probe tip rotation is increased. The increase of the intensity amplitude or amount of energy released is a function of the probe tip length and selected threshold. On the other hand, it found that the intensity of different materials such as brass, glass, and steel as shown in Figure 124 have almost closer intensity between (-35 and -20 dB), so the geometry of the probe tip and the magnitude of the threshold are the main two factors to determine the intensity of sound during sensing the part surface, and this is due to the impact force between the tip and measured part.

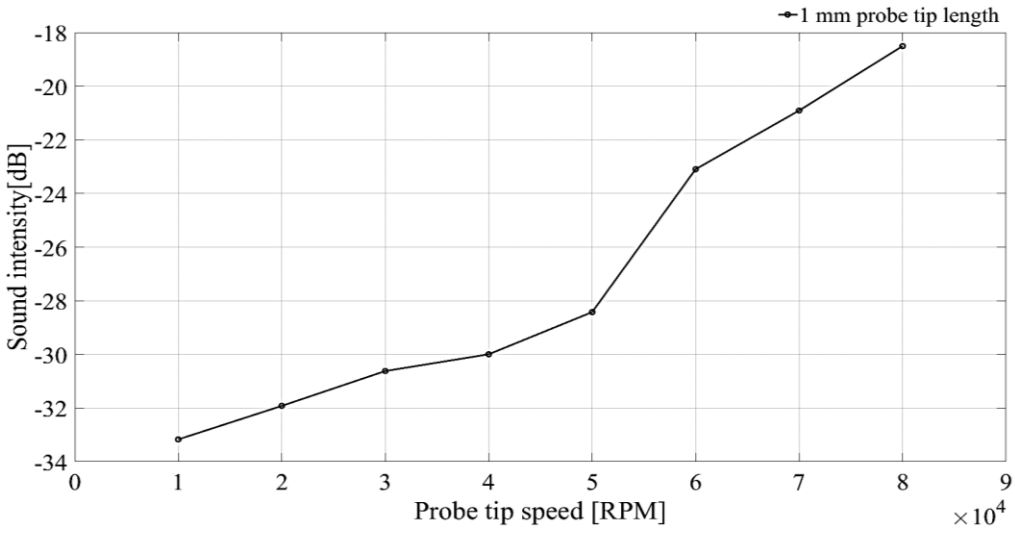

Figure 123 the sound intensity of probe tip during sensing operation

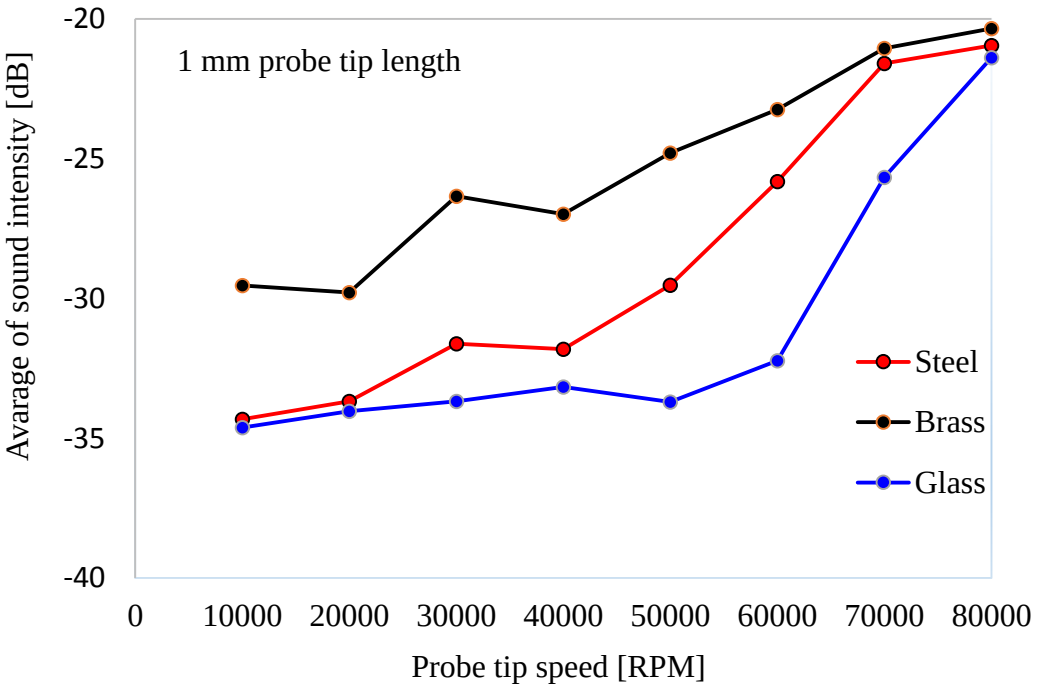

Figure 124 the sound intensity during sensing different materials

5.9 Acoustic emission signal RMS of the raw signal

The RMS is the root-mean-square of AE signal. It presents the average intensity of AE signal and shows the entire strength of AE signal. The experimental test for non-metallic materials (Glass, Fiber glass and Acrylic) can also be seen from AE signal RMS

of the raw signal as shown in Figure 125. The AE signal RMS values from the signal indicate that the while the influence of speed is clear to see, the variation in small RPMs up to 60K RPM does not give significant different because of less power generated at this level of speeds. In opposite only at maximum speeds do there appear to be significant differences in RMS values with 70,80K RPMs because of a high volume of a number of touches. So with the speed increasing, the RMS increases a lot.

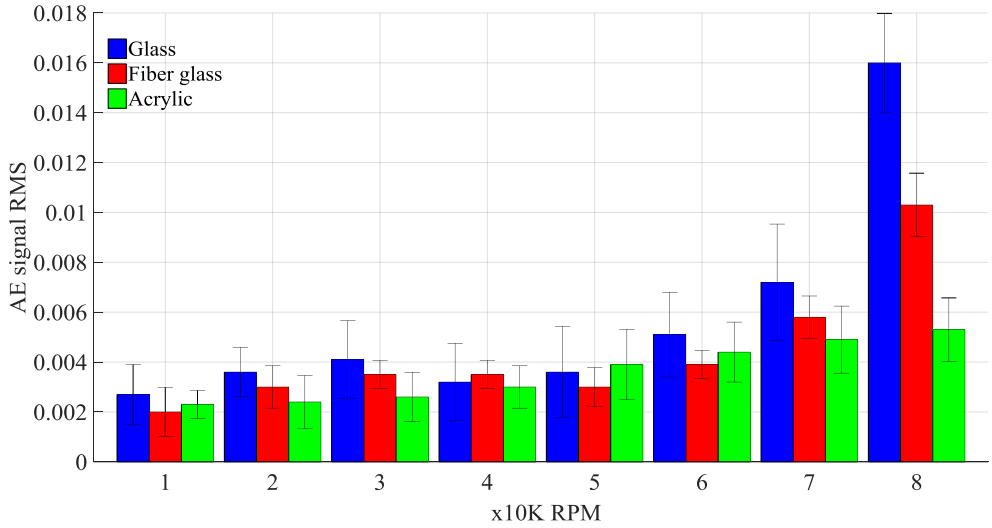

Figure 125 AE signal RMS values from the raw signal of glass, fiber glass and Acrylic materials at different probe tip speeds

Figure 126 shows the average RMS amplitude of the raw AE signal for five different contacted area for carbide steel material. There is very little difference of the average RMS amplitude for the area between 300 and 875 $mm^{2.}$ All tested area including the one less than 300 mm^2 (5 mm block gauge) the RMS values of the AE signals did not effect on the measurements sensitivity as shown in the previous chapter Figure 73 to Figure 77.

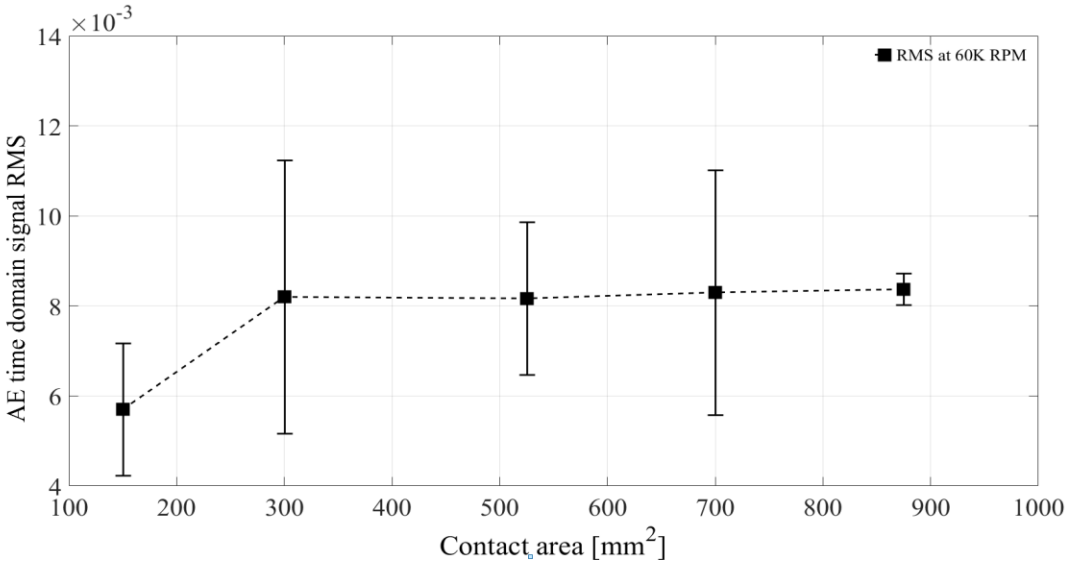

Figure 126 the effect contacted area to signal generation during sensing

5.10 Compensating for background noises

Due to the above background noises that hide the sound of probe tip rubbing which makes the peak amplitude of the tip rubbing is not large enough to cross the threshold. Therefore, a variable threshold was used to avoid this situation. On the other hand, setting the threshold too large will prevent potentially important signals from being recorded but this we increase the number of scratches on the measured surface, and setting the threshold too low will cause the background noise to cross the threshold and will result in a great deal of unwanted data to be recorded and in the meanwhile the machine stages will not move to execute the CNC program. Before filtering the noises, one should notice that the employed threshold is chosen randomly during the experiments, since noises not defined yet. Such region is required in order to find the acoustic emission signal threshold when the probe tip does not to touch the workpiece and to close to it.

FFT already introduced in the last section have been used for AE noise signal analyses. Next, the study will use filter method which could remove noise and interference

partly, but the processed signals could not provide effective data, or it is too complex. For AE signals, bandpass filter will be used to ensure the low and high frequencies are removed giving a resultant quality signal in the middle of these filter.

5.11 Signal to noise ratio (SNR) measurement

Most of the electronic audio devices such as acoustic emission sensors, amplifiers, and DAQ system create some level of electronic noise in audio signals to the signals passing through them or external sounds from the noisy world around us such as mechanical noise. These noises floor (unwanted sound) are usually inaudible to the human ear. The signal-to-noise ratio S/N typically rated in decibels (dB) used to describe how much-desired signal is present in the main signal, as opposed to unwanted signal (noise). The ratio between variance of input (rubbing sound) and variance of noise and it is defined as:

$$S/N = 20 \log10 (V_s/V_n) \quad (5.3)$$

Where the signal strength (V_s) and the noise level is (V_n) in volts.

As mentioned earlier that the preamplifiers are inevitably generating noise. The improving AE measurements system requires the optimization of AE sensor/preamplifier connection and minimization of the preamplifier noise [152]. To improve the SNR and to optimize our system measurements the AE sensor is connected to the preamplifier via a coaxial cable, with 50 Ω BCN connectors at both ends, which transmit the signal. Figure 127 shows the comparison of SNR for the different measured materials, as it can be seen that the SNR is increased as the frequency increased (10-80K RPM). For all measured materials, the SNR increases at a higher frequency (higher RPM) is due to the bandwidth limitation.

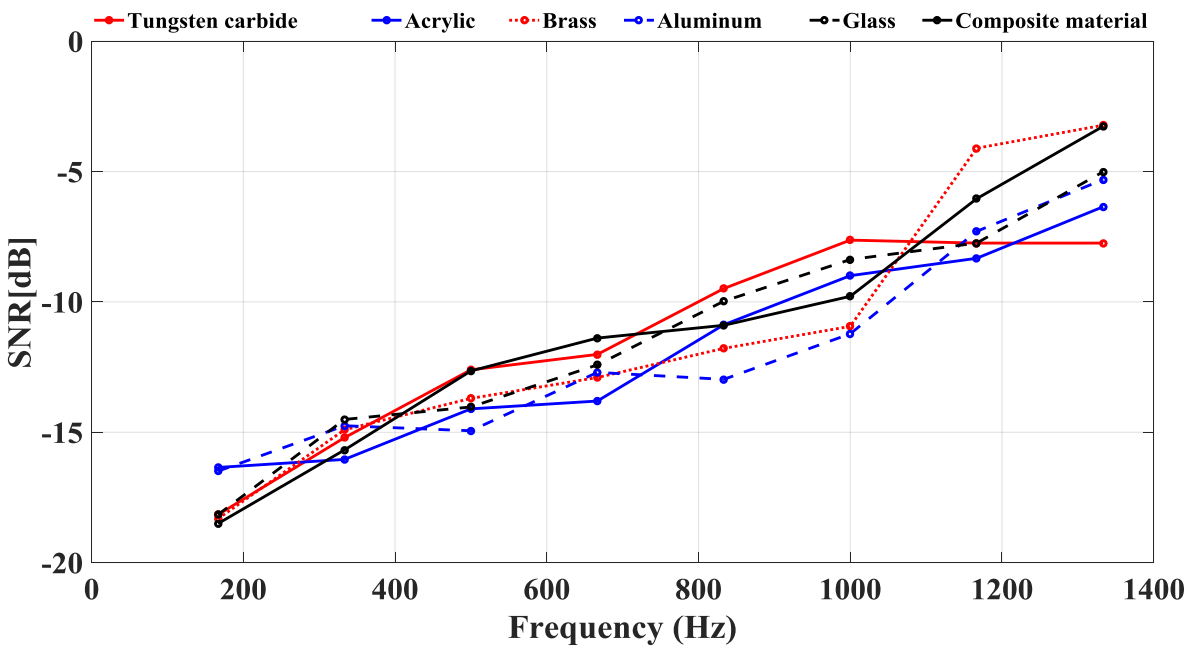

Figure 127 the measured SNR vs. frequency for different measured materials

5.12 conclusion

The acoustic emission signals during sensing have been investigating the unexplained phenomenon in order to understand their cause and to determine if they can be used to provide useful information about the rubbing the measured surface by the rotating wire probe tip.

The speed of the spindle is proportional to the sound pressure level, and the knocking due to rubbing produce sounds have slight variation at different RPM. In general, we can observe that the sound intensity for all RPMs are between (-34 and -18 dB) and the sound generated during rubbing is proportional to the probe tip length (dB α L). Moreover, the SNRs for different materials are much higher at RPMs, and this will effect on the threshold.

Acoustic emission signals during the surface measurement are primarily influenced by dynamic impact behavior for each measured material type, each corresponding to the

unique amplitude of energy at same frequency band and constant wire probe tip length. This finding that the realized energy of the physical impact or dynamic response of the measured surface at the touch point may be associated with component physical properties.

In conclusion, this work in this chapter has focused on determining the cause and interpretation of AE signals during measurement. Results have shown a strong relationship between rotational speed of probe tip effects and a number of probe tip touches and how they influence AE spike behavior and amplitude.

Chapter 6 - Micro-scale hole profile measurement using rotating wire probe and acoustic emission contact detection and scanned features

6.1 Introduction

Recently, a cost effective probing system was developed based on a probe that consists of a rotating wire and touch detection with an acoustic emission sensor. After being evaluated for its repeatability and potential surface deformation, this probing system was, shown to be a promising tool for the measurement of micro-scale holes. In this chapter, a wire-based rotating probe, and an acoustic emission touch detection system is used to measure the inside of micro-scale holes.

In order to reduce the effective rotating diameter of the probe, straight wires are used instead of bent wire, and resulting elastic wire bending, due to the centrifugal force during rotation, is utilized. Micro-scale holes as small as 0.5 mm in diameter are measured using the method. Micro-scale holes with different diameters were fabricated using femtosecond laser machining. The roundness and cylindricity of the micro-scale holes is also characterized in this work.

First presented in this chapter is the fabrication of the wire probe, followed by the experimental setup for the measurement of micro-scale holes. Since centrifugal forces result in the probe's wire bending, the effect of spindle speed on the rotating effective diameter (De) of the probe at different overhang lengths is investigated. Three micro-scale holes were fabricated at targeted diameters of 1.0, 0.8, and 0.5 mm, with the femtosecond laser machining setup as described. Measurement of the micro-scale holes was conducted and the results are as presented, followed by analysis.

6.2 Experimental procedure

6.2.1 Fabrication of the rotating wire probe

The wire probe tip was fabricated using several pieces of the stainless steel micro tube (Stainless Steel 304). First, three segments of micro tubes were cut to an appropriate length and adjusted further in length using a grinding machine. Second, the smallest tube was inserted concentrically into the next largest tube, continuing by inserting this assembly into the third and largest tube concentrically, creating a final assembly of three concentric tubes. The binding agent between these tubes was a thermal glue manufactured by Universal Photonics Company, setting at 85ºC. The largest tube's outer surface was used as a shank to fit into the spindle.

The stainless steel wire probe tip – with a diameter of 0.152 mm – was cut and bonded within the smallest tube diameter using 85˚C thermal glue, as shown Figure 128. Due to the tolerance stack-up between the inner, outer, and wire diameters, inevitably, there was an offset of δ between the spindle and probe axis of several microns. This offset affected the resulting De size; however, it did not affect the measurement operation. De is determined after calibration of the probe as an assembly. The system is then evaluated against calibration artifacts, followed by measurements of machined micro-scale holes.

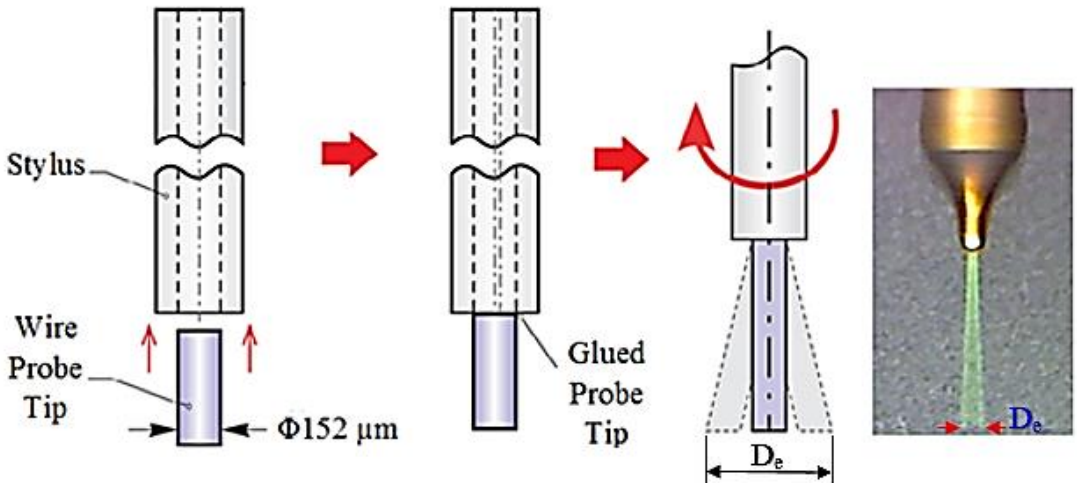

Figure 128 Procedure for probe fabrication using Ø152 µm diameter wire and a photograph of fabricated probe

6.2.2 Experimental setup

The inside dimensions of the micro-scale holes were measured using a precise, custom-made CNC machine (ALIO Industries). Also, the ultimate resolution can be estimated for our system is 50 µm. The resolution of the XYZ stages is 100 nanometers. The probe is rotated using an NSK E3200 spindle with the maximum rotational speed up to 80,000 rpm. A Physical Acoustics Nano 30 acoustic emission (AE) sensor placed beneath the fixture plate that holds the sheet with micro-holes. The AE sensor was used to detect contact when the rotating probe was translated using the linear stage within the micro-holes. A model of the experimental setup is shown in Figure 129.

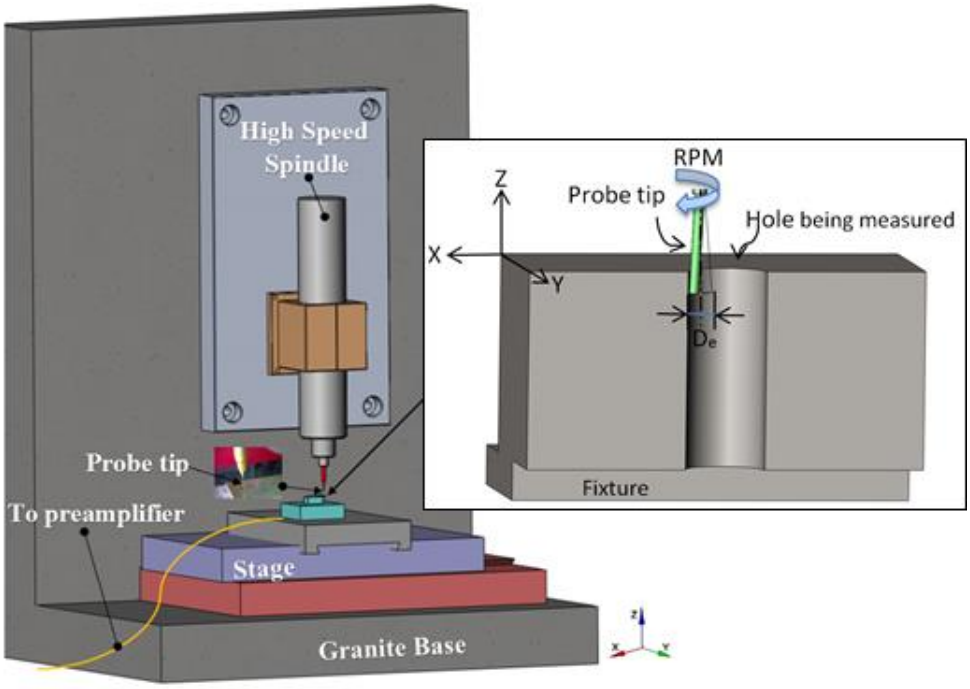

Figure 129 Experimental setup of the micro-hole profile measurement system

6.2.3 Preparation of micro-holes

Three micro-holes of 0.5, 0.8, and 1.0 mm diameters were prepared by drilling a 1 mm thick steel plate using a Ti: Sapphire femtosecond laser (seed laser: Millenia -Tsunami, amplifier: Spitfire-Empower) by Spectra Physics with the central wavelength of 800 nm, pulse duration of approximately 120 fs, repetition rate of 1 kHz, and maximum continuous equivalent power output of up to 800 mW. A 20x Mitutoyo LWD objective lens was used to focus the beam and machine the hole. The holes were machined by moving the laser beam helically down in the Z-axis. An optical profiler (Zeta-20, Zeta Instruments) was used to image the holes and measure the hole profile at the top and bottom, and the images are shown in Figure 130 for 0.5, 0.8, and 1.0 mm diameter holes, respectively, The heat, affected zone on the edges of the top side of the laser-cut hole can be observed. The heat affected zone is due to the laser heat build-up as the laser continues to ablate material from

the top to the bottom. The holes from the bottom do not seem to be perfectly circular, which may be due to errors associated with the laser machining process.

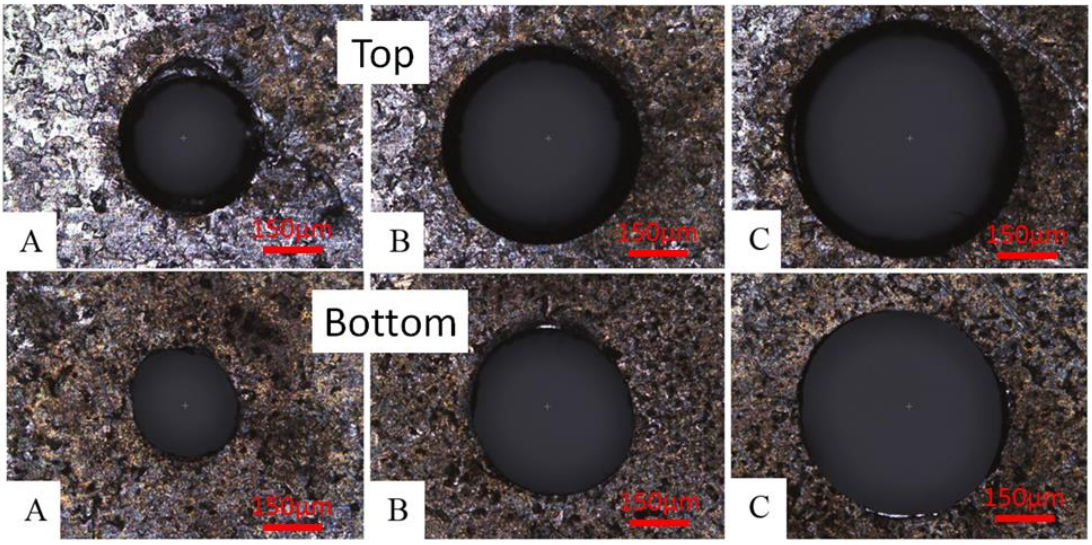

Figure 130 Optical profiler top and bottom images of the micro-scale holes: (A) Ø0.5 mm, (B) Ø0.8 mm, (C) Ø1.0 mm

The heat affected zone can be more clearly seen in the SEM images shown in Figure 131. The heat affected zone seems to be tapered to a certain point in the hole. Diameter measurements from the SEM images are also shown in Figure 131. The taper at the top of the hole can also be observed from the images of the optical profiler measurement. It is also observed that hole periphery area is bulged up, tapered, and this was well captured by the optical profiler. However, the optical profiler was not able to measure the inside the hole due to the limitations associated with the optical method.

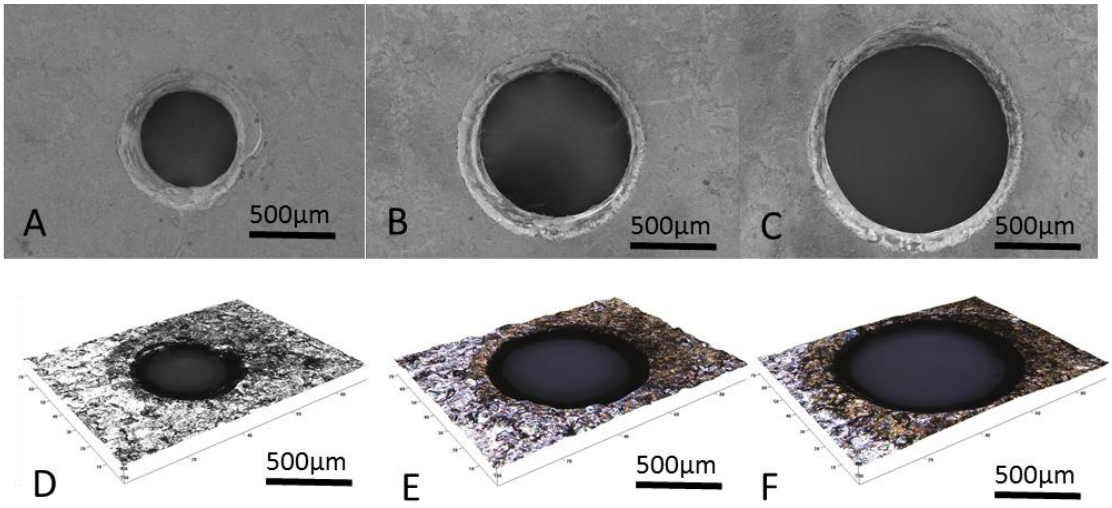

Figure 131 SEM images (A, B, C) and Optical profiler images (D, E, F) of the top of the micro-scale holes: (A, D) Ø0.5mm, (B, E) Ø0.8mm, (C, F) Ø1.0 mm

6.3 Calibration

Before measuring a micro-hole, the probe needs to be calibrated against a reference object. Calibration was necessary to determine the probe's effective diameter (D_e). The D_e of the rotating straight probe tip was measured using a 20 mm width (B_w) block gauge (Mitutoyo Grade 0) for precise measurement (Figure 132). Because the block gauge may not be positioned perfectly perpendicular to the approach direction for contact detection, contact positions at multiple locations on both sides of the block gauge were determined in order to compensate for the tilt angle (θ) between the block gauge width and the approach direction. From the contact positions from both sides, the tile angle can be calculated, and the length L can be determined. Then, the effective diameter (D_e) can be calculated by subtracting the length L from the average length between contact positions of both sides (P_w, see Figure 132).

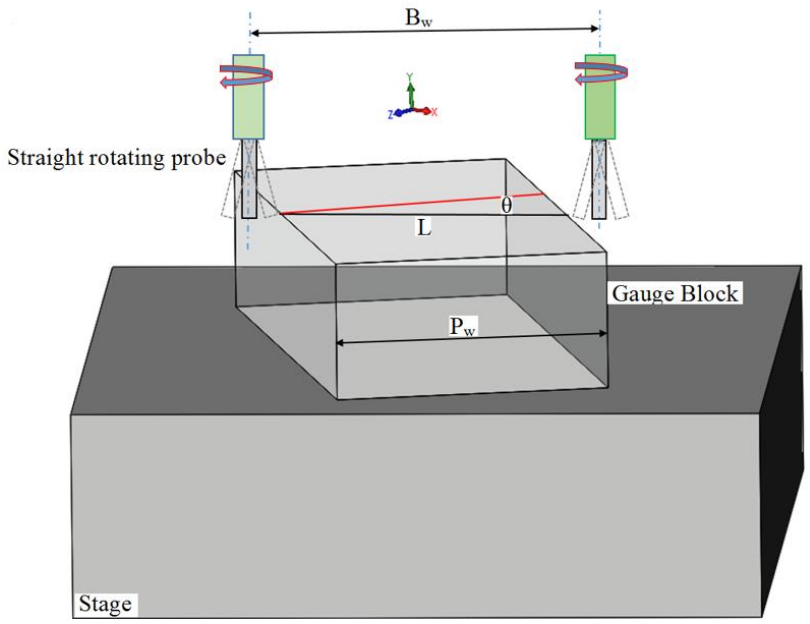

Figure 132 Diagram for the effective diameter (D_e) calibrations

6.4 Micro-hole profile measurements

In order to measure the hole profile, the wire probe tip was carefully inserted into the center area of the hole and was then rotated. The probe was then translated at 0.05 mm/s to the side of the hole at a given feed rate until the tip came into contact with the surface. The AE signal is generated as a result, due to the contact between the rotating wire tip and the side surface of the hole. The AE signal was sampled at 100 kHz and sent to the control software. The signal processing module determined the point of contact between the probe and the component using the threshold value of 10 mV. When the magnitude of the AE signals crossed the threshold point, contact was detected, and the wire probe was stopped. This was accomplished by calling a function in the command manager to generate a command for the CNC controller, as shown in Figure 133. Pulses generated due to subsequent AE signals were neglected. The contact coordinates of the probe were also recorded and the probe immediately returned to the start position. An automated scanning algorithm was

developed and a controller software was developed to perform point-to-point scanning . The controller allows automated scanning of a hole in the X-Y plane regardless of the hole diameter or geometry. From the hole center, the probe was moved in the X direction to measure two initial positions of the hole surface. Then, the approach direction from the hole center was determined for the next position based on the measurement of the two initial positions. The approach directions for subsequent positions were then determined from the previous two measurements until the probe passed the original approach direction. The probe was then lowered in the Z direction to measure the hole profile in the next X-Y plane. The measurement of the X-Y plane profile of the hole was repeated until the bottom of the hole was measured. Each circle in the X-Y plane was measured at uniformly distributed positions using the automated scanning algorithm, and these planar measurements were conducted at 20 sections along the Z-axis with 50 µm increment.

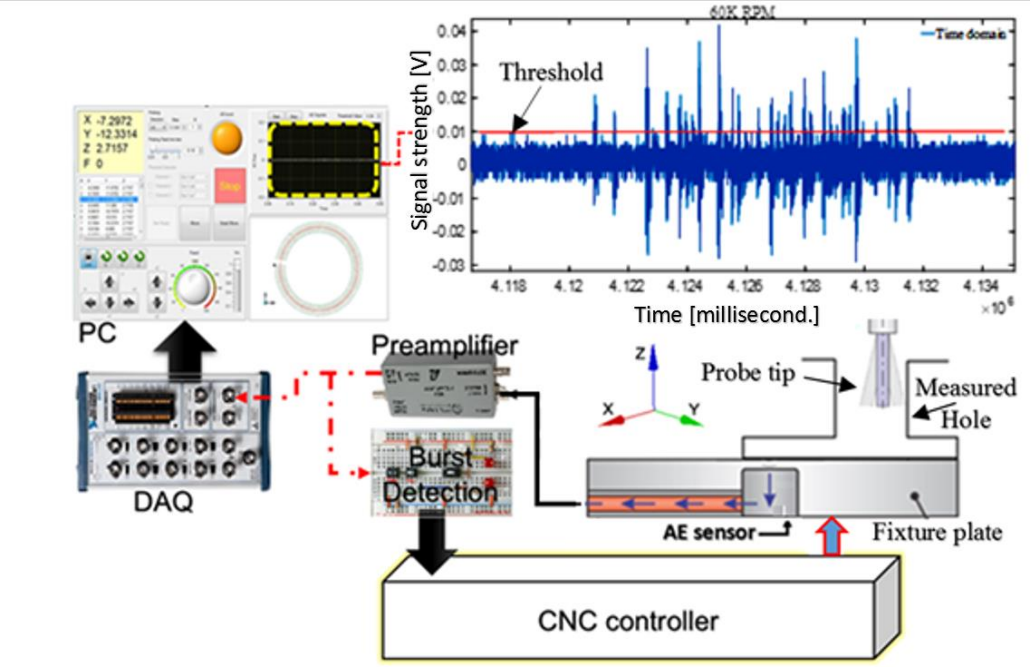

Figure 133 Micro-hole probing measurement AE system

6.5 Experimental results

6.5.1 Effect of spindle speed on the effective diameter

When measuring the inner surfaces of a given hole, the effect of the spindle's centrifugal force on the probe tip is driven by the angular velocity (i.e., revolutions per minute [rpm]). The resulting elastic deformation or bent angle of the probe tip defines the effective diameter (D_e), which is dependent upon the selected wire length and the rotational speed of the spindle. An initial study was carried out to explore the effect of varying spindle speed on the D_e of the probe wire tip of diameter 157 μm. Four different wire probe tip lengths were used (2, 4, 6, 8 mm) at different spindle speeds of 10,000 - 80,000 rpm. The results of these measurements are summarised in Figure 134.

This shows the effective diameters of the four different wire lengths of each probe tip as a function of spindle speed used. As expected, the effective diameter increases as the spindle speed increase at all probe tip lengths. At probe tip lengths greater than 4 mm, the effective diameter continuously increases as the spindle speed increases, indicating that wire bending causes increase in mass imbalance and consequently more bending. At probe tip length smaller than 4 mm, the effective diameter seems to stabilize with the increase of the rotational speed, which is desired for measurement precision. This indicates that at shorter wire lengths, the probe is less affected by the mass imbalance and shaft dynamics. In this work, the probe tip length of 2 mm and the rotational speed of 60,000 rpm were selected to measure the hole profiles. The spindle speed of 60,000 rpm was selected because the AE sensor is more sensitive at higher spindle speeds. The effective diameter of the probe at the probe tip length of 2 mm was measured to be 302.2 μm.

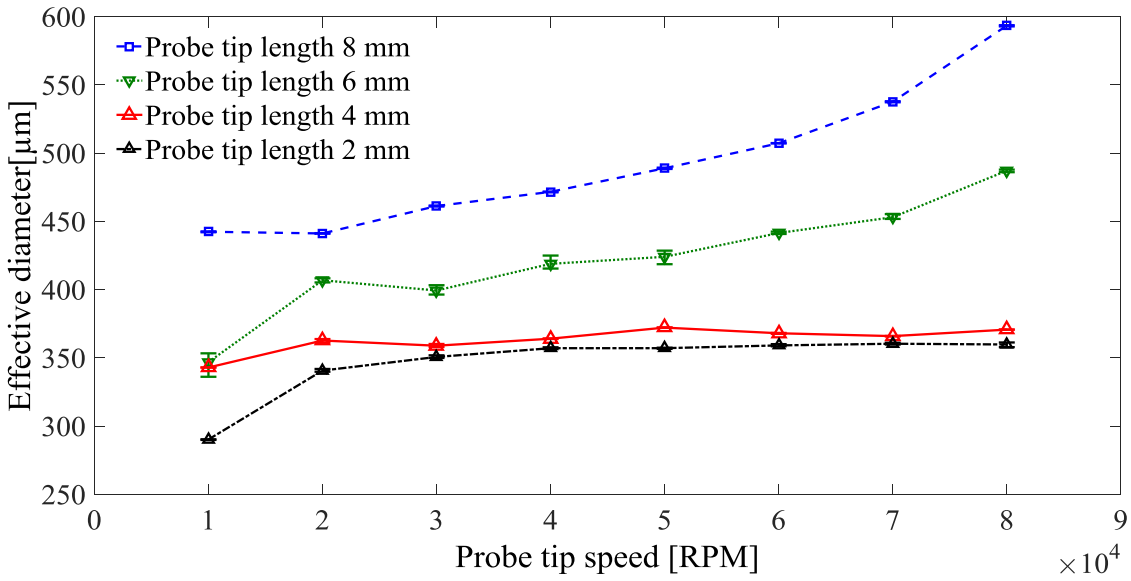

Figure 134 Relationship between the rotational speed [rpm] and the effective diameter (D_e)

6.5.2 Repeatability test

In order to evaluate the repeatability of the probing system, the wire probe rotating at 60,000 rpm was contacted against a Mitutoyo gauge block (ASME grade 0), and the detected contact position was recorded. The contact detection was repeated at the same location 100 times. The detected contact position variation is shown in Figure 135. As shown, the contact position varies within ±0.2 μm. The standard deviation of the variation for the repeatability measurements is $\sigma = 0.126$ μm. The repeatability measurement results show that the probing system is capable of dimensional measurement within submicron precision.

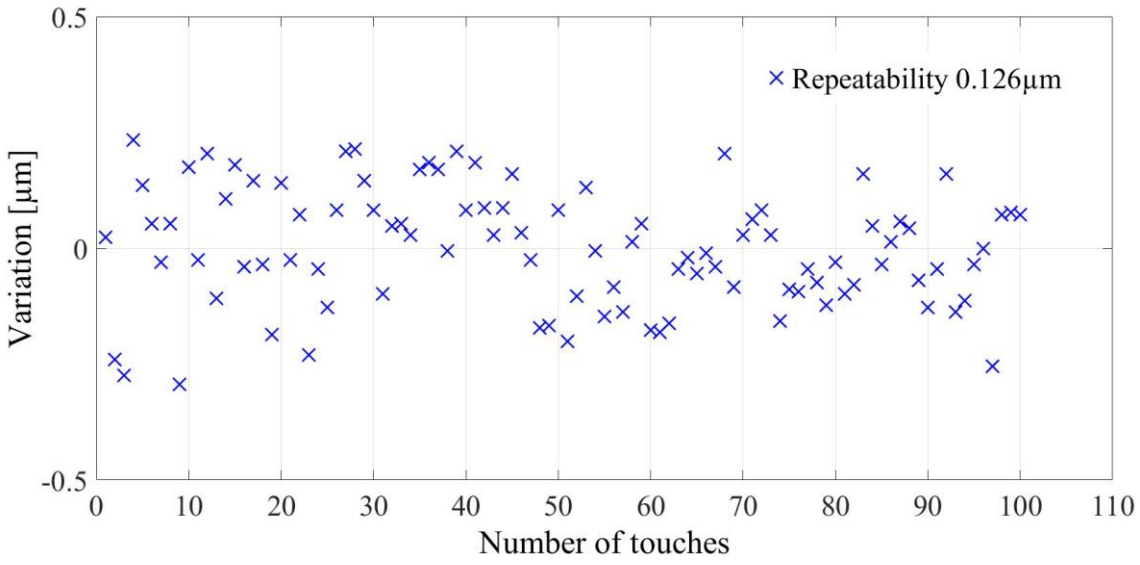

Figure 135 Repeatability results against a gauge block

6.5.3 Micro-hole measurement

The measurement results for three micro-holes are shown in Figure 136, which shows measured points after compensation of the effective diameter. It shows that the probing system is able to measure inside micro-holes, and the automated scanning method successfully measured contact positions against inner surfaces of the hole. As shown, the taper at the top of the holes can be clearly seen as well as the variation in the diameter. There seems to be slightly more variation in the measurements with the Ø0.5 mm hole. This may be due to the difficulty involved with the laser fabrication process as the hole diameter is decreased. Laser focusing becomes more difficult with smaller diameter holes. Also, the focused laser is more affected from the focused laser at other positions with the smaller diameter hole because the laser beam is much closer to each other.

Figure 137 shows a comparison of the measurement points with cross-sectional measurement of the holes using an optical profiler. It shows that the measured points match well with optical profiler measurements. However, the optical profiler measurements are

noisy close to the walls, and the measurements at the bottom of the holes are not correct. As shown, the optical profiler fails to measure the 0.5 mm diameter hole, whereas the probe was able to measure the inside hole profile close to the bottom.

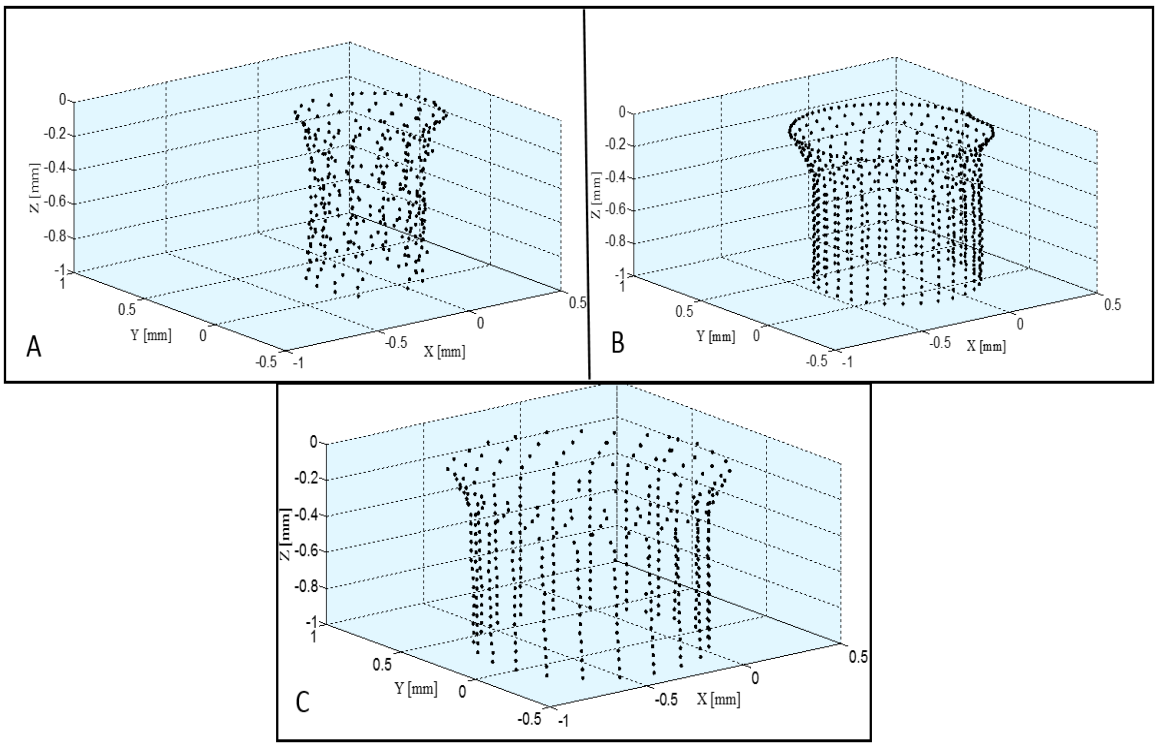

Figure 136 Measured points for (A) Ø0.5 mm hole, (B) Ø0.8 mm hole, and (C) Ø1.0 mm hole

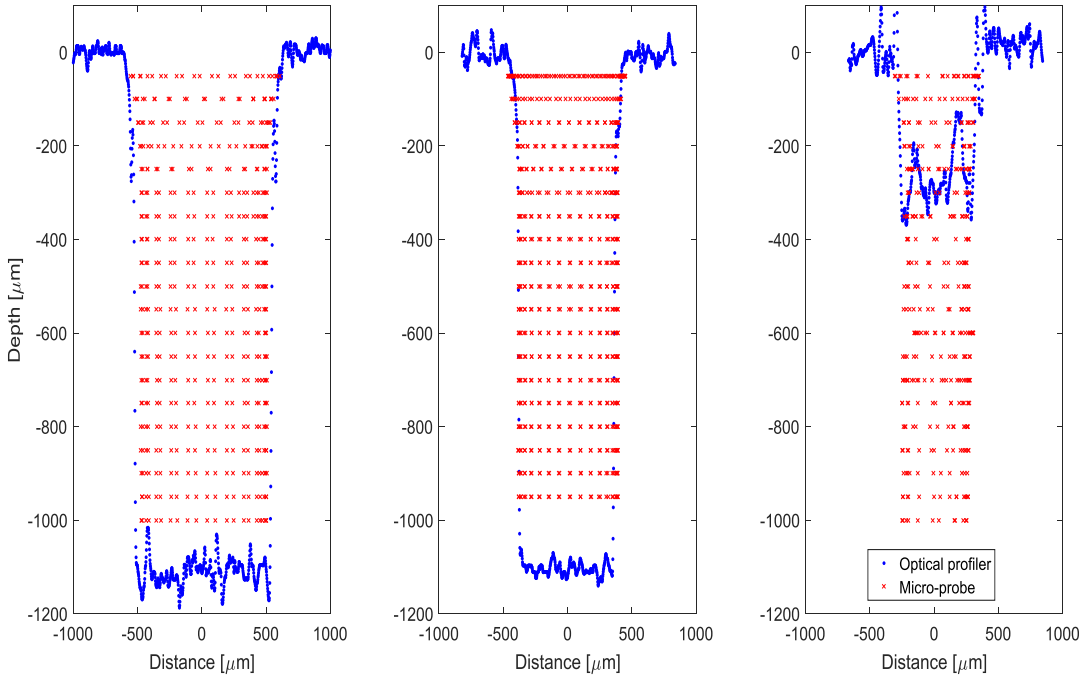

Figure 137 Comparison of measured points with optical profiler cross-sectional measurement

The diameters of the three measured micro-scale holes against hole depth are shown in Figure 138. The diameter of the hole at each depth was calculated by fitting a circle to the measured points using the least square method. As shown, the hole diameters near the top are greater than the diameters deeper into the hole due to the taper. Also, as mentioned previously, the variation in diameter is greater for the Ø0.5 mm hole.

The out-of-roundness values represented by the distance between the highest peak and the lowest valley are shown for different depths in Figure 139. The least square method was used to calculate the out-of-roundness values [37]. It can be clearly seen that the out-of-roundness values are much larger and fluctuate much more with the Ø 0.5 mm hole. It is also interesting that the out-of-roundness value fluctuates at different hole depths. This

must be related to the laser machining process. This indicates that the probing system can be used to evaluate the inequality of micro-holes.

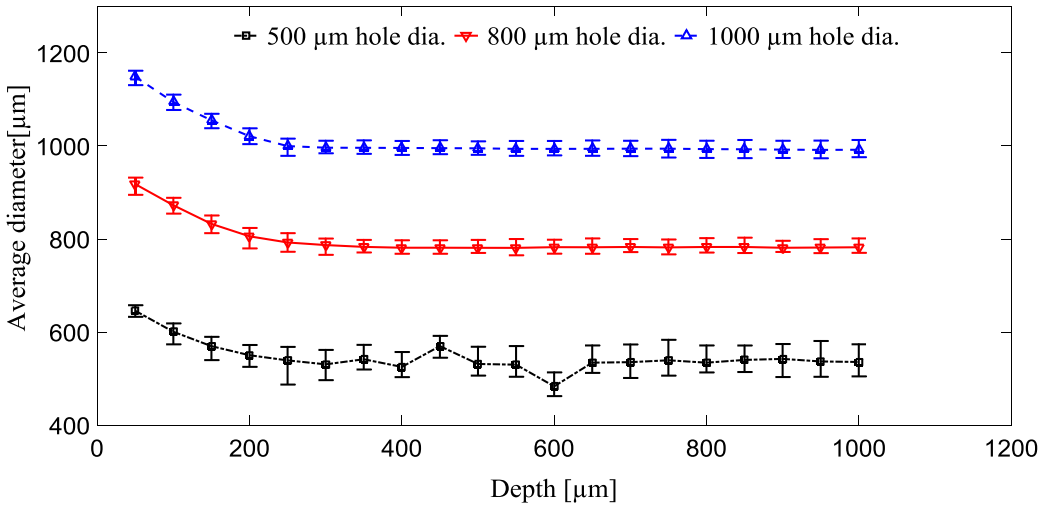

Figure 138 Diameter as a function of depth.

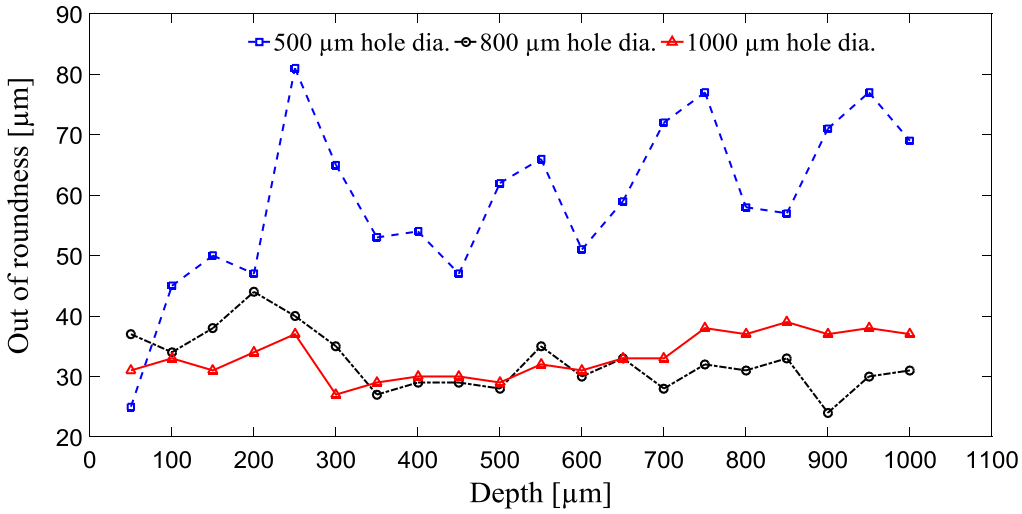

Figure 139 Out-of-roundness values as a function of depth.

In order to observe the hole profile in each X-Y plane, TrueRond software supplied by the TrueGage Surface Metrology was used. Figure 140 shows the hole profiles at hole depths of 100, 500, and 1000 µm from the top of the hole. As can be seen, due to laser machining errors and redeposition of micro-debris during machining, the hole is not

completely circular. This may also be due to errors in the circularity of the laser beam. This shows that the probing system is capable of capturing the profile inside the micro-holes.

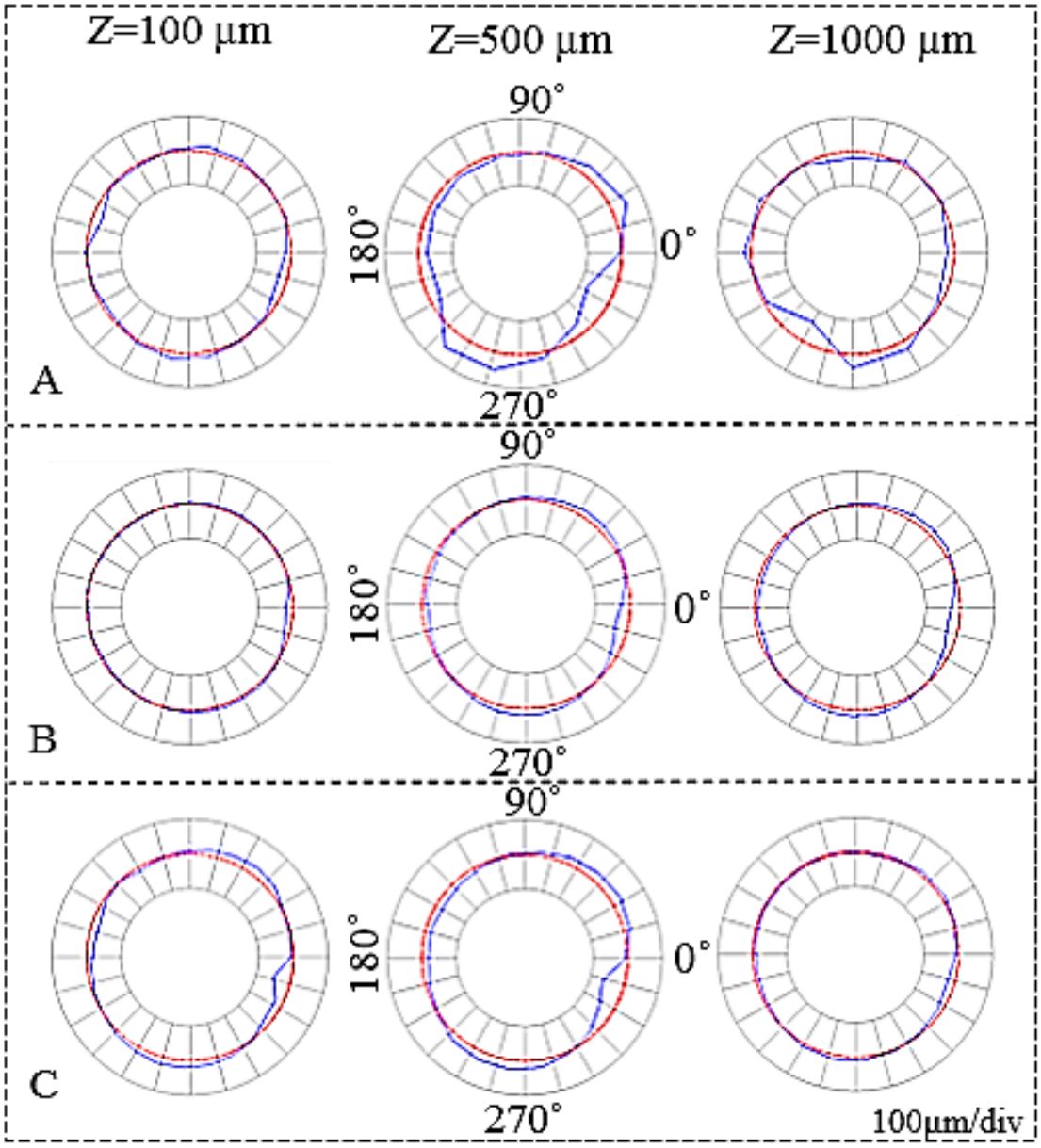

Figure 140 Hole measurement results at different depths: (A) Ø0.5mm, (B) Ø0.8mm, (C) Ø1.0 mm

To further examine the ability of the probing system, a semi-circular hole as shown in Figure 141 was machined from a 1 mm thick steel plate using the femtosecond laser

machining system. Also, the semi-circular hole was machined in order to be able to visualize the interior of the hole and verify the diameter variations inside the hole. Figure 141 shows optical profiler images of the top, bottom, and side views of the semi-circular hole. From the top and bottom views, it can be seen that the diameter measurements are different. Also, from the side view, the taper and irregularity in the interior of the hole can be seen. This implies that inner hole quality evaluation of micro-holes is important. The semi-circular hole profile measurements were conducted and the results are shown in Figure 142.

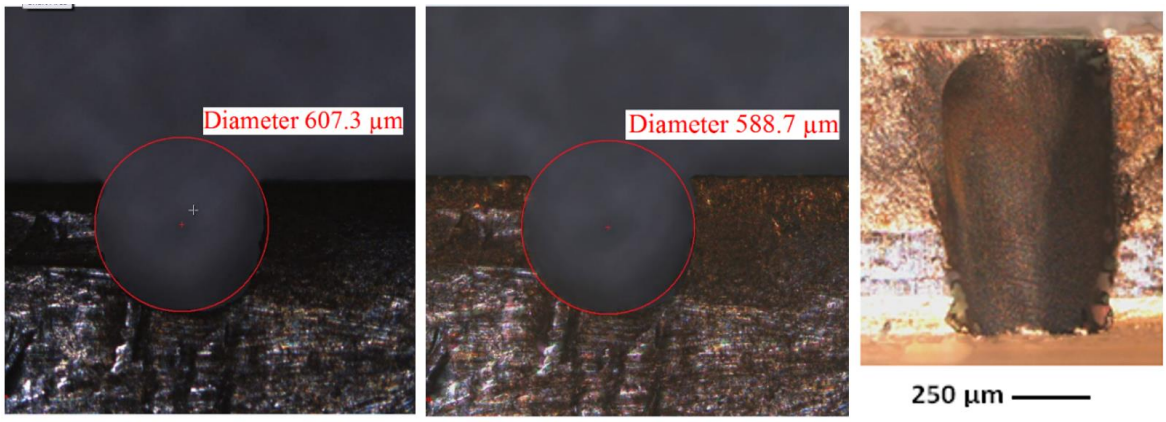

Figure 141 Optical profiler images of the top, bottom, and side views of femtosecond laser machined semi-circular hole

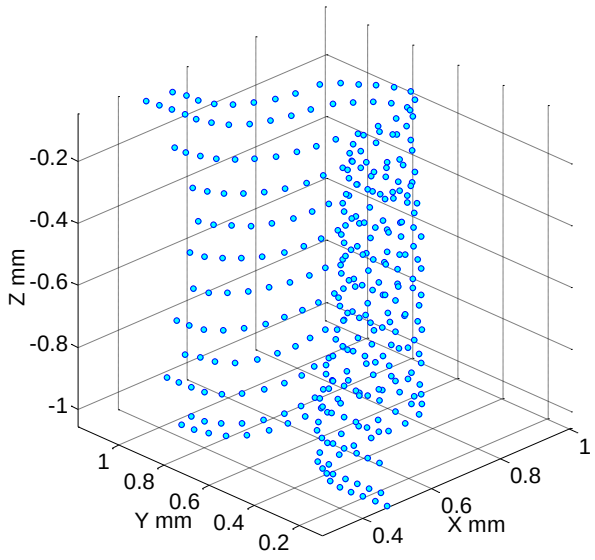

Figure 142 Measured contact positions of the semi-circular hole

6.5.4 Automated measurements

A micro end-mill machined pocket shown in Figure 143 and Figure 144 were scanned. The points taken during the automated scanning are shown in Fig. 144 with the pocket design geometry shown as a solid line. Deviations of the positions of the measured points from the pocket design geometry were as high as 80.0 µm because it was a rough milled pocket. These results show that the probing system can be effectively used to measure and verify the dimensions of machined features.

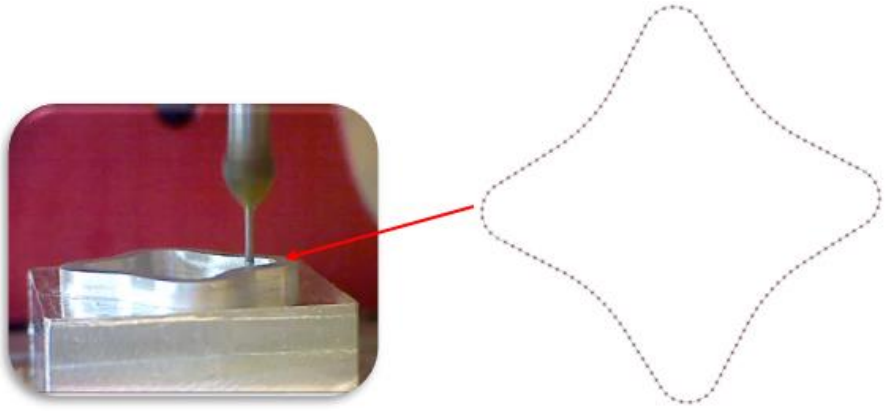

Figure 143 Automated scanning of a small milled contour

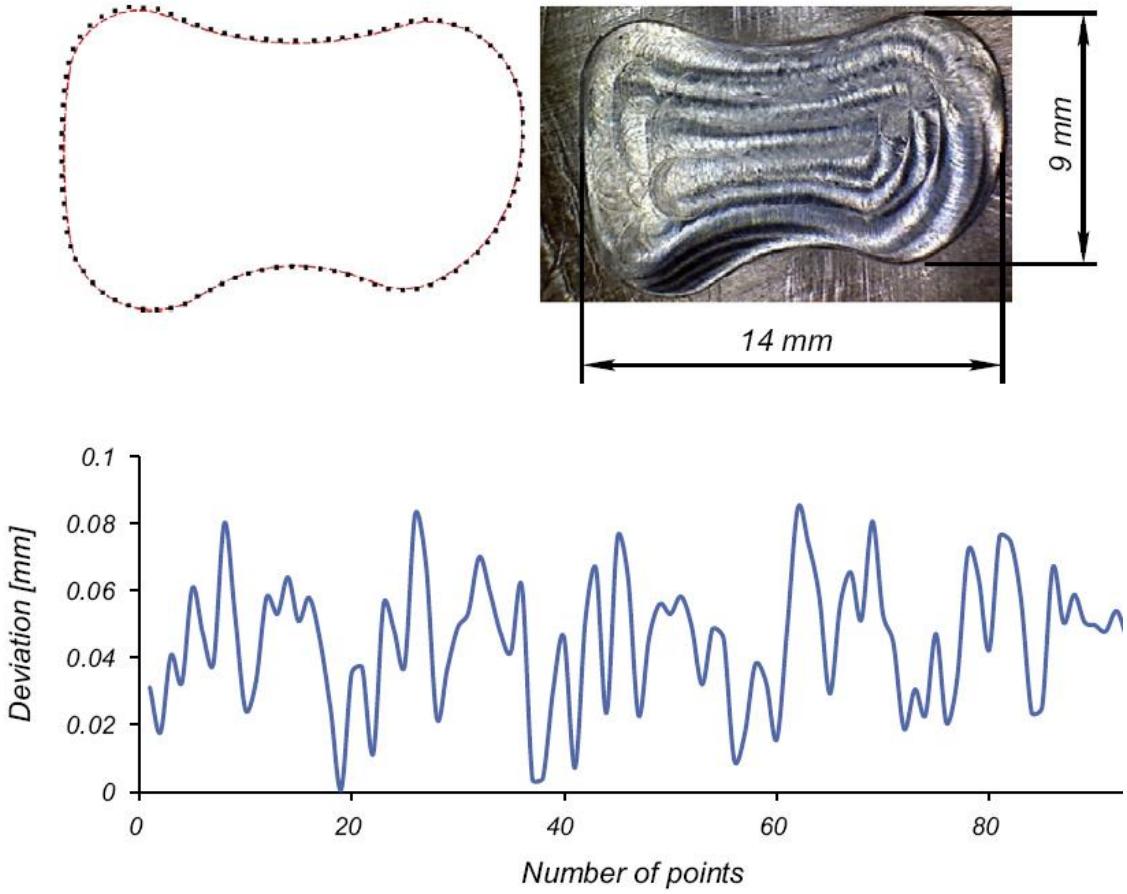

Figure 144 Automated scan results of a micro-milled pocket

6.6 Conclusion

In this chapter, a rotating wire probe with acoustic emission (AE) contact detection has been developed was used for dimensional measurement and evaluation of micro-scale holes, which were femtosecond laser machined. Inner profiles of micro-holes with a diameter as small as 500 μm was successfully measured and evaluated. The results show that there are significant variations in the inner hole quality due to laser machining process errors. Non-circular profiles inside holes have been measured, and out-of-roundness values have been calculated.

The measurement was also successfully conducted for a semi-circular hole. Measurement of smaller diameter micro-holes can be possible if the effective diameter can

be reduced. Also, automated scanning of artifacts and machined features have been achived and probing system can be effectivily used to measure and verify the dimensions of machined features.

Chapter 7 - Conclusion and Future Work

To address this thesis aim, which can be considered to be an overall aim for the area of micro probing measurements based on acoustic emission sensing development, three thesis objectives were developed specifically for this work. These thesis objectives were developed through identification of specific knowledge gaps in this research area. The concluding remarks with regards to these thesis objectives, along with the several research achievements, will be reported here.

7.1 Conclusions on the Thesis Objective

A dimensional probing system using a rotating wire and AE sensor for touch detection and an automated scanning algorithm have been developed. From the previously define micro-CMM probing requirements, besides the thesis objectives and to develop and validate a new micro-CMM that can be applied to AE sensing: the designed stylus has a stylus probe tip effective diameter below than 500 µm, an aspect ratio similar to existing micro manufactured CMM probe tip, and is suitable for use with a rotating wire probe tip based on acoustic emission sensing. Also, easy to fabricate calibrate rotated wire probe tip. A stylus was designed with an angle and straight wire probe-tip with different lengths and with a minimum effective working diameter of 302µm. When the wire probe-tip was analyzed for its dynamic properties at different rotational speed and approaching feed, its frequency was between (167-1333 Hz). Usually, we use an effective work diameter during measurements between 300-700 µm, we investigate the probe tip vibrations at different working effective diameter, and it was resulting no vibration will effect on these lengths at these working rotational speeds (10-80 K RPM). It was concluded that it was unlikely that

these frequencies would cause any vibration or to exciting the stylus through probe rotation, the used frequency would be below the natural frequency for this kind of probe tip geometry. This stylus was successfully manufactured and assembled in the Laboratory for Advanced Multi-scale Manufacturing (Lamm) through different steps and was successfully assembled onto high speed rotating spindle (NSK E800Z) chuck to form a working micro-CMM probe.

Also, the measurement repeatability and accuracy of the used probes are excellent, micro probing based on acoustic emission, for example, is capable of performing measurements with a repeatability and accuracy. It can be concluded that WPAES is capable of less than 1.0 µm repeatability. an often performs better. Moreover, multiple AE sensors and the setting of the appropriate thresholds optimizing the measurement quality. The geometry of the probes and the use of the AE sensor enable the probing system to be cost-effective and easily scalable for micro-scale components. The results of the evaluation indicate that the probing system can be used to measure a micro-scale part within one-micron accuracy with negligible probe wear and surface damage for dimensional measurement of most components, and this is due to better comparator sensitivity.

Acoustic emission signals during the surface measurement are primarily influenced by dynamic impact behavior for each measured material type, each corresponding to the unique amplitude of energy at same frequency band and constant wire probe tip length. This finding that the realized energy of the physical impact or dynamic response of the measured surface at the touch point may be associated with component physical properties. As mentioned early in this study the S-curve acceleration and deceleration time in the used Alio Industries linear motion system stage is only 50 milliseconds. If the output voltage

during touches acceding the recommended threshold within this time, the probe tip will stop touching the measured surface. If not it will acceding this time till reaching the threshold which will increase the number of touches and subsequently the number of touches will increase and effect the measurement quality. It is concluded that the materials having a high amplitude of power spectrum density may have the ability to have less number of touches. However, it can be concluded, from all of the tests completed during the experimental stage of this work, that the highest, the lowest rotational speed, lowest feed rate and minimum threshold is more appropriate parameters for high-quality measurements to minimizing the surface damage, and the probe tip wear rate too. Results have shown a strong relationship between rotational speed of probe tip effects and a number of probe tip touches and how they influence AE spike behavior and amplitude.

We have presented a new measurement application technique for measuring the inside dimensions of micro-holes. The rotating wire probing based on AE detection of the returning AE signal and the corresponding measuring method is proposed of micro-holes. A micro- scale holes, which were femtosecond laser machined with a thickness of 1 mm has been measured. Inner profiles of micro-holes with a diameter as small as 500 μm was successfully measured and evaluated. The results show that there are significant variations in the inner hole quality due to laser machining process errors. Non-circular profiles inside holes have been measured and out-of-roundness values have been calculated. Thus, it can be concluded that the straight probe tip can be used for micro- scale holes measurement. Measurement of smaller diameter micro-holes can be possible if the effective diameter can be reduced. This new technique of micro-probing will be able to add another capability of being able to measure micro holes smaller than 200 μm.

In general, this work is representative of an important contribution in the field of engineering measurements using rotating wire probe tip and AE sensors. Our promising results showed how significantly industrial coordinate measurement technology could be presented by novel technique and dimensional measurements based rotating wire probe and acoustic emission touch sensing to measure micro components.

7.2 Future Work

Any development is an endless process. Throughout the completion of this thesis, it has become apparent that several issues related to this new technique and validation of the micro WPAES system require further study. These issues had little effect on the successful completion of the thesis but are pertinent when considering the thesis aim of developments in the micro-CMM community.

For this thesis, all of experiments reported conducted using few different materials as a workpiece. Therefore the speed in which the sound wave travelled through the measured material was always not constant even for same frequency. Test other isotropic or non-isotropic materials and others with internal cavities and different shapes would change the way in which the acoustic wave are produced and how they are propagate through the materials at different frequencies. Due to the different measured materials properties, the AE signal data obtained would be related to the specific materials. Further work could be done specifically to characterize the acoustic emission raw data signal as a function of the measured material.

Since this technique is good only with solid materials, which are good conductors of sound waves and these materials having different hardness and stiffness. The probing force might be more than enough for some of them i.e soft materials; it will require some careful

consideration when the probe tip materials and measured parameters are selected. Also, we need to know the effect of the overtravel force of the probe tip wire dynamic i.e. vibration.

This work has provided a solid argument for using numerical modelling scanning techniques (point to point). To reduce the measuring time, to allow accelerated/decelerated approach feed rates before slowing the approach speed for contact at a reduced distance from the measured part. A camera-based image processing monitoring system could be applied for this purpose to reduce unnecessary travel time before contact. On the other hand, it would be beneficial to WPAES measurement to improve the numerical modelling scanning techniques to continue scanning techniques. This will accelerate the setup and measurement time.

One of the main focuses of this research was the repeatability, and therefore the AE sensor was placed underneath the fixture carried the measured material. The fact that the probe tip used for this research was rotating, placing an acoustic sensor on the styles of probe tip was not a simple task, and was not investigated because it was not an area of interest in the scope of this thesis. In order to receive the full benefits of using AE sensors, it may be worth investigating the placement of AE sensor on the probe tip. The work done in this thesis shows a broad spectrum of the capabilities and benefits of acoustic emission sensor in micro CNC machine measurement. From the several successful results obtained, it is believed that acoustic emission sensors have a promising future in the coordinate metrology industry. Continuing research in this area will provide several opportunities to gain practical knowledge of acoustic emission in Ultra micro CNC coordinate measurements.

There are three AE sensors currently being implemented in order to sense the measurement process and being able to detect surface measurement contact, which integrated with a controller and allowed for greater process control. It became apparent, while completing the measurement sensing during probe touches, that the AE signal characteristics of each probe are unique depending on probe tip geometry and measured material type. If a simple hardware band-pass filter, with amplification, is designed to consider the minimum requirements of the threshold, this will increase confidence in the measurement results in enhanced performance and improved quality measurement.

Throughout the measurements operation, several important factors proved to be detrimental to the operation of the probe. Two of these factors, the intensity noises of the spindle during rotation and the acoustic emission sensor sensitivity, can be improved through design changes to the probing system. Initially, a barrier layer of insulation was incorporated into the design of the probe to counteract sound spindle changes during the measurement operation. The ability of this insulation layer should be confirmed, and other methods for protecting the probe should be considered. One such method may be a complete encapsulation of the spindle.

The other issue arose during frequencies analysis it was found that the spindle frequencies range are between 100 to 1500 Hz, where the current AE sensor bandwidth from is 150 to 750 kHz. To ensure this did not affect any of the measurements, it is, therefore, suggested that a new AE sensor has a bandwidth from 1 to 50 kHz should be used i.e. R3a-30KHz (Physical Acoustics).

Due to the limitation of the probe tip fabrications and its run out which will effect on the effective diameter size. The current straight probe tip is best used to measure micro

holes up to 500 μm in diameter and thin through holes with thickness of 0.1-1mm. In future studies to measure holes smaller than 500 μm a new development probe with new tip dimeter i.e. 100 μm at a certain length will applicable to measure this type of micro-holes.

Due to delays inherent in AE signal processing and communication between the micro CNC machine controllers, the effective advance rate of the probe tip was limited to about 50 milliseconds without considering feedback time delay. Measuring WPAES probing force and reducing the over travel of the probing tip may be result in a better repeatability of the WPAES system and reduce the measuring time.

Bibliography

1. Brousseau, E.B., S.S. Dimov, and D.T. Pham, *Some recent advances in multi-material micro- and nano-manufacturing.* The International Journal of Advanced Manufacturing Technology, 2009. 47(1-4): p. 161-180.
2. Fan, K.-C., et al., *Study of a noncontact type micro-CMM with arch-bridge and nanopositioning stages.* Robotics and Computer-Integrated Manufacturing, 2007. 23(3): p. 276-284.
3. Dai, G., et al., *A high precision micro/nano CMM using piezoresistive tactile probes.* Measurement Science and Technology, 2009. 20(8): p. 084001.
4. Weckenmann, A., G. Peggs, and J. Hoffmann, *Probing systems for dimensional micro- and nano-metrology.* Measurement Science and Technology, 2006. 17(3): p. 504-509.
5. Han Haitjema, W.P., and P. H. J. Schellekens, *A silicon-etched probe for 3-D coordinate measurements with an uncertainty below 0.1 mm.* IEEE, 2001. 50(6).
6. Oiwa, T. and H. Nishitani, *Three-dimensional touch probe using three fibre optic displacement sensors.* Measurement Science and Technology, 2004. 15(1): p. 84-90.
7. Oiwa, T. and T. Tanaka, *Miniaturized three-dimensional touch trigger probe using optical fibre bundle.* Measurement Science and Technology, 2005. 16(8): p. 1574-1581.
8. Claverley, J.D. and R.K. Leach, *Development of a three-dimensional vibrating tactile probe for miniature CMMs.* Precision Engineering, 2013. 37(2): p. 491-499.
9. Fan, K.C., et al., *Analysis of the contact probe mechanism for micro-coordinate measuring machines.* Optoelectronics, Instrumentation and Data Processing, 2010. 46(4): p. 340-346.
10. Liang, Q., et al., *Development of a touch probe based on five-dimensional force/torque transducer for coordinate measuring machine (CMM).* Robotics and Computer-Integrated Manufacturing, 2012. 28(2): p. 238-244.
11. T. Liebrich, W.K., *New Concept of a 3D- probing system for micro – components.* CIRP Annals - Manufacturing Technology, 2010. 59(1):513-516.
12. Alting, L., et al., *Micro Engineering.* CIRP Annals - Manufacturing Technology, 2003. 52(2): p. 635-657.
13. Robert J. Hocken, P.H.P., *Coordinate Measuring Machines and Systems*. Second ed. 2012: CRC Press Taylor & Francis Group.
14. Fan, K.C., et al., *Development of a low-cost micro-CMM for 3D micro/nano measurements.* Measurement Science and Technology, 2006. 17(3): p. 524-532.
15. Marcin B. Bauza, S.C.W., Stuart T. Smith, Robert J. Hocken, *Utraprecision microscale hole scanning metrology*, in *American Society for Precision Engineering Proc. ASPE*. 2006.
16. Sommargren, G.E., *An optical measurement of surface profile.* Precision Engineering, 1981. 3: p. 131-136.
17. Hidaka, K. and P.H.J. Schellekens, *Study of a Small-sized Ultrasonic Probe.* CIRP Annals - Manufacturing Technology, 2006. 55(1): p. 567-570.

18. Butefisch, S., et al., *Tactile metrology for active microsystems.* Microsystem Technologies-Micro-and Nanosystems-Information Storage and Processing Systems, 2008. 14(12): p. 1933-1939.
19. Dobosz, M., Woźniak, Adam, *CMM touch trigger probes testing using a reference axis.* Precision Engineering, 2005. 29(3): p. 281-289.
20. Bos, E.J.C., *Aspects of tactile probing on the micro scale.* Precision Engineering-Journal of the International Societies for Precision Engineering and Nanotechnology, 2011. 35(2): p. 228-240.
21. Kuang-Chao Fan, Y.C., and Weili Wang, *Probe Technologies for Micro-Nano Measurements*, in *Proceedings of the 7th IEEE International Conference on Nanotechnology*. 2007, IEEE: Hong Kong. p. 989 - 993.
22. Ji, H., et al., *Development of a contact probe incorporating a Bragg grating strain sensor for nano coordinate measuring machines.* Measurement Science and Technology, 2009. 20(9): p. 095304.
23. Weckenmann, A., et al., *Probing systems in dimensional metrology.* Cirp Annals-Manufacturing Technology, 2004. 53(2): p. 657-684.
24. *Hexagon Metrology probes catalogue*, in *Probes & Sensors for Coordinate Measuring Machines Product Catalogue*. 2012: Germany.
25. Brand, U. and J. Kirchhoff, *A micro-CMM with metrology frame for low uncertainty measurements.* Measurement Science and Technology, 2005. 16(12): p. 2489-2497.
26. al., R.S.G.e., *Tool tip conductivity contact sensor and method*, U.S. Patent, Editor. 2002.
27. Tlusty, J. and G.C. Andrews, *A Critical Review of Sensors for Unmanned Machining.* CIRP Annals - Manufacturing Technology, 1983. 32(2): p. 563-572.
28. Popov, K., et al., *New tool-workpiece setting up technology for micro-milling.* The International Journal of Advanced Manufacturing Technology, 2009. 47(1-4): p. 21-27.
29. Moriwaki, T. and K. Okushima, *Detection for Cutting Tool Fracture by Acoustic Emission Measurement.* CIRP Annals - Manufacturing Technology, 1980. 29(1): p. 35-40.
30. Thomas, C.E., *Acoustic detection of milling tool touch to a workpiece*, in *United State Patent* G.E. Company, Editor. 1988.
31. Al-Dossary, S., R.I.R. Hamzah, and D. Mba, *Observations of changes in acoustic emission waveform for varying seeded defect sizes in a rolling element bearing.* Applied Acoustics, 2009. 70(1): p. 58-81.
32. Miinshiou Huang, L.J., Peter K. Liaw, Charlie R. Brooks, Rodger Seeley, and Dwaine L. Klarstrom, *Using Acoustic Emission in Fatigue and Fracture Materials Research.* Journal of The Minerals, Metals & Materials Society JOM, 1998. 50(11).
33. Jun-Hong Zhou, C.K.P., Zhao-Wei Zhong and Frank L. Lewis, *Tool Wear Monitoring Using Acoustic Emissions.* IEEE Transactions on Instrumentation And Measurement, 2011. 60, No. 2.
34. E. Gandarias, S.D., D. T. Pham, A. Ivanov, K. Popov, R. Lizarralde, P.J. Arrazola, *New methods for tool failure detection in micro milling*, in *1st International Conference on Multi-Material Micro Manufacture*. 2005: Spain.

35. P. SUTOWSKI, S.P., *An investigation of the grinding wheel wear with the use.* Archives of Civil and Mechanical Engineering- Published by Elsevier, 2006. 6(1): p. 87–98.
36. Li, X., *A brief review acoustic emission method for tool wear monitoring.* International Journal of Machine Tools and Manufacture- ElSEVIER, 2002. 42(2): p. 157–165.
37. David Dornfeld, D.-E.L., *Precision Manufacturing*. 2008, New York, NY 10013, USA: Springer Science+Business Media, LLC.
38. Hoffmann, J., A. Weckenmann, and Z. Sun, *Electrical probing for dimensional micro metrology.* CIRP Journal of Manufacturing Science and Technology, 2008. 1(1): p. 59-62.
39. Hansen, H.N., et al., *Dimensional Micro and Nano Metrology.* CIRP Annals - Manufacturing Technology, 2006. 55(2): p. 721-743.
40. Grous, A., *Applied Metrology for Manufacturing Engineering*. 2011, 111 River Street Hoboken, NJ 07030 USA: John Wiley & Sons, Inc.
41. Flack, D., *Fundamental good practice in dimensional metrology*, in *Reprinted with minor corrections/amendments* J. Hannaford, Editor. 2005, National Physical Laboratory: UK.
42. Leach, R., *Fundamental Principles of Engineering Nanometrology*. Second ed. 2014, United States: William Andrew is an imprint of Elsevier.
43. Jagani, V.P.a.A., *Evaluation of Circle Fitting Algorithm for Coordinate Measuring Machine.* International Journal of Material Research, Electronics and Electrical Systems 2011. Volume 4, Number 1-2: p. 39– 57.
44. Renishaw. *A 'one stop shop' retrofit solution by Renishaw*. Available from: http://www.renishaw.com/en/a-one-stop-shop-retrofit-solution-by-renishaw--10512.
45. Yueh-Jaw Lin, P.M., *A new algorithm for determining a collision free path for a CMM probe.* International Journal of Machine Tools & Manufacture 1999. 39: p. 1397–1408.
46. Ali Kamrani, E.A.N., *Rapid Prototyping: Theory and Practice* Manufacturing Systems Engineering Series. 2006, United States of America.: Springer.
47. Peggs, G.N., A.J. Lewis, and S. Oldfield, *Design for a Compact High-Accuracy CMM.* CIRP Annals - Manufacturing Technology, 1999. 48(1): p. 417-420.
48. Muammer Koc, T.O.-M., *Manufacturing: Design and Manufacturing of Micro-Products*. 2011.
49. Richard Leach, J.H., Keith Jackson, Andrew Lewis, Simon Oldfield and Andrew Yacoot, *Advances in traceable nanometrology at the National Physical Laboratory.* INSTITUTE OF PHYSICS 2001.
50. Flack, D., *CMM Probing Measurement Good Practice Guide* in *Engineering Measurement Division Measurement Good Practice Guide No. 43*. 2011, National Physical Laboratory.
51. Seggelen, J.K.v., et al., *An Elastically Guided Machine Axis with Nanometer Repeatability.* CIRP Annals - Manufacturing Technology, 2005. 54(1): p. 487-490.
52. Küng, A., F. Meli, and R. Thalmann, *Ultraprecision micro-CMM using a low force 3D touch probe.* Measurement Science and Technology, 2007. 18(2): p. 319-327.
53. Zeiss, C., *measuring Nanometrs*, I.m.t. GmbH, Editor.

54. Schwenke, H., et al., *Geometric error measurement and compensation of machines—An update.* CIRP Annals - Manufacturing Technology, 2008. 57(2): p. 660-675.
55. Umetsu, K., et al., *Geometric calibration of a coordinate measuring machine using a laser tracking system.* Measurement Science and Technology, 2005. 16(12): p. 2466-2472.
56. Makoto Abbe, K.T.a.S.O., *Calibration of CMM by 3-dimensional coordinate comparison.*
57. Harris, J.O. and A.D. Spence, *Geometric and quasi-static thermal error compensation for a laser digitizer equipped coordinate measuring machine.* International Journal of Machine Tools & Manufacture, 2004. 44(1): p. 65-77.
58. *Precision styli*, Renishaw, Editor.: United Kingdom.
59. Pril, W.O., *Development of High Precision Mechanical Probes for Coordinate Measuring Machines*. 2002, CIP-data library technische universiteit eindhoven: Wageningen.
60. van Vliet, W.P. and P.H.J. Schellekens, *Development of a fast mechanical probe for coordinate measuring machines.* Precision Engineering, 1998. 22(3): p. 141-152.
61. *Touch Probe Systems for Machine Tools*, HEIDENHAIN, Editor. 2010.
62. Wang, L., Xi, Fengfeng, *Smart Devices and Machines for Advanced Manufacture*. 2008: Springer-Verlag London Limited.
63. A Kung, F.M.a.R.T., *Ultra precision micro-CMM using a low force 3D touch probe.* MEASUREMENT SCIENCE AND TECHNOLOGY, 2007: p. 319–327.
64. *Triskelion Ultra Precision Tactile Probe System*, I.P.E.D. GmbH, Editor., Stuttgart, Germany.
65. Haitjema, H., W.O. Pril, and P.H.J. Schellekens, *Development of a silicon-based nanoprobe system for 3-D measurements.* Cirp Annals-Manufacturing Technology, 2001. 50(1): p. 365-368.
66. Heinrich Schwenke, F.H., Klaus Wendt, Franz Wäldele, *Future challenges in coordinate metrology: ADDRESSING METROLOGICAL PROBLEMS FOR VERY SMALL AND VERY LARGE PARTS*, in *INFORMATION DEVELOPMENT WORLD IDW*. 2001. p. 1–12.
67. Schwenke, H., et al., *Opto-tactile Sensor for 2D and 3D Measurement of Small Structures on Coordinate Measuring Machines.* CIRP Annals - Manufacturing Technology, 2001. 50(1): p. 361-364.
68. Cao, S., et al., *Recent developments in dimensional metrology for microsystem components.* Microsystem Technologies, 2002. 8(1): p. 3-6.
69. *<assets-AMA-Conferences-SENSOR+TEST-Konferenzen-2009-SENSOR-2009-Volume-II-B8.1-Proceedings-SENSOR2009Volume2.pdf>*.
70. K Enami, C.K., T Nogami, M Hiraki, *Development of nano-probe system using optical sensing*. 1999, IMEKO-XV World Congress. p. 189-192.
71. Cui, J., L. Li, and J. Tan, *Opto-tactile probe based on spherical coupling for inner dimension measurement.* Measurement Science and Technology, 2012. 23(8): p. 085105.
72. N. Ferreira, A.B., A. Dietzel, S. Büttgenbach, T. Krah, D. Metz, K. Kniel and F. Härtig, *Reducing the Probe Ball Diameters of 3D Silicon Based Microprobes for*

Dimensional Metrology, in *Seventh International Conference on Sensing Technology*. 2013.
73. Fan, K.-C., et al., *Design of an analogue contact probe for nano-coordinate measurement machines (CMM).* 2011. 8321: p. 832114.
74. Chu, C.-L. and C.-Y. Chiu, *Development of a low-cost nanoscale touch trigger probe based on two commercial DVD pick-up heads.* Measurement Science and Technology, 2007. 18(7): p. 1831-1842.
75. Chu, C.-L. and C.-H. Lin, *Development of an optical accelerometer with a DVD pick-up head.* Measurement Science and Technology, 2005. 16(12): p. 2498-2502.
76. Fan, K.-C., et al., *A scanning contact probe for a micro-coordinate measuring machine (CMM).* Measurement Science and Technology, 2010. 21(5): p. 054002.
77. Li, R.-J., et al., *An analogue contact probe using a compact 3D optical sensor for micro/nano coordinate measuring machines.* Measurement Science and Technology, 2014. 25(9): p. 094008.
78. Shimin Yang, S.L., Mark J Kaiser and Fung Hoi Kwun Eric, *A probe for the measurement of diameters and form errors of small holes.* IOPscience, 1998: p. 1365–1368.
79. Kim B J, M.T., Fujita H and Tominaga A, *Dimensional measurement of micro-scale holes with silicon-based micro twin probes.* IEEE Int. , 1998: p. 334–9.
80. Murakami, H.K., Akio; Onikura, Hiromichi; Sajima, Takao; Kawagoishi, Norio; Kondo, Eiji, *Development of a System for Measuring Micro Hole Accuracy Using an Optical Fiber Probe.* ournal of Advanced Mechanical Design, Systems, and Manufacturing, 2010. 4(5): p. 995-1004.
81. Muralikrishnan, B., J.A. Stone, and J.R. Stoup, *Fiber deflection probe for small hole metrology.* Precision Engineering, 2006. 30(2): p. 154-164.
82. Takao Sajima*, H.M., Akio Katsuki, Daisuke Tabuchi, Osamu Ohnishi, Syuhei Kurokawa, Hiromichi Onikura and Toshiro K. Doi, *Precision Profile Measurement System for Microholes Using Vibrating Optical Fiber.* Sensors and Materials, 2012. 24(7): p. 387-396.
83. Beomjoon Kim, T.M.a.T.B., *The vibroscanning method for the measurement of micro-hole profiles.* IOPscience, 1999. 10(8): p. 697–705.
84. Bauza, M.B., et al., *Development of a virtual probe tip with an application to high aspect ratio microscale features.* Review of Scientific Instruments, 2005. 76(9): p. 095112.
85. Bauza, M.B.W., S. C. Woody, B. A. Smith, S. T., *Surface profilometry of high aspect ratio features.* Wear, 2011. 271(3-4): p. 519-522.
86. Takaki Hashimoto, Y.T., Takashi Miyoshi, Ryusuke Nakajima *Fundamental analysis on the novel 3 D probing technique for micro parts using the optical fiber trapping.* Proceedings of the Annual Meeting of the ASPE, 2003: p. 83-86.
87. Chan-Seo Gooa, M.B.G.J., Akinori Saitob, *Probing system for measurement of micro-scale components.* Journal of Manufacturing Processes 14 (2012) 174–180, 2012.
88. Liebrich, T. and W. Knapp, *New concept of a 3D-probing system for micro-components.* CIRP Annals - Manufacturing Technology, 2010. 59(1): p. 513-516.
89. Lanceros, J.G.R.a.S., *Sensors: Focus on Tactile, Force and Stress Sensors*. 2008.

90. Savio, C.D., et al., *3D metrology with a compact scanning probe microscope based on self-sensing cantilever probes.* Measurement Science and Technology, 2007. 18(2): p. 328-333.
91. Pi, U.H.K., J. I.; Shin, S.; Khim, Z. G, *Electrostatic Force Microscopy with a Self-Sensing Piezoresistive Cantilever.* The International Nuclear Information System (INIS), 2003. 35(22): p. 209-212.
92. Takefumi Kanda, M.K.K., Toshiro Higuchi *Sensitivity of a miniaturized touch probe sensor using PZT thin film vibrator.* Ultrasonics, 2002: p. 61-65.
93. Masuzawa, T., et al., *Twin-Probe Vibroscanning Method for Dimensional Measurement of Microholes.* CIRP Annals - Manufacturing Technology, 1997. 46(1): p. 437-440.
94. Masuzawa, T., Y. Hamasaki, and M. Fujino, *Vibroscanning Method for Nondestructive Measurement of Small Holes.* CIRP Annals - Manufacturing Technology, 1993. 42(1): p. 589-592.
95. M. B. Bauza, S.C.W., R. M. Seugling, S. T. Smith, Craig, *Dimensional measurements of ultra*, in *25th Annual Meeting of the American Society for Precision Engineering*. 2010: Atlanta, GA, United States.
96. Seugling, R.M.D., I ; Florando, J ; Bauza, M ; Woody, S ; Smith, S, *Investigating scaling limits of a fibre based resonant probe for*, in *23rd ASPE Annual Meeting and 12th ICPE*. 2008: Portland, OR, United States.
97. Marcin B. Bauza, S.C.W., Stuart T. Smith, Richard M. Seugling, Ian M. Darnell and Jeffery N. Florando, *Microscale metrology using standing wave probes*, in *23rd ASPE Annual Meeting and 12th ICPE*. 2008: United States.
98. R. M. Seugling, S.C.W., M. B. Bauza, *Standing wave probes for dimensional metrology of low density foams*, L.B.N.L. Researcher, Editor. 2010, United States. Dept. of Energy. Sponsor: USA.
99. Schwenke, H., et al., *Optical Methods for Dimensional Metrology in Production Engineering.* CIRP Annals - Manufacturing Technology, 2002. 51(2): p. 685-699.
100. Michihata, M., Y. Takaya, and T. Hayashi, *Development of the nano-probe system based on the laser-trapping technique.* CIRP Annals - Manufacturing Technology, 2008. 57(1): p. 493-496.
101. Tan, J.B. and J.N. Cui, *Ultraprecision 3D probing system based on spherical capacitive plate.* Sensors and Actuators A: Physical, 2010. 159(1): p. 1-6.
102. Fraden, J., *Handbook of Modern Sensors*. Physics, Designs, and Applications. 2015, San Diego, CA, USA: Springer.
103. Crowder, R.M. *Automation and Robotics*. 1998; Available from: http://www.southampton.ac.uk/~rmc1/robotics/artactile.htm.
104. Vallen, H., *AE Testing Fundamentals,Equipment, Applications.* e-Journal of Nondestructive Testing 2002.
105. Carlos, M.F., *Heeding the warning sounds from materials.* ASTM International, 2003. 31(10): p. 26-29.
106. M. Surgeon, M.W., *One sensor linear location of acoustic emission events using plate wave theories.* Materials Science and Engineering, 1999: p. 254-261.
107. Wevers, M., *Listening to the sound of materials Acoustic Emission for the analysis of material behaviour.* NDT & E International- Journal - Elsevier, 1997. 30(2): p. 99-106.

108. Carlos, M.F. *Acoustic Emission: Heeding the Warning Sounds from Materials*. Available from: http://www.astm.org/SNEWS/OCTOBER_2003/carlos_oct03.html.
109. Li, X., *A brief review acoustic emission method for tool wear monitoring.* International Journal of Machine Tools & Manufacture, 2002. 42 (2002) 157–165.
110. Ohtsu, C.U.G.M., *Acoustic Emission Testing*. 2008, Verlag Berlin Heidelberg, Germany: Springer.
111. Ronnie K. Miller, E.v.K.H., Patrick O. Moore, *Nondestructive Testing Handbook:Acoustic Emission Testing*. August 30, 2005: Amer Society for Nondestructive; 3 edition.
112. Gautschi, D.-I.E.G., *Piezoelectric sensors*. 2002: Springer.
113. Center, N.R., *Introduction to Acoustic Emission Testing.* 2001-2014.
114. Mba, D. and J.Z. Sikorska, *Challenges and obstacles in the application of acoustic emission to process machinery.* Proceedings of the Institution of Mechanical Engineers, Part E: Journal of Process Mechanical Engineering, 2008. 222(1): p. 1-19.
115. Vahaviolos, S.J., *Acoustic Emission Standards and Technology Update*, ed. A.s.t.p. 1353. 1999, West Conshohocken, USA: ASTM.
116. Kocur, G.K., *Time Reverse Modeling of Acoustic Emissions in Structural Concrete*. 2012, ETH Zurich: Germany.
117. Bucur, V., *Acoustics of Wood*. Second ed, ed. T.E. Timell. 2006: Springer.
118. Miller, R.K.a.P.M., *Acoustic Emission Testin.NDT Handbook*. 3rd ed ed. Vol. Vol. 5. 2005.
119. Shirane, G., E. Sawaguchi, and Y. Takagi, *Dielectric properties of lead zirconate.* Physical Review, 1951. 84(3): p. 476.
120. Gautschi, D.-I.E.G., *Piezoelectric Sensorics*. Force Strain Pressure Acceleration and Acoustic Emission Sensors Materials and Amplifiers 2002, Berlin Springer-Verlag Berlin Heidelberg
121. Wolfgang Sachse, J.R., and Kusuo Yamaguchi, *Acoustic Emission: Current Practice and Future Directions*. February 1991, Baltimore.
122. Available from: https://www.nde-ed.org/EducationResources/CommunityCollege/Other%20Methods/AE/AE_Intro.php.
123. GmbH, V.S. *Acoustic Emission Sensors Specification*. 2015; Available from: http://www.vallen.de/zdownload/pdf/sov1507.pdf.
124. Acoustics, P. *2/4/6 - Switch Selectable Gain Single Ended and Differential Preamplifier*. Available from: http://www.physicalacoustics.com/by-product/2-4-6/.
125. H.M. van Roermund, A.B., Michiel Steyaert, *Nyquist AD Converters, Sensor Interfaces, and Robustness*. 2012: Springer.
126. Hendrik van der Ploeg, B.N., *Calibration techniques in nyquist A/D converters*. Vol. 873. 2006: The Springer International Series in Engineering and Computer Science.
127. Bourchak, M., et al., *Acoustic emission energy as a fatigue damage parameter for CFRP composites.* International Journal of Fatigue, 2007. 29(3): p. 457-470.

128. Güemes, W.O.J.A., *New Trends in Structural Health Monitoring*. International Centre for Mechanical Sciences. Vol. 542. 2013, Wien Heidelberg New York Dordrecht London: Springer
129. Center, N.R. *Introduction to Acoustic Emission Testing*. Available from: http://www.ndt-ed.org/
130. Ativitavas, N., *ACOUSTIC EMISSION SIGNATURE ANALYSIS OF FAILURE*. 2002, The University of Texas at Austin.
131. Patrick O. Moore, T.E.K.M.a.E.v.K.H., *Nondestractive testing Handbook*. Vol. Vol. III. . Columbus: Published by the American Socity for Nondestractive Testing USA.
132. Kuo, C.-C., *Artificial recognition system for defective types of transformers by acoustic emission.* Expert Systems with Applications, 2009. 36(7): p. 10304-10311.
133. Tilley, J.M.R.B.C.M.R.M., *Acoustic emission monitoring for inspection of seamwelded hot reheat piping in fossil power plants*, in *Nondestructive Evaluation of Utilities and Pipelines*. 1996, The International Society for Optical Engineering SPIE: Scottsdale, USA.
134. He, Y., X. Yin, and F. Chu, *Modal Analysis of Rubbing Acoustic Emission for Rotor-Bearing System Based on Reassigned Wavelet Scalogram.* Journal of Vibration and Acoustics, 2008. 130(6): p. 061009.
135. WELCH, P.D., *The use of fast Fourier transform for the estimation of power spectra a method based on time averaging over short modified periodograms.* IEEE TRANSACTIONS ON AUDIO AND ELECTROACOUSTICS,, 1967. AU-1,No. 2.
136. Webster, J., W.P. Dong, and R. Lindsay, *Raw Acoustic Emission Signal Analysis of Grinding Process.* CIRP Annals - Manufacturing Technology, 1996. 45(1): p. 335-340.
137. Karakehayov, Z., *Data Acquisition Applications*. August 23, 2012
138. Nivesrangsan, P., J.A. Steel, and R.L. Reuben, *Source location of acoustic emission in diesel engines.* Mechanical Systems and Signal Processing, 2007. 21(2): p. 1103-1114.
139. Nair, A. and C.S. Cai, *Acoustic emission monitoring of bridges: Review and case studies.* Engineering Structures, 2010. 32(6): p. 1704-1714.
140. M. Sison, J.C.D., M. G. Lozev, G. G. Clemeña, *Analysis of Acoustic Emissions from a Steel Bridge Hanger.* Springer, 1998. 10(3): p. 123-145.
141. Peacock, M., *Acoustic emission for detection of process related damage in pressure vessels and piping*, in *Nondestructive Evaluation of Utilities and Pipelines*. 1996, he International Society for Optical Engineering SPIE.
142. Miinshiou Huang, L.J., Peter K. Liaw, Charlie R. Brooks, Rodger Seeley, and Dwaine L. Klarstrom, *Using Acoustic Emission in Fatigue and Fracture Materials Research.* Journal of the Minerals, Material & Material Society JOM, 1998. 50,No. 11.
143. Theobald, P., B. Zeqiri, and J. Avison, *Couplants and their influence on ae sensor sensitivity.* Journal of acoustic emission. 26: p. 91.
144. Materials, A.S.f.T.a., *Standard Guide for Mounting Piezoelectric Acoustic Emission Sensors*. 2007, ASTM-E-650-97.

145. Bourne, K.A., et al., *An Acoustic Emission-Based Method for Determining Contact Between a Tool and Workpiece at the Microscale.* Journal of Manufacturing Science and Engineering, 2008. 130(3): p. 031101.
146. Salah Elfurjani, B.V., and Martin B. G. Jun, *Evaluation of Rotating Probes for Acoustic Emission Contact Sensing*, in *8th International Conference on MicroManufacturing ICOMM 2013*. 2013: Victoria, Canada 25 – 28 March 2013
147. Elfurjani, S., et al., *Dimensional measurement based on rotating wire probe and acoustic emission.* Measurement, 2015. 59: p. 329-336.
148. Salah Elfurjani, A.B., Martin B. Jun, *Experimental Study of Microscale Probe Measurement System Using Wire-Based Probe and Acoustic Emission Sensor*, in *7th International Conference on Micromanufacturing ICOMM*. 2012: March 12-14, 2012, Norris University Center, Northwestern University, IL, USA.
149. Salah Elfurjani, A.B., and Martin B.G. Jun, *Evaluation of a Probing System Using Acoustic Emission Sensors and a Rotating Probe for Measurement of Miniature Components*, in *1st International Conference on Virtual Machining Process Technology VMPT 2012, CIRP Sponsored Conference* 28 May- 1 June, 2012: Ecole Polytechnique, Montréal, Canada
150. Elfurjani, S., J. Ko, and M.B.G. Jun, *Micro-scale hole profile measurement using rotating wire probe and acoustic emission contact detection.* Measurement, 2016. 89: p. 215-222.
151. Den Hartog, J.P., *Mechanical Vibrations* 1985, Dover Publications.
152. Fernando, R., *Health Monitoring of FRP using Acoustic Emission and Fiber Optic Techniques*. 2004, Porto. p. 257.